Aus dem Walther-Straub-Institut für Pharmakologie und Toxikologie,

Institut der Ludwig-Maximilians-Universität München

Dissertation

zum Erwerb des Doctor of Philosophy (Ph.D.)

an der Medizinischen Fakultät der

Ludwig-Maximilians-Universität München

Modulation of plasmin activity by TRPM7 and TGF-β in lung cells

vorgelegt von:

Sarah Zeitlmayr

aus:

Trostberg

Jahr:

2023

Mit Genehmigung der Medizinischen Fakultät der

Ludwig-Maximilians-Universität zu München

First evaluator (1. TAC member):   Prof. Dr. med. Thomas Gudermann

Second evaluator (2. TAC member): PD Dr. habil. med. Claudia Staab-Weijnitz, PhD

Third evaluator: Prof. Dr. med. Jürgen Behr

Fourth evaluator: Prof. Dr. rer. nat. Markus Rehberg

Dean: **Prof. Dr. med. Thomas Gudermann**

date of the defense: 12.06.2023

Table of Contents

1.   Abstract

Aberrant regulation of extracellular matrix (ECM) proteins such as fibronectin or collagens is characteristic for lung fibrosis and lung tumor progression. Activity of the protease plasmin and subsequent ECM degradation is crucial in the progression of these diseases. Despite that, plasmin activity of lung cells has rarely been measured directly and regulatory processes are barely understood. Plasmin activity is decreased by the plasminogen activator inhibitor 1 (PAI1), which is induced by transforming growth factor β (TGF-β) - promoted activation of SMAD transcription factors. In this work, TGF-β-induced inhibition of plasmin activity, monitored by a fluorogenic plasmin substrate, could be correlated with TGF-β/SMAD-induced PAI1 expression in primary human pulmonary fibroblasts (pHPF). In addition, the transient receptor potential cation channel, subfamily M, member 7 (TRPM7) was found to restrain plasmin activity, since two structurally unrelated TRPM7 blockers enhanced plasmin activity. This increase could be correlated with decreased PAI1 levels, most likely due to functional interactions between TRPM7 and TGF-β on the level of SMAD proteins. Accordingly, TRPM7 blockers antagonized TGF-β-mediated fibronectin or collagen deposition and fibroblast-to-myofibroblast differentiation. Thus, TRPM7 blockade emerges as a novel tool to target ECM accumulation in pHPF and thus to ameliorate lung fibrosis.

TGF-β has also been reported to act as a tumor-suppressor or tumor-promoter depending on the stage of the disease. Further, plasmin activity has been proposed to be higher in late stages of lung tumors. When basal plasmin activity in early stage (A549) cells was compared to late stage tumor cells (H1299), higher activity was surprisingly found in A549 cells. However, when TGF-β was applied, reduced plasmin activity was observed in A549 cells, but an increase in H1299 cells. Thus, effects of TGF-β on plasmin activity might depend on the stage of the lung tumor and elevated plasmin activity proposed for late stage tumor cells might depend on the presence of TGF-β. Extracellular signal-regulated kinases 1/2 (ERK1/2) signaling is provided as a possible pathway accounting for the differences among tumor cells, since ERK1/2 blockade not only prevented the TGF-β-mediated increase in plasmin activity in H1299 cells, but even led to a decrease as observed

in A549 cells. Hence, this work reveals so far unappreciated roles for TGF-β and ERK-1/2 in the elevated activity of plasmin in late stage lung tumor cells.

2. Zusammenfassung

Eine Fehlregulation in der Expression von Proteinen der extrazellulären Matrix (ECM) wie Fibronektin oder Kollagen ist charakteristisch für Lungenfibrose und das Fortschreiten von Lungentumoren. Die Aktivität der Protease Plasmin und der anschließende Abbau der ECM sind ein entscheidender Faktor für das Fortschreiten dieser Krankheiten. Die Plasminaktivität von Lungenzellen wurde bisher jedoch nur selten direkt gemessen und die involvierten regulatorischen Prozesse sind wenig verstanden. Aktivität von Plasmin wird durch den Plasminogen-Aktivator-Inhibitor 1 (PAI1) verringert, welcher durch die vom transformierenden Wachstumsfaktor β (TGF-β) geförderte Aktivierung der SMAD-Transkriptionsfaktoren induziert wird. In der vorliegenden Arbeit wurde die Plasminaktivität mittels eines fluorogenen Plasminsubstrates gemessen. Damit konnte eine TGF-β-vermittelte Aktivierung von SMAD Proteinen und die Hemmung der PAI1-Expression mit einer verringerten Plasminaktivität in primären humanen Lungenfibroblasten (pHPF) korreliert werden. Darüber hinaus wurde festgestellt, dass der Ionenkanal die Plasminaktivität hemmt, da TRPM7-Blocker die Plasminaktivität erhöhten. Dieser Anstieg könnte mit verringerter PAI1 Expression korreliert sein, welche vermutlich auf funktionelle Interaktionen zwischen TRPM7 und TGF-β auf der Ebene der SMAD-Proteine zurückzuführen ist. Dementsprechend hemmten TRPM7-Blocker die TGF-β-vermittelte Fibronektin- oder Kollagenablagerung sowie die Differenzierung von Fibroblasten zu Myofibroblasten. Somit erweist sich die TRPM7-Blockade als eine neuartige Möglichkeit, die ECM-Akkumulation in pHPF zu bekämpfen und Lungenfibrose zu lindern.

TGF-β kann je nach Stadium als Tumorsuppressor oder Tumorpromotor wirken. Außerdem wird angenommen, dass die Plasminaktivität in späten Stadien von Lungentumoren höher ist. Beim Vergleich der basalen Plasminaktivität in A549-Zellen (Zellen aus einem Primärtumor) mit H1299-Zellen (Tumorzellen isoliert aus Lymphknoten) wurde überraschenderweise eine höhere Aktivität in A549-Zellen festgestellt. Nach Stimulation mit TGF-β wurde in A549-Zellen eine verringerte Plasminaktivität, in H1299-Zellen dagegen eine erhöhte Aktivität festgestellt. Somit könnten die Auswirkungen von TGF-β auf die Plasminaktivität

vom Stadium des Lungentumors abhängen. Die für migrierende Tumorzellen vorgeschlagene erhöhte Plasminaktivität könnte ebenfalls von TGF-β abhängen. Die Signalübertragung durch ERK1/2 (extracellular signal-regulated kinases 1/2) könnte für die Unterschiede zwischen den Tumorzellen verantwortlich sein, da eine Blockade der ERK1/2 Aktivität nicht nur den TGF-β-vermittelten Anstieg der Plasminaktivität in H1299-Zellen verhinderte, sondern sogar zu einer reduzierten Plasminaktivität ähnlich zu A549-Zellen führte. Diese Arbeit deckt somit eine bisher nicht beachtete Rolle von TGF-β und ERK-1/2 bei der erhöhten Plasminaktivität in Lungentumorzellen im Spätstadium auf.

3. Introduction

3.1 The fibrinolytic system and its role in the lung

In 1893, Albert Dastre studied the dissolution of fibrin clots in the blood and coined the term "fibrinolysis", marking the start of extensive research in the field of hemostasis [1]. Hemostasis describes the dynamic balance between coagulation, where platelets and fibrin polymers clot to close wounds, and fibrinolysis, which leads to the dissolution of fibrin clots and subsequently prevents clogging of blood vessels and thrombosis [2-5]. Cleavage of fibrin by plasmin results in the generation of fibrin degradation products (FDPs) that are then cleared by blood circulation [6].

All processes of hemostasis are subject to a complex regulation to maintain proper physiological function. Failure of physiological fibrinolysis has dreadful consequences, leading to either bleeding disorders when overactive, or thrombus formation upon decreased activity [2]. Inability to dissolve blood clots e.g. in the leg creates a significant risk for movement of the thrombus to the lung arteries, resulting in pulmonary embolism, which is often fatal when untreated [7]. Therapeutics for pulmonary embolism target the halting of coagulation and in severe cases, activation of the fibrinolytic system to achieve thrombolysis [8, 9]. Besides its thrombolytic function, the fibrinolytic system has been linked to immunological responses and tissue remodeling, thus playing an important role in various pathological conditions [10].

The protease plasmin as the central enzyme of the fibrinolytic system degrades fibrin formed in blood vessels as well as proteins of the extracellular matrix, thus affecting tissue remodeling and cell migration [11]. As a major regulator of extracellular matrix (ECM), the fibrinolytic system is thus crucial in diseases displaying dysfunctional ECM remodeling, like pulmonary fibrosis or tumorigenesis [12-16].

Crucial steps in the regulation of plasmin activity and the fibrinolytic system are described in detail in the following section.

3.1.1 The plasminogen activation system and its modulators

The serine protease plasmin is generated by cleavage of the zymogen plasminogen, its inactive precursor. Plasminogen is cleaved by tissue-type (tPA) or urokinase-type plasmin activators (uPA) via the lysine binding site of plasminogen [17, 18]. Circulating plasminogen is mainly synthesized in the liver, but lower levels of tissue-derived plasminogen have been reported to be produced in several extrahepatic sites including lung, heart and kidney among others [19-21]. Generation of plasminogen at tissue sites results in plasmin activation independently of circulating plasminogen and is thought to be important for physiological implications of plasmin [19].

Plasminogen is a single-chain glycoprotein consisting of 810 amino acids and is cleaved by both tPA or uPA at Arg561-Val562 [22, 23]. Interestingly, tPA is produced in endothelial cells and requires binding to fibrin for efficient cleavage [24]. uPA on the other hand is primarily released from fibroblasts and epithelial cells in wounded tissues. Cleavage of plasminogen by uPA is independent of fibrin binding and can occur when uPA is in solution or cell-associated to its receptor [25, 26]. The primary function of tPA and uPA is considered to be fibrinolysis in blood vessels, however, uPA is additionally associated with tumor and fibrosis [26]. Plasminogen, tPA and uPA are bound to the plasma membrane by their receptors [27-29]. Thus, active plasmin can be found associated to the membrane or when it is released to the extracellular fluid [30, 31]. Plasminogen cleavage by tPA or uPA results in the formation of plasmin, a two-chained protease linked by two disulfide bonds [23]. Two isoforms of plasminogen exist, the native form of plasminogen glu-plasminogen can be further activated to lys-plasminogen by additional cleavage of a glutamic acid at the N-terminus. Lys-plasminogen exhibits a shorter half-life in plasma and higher affinity for fibrin-binding than glu-plasminogen and it is proposed that the additional cleavage step to form lys-plasminogen depends on whether the cleavage is taking place on the cell surface or in solution [32]. Active plasmin then binds to substrates like fibrin or fibronectin via lysine recognition sites to trigger cleavage of the substrates.

The plasmin system is regulated by expression of the plasminogen-activator-inhibitor 1 (PAI1), a member of the serine protease inhibitor (serpin) gene family. PAI1 protein levels or mRNA expression are generally elevated by TGF-β/SMAD signaling and TGF-β-dependent pathways and its implications on physiological and pathophysiological conditions will be highlighted in chapter 3.4.
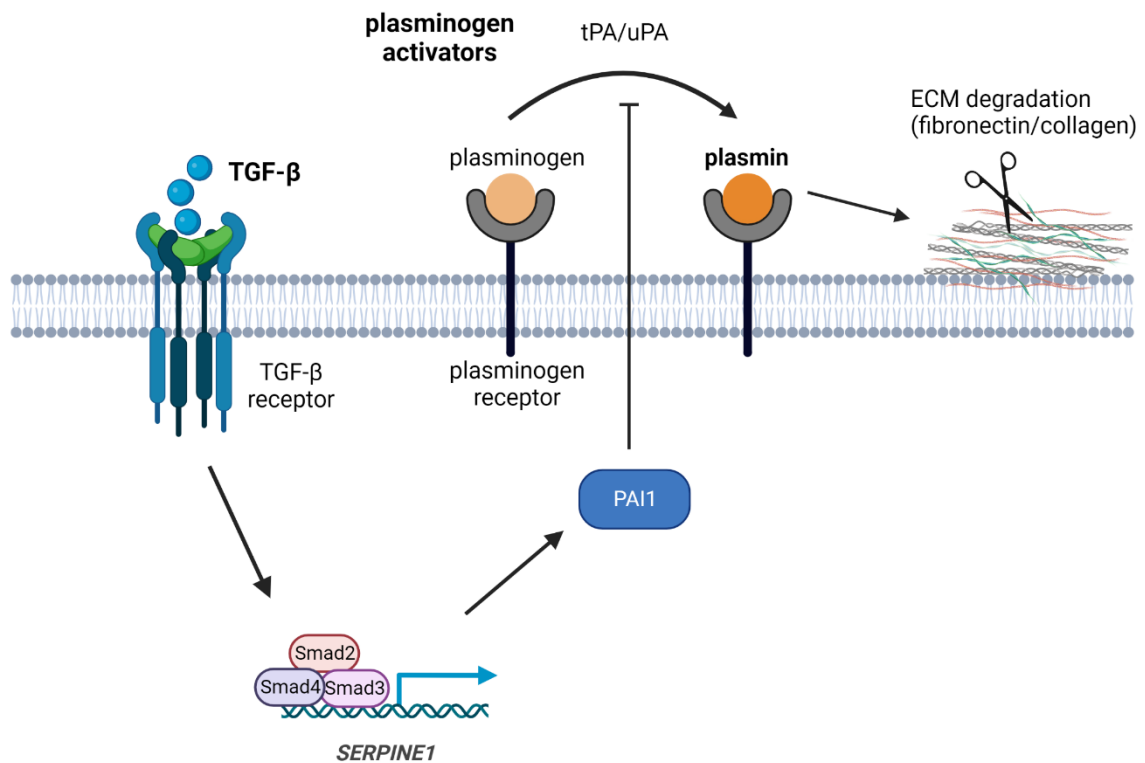
Figure 1: Schematic overview of the fibrinolytic system

Plasminogen to plasmin activation is mediated by plasminogen activators tPA and uPA. Active plasmin degrades components of the extracellular matrix (ECM) like fibronectin and collagens. TGF-β-signaling via SMAD proteins induces expression of plasminogen-activator-inhibitor 1 (PAI1), thereby inhibiting plasmin activation.

A schematic overview of the fibrinolytic system and its regulation is displayed in fig 1. PAI1 is produced by several cells, including endothelial cells, hepatocytes, fibroblasts and macrophages [33]. It contains three β-sheets and nine α-helices and two highly conserved functional domains have been identified: One domain is

required for connecting PAI1 to ECM via binding to vitronectin and the second domain confers inhibition of tPA/uPA activity [34, 35]. By inhibiting soluble or cell-associated tPA or uPA, PAI1 leads to the inhibition of plasminogen to plasmin conversion [36]. PAI2 and PAI3 are closely related to PAI1, however PAI2 is mostly important in fetal growth regulation during pregnancy and PAI3 is thought to be a regulator of plasmin activators in the male reproductive tissue [37, 38].

Mutations in the *SERPINE1* gene leading to PAI1 deficiency are associated with dysfunctional wound healing and bleeding disorders and *SERPINE1* polymorphisms are linked to coronary artery disease [39-42]. Furthermore, increased PAI1 protein levels are associated with development of multiple diseases like thrombosis, cancer, fibrosis and atherosclerosis [33, 43, 44]. Besides PAI1, the serpine α2-antiplasmin is the second major inhibitor of plasmin activity, which is synthesized in the liver and circulates in the blood [45]. In contrast to the indirect inhibition of plasmin by PAI1, α2-antiplasmin is a fast-acting and direct inhibitor of free plasmin [46]. Recently, *SPINT2*, encoding hepatocyte growth factor activator inhibitor 2 (HAI2), has been proposed to directly inhibit plasmin [14]. Accordingly, HAI2 has been found to suppress cell invasion and metastasis and low HAI2 expression has been linked to tumor progression [47-49].

Key components of the plasminogen activation system like plasminogen receptors and serine proteases are conserved among mammals and likely emerged from a common ancestor [50-55]. However, in chickens, the loss of a plasminogen receptor encoding gene has been reported and despite sharing a homology of 82 %, mouse and human PAI1 differ slightly in important features [56, 57]. PAI1 levels in mouse plasma and platelets are considerably lower than in humans and structural differences have been found concerning the α-helix and functional domains [58, 59]. Besides, additional proteinase inhibitors other than PAI1 seem to be of importance to inhibit tPA function in mice [60]. These differences could possibly affect targeting PAI1 in different species.

Ultimately, activation of the fibrinolytic system and its consequential proteolytic activity is tightly regulated and misregulation is associated with multiple pathological conditions. Bleeding disorders occur upon increased activity of plasminogen activators or deficiency of α2-antiplasmin and can be treated with

14

lysine analogues like epsilon aminocaproic acid or Tranexamic acid, which inhibit fibrinolysis by competitively inhibiting the binding of plasmin to fibrin [61, 62]. Since these drugs generally target fibrinolysis in the body, they are accompanied with severe side effects like thrombosis [63]. Thrombotic diseases are related to deficiency of plasminogen or plasminogen activators [64]. Therapy includes anticoagulants like heparins, vitamin K-antagonists or direct oral anticoagulants. Warfarin, a vitamin K-antagonist, reduces activity of Vitamin K, which is needed for generation of crucial proteins within the coagulation process, however correct dosing is complicated due to its interactions with other drugs or intake of particular food, thus risking severe side effects like bleeding [65]. Direct oral anticoagulants like rivaroxaban or apixaban directly target coagulation factors and present an alternative to vitamin K-antagonists, since they have less interactions with drugs or food and are safer to use due to the availability of specific antidotes in the case of severe side effects [66]. Usage of anticoagulants is however limited, since life threatening cases of thrombosis like clot formation in heart or lung arteries require thrombolysis. Thus, activating the fibrinolytic system is an established emergency treatment to prevent heart attacks or acute pulmonary embolisms. Prominent thrombolytic drugs induce plasminogen-to-plasmin conversion, including tPA, uPA or streptokinase [67]. However, correct dosage is difficult and side effects include life-threatening hemorrhage and neurotoxic effects, thus new treatments with less severe side effects are needed [68, 69]. Recently, inactivation of α2-antiplasmin has been shown to dissolve pulmonary blood clots in mice with lower bleeding risk compared to tPA, thus being proposed as treatment for pulmonary embolism [70].

Besides these implications in hemostasis, the fibrinolytic system is crucial in regulation of ECM and is thus strongly associated with tissue fibrosis, which is characterized by excessive accumulation of ECM proteins. Plasmin binds and digests fibronectin and collagen, which are major components of the ECM [71, 72]. An implication of PAI1 on the activation of the fibrinolytic system and subsequent modulation of ECM levels in lung fibrosis has been indicated in several studies [73-75]. For instance, Sisson et al suggested that PAI1-deficient mice showed reduced fibrosis due to the activity of the fibrinolytic system and showed that treatment of mice with uPA significantly ameliorated lung fibrosis [74]. Mice lacking PAI1 or mice

15

instilled with PAI1-siRNA have been shown to be protected from pulmonary fibrosis and increased PAI1 levels lead to accumulation of ECM components like collagen or fibronectin in mouse lungs [13, 73, 76].

Increased levels of PAI1 are associated with dermal fibrosis and PAI1 has been shown to regulate levels of collagens in skin fibroblasts [77, 78]. Further, PAI1 – deficient mice show reduced dermal fibrosis [79]. According to these findings, PAI1 deficiency is also correlated with reduced renal and kidney fibrosis [80, 81]. Thus, PAI1 seems a promising target to modulate activation of the fibrinolytic system in the context of fibrosis. Additionally, by degradation of ECM proteins, plasmin allows for cellular migration and invasion, thus high levels of plasmin are thought to be key drivers of migratory abilities in advanced stages of cancers [14, 82]. Thus, signaling pathways targeting the fibrinolytic system are suggested as tools for modulating ECM protein levels.

3.2   Pulmonary fibrosis

Pulmonary fibrosis (PF) belongs to the group of interstitial lung diseases (ILD), which describes rare and chronic diseases affecting the tissue surrounding alveoli, also known as pulmonary interstitium. The prevalence of interstitial lung diseases per 100,000 people is 6.3 to 71 and includes several subgroups of diseases [83]. Of these subgroups, idiopathic pulmonary fibrosis (IPF), referring to a disease progression without a known cause, is the most common one [84]. IPF has a prevalence per 10,000 of the population of 0.33 to 2.51 in Europe, and 2.40 to 2.98 in North America a median survival rate of 3-5 years after diagnosis [85]. Lung fibrosis in general is often diagnosed in late stages of the disease. Known causes of PF include occupational risks like inhalation of substances like asbestos, silica, vinyl chloride, nylon flock or metal dust [86-89]. Age is also a severe risk factor and several diseases are an additional risk to manifest in fibrosis, like pulmonary hypertension or cancer. Radiation and chemotherapy as well as cigarette smoke have been linked to pulmonary fibrosis and PF is indeed a common co-morbidity of lung cancer [90-92].

Just recently, pulmonary fibrosis has been proposed as long term consequence of the Covid-19 acute respiratory stress syndrome, thus the incidence of IPF might

further increase in the coming years [93-95]. George et al proposed drugs used for the treatment of idiopathic pulmonary fibrosis like pirfenidone as possibility to reduce development of severe Covid-19 cases [93].

Currently, therapy for ILDs includes immunosuppressants or systemic steroids [96]. These therapies are, however, only used in non-IPF ILDs, since the usage of immunosuppressants in IPF patients has been shown to aggravate the disease [97]. No efficient therapy for the treatment of IPF is available until now, and treatment of lung fibrosis mainly aims at easing symptoms by supplying oxygen. Two FDA (US food and drug administration) and EMA (European medicines agency) approved drugs are currently used: Nintedanib, a receptor tyrosine kinase inhibitor, and Pirfenidone, which inhibits TGF-β signaling [98, 99]. Of note, pirfenidone has recently been suggested as additional treatment strategy for non-IPF ILDs [100]. However, these drugs are only able to slow the progression of IPF, but not to stop or even cure the disease. As a consequence, lung transplantation remains as the only possibility to cure IPF, but it is rarely performed due to the limited availability of donor lungs and the low survival probability in patients as consequence of old age or comorbidities [99, 101]. Thus, new strategies for effective therapy of PF and IPF are needed, especially to achieve restoration of the affected tissue in late stages of the disease [102].

The main process responsible for the progression of pulmonary fibrosis is the misregulation of ECM. ECM remodeling during wound healing is crucial for proper function of the lung and fibroblasts are most abundant in wound healing. Fibroblasts are mesenchymal cells originating from embryonic mesoderm tissue. During wound healing, fibroblasts differentiate to myofibroblasts, which are able to migrate to the site of the injury and produce ECM components like fibronectin, collagen and elastin [103]. Once the injury is repaired, under physiological conditions, ECM production is stopped by apoptosis of myofibroblasts and proteolytic ECM degradation [104]. Misregulation of ECM remodeling often includes uncontrolled fibroblast to myofibroblast differentiation leading to excessive ECM accumulation, eventually resulting in scarring of tissue and fibrosis [105, 106]. In addition to resident fibroblasts, other cell types can also be transformed to fibroblasts by epithelial to mesenchymal transition (EMT). This process is

characterized by reduction of epithelial markers like E-cadherin and induction of mesenchymal markers like vimentin and α-smooth muscle actin (α-sma) [107].

Excessive ECM accumulation mostly affects the interstitial space in alveolar regions and results in a stiffening of the lung, accompanied by a reduction of total lung volume and reduced gas exchange. It is thus classified as restrictive lung disease [108]. Histochemical analysis of lung fibrosis often reveals "fibroblast foci", which are characteristic for pulmonary fibrosis. They describe an accumulation of fibroblasts, myofibroblasts and ECM and are regarded as main reasons for tissue destruction in fibrotic disease [105]. Studies revealed deposition of collagens and fibronectin at these sites, with collagen1 increasing in the progression of the disease and thus being a marker of late stages of fibrosis [109, 110]. It has been shown that not only the ECM but also fibroblasts themselves become stiff and less elastic in patients [111]. By increasing cellular migration and proliferation in areas with stiffer ECM, ECM proteins are highly involved in cellular features of fibroblasts and progression of the disease [112].

Inhibition of plasmin activation by PAI1 is initially required for wound healing to stop ECM degradation, however upregulation of PAI1 has been reported to lead to reduced ECM digestion and is regarded as marker of fibrotic tissues. Extensive amounts of ECM can thus be the consequence of increased ECM production as well as reduced degradation. As mentioned above, studies have shown that PAI1 deficiency can protect lungs from bleomycin-induced fibrosis and increased PAI1 levels have been associated with fibrosis [13, 79, 113, 114]. Thus, targeting PAI1 and consequently the activity of plasmin may be a promising approach to achieve tissue restoration in late stages of pulmonary fibrosis.

3.3   Lung carcinoma

With 11.4 % of total cancer cases and 18.0 % of total cancer deaths in 2020, lung cancer is the second-most frequent type of cancer and the leading cause of cancer-related deaths [115]. In 2018, survival of lung cancer patients 5 years after diagnosis was 10 % to 20 %, and prognosis is best upon diagnosis at early stages and surgical removal of cancerous tissues [116]. Unfortunately, no characteristic

early symptoms are defined and most patients with non-small cell lung cancer (NSCLC) are diagnosed at a late stage of disease, thus limiting treatment options to chemo- or radiotherapy [117]. Attributing for two-thirds of lung cancer deaths worldwide, the leading cause of lung cancer is tobacco smoking [118]. Of note, lung fibrosis increases the risk for developing lung cancer, but the mechanism of interaction between these two diseases remains unclear [119].

Lung cancers are divided into two main groups, small cell lung cancer and non-small cell lung cancer. With 80 to 85 %, NSCLC is the most common type and is classified in 3 groups: adenocarcinoma, squamous cell carcinoma and large cell carcinoma [120]. Adenocarcinoma is the most common type and affects the bronchioles, squamous cell carcinoma originates from squamous cells lining the lung surface and large cell carcinoma is the least common and is characterized by rapid growth [121].

Due to the lack of treatment options, novel therapeutic approaches including targeted therapies are needed, therefore it is crucial to understand cellular mechanisms and pathways contributing to tumor progression [118]. One successful example of targeted therapy that arose in the last years is targeting the epidermal growth factor receptor, which is often elevated in NSCLC. By inhibiting tyrosine kinase activity of epidermal growth factor receptor (EGFR) with the small molecule tyrosine kinase inhibitors gefitinib or erlotinib, downstream signaling pathways are blocked and survival of patients carrying EGFR mutations significantly improved [122, 123]. Similarly, mutations in the TGF-β receptor have been shown to increase invasiveness of tumor cells by enhancing SMAD signaling. With misregulated TGF-β-induced SMAD signaling being a prominent pathway in EMT of tumor cells, this work focuses on targeting the role of TGF-β in the progression of lung tumors at different stages.

The process of epithelial to mesenchymal transition is key in tumor progression and initiation of metastasis. During EMT, cancer cells lose their epithelial characteristics, e.g. downregulation of cell adhesion proteins like E-cadherin and loss of ECM proteins. Thus, cells acquire invasive properties and exhibit characteristics of mesenchymal cells like expression of N-cadherin or fibronectin [124, 125]. Besides EMT, degradation of ECM is crucial for tumor migration and

19

invasion. Fibronectin is a prominent member of ECM, but has also been reported as marker for EMT, thus studying fibronectin levels seems promising in this context [126, 127]. Degrading ECM proteins in the tumor environment is often triggered by TGF-β signaling and leads to reduced cell-cell-adhesions, thereby facilitating cellular migration [128]. Inhibition of plasmin activation and subsequent ECM degradation thus seems a logical possibility to inhibit tumor progression. However, PAI1 is a marker of migratory cells and thus correlated with poor prognosis in several cancers and PAI inhibitors are being researched as cancer therapy [129-131]. It has been shown to promote actin reorganization, which is essential for migration of cancer cells [132]. Besides, PAI1 promotes proliferation by inhibiting apoptosis of cancer cells [133]. PAI1 is a prominent target of TGF-β signaling, which will be highlighted in the following chapter.

3.4 Implications of transforming growth factor β in the regulation of extracellular matrix in pulmonary diseases

Extracellular matrix consists of various collagens, actins, proteoglycans and glycoproteins and provides elasticity, mechanical stability, tissue separation and intercellular communication [134]. Fibroblasts and macrophages migrating to the wound are the main producers of TGF-β and promote production of ECM at the site of the wound [135, 136]. Fibronectin, one of the key components of ECM, exists in a plasma form and in a cellular form. The plasma form is circulating in the blood and is accumulated into fibrin clots upon injuries. At the site of the injury, cellular fibronectin is then synthesized and aberrant synthesis of fibronectin leads to dysfunctional tissue repair and fibrosis [137]. In response to injuries, ECM is crucial for stimulating cell proliferation, differentiation or apoptosis and leads to more fibroblasts attaching to the ECM at the site of injury [138]. Cells bind to the ECM via focal adhesion to cellular actins. Cell adhesion is facilitated by integrins, which require binding to fibronectin of the ECM [139]. Loss of ECM and consequent intercellular adhesive connections results in reduced tissue integrity and polarity, thereby promoting cellular mobility and facilitating cell migration, which is especially important in the context of cancer. TGF-β signaling pathways e.g. via the small

G protein Ras homolog family member A (RhoA) are key in actin reorganization in the tumor cell environment and will be further explained in the following chapters

ECM can be divided into two layers: the basement membrane and the interstitial ECM. Basement membrane provides mechanical support and is located beneath the epithelium. Interstitial ECM is located in the lung parenchyma and thus affects gas exchange [140]. Several chronic diseases are correlated to an altered ECM composition, including asthma, chronic obstructive pulmonary disease, cancers and pulmonary fibrosis [30]. Regulation of ECM remodeling during wound healing is crucial for proper function of the lung and fibroblasts are most abundant in wound healing [108]. As stated above, key factor in the degradation of ECM is plasmin, which directly binds and digests fibronectin and collagens, leading to reduction of ECM protein levels [71, 72]. Besides, plasmin can also degrade ECM proteins indirectly by activation of matrix-metalloproteinases (MMPs), which is especially important in the degradation of collagens [134, 141, 142].

An important factor in the regulation of extracellular matrix is TGF-β, as increased levels of TGF-β are associated with aberrant regulation and consequent accumulation of ECM. TGF-β has been shown to directly induce expression of ECM components, however, it can also modulate ECM levels via interacting with the fibrinolytic system, thereby modulating the extent of ECM degradation. The mechanism by which TGF-β influences ECM proteins are discussed in detail in the following chapters.

3.4.1 Physiological roles of transforming growth factor β

Three isoforms of TGF-β (TGF-β1, 2 and 3) are expressed in mammalians, however TGF-β1 is most abundant, ubiquitously expressed and commonly associated with diseases [143-145]. Thus, for the sake of simplicity, TGF-β refers to TGF-β1 in this work.

TGF-β is involved in a variety of cellular processes like differentiation, proliferation, embryogenesis, migration, apoptosis and wound healing [146]. Due to its importance in crucial cellular processes, misregulation of TGF-β signaling is associated with various diseases like tissue fibrosis or tumor progression [144]. TGF-β signaling is essential for the immune system, as lack of TGF-β in mice is

lethal due to multiorgan inflammation [147]. This is due to its activating role for T-lymphocytes and T helper cells [148]. Besides, TGF-β inhibits proliferation of B lymphocytes and inhibits macrophage activity [149]. Misregulation of TGF-β conferred actions on components of the immune system is associated with autoimmune diseases like multiple sclerosis [150]. Under physiological conditions, TGF-β blocks progression of the cell cycle at G1 phase, thereby inducing apoptosis and reducing cell proliferation [151]. In malignant diseases, TGF-β signaling is often aberrant, leading to uncontrolled proliferation of cancer cells. Angiogenesis and invasion of cancer cells are also attributed to TGF-β. However, TGF-β exhibits both characteristics of tumor suppressor and tumor promoter, which will be discussed in more detail in chapter 3.4.4.

Further, cholesterol has been shown to decrease binding of TGF-β to its receptors, thereby increasing the risk for heart diseases like atherosclerosis [152-154]. TGF-β signaling via SMAD3 suppresses proliferation of pancreatic β-cells, therefore, it plays an important role in regulation of blood glucose levels and is associated with diabetes [155]. Dysfunctional TGF-β-signaling is also associated with neurodegeneration in Alzheimer's disease [156]

Mutations in the TGF-β receptors lead to the Loeys-Dietz syndrome, a rare autosomal dominant genetic disease, which is characterized by dysregulated connective tissue and increased risks for aneurysms [157].

With the lungs being especially exposed to external pathogens or toxins, TGF-β plays a crucial role in pulmonary inflammatory processes and cellular homeostasis. Infection with *Mycobacterium tuberculosis* results in increased TGF-β activity, leading to immune suppression within the lung and reducing TGF-β activity has emerged as therapy for tuberculosis [158]. Furthermore, TGF-β signaling is associated with pathogenesis of pulmonary emphysema, chronic obstructive pulmonary disease, asthma, lung fibrosis and lung carcinoma [159].

TGF-β confers its implications on various cellular and physiological roles via induction of the canonical SMAD pathway as well as several other pathways independent of SMAD proteins, which will be described in the following chapters.

3.4.2 Transforming growth factor β signaling pathways

3.4.2.1   SMAD-dependent signaling cascade

The TGF-β signaling cascade is initiated by binding of the TGF-β ligand to dimeric serine/threonine kinase TGF-β receptors, which consist of a transmembrane domain, a cysteine rich extracellular domain and a serine/threonine domain in the cytoplasm [144]. TGF-β initially binds the type II TGF-β-receptor, which phosphorylates serine residues of the type I TGF-β-receptor, leading to the formation of a tetrameric receptor-ligand complex [160, 161]. The activated type I TGF-β-receptor then confers downstream signaling via different pathways. The classical and most abundant pathway via SMAD proteins is illustrated in figure 2 [160].

The term SMAD stems from the discovery of *mother against decapentaplegic* (MAD) in *Drosophila melanogaster* and the protein SMA (small body size) in *Caenorhabditis elegans* [162, 163]. The human homologues were therefore named SMAD proteins [164]. SMADs are compromised of the n-terminal MH1 (Mad homology 1) domain required for DNA binding and nuclear translocation, a linker region and a c-terminal MH2 (Mad homology 2) domain required for binding to type I receptors and SMAD oligomerization. Mad homology domain 1 is highly conserved in R-SMADs and Co-SMADs whereas MH2 is highly conserved among all SMADs [165].

The eight vertebrate SMAD proteins are classified in three functional groups: SMAD4 is a co-mediator SMAD (Co-SMAD), SMAD6 and SMAD7 are inhibitory SMADs (I-SMADs) and the remaining SMADs are receptor-regulated SMADs (R-SMADs). SMAD2 and -3 are activated by TGF-β-receptor I-mediated phosphorylation. SMAD1, -5 and -8 are activated in response to signaling by bone morphogenetic proteins [165]. R-SMAD phosphorylation requires binding to the TGF-β-receptor-complex by the SMAD anchor for receptor activation (SARA) protein. Receptor-activated SMAD2 and SMAD3 proteins are phosphorylated at two serine residues (Ser465, Ser467) of the SSXS motif at the C-terminus and thereby form a heterotrimeric complex with SMAD4, leading to a translocation to the nucleus and transcriptional activity [166, 167]. I-SMADs have been shown to

bind to type I TGF-β-receptors via their MH2 domain and are thus competitive inhibitors of R-SMADs. I-SMADs also inhibit TGF-β signaling by competing SMAD4, thereby preventing nuclear translocation of the SMAD complex [168-171].

Despite being highly conserved, species specific differences in TGF-β-SMAD signaling have been reported [172]. Upon TGF-β stimulation, total SMAD3 protein levels are reduced in human lung fibroblast, whereas rat fibroblasts show increased SMAD3 levels, suggesting differences of TGF-β signaling in distinct species [173-175].

Of note, in contrast to carboxy - terminal phosphorylation, extracellular signal-regulated kinase 1/2 (ERK1/2)-mediated phosphorylation of the SMAD2 linker region at serines 245, 250 and 255 leads to inhibition of nuclear translocation and downstream signaling [176-178].

The SMAD signaling pathway is crucial for the regulation of ECM levels of cells. TGF-β-induced SMAD signaling regulates various genes, including the protein PAI1, which plays an essential part in the regulation of the fibrinolytic system. Via binding of SMAD3/4 to the promotor of the *SERPINE1* gene, PAI1 protein levels are enhanced, which reduces proteolytic activity of plasmin and reduces the degradation of ECM components [179-181]. Besides, SMAD3 directly induces transcription of collagen1 and fibronectin, leading to increased levels of ECM proteins [182-184]. Thus, two modes of action promote accumulation of ECM in fibrotic diseases by SMAD signaling.

In addition to the activation of the SMAD signaling cascade, TGF-β activates several distinct pathways that additionally contribute to cellular responses of TGF-β.
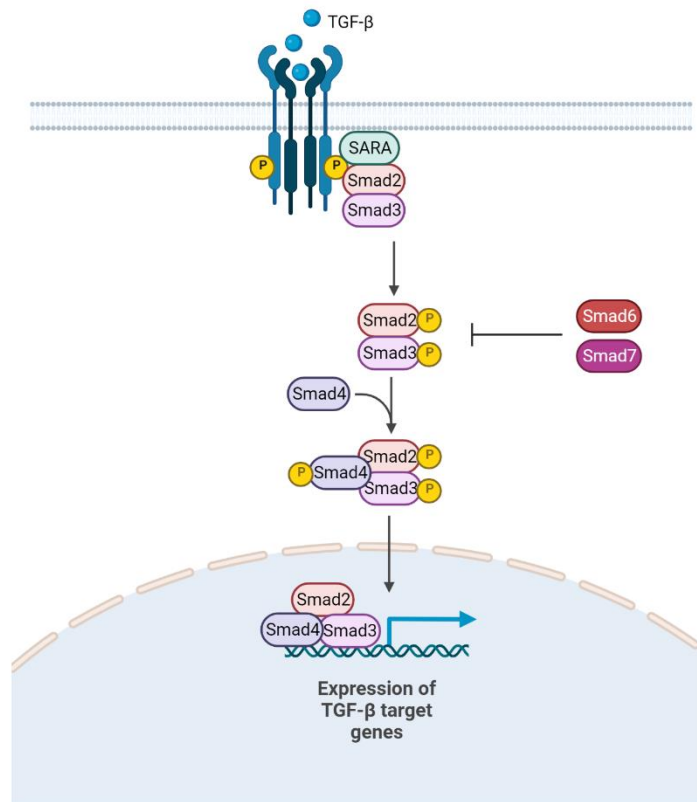
Figure 2: Overview of the TGF-β / SMAD signaling pathway

Binding of TGF-β to type II receptors leads to phosphorylation of type I receptors, resulting in a tetrameric receptor-ligand complex. The SMAD anchor for receptor activation (SARA) protein enables binding of SMAD2/3 to the receptor complex, leading to SMAD2/3 phosphorylation by type I TGF-β receptor. SMAD2/3 activation is inhibited by SMAD6 and SMAD7. Phosphorylated SMAD2/3 forms a complex with SMAD4, followed by translocation into the nucleus and downstream signaling.

3.4.2.2   SMAD-independent signaling pathways

In addition to the SMAD signaling pathway, TGF-β activates multiple other signaling pathways independent of SMAD proteins, some of which have been proposed to play crucial roles in various diseases. Activation of different signaling molecules by TGF-β can additionally lead to a crosstalk with the SMAD signaling pathway to modulate cellular responses. The major SMAD-independent TGF-β signaling pathways involve Rho-GTPases, mitogen activated protein kinases (MAPK) and YAP/TAZ signaling pathways. The cellular mechanisms underlying SMAD-independent TGF-β signaling will be highlighted in the following chapters.

3.4.2.2.1   Rho-GTPase signaling pathways

The Rho family of GTPases are small G proteins and prominent members include RhoA, Rac and Cdc42. Their activation is associated with malignant diseases due to their importance in the organization of the cytoskeleton and cell motility [185]. Rho GTPases exist as active form when bound to guanosine triphosphate (GTP) or inactive when bound to guanosine diphosphate (GDP). Activation of Rho GTPases requires the exchange of GDP to GTP, which is catalyzed by guanine nucleotide exchange factors (GEFs) [186]. Intrinsic GTPase activity of Rho GTPases leads to inactivation via hydrolization of GTP to GDP, which is supported by GTPase activating enzymes.

TGF-β-induced activation of RhoA has not been studied in depth, but signaling via activated type I TGF-β receptor has been suggested. [187, 188]. Interestingly, TGF-β has been suggested to induce expression of nuclear RhoA exchange factor, a GEF specifically targeting RhoA [189, 190]. RhoA leads to activation of Rho-associated kinase (ROCK), which has been related to mobilization of actin cytoskeleton leading to tumor cell invasion and metastasis in various types of cancer [191]. However, reduction of RhoA protein levels after TGF-β stimulation have also been reported. TGF-β-receptor-induced phosphorylation of the protein Par6 leads to recruitment of Smurf1 and subsequently leads to ubiquitination and degradation of RhoA [192, 193]. This process was reported to dissolve tight junctions, thereby enhancing EMT. Thus, TGF-β likely regulates RhoA activity via different modes of action [194].

ROCK signaling has been implicated in both cancer and fibrotic diseases. Loss of the tumor suppressor DLC1 (deleted in liver cancer 1) leads to hyperactivation of RhoA and downregulation of DLC1 is commonly found in tumor patients [195]. Activation of ROCK has been shown to promote myocardial fibrosis [196, 197]. Interestingly, a crosstalk between RhoA- and SMAD-signaling has been proposed: RhoA promotes SMAD signaling and is required for TGF-β/SMAD-induced differentiation of human embryonic lung fibroblast cell line WI-38 [198, 199]. It has been proposed that activation of RhoA signaling leads to reduced levels of the SMAD2/3 phosphatase PPM1A (protein phosphatase, Mg^{2+}/Mn^{2+} dependent 1A), thereby increasing levels of phosphorylated SMAD2/3 [200, 201]. Further, TGF-β-induced SMAD3 activation leads to activation of RhoA via directly targeting the *NET1* gene, which encodes a GEF, leading to consequent actin reorganization and EMT induction in human retinal epithelial cells [190].

3.4.2.2.2 Mitogen activated protein kinase pathways

Several important pathways activated by TGF-β are dependent on MAP kinases and according to this, TGF-β has been shown to activate MAP kinases like c-Jun amino terminal kinases (JNK), ERK1/2 or p38 in different cell lines [202-205]. MAP kinase kinase kinases (MAP3K) activate MAP kinase kinases (MAP2K) by phosphorylation of serine/threonine residues. MAP2K then activate MAPK like ERK1/2 or JNK. Accordingly, TGF-β-signaling via mitogen activated protein kinases like ERK1/2 or JNK is associated with fibrotic diseases [206-209].

TGF-β triggers activation of TGF-β-activated kinase 1 (TAK1), an upstream MAP3K that further activates several signaling cascades. TAK1 activation follows a distinct mode of action compared to SMAD activation: TGF-β-induced activation of TAK1 is independent of kinase activity of the type I TGF-β-receptor. In the absence of TGF-β, TAK1 is associated with the type I TGF-β-receptor and inactive. Stimulation with TGF-β and consequent receptor-complex formation leads to the dissociation of TAK1 from the receptor and its activation by autophosphorylation [210, 211]. TAK1 then phosphorylates a number of downstream signaling targets, like JNK, ERK1/2 or p38 MAPK [210, 212, 213]. While TGF-β-induced TAK1 signaling is generally considered as a SMAD-independent pathway, a crosstalk between these pathways is not excluded, e.g. in renal fibrosis, JNK signaling

directly phosphorylates SMAD3 [214]. Besides, TAK1 has been reported to induce expression of SMAD7, thereby inhibiting the SMAD pathway [215]. Interestingly, TAK1/JNK signaling has been reported to promote renal fibrosis and inflammation and leads to fibronectin expression in NIH3T3 embryonic fibroblasts [214, 216, 217].

As an important member of MAPK signaling pathways, the MEK/ERK1/2 pathway is dependent on TGF-β signaling. First evidence that TGF-β activates ERK1/2 signaling was found by Mulder et al, who observed activation of Ras, leading to ERK1/2 activation in rat epithelial cells [218]. Although TGF-β-receptors are classified as serine/threonine kinases, the type II TGF-β-receptor shows autophosphorylation at tyrosines, however at a much lower level than at serines and threonines [219]. Further, TGF-β has been shown to phosphorylate tyrosines of the type I TGF-β-receptor. Active type I TGF-β-receptor can phosphorylate serine and tyrosine residues of the ShcA adaptor protein [220]. Phosphorylated tyrosines of ShcA act as binding sites for proteins with a Src homology 2 domain like growth factor receptor bound protein 2 (Grb2) [221, 222]. Binding of GrB2 results in recruitment of the guanine exchange factor Son of Sevenless via Ras [223]. Activation of Ras by TGF-β requires the exchange of GDP to GTP by Son of Sevenless. GTP-bound Ras then recruits the MAP3K Raf, leading to activation of the MAP2K MAPK/ERK1/2 kinase (MEK)1/2 and subsequent ERK1/2 activation [218, 224].

TGF-β-induced activation of ERK1/2 has been reported in several cell types, including lung and breast cancer cells and fibroblasts [225-228]. It is especially important in TGF-β-mediated EMT, by dissolving tight junctions and promoting cellular mobility [229]. Accordingly, ERK1/2 activity is required for proliferation of NIH3T3 mouse embryonic fibroblasts [208]. ERK1/2 inhibition has been shown to decrease EMT in pulmonary fibrosis [230]. In breast cancer cells, ERK1/2 promotes TGF-β-induced EGFR expression associated with cancer progression [209]. Increased levels of phosphorylated ERK1/2 are associated with poor survival and late stages of NSCLC [227]. Interestingly, Ras-induced MAPK pathway targets SMAD signaling via inactivation of SMAD2, thus further implicating a crosstalk between these pathways [177]. Importantly, ERK1/2 is required to induce activator

protein 1 (AP-1), which has been reported to contribute to proliferation of cancer cells and to induce expression of PAI1 [231, 232]. AP-1 is a heterodimer formed of two proteins: c-Jun, which is activated by JNK signaling, and c-Fos, which is activated by ERK1/2 signaling [233-235].

3.4.2.2.3   YAP/TAZ signaling pathways

The Hippo signaling pathway is crucial for organ growth by controlling proliferation and apoptosis of cells and was originally discovered as tumor suppressor in Drosophila [236, 237]. The mammalian Hippo pathway includes mammalian sterile 20-like kinase 1/2 (MST1/2), which phosphorylate large tumor suppressor kinase 1/2 (LATS1/2) [238]. Active LATS1/2 phosphorylates serine residues of the Yes-associated protein (YAP) and the WW domain-containing protein (TAZ). YAP/TAZ are normally located in the nucleus, acting as transcriptional coactivator for TEAD (TEA domain family member) or SMAD transcription factors [239, 240]. Phosphorylated YAP/TAZ, however, interacts with 14-3-3, which prevents translocation to the nucleus and subsequent transcriptional activity [241].

YAP/TAZ signaling has been shown to drive the expression of several profibrotic and EMT-promoting genes like *COL1A1* (collagen1), *ACTA2* (α-sma) and *SERPINE1* (PAI1), thus YAP/TAZ has been associated with promoting EMT in cancer cells and ECM stiffness in lung fibroblasts [241-244]. Of note, *COL1A1* and *SERPINE1* promoters contain binding sites for AP-1, which is activated by YAP/TAZ signaling [245, 246].

Importantly, YAP/TAZ act as mechanosensors and mechanotransducers (Calvo et al. 2013, Liu et al. 2015). Accordingly, TGF-β induced RhoA signaling is key in actin polymerization and YAP/TAZ are activated in response to actin remodeling [247, 248]. Protease-activated receptors (PARs) have been shown to inhibit LATS1/2 kinase function via Rho GTPases, thereby dephosphorylating YAP/TAZ and promoting activity in the nucleus, however the mechanism by which Rho inhibits LATS1/2 needs to be clarified [249, 250]. Further, TGF-β has been shown to activate YAP/TAZ via ERK1/2 and RhoA led to a dephosphorylation and consequent activation of YAP/TAZ, presumably via LATS1/2 modulation, however the exact mechanisms remain unclear [251, 252].

In summary, YAP/TAZ are associated with the promotion of tissue fibrosis and tumor progression [253]. YAP/TAZ act upon stiffening of ECM in fibroblasts and promote the production of fibrotic proteins, thereby driving fibroblast differentiation [254, 255]. Similarly, polarity changes in epithelial cells during EMT induce YAP/TAZ, leading to further promotion of EMT [256]. Accordingly, YAP/TAZ has been suggested as the mechanism linking fibrosis and cancer, since each of the diseases increases the risk to develop the other. By sensing cellular mechanical changes during EMT or fibrosis, YAP/TAZ signaling promotes fibroblast activation or tumorigenesis, respectively [253]. In dermal fibroblasts, YAP/TAZ regulates SMAD signaling by inducing the inhibitory SMAD7 via AP-1 [257]. YAP/TAZ is highly expressed in fibroblast nuclei from PF patients [242, 243]. In NSCLC, elevated YAP/TAZ expression is associated with poor prognosis and increased lymph node metastasis [258].

3.4.3 Transforming growth factor β signaling in fibrosis

TGF-β is released by immune cells at the site of an injury and TGF-β-signaling via SMAD proteins is the main driver of fibroblast to myofibroblast differentiation. Accordingly, increased TGF-β levels are found in IPF patients and targeting TGF-β-signaling became a focus of fibrosis research [259]. TGF-β/SMAD signaling leads to enhanced PAI1 expression, which is correlated with reduced proteolytic activity of the fibrinolytic system and enhanced levels of ECM.

As stated earlier, TGF-β/SMAD signaling can enhance ECM production relevant for tissue fibrosis via two different pathways: Firstly, SMAD proteins are known to directly induce transcription of fibronectin and collagens [183, 260]. Secondly, SMAD signaling can indirectly affect ECM levels via modulation of PAI1 levels and activity of the plasmin system [180, 181]. Targeting the latter would be especially important in late stages of fibrosis and could even lead to tissue repair by degradation of ECM [102].

TGF-β signaling leads to binding of SMAD3 and SMAD4 to CAGA boxes within the human *SERPINE1* (PAI1) promoter. These SMAD3/4 binding sites are essential for TGF-β-mediated PAI1 induction [179]. Importantly, AP-1 can also bind to the human PAI1 promoter to induce transcriptional activity [245, 261, 262]. It has

recently been reported that YAP/TAZ promotes transcription of c-Fos in cancer cells, thereby contributing to induction of AP-1 and proliferation [232].

The anti-fibrotic agent pirfenidone inhibits TGF-β signaling by preventing nuclear translocation of phosphorylated SMAD2/3, resulting in reduced collagen levels and fibroblast proliferation [263-266]. As mentioned before, SMAD signaling could directly induce expression of collagens or reduce their degradation via PAI1. Pirfenidone has been shown to reduce mRNA levels of collagen1, thus likely acting on direct effects on collagen expression conferred by SMAD signaling [263]. However, therapeutic success with pirfenidone is limited and late stages of IPF, that would require restoration of the affected tissue and degradation of excessive ECM, remain pharmacologically incurable. Recently, MMPs have come to focus as treatment option for IPF due to their involvement in ECM degradation [267]. The MMP inhibitor doxycycline significantly improved quality of life and survival in IPF patients to a certain extent [268, 269]. But according to a meta-analysis of randomized controlled trials, MMP inhibitors should not be recommended, since they did not significantly improve mortality, but had an increased risk for severe side effects, in particular gastrointestinal toxicity [270]. Researchers in the field of pulmonary fibrosis suggest that targeting specific parts of profibrotic pathways is insufficient and does not do justice to the complexity of the disease. Thus, new therapeutic approaches are needed, specifically for achieving restoration of the affected tissue [102, 271]. Targeting ECM degradation via the fibrinolytic system therefore seems a promising approach.

3.4.4 Transforming growth factor β signaling in lung carcinoma

The role of TGF-β in tumor cells is complex and depends on the stage of carcinogenesis. While TGF-β acts as tumor suppressor in early-stage tumors, it promotes tumor progression and metastasis in later stages. This dual role of TGF-β is often referred to as the "TGF-β-paradox" [272-274]. Accordingly, high levels of TGF-β are correlated with advanced stages of the disease, lymph node metastasis and lower survival [275, 276].

Inhibition of TGF-β signaling in late tumor stages is investigated as possible treatment strategy [277-279]. TGF-β induces EMT via SMAD-dependent and

SMAD-independent pathways like RhoA, ERK1/2 or PI3K/Akt [280-283]. Importantly, EMT induced by TGF-β has been achieved in the human lung tumor cell line A549 after 48 h stimulation [284].

Besides the induction of EMT, TGF-β signaling can contribute to the pathogenesis of lung cancer by targeting the ECM proteins in the tumor microenvironment via regulation of plasmin activity. Degradation of ECM proteins leads to reduced cell-adhesion, thereby facilitating cell invasion and metastasis [128]. Targeting the plasmin activation system has previously been proposed as potential drug target for cancer therapy [36]. Accordingly, enhanced activation of the plasmin system is associated with increased invasion and proliferation of tumor cells and increased levels of uPA, uPAR and decreased PAI1 expression are well established biomarkers for cancer [285, 286]. Despite linking the plasmin activation system to increased metastasis and progression in a variety of cancer types, plasmin activity has rarely been measured directly [14, 287-290].

In this work, two distinct lung tumor cells originating from lung epithelial cells are used, which exhibit differences in several crucial cellular characteristics. A549 cells were isolated from a primary tumor and therefore represent early stage, stationary tumor cells [291]. In contrast, H1299 cells derived from a lymph node metastasis of a lung tumor and thus represent late-stage, invasive tumor cells [292]. Indeed, a previous work suggested that invasive H1299 cells exhibit higher plasmin activity than non-invasive A549 cells [14]. An indirect correlation between plasmin activity and metastatic activity has also been found, since A549 cells express higher levels of the plasmin inhibitor HAI2 than H1299 cells [14]. In accordance with this finding, high expression levels of the inhibitory SMAD6 have been reported in H1299 cells, which could account for an inhibition of TGF-β-induced SMAD signaling and consequent decrease in PAI1 levels [293]. Further, A549 show no expression of DLC1 in contrast to H1299 cells, thus an increase in ROCK activity is assumed in A549 cells [294]. ROCK activity has been shown to induce YAP/TAZ signaling and consequent AP-1 activation. The *SERPINE1* promoter contains an AP-1 binding site, thus AP-1 induction leads to expression of PAI1 [245, 295]. Besides, A549 and H1299 cells differ in the activity of the MEK/ERK1/2 signaling. Mutations in the proto-oncogene Ras are commonly found in NSCLC, predominantly mutations in

K-ras, but to a lesser extent also in N-ras and H-ras [296]. The cell lines used in this work both carry a Ras-Mutation, A549 cells carry a mutation in K-ras, which leads to increased activation of the MEK/ERK1/2 signaling pathway [297, 298]. Similarly, H1299 carry a mutation in N-ras, also leading to a possible activation of ERK1/2 signaling [299-301].

Differences in the oncogenic phenotype between K-ras and N-ras mutations have been reported in colon cancer as well as in melanoma, thus the mutations might be of distinct importance in different tumor cells [302, 303]. MEK/ERK1/2 signaling has been shown to interact with TGF-β signaling and the plasmin system: TGF-β-induced PAI1 expression was dependent on ERK1/2 activity in vascular smooth muscle cells [304]. Interestingly, ERK1/2 signaling has previously been linked to the YAP/TAZ signaling pathway and SMAD signaling in lung cells. In human NSCLC cells, inhibition of ERK1/2 led to a down-regulation of the YAP/TAZ signaling pathway [252]. Thus, ERK1/2 signaling promotes formation of AP-1 via induction of cFos as well as via YAP/TAZ signaling, thereby further suggesting enhanced PAI1 expression in A549 cells [233].

In summary, these pathways support the assumption that the metastatic tumor cell line H1299 exhibits increased plasmin activity due to lower PAI1 levels compared to the stationary tumor cell line A549 and an overview of the contributing pathways is shown in figure 3.
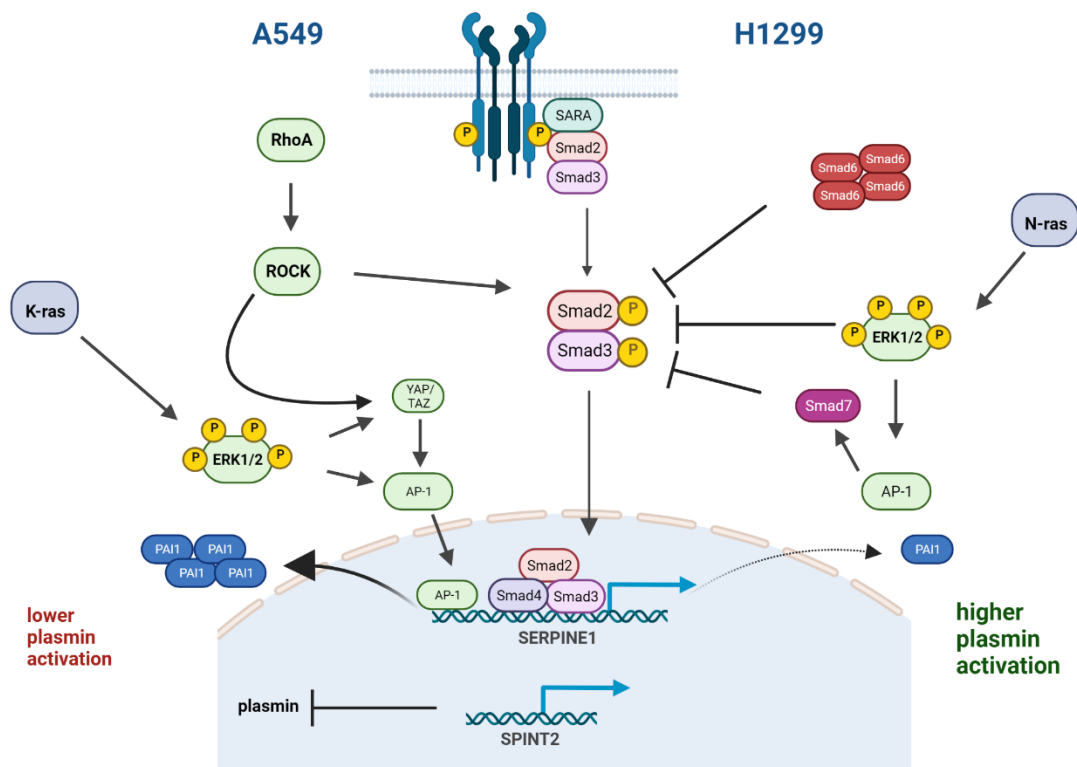
Figure 3: Summary of pathways supporting increased plasmin activity postulated for H1299 cells.

Increased levels of RhoA/ROCK and ERK1/2 signaling in A549 cells lead to induction of YAP/TAZ and consequently of AP-1. ERK1/2 additionally induces AP-1 via c-Fos. The *SERPINE1* promoter contains an AP-1 binding site, thus leading to increased PAI levels and lower plasmin activity in these cells. H1299 highly express SMAD6, which inhibits SMAD2/3 activation and leads to reduced PAI1 levels, thus suggesting an increased plasmin activity in H1299 cells.

Despite these findings, several pathways have been described that speak against an increase in plasmin activity in H1299 cells and a summary is shown in figure 4. TGF-β-induced upregulation of PAI1 and uPA is dependent on SMAD2 and MEK/ERK1/2 signaling in dental pulp cells and in stem cells from the apical papilla [305, 306]. Indeed, increased Ras signaling and consequent ERK1/2 activation led to an inhibition of TGF-β-induced SMAD signaling by phosphorylating SMAD2 and SMAD3 at specific sites in their linker regions, thereby inhibiting translocation to

34

the nucleus [177]. Thus, increased ERK1/2 activity in A549 may lead to reduced PAI1 expression and consequently increased plasmin activity. Further, both ROCK signaling and ERK1/2 signaling lead to activation of YAP/TAZ and consequent AP-1 formation as stated above. AP-1 leads to production of the inhibitory SMAD7, thereby reducing SMAD activity and PAI1 expression [257]. Thus, increased activity of ROCK and ERK1/2 in A549 cells suggest lower levels of PAI1 and consequently higher plasmin activity compared to H1299.

Thus, TGF-β-signaling via distinct pathways seems of utmost importance in the pathogenesis of malignancies, however the role of TGF-β-signaling on PAI1 is not clear. Also, despite its crucial role in cell migration leading to progression of the disease, plasmin activity of lung cancer cells has rarely been studied and interactions with TGF-β signaling in different stages of the disease need to be studied further.
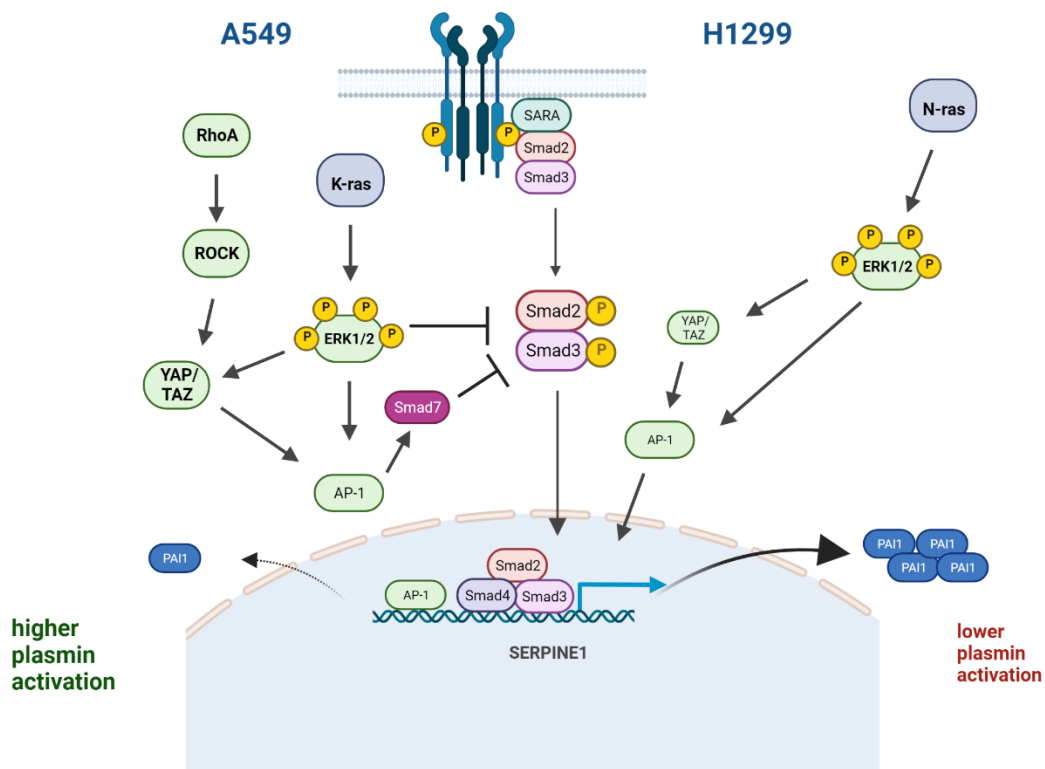
Figure 4. Summary of pathways conflicting with the increased plasmin activity postulated for H1299 cells.

Increased RhoA/ROCK and ERK1/2 activity in A549 cells leads to induction of AP-1 via YAP/TAZ. AP-1 activates the inhibitory SMAD7, thereby decreasing SMAD2/3 activity. Additionally, increased ERK1/2 activity in A549 cells leads to phosphorylation of linker regions of SMAD2/3, thereby inhibiting translocation to the nucleus. Thus, reduced activity of SMAD2/3 in A549 cells suggested, followed by decreased PAI1 expression and ultimately increased plasmin activity.

3.5 Transient receptor potential cation channel, subfamily M, member 7 (TRPM7)

3.5.1 Structure and function

The first transient receptor potential (TRP) protein was found in photo receptor cells of *Drosophila melanogaster* in 1989 and has soon been identified as cation channel [307]. The name transient stems from the response to a continuous light stimulus from *Drosophila melanogaster* carrying a trp mutation, which was short or transient rather than continuous as observed in the wildtype flies [307, 308]. Today, 27 human TRP channels are categorized in seven subfamilies based on their amino acid sequence: TRPC (canonical), TRPV (vanilloid), TRPA (ankyrin), TRPM (melastatin), TRPN (no mechanoreceptor potential C), TRPP (polycystin) and TRPML (mucolipin). An eighth subfamily, TRPY (yeast), includes TRP channels found in yeast [309, 310].

All TRP channels consist of six transmembrane segments with a channel pore between the transmembrane segments 5 and 6 and cytosolic N- and C-termini and can be found as either homo- or hetero-tetramers [310]. TRP channels are multifunctional proteins with crucial implications for cellular physiology and have thus been associated with multiple pathological conditions. As a result, TRP channels are being researched as potential drug targets in several diseases [311].

The melastatin-related transient receptor potential cation channel subfamily consists of eight members (TRPM1-8), which display distinct expression patterns and ion selectivity. Among them, TRPM2, TRPM6 and TRPM7 are bifunctional proteins which contain, in addition, a c-terminal domain with enzymatic activity fused to the transmembrane segments, thus being referred to as chanzymes [309, 312]. TRPM2 contains an ADP-ribose phosphatase domain and is mostly expressed in the brain tissue, while TRPM6 and TRPM7 contain a serine/threonine kinase domain and are linked to cellular magnesium homeostasis.

TRPM6 and TRPM7 share a sequence homology of around 50 %, both are divalent cation channels and are regulated by intracellular Mg^{2+} and phosphatidylinositol 4,5-biphosphate levels [309]. Importantly, TRPM6 is highly expressed in the

intestine and in the kidney and thus considered of great importance in these tissues [310]. TRPM7 on the other hand is ubiquitously expressed and important for cellular processes like cell proliferation, proliferation or apoptosis [313].

The human *TRPM7* gene encodes a 220 kilo dalton (kDA) protein with 1,865 amino acids. TRPM7 orthologues have been found in mouse, rat, chimpanzee, cow, and dog as well as in zebrafish [314]. As stated above, TRPM7 is ubiquitously expressed, however the highest mRNA expression in humans is found in the heart, bone and adipose tissue, whereas in the mouse, it is highly expressed in intestine, kidney, lung and brain [315, 316]. TRPM7 is fundamental for cell survival and activity due to its regulation of uptake of divalent cations like Mg^{2+}, Zn^{2+} and Ca^{2+}. Knockout of TRPM7 in mice is thus lethal in early embryonic stages [317].The role of the TRPM7 kinase domain is not well understood and while it is not necessary for channel function, it is believed to regulate sensitivity towards intracellular Mg^{2+} [318-320].

Due to its importance in multiple cellular processes, pharmacological tools for selective inhibition of TRPM7 are needed. Several compounds have initially been used to inhibit TRPM7, however they were rather unspecific channel inhibitors like Gd^{3+} or 2-APB, thus selective blockade of TRPM7 remained unachieved [321, 322]. Only later, when specific blockers like Waixenicin A and NS8593 were discovered, selective targeting of TRPM7 became possible [323-325].

Both NS8593 and Waixenicin A were used in this work. The small molecule NS8593 blocks TRPM7 channel function with an IC_{50} value of ~1.6 µM under Mg^{2+}-free conditions [325]. Importantly, NS8593 has also been reported as blocker of small conductance Ca^{2+} -activated K^+ (SK) channels. NS8593 blocks SK channels with an IC_{50} value of ~90 nM, thus the selective SK blocker apamin was used as control in this work [325, 326]. Waixenicin A, a diterpenoid from the soft coral *Sarcothelia edmondsoni*, blocks TRPM7 channel function with an IC_{50} value of ~7 µM in Mg^{2+}-free conditions [323]. So far, no off targets for Waixenicin A have been published. Using these blockers, implications of TRPM7 in cell cycle regulation, hypertension, immune cell signaling, fibrosis and cancer have been reported.

Selectively targeting TRPM7 channel or kinase function may give further insights into the cellular implications of TRPM7. TG100-115 is the only compound available

that has been proposed to selectively inhibit TRPM7 kinase but not channel function [327]. However, selective inhibition of TRPM7 kinase remains questionable since it was initially introduced as inhibitor of phosphoinositide 3-kinase isoforms gamma and delta [328]. Thus, so far, no pharmacological tools are available to specifically target kinase or channel function. Consequently, usage of TRPM7 blockers leads to blockade of both TRPM7 functions. Therefore, data indicating specific effects of the TRPM7 kinase on cellular signaling have solely be based on genetic approaches using modified mouse models (TRPM7-K1646R mice), in which TRPM7 kinase activity has been inhibited by replacing lysine at position 1646 by an arginine [329]. Interestingly, using these mice, it was shown that TRPM7 kinase interacts with the TGF-β/SMAD signaling pathway in T-cells via direct phosphorylation of SMAD2 at Ser465/467 [329]. As TGF-β signaling via SMAD proteins is of utmost importance in the progression of tissue fibrosis and malignant diseases, this work hypothesized a role of TRPM7 on SMAD signaling and cellular markers of the diseases in pulmonary fibroblasts and lung cancer cells.

3.5.2 Role of TRPM7 in fibrosis

Several implications of TRPM7 in fibrotic diseases have been reported, e.g. elevated TRPM7 activity has recently been reported to support cardiac and kidney fibrosis [312, 330, 331].

In cardiac fibroblasts, TRPM7 led to enhanced proliferation and differentiation, accompanied by an increase in ECM production, thus TRPM7 has been proposed as potential target for therapy of cardiac fibrosis [330, 332]. Mice with a truncated TRPM7 kinase-domain mice showed cardiac fibrosis, inflammation and increased SMAD3 signaling [312].

Interestingly, TRPM7 mediated Ca^{2+} levels have been reported to support TGF-β-signaling and contribute to atrial fibroblast differentiation, whereas TRPM7 mediated Mg^{2+} signals protect against cardiovascular fibrosis [312, 330]. Additionally, TRPM7 regulates the differentiation of the fetal human lung fibroblast cell line MRC5 via PI3K/Akt (Phosphoinositide 3-kinase/ protein kinase B) signaling. In these cells, downregulation of TRPM7 led to reduction of TGF-β-induced collagen expression [333].

As mentioned above, TRPM7 kinase has been reported to interact with TGF-β/SMAD signaling by directly phosphorylating SMAD2 in T-lymphocytes [329]. In fibrotic kidneys, TRPM7 expression is elevated and blockade of TRPM7 reduced cell proliferation and TGF-β/SMAD signaling in these cells [331]. Further evidence that TRPM7 might affect SMAD signaling in the context of fibrosis has been reported in liver myofibroblasts, where blockade of TRPM7 reduced TGF-β/SMAD signaling and expression of myofibroblast markers collagen1 and α-SMA [334].

Interestingly, Yu et al. stated that TRPM7 blockade with Gd^{3+} or 2-APB decreased proliferation and differentiation of the MRC5 lung fibroblast cell line, thus linking TRPM7 to pulmonary fibrosis [333]. However, the blockers used in this study are not generally used as specific TRPM7 blockers and specific TRPM7 blockers like NS8593 were not yet described. Of note, it has been proposed that 2-APB does not directly inhibit TRPM7 channels [335]. Further, Gd^{3+} has been reported to inhibit calcium release-activated calcium channels, but not TRPM7 [336, 337]. Thus, besides substantial evidence for the implication of TRPM7 in fibrotic diseases, cellular mechanisms underlying this interaction remain unclarified. Of note, no data at all are available demonstrating effects of TRPM7 on pulmonary fibrosis.

3.5.3 Role of TRPM7 in lung tumor

TRPM7 is a key driver of cell proliferation and is thus linked to cancer. Indeed, increased TRPM7 activity has been associated with invasion, migration, proliferation and EMT of several tumor types [338-341]. Blockade of TRPM7 has been reported to inhibit cell proliferation, thus making it a promising therapeutic target for malignant diseases [324, 342]. Of note, blockade of TRPM7 by NS8593 *in vitro* and *in vivo* induced senescence of hepatocellular carcinoma cells [343]. Blockade of TRPM7 kinase was reported to reduce migration of breast cancer cells, however, involvement of TRPM7 kinase remains questionable due to the usage of the rather unspecific blocker TG100-115 in this study [327].

Besides its ability to influence signaling pathways like the above-mentioned SMAD signaling pathway via its kinase domain, TRPM7 influences cellular processes via

regulation of intracellular Ca^{2+}-levels. Misregulation of calcium signaling leading to aberrant cell proliferation has often been linked to tumorigenesis, especially in the lung [344, 345]. Enhanced expression of TRPM7 has been reported in several types of lung cancer cells, including squamous, large-cell and non-small-cell lung tumor cells [345]. In line with these findings, database analysis revealed a correlation of high TRPM7 expression, high metastasis levels and lower survival rates of patients [344]. Accordingly, upregulation of TRPM7 upon EGF (epidermal growth factor) stimulation was reported to increase migration of A549 cells [346]. Thus, TRPM7 emerged as a promising target for lung cancer therapy.

3.5.4 Implications of TRPM7 on the fibrinolytic system

Despite the importance of the plasmin system as well as of TRPM7 on cellular processes like proliferation and migration, interactions of these two have rarely been studied. Liu et al reported that TRPM7 silencing suppresses EMT in lung cancer cells and propose Waixenicin A as antitumor drug through its ability to inhibit the plasminogen activator uPA [345]. Similarly, TRPM7 has been reported to regulate invasion of pancreatic cancer cells via activation of uPA [347]. Apart from these two publications, no implications of TRPM7 on the plasmin activation system have been reported yet. Most importantly, plasmin activity has rarely been measured directly. However, the previously described reduction of collagen1 expression in MRC5 cells after TRPM7-downregulation strongly suggest an involvement of the plasmin system, since collagen is a major substrate of active plasmin.

Thus, studying the role of TRPM7 on the plasmin activation system seemed a promising approach in the context of lung fibrosis and tumor.

41

3.6   Aim of study

Regulation of plasmin activity within the fibrinolytic system is crucial for EMT remodeling and misregulation has been linked to tissue fibrosis and tumor progression. In spite of its critical importance, plasmin activity has rarely been measured directly. Instead, levels of components of the fibrinolytic system like uPA or PAI1 have been measured and an assumption on plasmin activity has been made. Thus, the first aim was to establish a protocol for reliable measurements of plasmin activity in lung cells.

TGF-β signaling via SMAD proteins is crucial in the development of fibrosis and cancer. By inducing expression of PAI1, SMAD signaling was hypothesized to modulate plasmin activity in lung cells. Second aim of this project was thus to monitor the effects of TGF-β on SMAD activation, plasmin activity and migration in pHPF and lung cancer cells. Due to its bi-functional effects on tumor progression depending on the stage of the disease, effects of TGF-β were compared in early (A549) and late (H1299) stage lung cancer cells. Modulation of plasmin activity is key in targeting ECM remodeling. Due to its ability to phosphorylate SMAD2 in T-lymphocytes, an interaction of TRPM7 and the fibrinolytic system has been hypothesized. Thus, this project further aimed at analyzing the consequences of TRPM7 blockade on plasmin activity in pHPF and lung cancer cells.

While a reduction of ECM after TRPM7 blockade has been suggested in MRC5 cells, no such effects have been reported for primary human fibroblasts yet. Hence, the third aim was to establish TGF-β-induced fibroblast to myofibroblast differentiation of pHPF and analyze effects of TRPM7 blockade. To assess whether TRPM7 kinase or channel function are involved in the regulation of the fibrinolytic system, this project aimed at analyzing genetically modified mice with eliminated TRPM7 kinase activity. Similarly, analysis of an interaction of TRPM7 activity and TGF-β-induced EMT of lung cancer cells was intended. Ultimately, this project aimed at analyzing a potential role of TRPM7 in regulating TGF-β signaling, plasmin activity and ECM levels on a cellular level in the context of pulmonary fibrosis and lung cancer.

4. Materials

4.1 Instruments

Instrument	Manufacturer
Cell culture incubator PHCbi	PHC, Etten-Leur
Centrifuge Heraeus Biofuge Stratos	ThermoFisher, Waltham
Centrifuge Heraeus Fresco21	ThermoFisher, Waltham
Centrifuge Labofuge 400	ThermoFisher, Waltham
ChemiSmart 5000	Peqlab, Erlangen
Dissecting instruments	KOBE, Marburg
Gel electrophoresis Mini-PROTEAN Tetra	BioRad, Hercules
Hellma® TrayCell™	Sigma Aldrich, Taufkirchen
Incubated orbital shaker MaxQ 6000	ThermoFisher, Waltham
Light microscope CKX31	Olympus, Hamburg
LightCycler® 480	Roche, Penzberg
Magnetic stirrer MR 3000	Heidolph, Schwabach
Micro pipettes	Peqlab, Erlangen
Mini TransBlot ® tank transfer system	BioRad, Hercules
Multi-channel pipette	Thermo Scientific, München
Neon® electroporation system	ThermoFisher, Waltham
Neubauer chamber	Brand, Wertheim
Orbital shaker Polymax 1040	Heidolph, Schwabach
pH-Meter FiveEasy	Mettler Toledo, Columbus
Photometer BioPhotometer Plus	Eppendorf, Hamburg
Pipetus®	Hirschmann Laborgeräte, Eberstadt
Plate Reader FluoStar Omega	BMG Labtech, Offenburg
Scale EG620	Kern, Balingen
Sonopuls™ Ultrasonic Homogenizer	Bandelin, Berlin
Sterile laminar flow hood HERAsafe KS18	ThermoFisher, Waltham
Thermo shaker TS-100	Peqlab, Erlangen
Vortex REAX1DR	Heidolph, Schwabach
Water bath HI 1210	Memmert, Schwabach

4.2 Consumable materials

Material	Manufacturer
20 ml syringe	Braun, Tuttlingen
Armadillo 96-well PCR plates	ThermoFisher, Waltham
Cell culture 12-well plates	Sarstedt, Nürnbrecht
Cell culture 24-well plates	Sarstedt, Nürnbrecht
Cell culture 6-well plates	Sarstedt, Nürnbrecht
Cell culture 96-well plates, clear bottom	Corning, Kennebunk
Cell culture 96-well plates, white bottom	Sarstedt, Nürnbrecht
Cell culture dishes TC100	Sarstedt, Nürnbrecht
Cell culture flask, 175 cm²	Sarstedt, Nürnbrecht
Cellulose swabs	Meditrade, Kiefersfelden
Cotton buds	Roth, Karlsruhe
Cryo pure tubes	Sarstedt, Nürnbrecht
Filter paper 2.45 mm	Bio-Rad, München
Multiply® µstrip pro PCR 8-strips	Sarstedt, Nürnbrecht
Neon™ Transfection System 100 µL Kit	ThermoFisher, Waltham
Nitrocellulose membrane 0.45 µm	GE Healthcare Life science, Freiburg
Nylon cell strainer, 70 µM	Corning, Durham
Optically clear adhesive seal sheets	ThermoFisher, Waltham
Pasteur pipettes	VWR, Darmstadt
Pipette tips	Sarstedt, Nürnbrecht
Reagent reservoirs	Sarstedt, Nürnbrecht
Safe seal micro tubes	Sarstedt, Nürnbrecht
Safety Multifly® needles	Sarstedt, Nürnbrecht
Screw cap tubes	Sarstedt, Nürnbrecht
Serological pipettes	Sarstedt, Nürnbrecht
Surgical disposable scalpels	Braun, Tuttlingen

4.3   Cell culture media and supplements

Medium	Manufacturer
DMEM + GlutaMAX™ (*Dulbecco's modified eagle medium)*	ThermoFisher, Waltham
DMEM/F-12 (Ham)	ThermoFisher, Waltham
Endothelial cell medium	PromoCell, Heidelberg
Endothelial cell supplement mix	PromoCell, Heidelberg
FBM™ basal medium	Lonza, Basel
FGM™-2 SingleQuots™	Lonza, Basel
Fibroblast medium 2	PromoCell, Heidelberg
Fibroblast supplement mix 2	PromoCell, Heidelberg
Normocin	InvivoGen, San Diego
Penicillin Streptomycin (15070-063)	Gibco, Waltham
RPMI 1640 *(Gibco Roswell Park Memorial Institute medium 1640)*	ThermoFisher, Waltham
SeraPlus FCS (*fetal calf serum)*	PAN-Biotech, Aidenbach

4.4   Reagents

Reagent	Manufacturer
Apamin	Santa Cruz Biotechnology, Dallas
BLUEplus prestained protein ladder (10-180 kDa)	Biomol, Hamburg
Bovine serum albumin (BSA)	Roth, Karlsruhe
cellQART® cell cuture inserts, 5 µM	SABEU, Northeim
Clarity WesternBlot substrate	BioRad, Hercules
Collagenase type I	Millipore, Temecula
DEPC H20	Sigma Aldrich, Taufkirchen
Dimethyl sulfoxide (DMSO)	Sigma Aldrich, Taufkirchen
D-Val-leu-Lys-AMC	Sigma Aldrich, Taufkirchen
Isofluorane (1 ml/ml)	CP-Pharma, Burgdorf
Lipofectamine™ RNAiMAX Transfection reagent	ThermoFisher, Waltham
Luciferase assay system	Promega, Fitchburg
Milk powder	Roth, Karlsruhe
NS8593	Sigma Aldrich, Taufkirchen

NucleoBond Xtra Midi kit for plasmid DNA	Macherey-Nagel, Düren
OptiMEM	ThermoFisher, Waltham
Page Ruler plus prestained protein ladder	ThermoFisher, Waltham
Paraformaldehyde	EMS, Hatfield
PathScan® Phospho-Smad2 Sandwich ELISA Kit	Cell-Signaling, Frankfurt; #7348
Phosphate buffered saline (PBS)	ThermoFisher, Waltham
PD184352	Sigma-Aldrich, Taufkirchen
Plasminogen	Sigma-Aldrich, Taufkirchen
Plasminogen	ThermoFisher, Waltham
Ponceau S	Sigma Aldrich, Taufkirchen
Primers	Metabion, Planegg
RevertAid First Strand cDNA Synthesis Kit	ThermoFisher, Waltham
Roche cOmplete™ protease inhibitor cocktail	Roche, Penzberg
Sircol soluble collagen assay	Biocolor, Carrickfergus
Sulforhodamine B based toxicology assay kit	Sigma-Aldrich, Taufkirchen
SYBR™ green Kappa Fast start qPCR Mastermix	Sigma-Aldrich, Taufkirchen
TE-buffer IDTE (nuclease free)	Integrated DNA Technologies, Coralville
TG100-115	Santa Cruz Biotechnology, Dallas
TGF-β1	Sigma-Aldrich, Taufkirchen
TMB substrate	Sigma-Aldrich, Taufkirchen
Trizol-reagent	ThermoFisher, Waltham
Trypsin EDTA	ThermoFisher, Waltham
TurboFect™ Transfection Reagent	ThermoFisher, Waltham
Ultrapure H_2O (nuclease free)	ThermoFisher, Waltham
Waixenicin A	Isolated as described previously [323] Kindly provided by Prof. Zierler
α2-antiplasmin	Sigma-Aldrich, Taufkirchen

Standard chemicals used in this work were obtained from Carl-Roth, Karlsruhe or Sigma-Aldrich, Taufkirchen.

4.5 Antibodies

Primary antibody	Donor	Manufacturer; purchase number
Histone H3	Rabbit	Abcam, Cambridge; ab1791
SDHA	Mouse	Abcam, Cambridge; ab14715
PAI1	Rabbit	Abcam, Cambridge; ab66705
Collagen1	Rabbit	Abcam, Cambridge; ab34710
α-SMA	Rabbit	Abcam, Cambridge ; ab5694
fibronectin	rabbit	Abcam, Cambridge; ab2413
pSMAD2 (Ser465/467)	Rabbit	Cell-Signaling, Frankfurt; clone 138D4,
SMAD2	Rabbit	cell signaling, Frankfurt; clone D43B4, #5339
SMAD3	Rabbit	cell signaling, Frankfurt; clone C67H9, #9523
pERK (Tyr204)	Mouse	Santa Cruz Biotechnology, Dallas; sc-7383
ERK1	Goat	Santa Cruz Biotechnology, Dallas; sc-94-G

Secondary antibodies (HRP-conjugated)	Manufacturer; purchase number
Anti-mouse-IgG	BioRad, Hercules; 1706516
Anti-rabbit-IgG (#1706515)	BioRad, Hercules; 1706515

4.6 siRNA

siRNA	Manufacturer	Purchase number
TRPM7	ThermoFisher, Waltham	AM16708: ID103360 and ID104677
control-siRNA	ThermoFisher, Waltham	AM4611

4.7 Plasmids

Plasmid	Provider	Bacterial resistance
8xGTIIC-luc (YAP/TAZ)	Addgene, Watertown	ampicillin
pCAGA-luc (SMAD3/4)	PD Dr. Claudia Staab-Weijnitz	ampicillin

4.8   Primary cells and cell lines

Primary cells	Provider; purchase number
pHPF	PromoCell, Heidelberg; C-12360
HPAEC	PromoCell, Heidelberg; C-12241
pHPF healthy donor (NHLF)	Lonza, Basel; CC-2512
pHPF IPF donor (DHLF-IPF)	Lonza, Basel; CC-7231
Cell lines	
A549	ATCC, Manassas; CCL-185
H1299	Provided by Dr. Georgios Stathopoulos, CPC München
16-HBE14o-	Sigma-Aldrich, Taufkirchen; SCC150
L929	ECACC, Salisbury ;85103115

5. Methods

5.1 Cell culture

5.1.1 Primary cells and cell lines used in this work

Primary human pulmonary fibroblasts (pHPF) and primary human pulmonary artery endothelial cells (HPAEC) were purchased from PromoCell®. These cells were isolated from human lung tissue and cryopreserved at passage 2. Cells were shipped on dry ice in cryo vials containing 500,000 viable cells. Since primary cells were not artificially immortalized, they cannot undergo as many population doublings as immortalized cell lines and were therefore used for experiments between passages 3 and 10 only.

Primary human pulmonary fibroblasts from one healthy donor and one donor with pulmonary fibrosis were purchased from Lonza. Cells were isolated from lung tissue and shipped cryopreserved in vials containing 500,000 viable cells.

H1299 cells are a human epithelial non-small-cell lung carcinoma (NSCLC) cell line derived from a lymph node metastasis from a 43-year-old male [292].

A549 cells are a human lung adenocarcinoma cell line established through an explant culture of carcinomatous lung tissue of a 58-year-old male [291].

16HBE14o- cells are a SV40 large T-antigen transformed human bronchial epithelial cell line established from a 1-year old male heart-lung transplant patient and were used as control to lung tumor cells [348].

L-929 cells are a mouse fibroblast cell line from subcutaneous connective tissue derived in 1948 from a 100-day-old C3H/An male mouse [349].

5.1.2 Isolation and cultivation of primary pulmonary mouse fibroblasts

Mouse pulmonary fibroblasts were isolated according to pre-established protocols [350, 351].

Mice used for this work were provided and already sacrificed by the group of Prof. Dr. rer. nat. Susanna Zierler. Mice were taken from the animal facility 1 to 2 hours prior to the start of the experiment. One mouse was carefully transferred to a tightly sealable container and 3 ml isoflurane were added to the container. After approximately 1 min, the mouse was fully anesthetized and a cervical dislocation was performed by a member of the group of Prof. Zierler. The mouse was put on a cork laying on the back and fixed with one needle through each paw. The head was fixed in an overextended state by a needle between the teeth to facilitate the following steps. Fur was moistened with 70 % ethanol and a median incision was performed from the umbilicus to the chin. The abdomen was opened and the diaphragm was punctured to detach it from the lung. The diaphragm was cut and removed. Ribs were cut to open the thorax and fixed sideways with needles. The heart was grabbed with blunt tweezers and the left heart ventricle was punctured until a drop of blood appeared. A Safety Multifly® needle attached to a 20 ml syringe containing 15 ml ice-cold phosphate buffered saline (PBS) was inserted into the right heart ventricle to rinse the lung. Blood and PBS were removed by cellulose swabs. When the lung was completely white, it was taken out of the thorax in small pieces and transferred into a 50 ml tube containing ice-cold PBS. The following steps were performed in the sterile laminar flow hood. As growth medium for primary mouse pulmonary fibroblasts (pMPF), DMEM/F-12 supplemented with 20 % fetal calf serum (FCS), 5 ml penicillin/streptomycin (100 U / ml) and 1 ml Normocin (0.1 mg/ml) was used. Lung pieces were put in a 10 cm dish containing 5 ml prewarmed growth medium and cut into 1 mm^2 pieces using a scalpel. Lung pieces and medium were transferred into a 50 ml tube. Lung was digested with 50 µl Collagenase (5 mg / 50 µl) for 2 h at 37 °C while shaking at 400 rpm. A 70 µM nylon cell strainer was placed on a new 50 ml tube and digested tissue pieces were transferred into the strainer and scratched through the mesh with the flat end of a 3 ml syringe piston. The strainer was rinsed with 15 ml prewarmed PBS, the tube was centrifuged at 400 x g for 5 min at room temperature and supernatant was

discarded. The pellet was resuspended in 10 ml growth medium, seeded onto a TC100 dish and incubated at 37 °C for 48 hours. 2 days after isolation, pMPF were checked and medium was changed or cells were split when reaching 80 – 90 % confluence. For splitting, cells were washed twice with 5 ml PBS and 1 ml Trypsin was added to the dish for 10 min. Once cells were detached, 9 ml growth medium were added and the total volume of 10 ml was distributed equally among 3 new TC100 dishes. After reaching 80-90 % confluency, cells were either split again to increase cell number as described above or seeded onto well plates for experiments.

5.1.3 Cell culture

The following paragraph describes cultivation of all used primary cells and cell lines, except primary mouse pulmonary fibroblasts (pMPF). For cultivation of pMPF see chapter 5.1.2. Cells were adherently cultured in growth medium on T175 flasks (175 cm^2 growth area) in a humid incubator with 5% CO2 at 37 °C. An overview of growth medium with the included supplements for the distinct cells is shown in table 1. When the cells reached approximately 80 % confluency, they were subcultured to prevent overgrowing. Subculturing and seeding of the cells was performed under a sterile laminar flow hood. Solutions required for subcultivation were prewarmed in a water bath at 37 °C. Cell medium was aspirated and cells were washed with 5 ml PBS twice. Then, 5 ml of a 0.25 % Trypsin-EDTA (Disodium ethylenediaminetetraacetic acid) solution was added and the flask was incubated at 37 °C for 5 min to release cell attachments to the plastic surface. EDTA is necessary to weaken cell-cell interactions by chelating bivalent cations. After cells were checked under the microscope for complete detachment, 5 ml of growth medium containing fetal calf serum (FCS) were added to the flask to stop proteolytic actions of trypsin. Cells were separated by carefully pipetting up and down and 10 ml suspension was transferred to a 15 ml tube. Cells were centrifuged for 5 min at 800 rpm, the supernatant removed and the pellet resuspended in 10 ml medium. A part of the suspension, normally 1 ml, was transferred to a new T175 flask containing 25 ml growth medium to reach 80 % confluency after 2-3 days. The remaining cell-suspension was used for experiments. The number of cells in the suspension was determined by adding 10 µL cell suspension to a Neubauer

counting chamber. Cell number in one gridded square (corresponds to 0.1 µL) was determined under the microscope and the number was multiplied with 10^4 to calculate the number of cells per mL of cell suspension. The desired cell numbers for individual experiments were seeded onto cell culture plates and incubated at 37 °C for 24 h.

Table 1: Overview of media and growth media supplements used for distinct cells

Cells	Basal medium	Supplements for growth medium
pHPF Promocell	Fibroblast medium 2 (PromoCell)	**Fibroblast supplement mix 2 (PromoCell):** Fetal calf serum 2 % Fibroblast growth factor 1 ng/ml Insulin 5 µg/ml
HPAEC	Endothelial cell medium (PromoCell)	**Endothelial cell supplement mix (PromoCell):** Fetal calf serum 2 % Endothelial cell supplement 0.004 ml/ml Epidermal growth factor 0.1 ng/ml Fibroblast growth factor 1 ng/ml Heparin 90 µg/ml Hydrocortisone 1 µ/ml
pHPF Lonza	FBM™ basal medium (Lonza)	**FGM™-2 SingleQuots™ for 500 ml medium:** Fetal calf serum 10 ml Insulin 0.5 ml Fibroblast growth factor 0.5 ml GA-1000 (gentamycin/amphotericin) 0.5 ml
A549	RPMI 1640	Fetal calf serum 10% Penicillin / streptomycin (100 U/ml)
H1299	RPMI 1640	Fetal calf serum 10% Penicillin / streptomycin (100 U/ml)

16-HBE	RPMI 1640	Fetal calf serum 10%
		Penicillin / streptomycin (100 U/ml)
L-929	DMEM + GlutaMAX™	Fetal calf serum 10%
	+ 4.5 g/l glucose	Penicillin / streptomycin (100 U/ml)

5.1.4 Cryoconservation of cells

Cells were detached and counted (as described in 4.1.3) and centrifuged at 800 rpm for 5 min. The supernatant was carefully aspirated and the pellet was resuspended in ice-cold FCS containing 10% dimethyl sulfoxide (DMSO) as frost protection agent. For 600,000 counted cells, 1 ml of DMSO/FCS solution was prepared. 1 ml cell suspension was then transferred to a cryo-tube and subsequently stored in a freezing container at -80 °C, which is designed to achieve the optimal cooling rate of -1°C/minute. After 24 h, tubes were transferred to the liquid phase of a nitrogen tank for long-term conservation. All above-mentioned steps were performed on ice.

5.1.5 Thawing of cryoconserved cells

After withdrawal from the nitrogen tank, cryo-tubes were immediately warmed up at 37 °C in a water bath and transferred to a T175 culture flask containing prewarmed growth medium. This ensured quick thawing of the cells [352]. After 24 h, medium in the flask was exchanged with fresh growth medium to remove DMSO.

5.1.6 Stimulation procedure

Two stimulation procedures were used in this work, which are indicated in the corresponding figure legend. In most experiments, cells were stimulated with the desired reagents for 24 h in cell-specific growth medium with FCS (see table 1). To achieve induction of fibroblast-to-myofibroblast differentiation or epithelial-to-mesenchymal transition of cancer cell lines, cells were stimulated with TGF-β or co-stimulated with the desired reagents in cell-specific basal medium containing 0.5 % FCS for 48 h. TGF-β was used at a concentration of 2 ng/ml, which correlates to 420 pM. Stimulation with TGF-β using this protocol has previously been

established to induce EMT as well as fibroblast differentiation [175, 284, 353, 354]. Besides, individual experiments required specific stimulation procedures, which are indicated the corresponding description of methods and likewise in the figure legends.

If reagents were dissolved in solutions other than H_2O, carrier controls were added to exclude misinterpretation of the data due to effects of the solvent. Table 2 summarizes the dissolving solution for the individual reagents together with the final concentration of the reagent used for experiments. Deviations of the standard concentrations are indicated in the corresponding figure legends.

Table 2: Overview of solvents and concentrations of individual reagents

Reagent	Solvent	Concentration
TGF-β	H_2O	2 ng/ml
NS8593	100 % DMSO	25 µM
Waixenicin A	100 % EtOH	10 µM
Apamin	H_2O	100 nM
PD184352	100 % DMSO	10 µM
α2-antiplasmin	H_2O	500 nM
Plasminogen	50% glycerol (v/v)	5 or 25 µg/ml
TG100-115	100 % DMSO	10 µM

5.2 Plasmin activity assay

5.2.1 Measuring fluorescence of D-Val-Leu-Lys 7-amido-4-methylcoumarin

Plasmin activity was measured using the fluorogenic plasmin substrate D-Val-Leu-Lys 7-amido-4-methylcoumarin. This synthetic substrate consists of a three amino acid sequence and an inactive fluorophore linked by an amido group (Fig 5). The chemical structure of the substrate was obtained and adjusted from the Sigma-Aldrich webpage and is displayed in fig 5 [355]. Plasmin cleaves this substrate by hydrolyzing the amido group attached to the lysine, resulting in the release of the active fluorophore that can be measured fluorometrically [356]. It has been shown that this substrate is hydrolyzed by plasmin (K_m = 0.1 mM) and to a lesser extent by kallikrein (K_m = 0.6 mM), but not at all by uPA, α-thrombin, Factor Xa, Factor IXa, Factor XIa, or Factor XIIa and can thus be used for specific and sensitive monitoring of plasmin activity [356, 357]. Indeed, it has previously been used to measure plasmin activity in airway smooth muscle cells and lung tumor cell lines [14, 358].
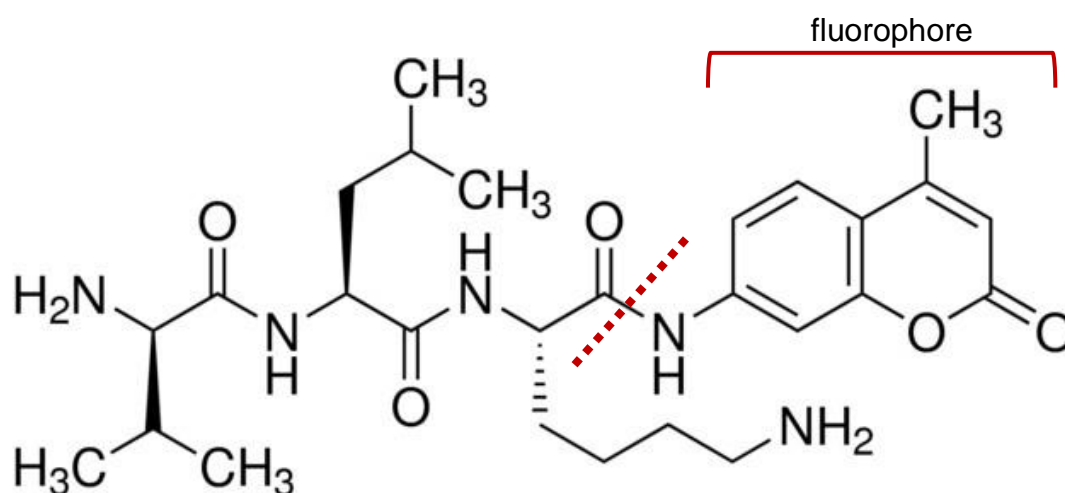
Figure 5: Chemical structure of D-Val-Leu-Lys 7-amido-4-methylcoumarin

Figure obtained and adjusted from the Sigma-Aldrich webpage. Red dotted line displays cleavage site of plasmin resulting in the fluorophore.

Plasmin activity was measured in two fractions: the cell-associated fraction, which includes plasmin that is bound to the cells as well as plasmin that is produced just at that time. Additionally, plasmin activity located in the supernatant was measured and termed plasmin activity of the secreted fraction. First, cells were seeded onto 96-well plates with each well containing 5000 cells in 100 µl medium. 24 h later, cells were stimulated in 50 µl for the desired time period. Then, 10 µl of the supernatant (1/5 of the total volume) of each well was transferred to a new 96-well plate that contained 90 µl plasmin substrate at a concentration of 55 µM in 20 mM Tris-(hydroxymethyl)-aminomethan -hydrochlorid (TRIS/HCl), resulting in a final substrate concentration of 50 µM. Pipetting of the supernatant was done carefully and without touching the base of the wells with the pipette tip to achieve clear separation of the secreted fraction. Remaining supernatant of the initial plate was aspirated completely and 50 µl plasmin substrate at a concentration of 50 µM in 20 mM TRIS/HCl was added. For each experiment, a blank was included: consisting of substrate without cells. Both plates were incubated at 37 °C for 3 hours and fluorescence was measured with the FLUOstar Omega microplate reader at 360 ± 20 nm excitation and 475 ± 20 nm emission. Underlying this detection is the ability of the substrate to use the energy of absorbed photons to elevate its electrons into an excited state. Consequent relaxation of the electrons to the ground state results in emission of light of a longer wavelength. Before the measurement, the gain was adjusted to determine the range of detection. Fluorescence was measured as random fluorescence units (RFU) and the mean RFU of the blank was subtracted from every sample's RFU. Since only one fifth (10 µl) of the secreted fraction were measured, RFU from the secreted fraction were multiplied by 5.

5.2.2 Total protein detection by Sulforhodamine B (SRB) assay

In order to normalize the measured plasmin activity to the number of cells and to eliminate possible cytotoxic effects by the stimulation agents, the sulforhodamine B (SRB) assay was performed as control assay. The SRB assay, established by Skehan et al., is an *in vitro* cytotoxicity assay, which determines total protein amount [359]. SRB is an aminoxanthene dye with two sulfonic groups and stoichiometrically binds to alkaline amino acids of proteins under acid conditions.

The resulting measurement of dye is therefore directly proportional to protein amount and cell number.

Cells were seeded in 96-well plates with each well containing 5000 cells in 100 µl medium and stimulated together with corresponding plate for the plasmin assay. It was paid attention that both plates were treated the same. After the stimulation, cell supernatant was aspirated to remove the serum from the medium that would distort the protein measurement. Cells were fixed to the plate by adding 25 µl cold trichloroacetic acid (50 % in H_2O) acid and incubating at 4 °C for 1 h. Trichloroacetic acid is a strong protein precipitant and fixates cells by interaction of the positively charged amino group of proteins and the negatively charged chloracetate anion [360]. Wells were washed carefully with H_2O 3 times and excessive water was removed by tapping the plate into paper towels. The plate was then allowed to air dry at room temperature for approximately 10 min. Afterwards, 50 µl SRB solution (0.057 % in methanol (wt/vol)) was added to the wells and the plate was incubated at room temperature for 1 h, while being covered to protect SRB from light. Wells were then rinsed 3 times with 1 % acetic acid to remove unbound dye, tapped into paper towels and air dried at room temperature for 10 min. Binding of SRB to proteins is reversible under alkaline conditions, therefore 100 µl of a 10 mM TRIS-base solution (pH 10.5) was added to each well, and the plate was put on a shaker for 20 min to solubilize SRB. For each experiment, a blank was added, consisting of TRIS-base solution without cells. Absorbance at 510 nm was measured with the FLUOstar Omega microplate reader and absorbance was displayed as optical density (OD). To determine the linear range of the assay, a cell number titration experiment was performed in pHPF, A549 and H1299 cells (Fig 6). As displayed, SRB signals differed for different cell types and the highest cell number tested resulted in a saturation of the dye. Thus, 5000 cells were defined as standard cell density for this experiment, since it represented the early exponential phase in all tested cells.
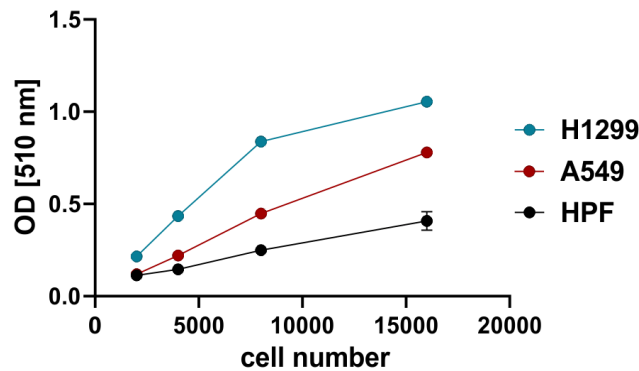
Figure 6: Correlation of SRB signal to cell number in pHPF, A549 and H1299

Different numbers of cells of pHPF, A549 and H1299 were seeded onto 96 - well plates, cultivated for 24 h and a SRB assay was performed. SRB signal is displayed as OD 510

5.2.3 Calculating plasmin activity over cell number

Plasmin activity measured as RFU was normalized to OD values of the SRB assay. For that, mean SRB values for each condition were calculated and RFU values of the corresponding condition divided by this SRB number. Both fractions, cell-associated and secreted were normalized to the same SRB values. The resulting value was defined as RFU / OD510 ratio. To visualize effects of the stimulation, the mean of basal (unstimulated) ratios was calculated and values of stimulated conditions were divided by this mean. The resulting value was defined as x-fold of basal value. An overview of all steps involved in the analysis is shown in figure 7.
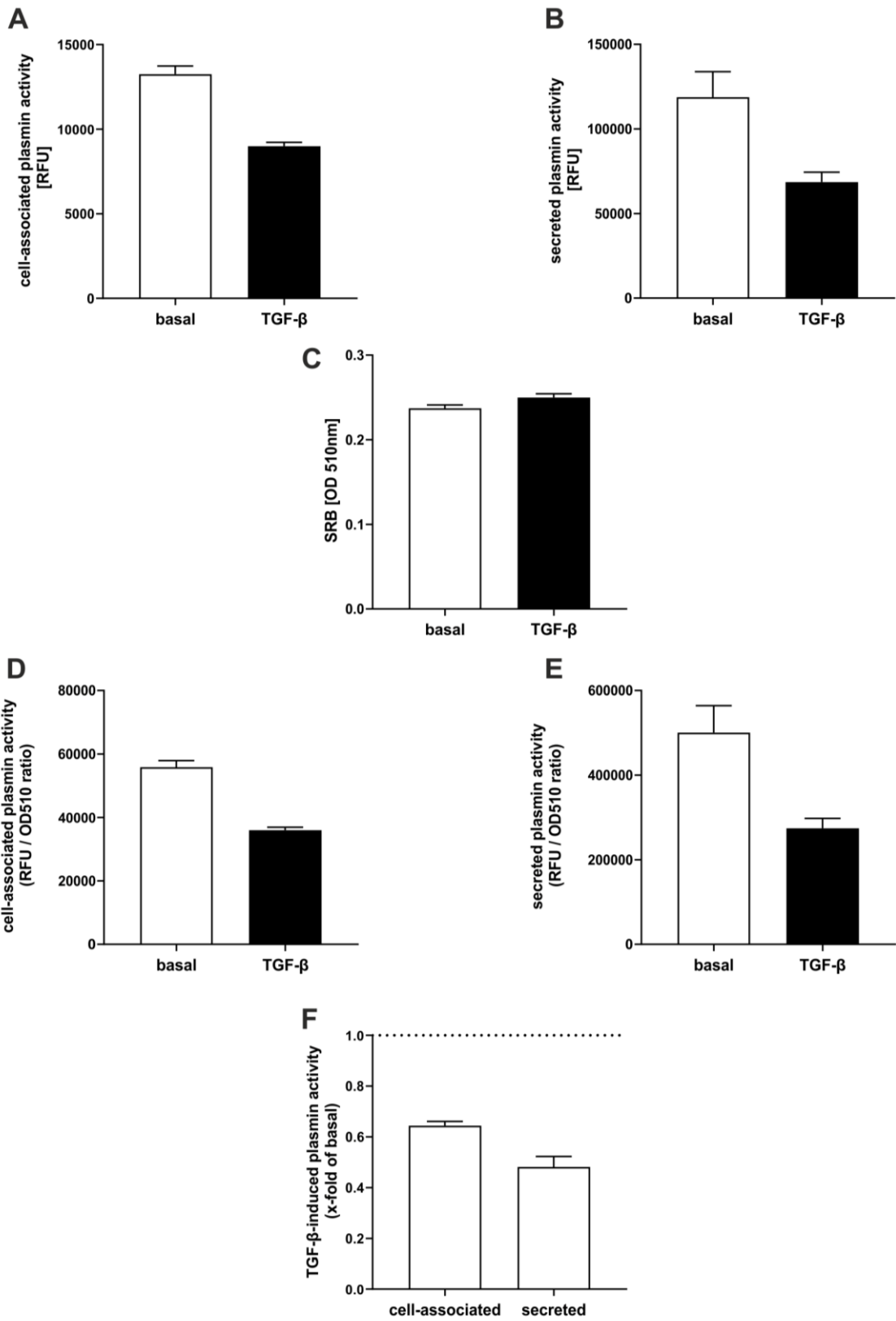
Figure 7: Fig 3 Example of plasmin assay analysis

pHPF were stimulated with TGF-β (2 ng/ml) for 24 h an plasmin assay and SRB assay were performed. Data shown was measured in octuplicates in one representative experiment. Plasmin activity is shown as RFU of cell-associated (**A**) and secreted (**B**) fraction. Data of SRB assay are displayed as OD510 in **C**. RFU values were normalized to OD values of the SRB assay and displayed as RFU / OD510 ratio of cell-associated (**D**) and secreted fraction (**E**). In **F**, the x-fold of stimulated to unstimulated cells was calculated.

5.3   Specific protein detection by Western Blot

5.3.1 Sample preparation

Proteins of the cellular as well as of the secreted fraction were denaturized with Laemmli buffer. Laemmli buffer consists of sodium dodecyl sulfate (SDS) and β-mercaptoethanol [361]. SDS confers a negative charge to the proteins and leads to disruption of secondary and tertiary protein structures. β-mercaptoethanol is a reducing thiol and cleaves disulfide bridges, resulting in disruption of quaternary protein structures. Eventually, proteins are linearized, denaturized and charged negatively proportionally to the chain length and their molecular mass [362].

Cells were seeded in 6-well plates with each well containing 100,000 cells in 2 ml medium and incubated at 37 °C for 24 h. Cells were then stimulated for the desired time period with 1 ml per well. The cell supernatant was transferred to a new tube and centrifuged at 13,000 rpm for 5 min to remove cells that detached during the stimulation. 150 µl of the supernatant were then transferred to a new tube and 20 µl 4x Laemmli buffer was added. The resulting samples of the secreted fraction were stored at -20 °C. Remaining supernatant was aspirated from the plates and 200 µl 1x Laemmli buffer was added per well. 4x Laemmli buffer was diluted in H_2O to generate 1x Laemmli buffer. After 3 min incubation, cell lysates were transferred to tubes, sonicated for 15 s, heated for 5 min at 65 °C to break down genomic DNA and centrifuged for 5 min at 13,000 rpm. Samples of the cell-associated fraction were also stored at -20 °C.

5.3.2 SDS-polyacrylamide gel electrophoresis (SDS-PAGE)

SDS-PAGE allows for protein separation based on their molecular weight. Negatively charged proteins move through an electric field towards the anode. SDS-PAGE consists of a running gel and stacking gel, which differ in pore size, pH and ion concentration. Proteins are administered to the stacking gel, where they are concentrated in one band to ensure migration into the running gel at the same time. Once in the running gel, proteins are then separated based on their molecular weight. Proteins with a higher molecular weight are moving slower than smaller proteins. Migration speed can be varied by changing concentration of polyacrylamide in the gel. The higher the polyacrylamid concentration, the smaller the pores and the smaller the migration speed. In this work, running gels with 10 % polyacrylamid were used and assembled in the Mini-PROTEAN Tetra Cell electrophoresis system from BioRad.

20 μl of protein lysates were loaded onto the wells of the gels and on each gel a protein ladder was added (4 μl). 80 V were applied until proteins reached the running gel. Voltage was then increased to 120 V. The bromphenole blue from the Laemmli buffer allowed for visual detection of the migration front to prevent proteins from running out of the gel.

Laemmli buffer 4x

0,025 % bromophenol blue (w/v)
5% glycerin (v/v)
1 % SDS (w/v)
15 mM TRIS/HCL pH 6.8 (w/v)
1,25 % β-mercaptoethanol (w/v)

10x SDS-buffer

25 mM TRIS/HCl
0.1 % SDS
190 mM glycine

Stacking gel pH 6.8

0.13 M TRIS
0.1 % SDS
5.4 % acrylamide
0.14 % bisacrylamide
0.001 % Temed
0.001 % Ammonium persulfate

Running gel pH 8.8

0.38 M TRIS
0.1 % SDS
10% acrylamide
0.3 % bisacrylamide
0.001 % Temed
0.001 % Ammonium persulfate

5.3.3 Western Blot

After proteins were separated by SDS-PAGE, they were transferred to a nitrocellulose membrane using the Mini TransBlot ® tank transfer system. Membrane, gel and filter papers were equilibrated in TGM buffer (TRIS-glycine methanol buffer). The gel was put on top of the membrane, put on top of a filter paper and covered with another filter paper. Any air bubbles were carefully removed with a roller. This stack was then covered in foam pads and placed in a gel holder cassette. A schematic overview of this setup is shown in figure 8. During assembly, all components were submerged in TGM to avoid air bubbles. Two gel holder cassettes were placed in one tank filled with TGM. An electric current was applied and negatively charged proteins were transferred to the membrane by moving towards the anode. The transfer was run at 250 V and 350 mA for 2 h at 4 °C.
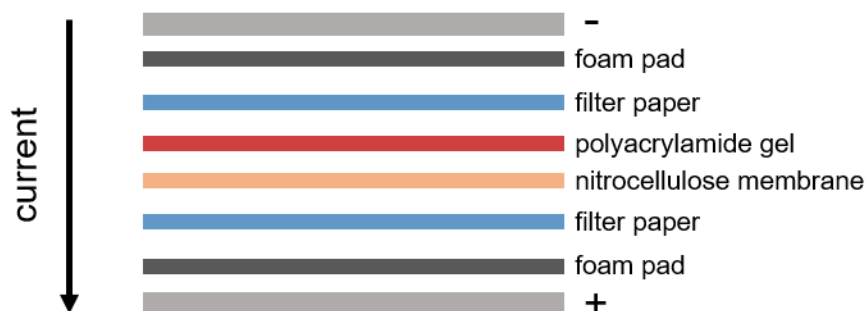
Figure 8: Schematic overview of a transfer stack within a gel holder cassette

Protein transfer was checked by staining proteins on the membranes with Ponceau S. Blots were cut horizontally in 2 or 3 pieces to detect proteins of interest with different antibodies. For each membrane, a loading control that was not affected by stimulation was added to check if the same amounts of protein were initially loaded onto the gels. Histone H3 or succinate dehydrogenase complex, subunit A (SDHA) were used as loading controls, depending on the size of the target proteins. Next, TRIS-buffered saline (TBST) was used to destain membranes, followed by incubation of the membranes with blocking solutions for 30 min on a shaker to block unspecific binding sites. Membranes were incubated with primary antibodies at 4 °C on a shaker overnight. Different antibodies required

different solvents and blocking solutions were chosen according to these solvents. Table 3 summarizes the utilized blocking solutions for distinct antibodies. Of note, all used antibodies are suitable for detection of the individual antigen in human and mouse cells according to the manufacturers. After washing the membranes with TBST three times for 10 min, they were incubated with the according horseradish-peroxidase-conjugated (HRP) secondary antibodies (see table 3) for 1 h at room temperature. Membranes were subsequently washed with TBST three times for 10 min and target proteins were detected by chemiluminescence. Membranes were incubated with luminol and hydrogen peroxide for 1 min during which the horseradish peroxidase from the secondary antibody catalyzes luminol by consuming H_2O_2, leading to a chemiluminescence detectable by ChemiSmart5000.

Table 3: List of primary antibodies with their corresponding blocking solutions, dilution factors and HRP-conjugated secondary antibodies

Primary Antibody	kDA	Solution for blocking & dilution	Dilution	Secondary antibody
Collagen1	130	1 % BSA/TBST	1 : 1000	Anti-rabbit
Fibronectin	280	1 % BSA/TBST	1 : 1000	Anti-rabbit
Histone	18	3 % milk powder	1 : 40000	Anti-rabbit
PAI1	45	1 % BSA/TBST	1 : 2000	Anti-rabbit
pSMAD2	60	5 % BSA/TBST	1 : 1000	Anti-rabbit
SDHA	70	1 % BSA/TBST	1 : 2500	Anti-mouse
SMAD2	60	5 % BSA/TBST	1 : 1000	Anti-rabbit
SMAD3	50	5 % BSA/TBST	1 : 1000	Anti-rabbit
α-SMA	42	1 % BSA/TBST	1 : 1000	Anti-rabbit
pERK	44/42	3 % milk powder	1:2000	Anti-mouse

ERK1	44	3 % milk powder	1:5000	Anti-goat

Secondary antibody			
Anti-mouse	3% milk powder	1:5000	
Anti-rabbit	3% milk powder	1:10000	
Anti-goat	3 % milk powder	1:2500	

10x TBST:

10 mM TRIS

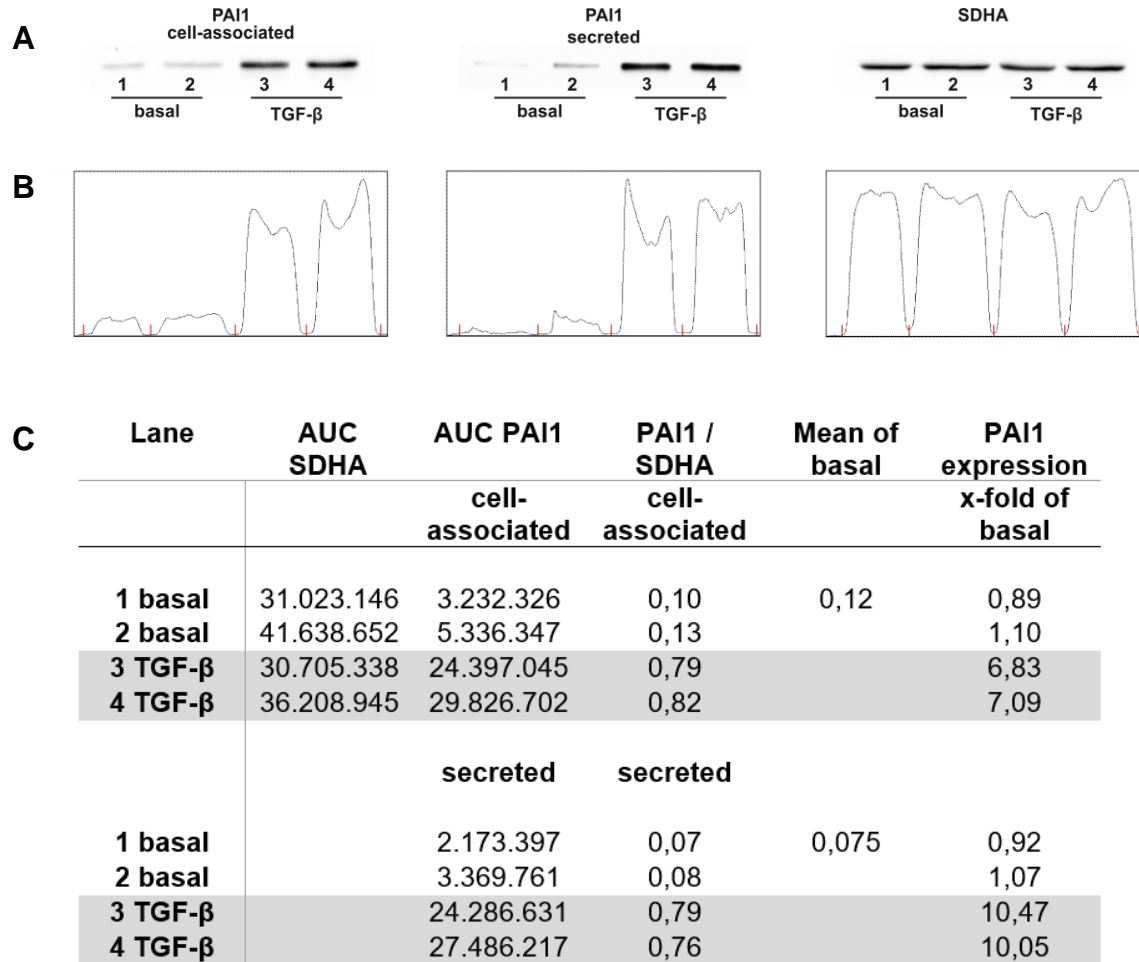150 mM NaCl

0.05% Tween (v/v)

pH 7.4

1x TGM:

25 mM TRIS

192 mM Glycine

20% MeOH

Ponceau S:

0.1% Ponceau

5% Acetic acid

5.3.4 Quantification

Pictures taken with the ChemiSmart camera were densitometrically analyzed with ImageJ by calculating the area under curve (AUC). AUC of the target protein was normalized to AUC of the loading control and protein expression was calculated as x-fold over basal (fig 9).

A

PAI1 cell-associated
1   2   3   4
basal   TGF-β

PAI1 secreted
1   2   3   4
basal   TGF-β

SDHA
1   2   3   4
basal   TGF-β

B

C

Lane	AUC SDHA	AUC PAI1	PAI1 / SDHA	Mean of basal	PAI1 expression x-fold of basal
		cell-associated	cell-associated		
1 basal	31.023.146	3.232.326	0,10	0,12	0,89
2 basal	41.638.652	5.336.347	0,13		1,10
3 TGF-β	30.705.338	24.397.045	0,79		6,83
4 TGF-β	36.208.945	29.826.702	0,82		7,09
		secreted	secreted		
1 basal		2.173.397	0,07	0,075	0,92
2 basal		3.369.761	0,08		1,07
3 TGF-β		24.286.631	0,79		10,47
4 TGF-β		27.486.217	0,76		10,05

Figure 9: Densitometric analysis of one exemplary western blot

pHPF were stimulated with TGF-β for 24 h, western blot was performed. Blots with the cell-associated fraction were cut in half to detect PAI 1 (45 kDa) and SDHA (70 kDa). The loading control of the cell-associated fraction was also used for the secreted fraction. **A** shows the inverted pictures taken with the ChemiSmart camera. In **B**, areas under curve (AUC) created with ImageJ are displayed. Red lines indicate helplines for AUC quantification. Quantification of AUCs, normalization to the loading control and calculation of PAI1 expression as x-fold of basal is summarized in **C**.

5.4 Detection of soluble collagens by Sircol™ assay

Secreted collagens were measured with the Biocolor Sircol™ Soluble Collagen assay kit and the assay was performed according to the manufacturer's protocol. The assay is based on the ability of the Sircol™ dye to precipitate and dye soluble collagens. Sircol™ dye contains Sirius Red, which is an anionic dye containing sulfonic acid side chains which binds to basic collagens with intact triple helix organization. All solutions used were included in the assay kit. 500,000 cells were seeded onto cell culture dishes, incubated overnight and stimulated for 48 h in 4 ml. 1.6 ml supernatant were transferred to a low-protein-binding tube to avoid albumin from the medium to bind to the tube, resulting in absorbance of Sircol™ dye. 330 µl cold collagen isolation & concentration reagent were added per tube. For each experiment, a negative and a positive control were added. For the negative control, 1.6 ml cell culture medium was added to 330 µl cold collagen isolation & concentration reagent. For the positive control, 60 µl Collagen standard (500 µg/ml), which equals 30 µg Collagen, was mixed with cell culture medium to obtain a finale volume of 1.6 ml, then 330 µl cold collagen isolation & concentration reagent was added. All samples were mixed and incubated in an ice/water bath overnight at 4 °C. Then, samples were centrifuged at 14,000 rpm for 30 min at room temperature (RT). Supernatant was removed by carefully inverting the tube and keeping tubes upside down on a tissue. During this step, the collagen pellet at the bottom of the tube was transparent, therefore it was refrained from pipetting supernatant from the tube. 1 ml Sircol™ dye was added per tube; tubes were inverted 5 times and agitated at 400 rpm for 30 min at room temperature. After centrifugation at 14,000 rpm for 30 min at room temperature, supernatant was removed by inverting tubes and putting them onto paper towels upside down. The pellet was now dyed and clearly visible. Any excess dye in the tube as well as in the lid was removed using small rolls formed from absorbent cellulose swabs and sharpened cotton buds. This step was performed very carefully to achieve complete removal of unbound dye without destroying the pellet in the process. 750 µl cold acid-salt-wash-reagent were added to each tube followed by centrifugation at 14,000 rpm for 30 min at room temperature. Supernatant was removed as described above, 750 µl cold acid-salt-wash-reagent was added and

tubes were centrifuged at 14,000 rpm for 30 min at room temperature. After removing supernatant as described above, 250 µl alkali reagent was added and the pellet was dissolved by vortexing for several minutes. Samples were transferred in duplicates (100 µl each) onto 96-well plates and absorbance at 555 nm was detected with the FLUOstar Omega microplate reader. Absorbance was displayed as OD.

5.5   Introduction of nucleic acids into eukaryotic cells

Several cell transfection methods were used to transiently introduce plasmid DNA or siRNA into living cells. Plasmid DNA was transfected via electroporation or using the TurboFect™ reagent, whereas siRNA was introduced into cells by Lipofectamine™ RNAiMAX transfection reagent.

5.5.1   siRNA transfection with lipofectamine

Translation of target genes can be stopped with small interfering RNAs (siRNAs). siRNAs are short, double stranded RNA segments consisting of 20 – 25 base pairs which bind to complementary RNA segments, leading to disabling of their function. This mechanism is known as RNA interference and naturally occurs in viruses [363]. The endoribonuclease Dicer cuts double stranded RNA to siRNA, which then builds RNA induced silencing complex (RISC) with other involved proteins. Once single stranded siRNA binds to the target genes' complementary strand, the RISC complex cuts this complementary strand leading to loss of expression of the target gene (Fig 10). A scrambled siRNA, which does not affect genome expression, is used as negative control to check for unspecific effects of the transfection method. Two predesigned siRNAs (Ambion) were introduced into pHPF by Lipofectamine™ RNAiMAX transfection reagent from Thermo Fisher. Lipofectamine entraps siRNA in liposomes which is able to fuse with negatively charged cell membranes leading to a release of siRNA into cytoplasm. For plasmin activity assays, 1 pmol siRNA was mixed with 0.3 µl Lipofectamine™ RNAiMAX in OptiMEM Medium for each well of a 96-well plate and incubated for 30 min at RT. 10 µl were then added to each well and 10,000 cells were added on top in growth medium. Cells were cultured for 72 hours, stimulated and plasmin activity was measured as described

in 2.2. For mRNA isolation, 25 pmol siRNA was mixed with 7.5 µl Lipofectamine™ RNAiMAX in OptiMEM Medium for each well of a 6-well plate and incubated for 30 min at RT. 250 µl were then added to each well and 200,000 cells were added on top in growth medium. Cells were cultured for 72 hours and mRNA was isolated as described in 4.11.1.

5.5.2 Transfection of plasmid DNA via electroporation

Cells were transfected with reporter plasmids by electroporation using the Neon™ transfection system from Invitrogen. Short electric impulses are applied to the cells, leading to the formation of pores in the cell membrane through which plasmids can enter the cells. Buffers used were provided by the manufacturers Neon Kit. Cells were detached and counted as described above and the desired amount of cells was centrifuged at 800 x g for 5 min. Supernatant was aspirated and cell pellet was resuspended in resuspension buffer (100 µl per electroporation step) and mixed with the plasmid DNA (5 µg per step). It is crucial that cell number and electroporation settings fit perfectly to ensure that the electric impulses lead to the desired effect. Therefore, for each cell line, electroporation settings and cell number were tested to figure out the perfect conditions. For A549 and H1299 cells, 500,000 cells were electroporated at 1450 V for 30 ms with 1 pulse. For pHPF, since they are considerably larger in size than A549 or H1299 cells, cell number was reduced to 250,000 cells per electroporation step and they were challenged with 1650 V 3 times for 10 ms. After electroporation, cells were placed on 96-well plates (20,000 cells per well) in their respective culture medium and cultured for 24 h. After stimulation, cells were lysed and luciferase activity was measured as described in 4.7.
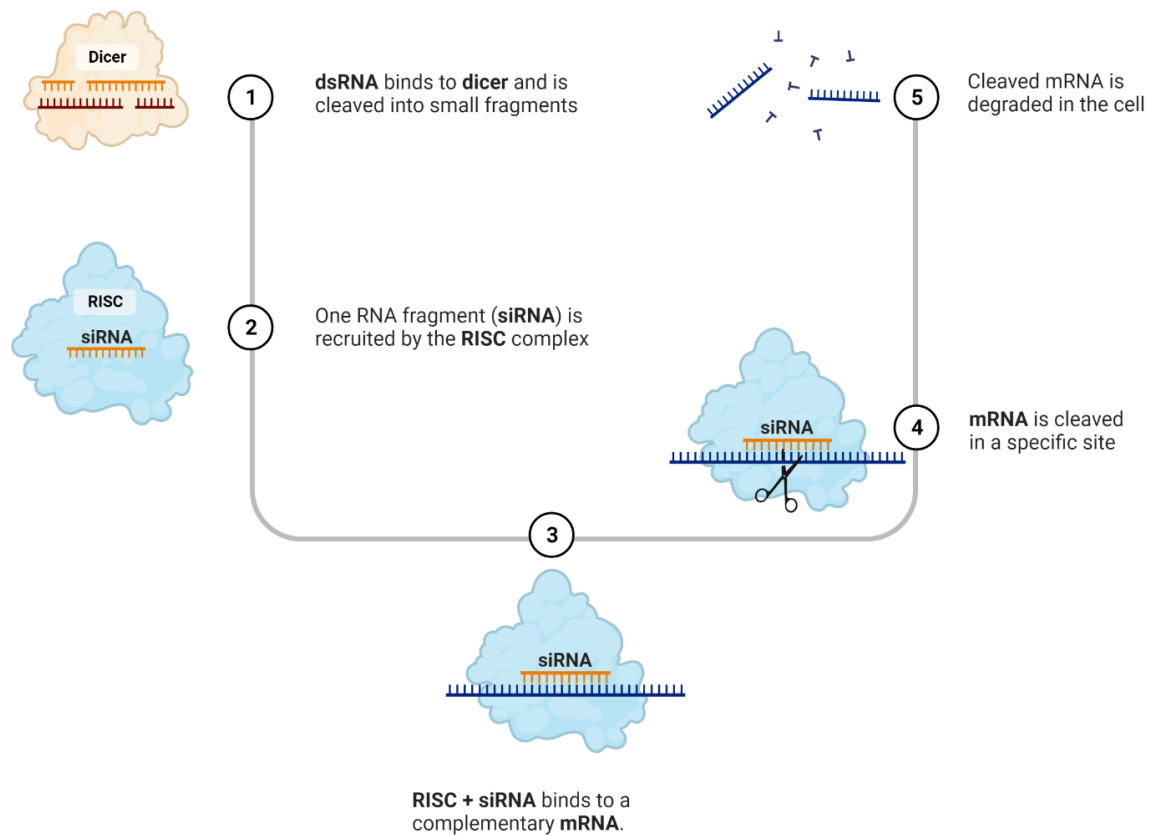
Figure 10: Mechanism of RNA interference

Dicer cuts double stranded RNA to siRNA which is then recruited by the RISC complex. RISC and siRNA bind to complementary mRNA of the target gene, leading to cleavage of the mRNA and subsequent degradation.

5.5.3 Transfection of plasmid DNA via TurboFect™

Cells were transfected with TurboFect™, a solution of cationic polymers which builds stabile, positively charged complexes with DNA. Thereby, entry of DNA into the cells is facilitated and DNA degradation within cells is prevented. 70,000 cells were seeded on 12-well plates and cultivated for 24 h. For each well, the equivalent volume to 250 ng Plasmid in 50 µl serum free medium was mixed with the double volume of TurboFect™ reagent in 50 µl serum free medium and incubated for 30 min at RT. 100 µl of this mixture was added to each well, cells were incubated for 24 h and hereafter stimulated for the desired time periods. After stimulation, cells were lysed and luciferase activity was measured as described in 4.7.

5.6   Plasmid isolation

Plasmids used for luciferase reporter gene assay were bought as bacteria in agar stab containing the plasmid. To isolate plasmids, a pipette tip was used to transfer a small amount of bacteria to a pre-culture tube containing 2 ml LB (lysogeny broth) medium and the respective antibiotic. After incubation overnight at 37 °C at 250 rpm, 200 µl of the preculture were transferred to a flask containing 200 ml LB medium with the respective antibiotic. After additional 24 h at 37 °C and 250 rpm, plasmid isolation was performed using the "NucleoBond Xtra Midi kit for transfection-grade plasmid DNA" from Macherey-Nagel according to the manufacturer's protocol. All used reagents were provided by the manufacturer. 200 ml bacteria suspension with an OD at 600 nm of about 2 were centrifuged for 15 min at 5000 x g at 4 °C and supernatant was discarded. Bacteria were resuspended in 8 ml resuspension buffer and 8 ml lysis buffer was added. To fasten cell lysis, tubes were inverted several times. After 5 min at room temperature, 8 ml neutralization buffer was added. A filter was added to a "NucleoBond Xtra" column, washed with 12 ml equilibration buffer and bacteria suspension was loaded onto the column. The filter was washed with another 5 ml equilibration buffer and removed. The column was washed with 8 ml washing buffer and plasmid DNA was subsequently eluted with 5 ml elution buffer. 3.5 ml 100 % isopropanol were added to precipitate DNA and the total volume of 8.5 ml was transferred to five 1, 5 ml Eppendorf tubes. After 2 min incubation, tubes were centrifuged for 30 min at

14,000 x g at 4 °C and pellets were washed with 70% EtOH. After centrifugation for 10 min at 14,000 x g at 4 °C, pellets were air-dried for approximately 15 min and dissolved in 50 µl IDTE (TRIS/EDTA buffer). DNA concentration and purity was measured in a photometer by determining absorbance at 260 nm and 280 nm. 1µl of DNA solution was added to the "TrayCell" extension on the BioPhotometer® from Eppendorf. DNA purity is sufficient when the 260/280 ratio is above 1.8. DNA was stored at -20 °C until further use.

LB medium:

85.5 mM NaCl

0.5 mM NaOH

1 % trypton/pepton

0.5% yeast extract

5.7 Luciferase reporter gene assay

Firefly luciferase reporter gene assays were used to measure the activity of SMAD3/4 and YAP/TAZ signaling. The luciferase gene is introduced into DNA and is transcribed if the respective signaling pathways are activated. Upon SMAD3/4 or YAP/TAZ activation, they bind to the reporter construct which results in generation of luciferase. Luciferase is an enzyme originating from the firefly *photinus pyralis* and catalyses adenosine-triphosphate-dependent oxidation of luciferine to oxyluciferine. This reaction results in the emission of bioluminescence which is directly proportional to the number of luciferase molecules and therefore proportional to the promoter activity. SMAD3/4 activation was measured using the pCAGA-luc reporter construct provided by PD Dr. habil. med. Claudia Staab-Weijnitz, PhD (CPC Munich), which contains the SMAD3/4 responsive part of the human *SERPINE1* promotor [179]. YAP/TAZ promoter dependent activation was measured with the 8xGTIIC-luciferase plasmid from addgene [364]. This synthetic plasmid contains 8 binding sites for TEAD, a transcription factor directly activated by YAP/TAZ. Plasmids were transfected into cells via electroporation or turbofect as described in chapter 4.5. After stimulation, 50 µl lysis buffer were added to the cells and samples were transferred to 96-well plates with white bottom. Luciferase activity was measured with the FLUOstar Omega microplate reader at 1 s steps for

10 s. 25 µl luciferase substrate were automatically injected at 2 s and light emission was displayed as random light units (RLU). The average of RLU from 3 – 10 s were calculated and background at 1 s was subtracted (Fig 7). Figure 11 shows an exemplary measurement of a luciferase reporter assay.

Lysis buffer

25 mM TRIS/HCl pH 7.4

4 mM ethylene glycol-bis(β-aminoethyl ether)-N,N,N′,N′-tetraacetic acid

8 mM MgCl2

1 mM DTT

1 % Triton-X-100
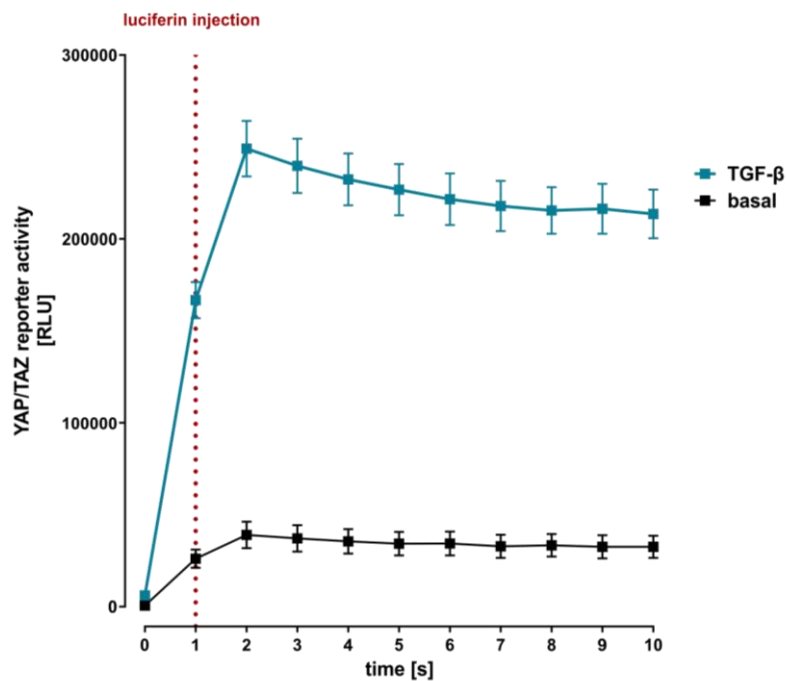
Figure 11: Exemplary luciferase reporter gene assay

A549 cells were transfected with the 8xGTIIC-luciferase plasmid and stimulated for 24 h with 2 ng/ml TGF-β. After cell lysis, YAP/TAZ activity was measured. Data shown were obtained from quadruplicates from one exemplary experiment. Light emission was measured for 10 s with luciferin being injected at 2 s. Results are displayed as random light units (RLU).

5.8 Phospho-SMAD2 enzyme-linked immunosorbent assay (ELISA)

Levels of activated SMAD2 phosphorylated at Serine 465 / 467 were determined using the PathScan® Phospho-Smad2 Sandwich ELISA Kit from CellSignal. 50,000 cells were seeded onto 24-well plates, kept overnight and stimulated for the desired times. ELISA was conducted according to the protocol provided by the manufacturer. All used solutions were included in the kit. After stimulation, cells were washed with 1 ml ice-cold PBS and lysed on ice for min with 200 µl ice-cold lysis buffer supplied with Roche cOmplete™ protease inhibitor cocktail. Cells were scraped from the microwell plates, transferred to a tube and sonicated on ice. Tubes were then centrifuged for 14,000 rpm at 4 °C for 10 min, supernatant containing the cell lysate was transferred to a new tube and tubes were kept on ice. Microwell-stripes coated with SMAD2 mouse monoclonal antibody were brought to room temperature before starting the assay. 100 µl cell lysate was added to each well, wells were sealed with adhesive film and incubated overnight at 4 °C, leading to capturing of phosphorylated and non-phosphorylated SMAD2. Film was removed and wells were washed by inverting the tubes and washing them 4 times with 200 µl washing buffer. After each washing step, wells were tapped onto paper towels to completely remove buffer, without letting them dry. 100 µl reconstituted phospho-SMAD2 rabbit detection antibody was pipetted into each well, wells were sealed and incubated at 37 °C for 1 h. Wells were then washed 4 times as described above. 100 µl reconstituted secondary anti-rabbit HRP-linked antibody was added to the wells, wells were sealed and incubated at 37 °C for 30 min. Wells were washed 4 times as described above. 100 µl 3,3′,5,5′-tetramethylbenzidine (TMB) substrate was added to the wells, wells were sealed and incubated for 30 min at room temperature. This step resulted in a blue color due to oxidation of TMB by horseradish-peroxidase. 100 µl acid stop solution was added to stop the reaction, leading to a color change from blue to yellow. Plates were carefully agitated and samples were transferred to a 96-well plate. Absorbance at 450 nm was detected with the FLUOstar Omega microplate reader and displayed as (OD). If OD values higher than 1 were measured, the protocol

was adjusted by shortening TMB incubation time and diluting cell lysates before adding them to the wells.

5.9 Whole cell PAI1 ELISA

PAI1 protein levels where detected using a second approach besides Western Blot. Whole cell PAI1 ELISA was performed according to a previously published protocol [365]. 25,000 cells were seeded onto 24- well plates and stimulated after 24h. Supernatant was aspirated and cells were fixed on the plate by adding 200 µl 4% paraformaldehyde. After 15 min, paraformaldehyde was aspirated and 200 µl of 50 % ice cold methanol/acetone was added for 5 min to permeabilize cell membranes. Cells were then washed with 1 ml phosphate-buffered saline (PBS) and unspecific binding sites were blocked by adding 200 µl 1% BSA/TBST for 15 min. PAI1 primary antibody was diluted 1:1,000 in 1 % BSA/TBST and as control, histone antibody was diluted 1:5,000 in 1% BSA/TBST. Cells were incubated with 200 µl primary antibodies for 1h at room temperature, followed by 3 washing steps with 1 ml PBS for 10 min each. Goat-anti-rabbit horseradish-peroxidase-conjugated secondary antibody was diluted 1:4,000 in 1% BSA/TBST and 200 µl were added to cells for 45 min. Cells were washed 3 times with 1 ml PBS for 10 min and 3,3′,5,5′-tetramethylbenzidine (TMB) was added which started the oxidation of TMB by horseradish-peroxidase, resulting in a blue color. After approximately 10 min incubation in the dark to protect TMB, the reaction was stopped by adding 50 µl sulfuric acid, resulting in a color change from blue to yellow. Samples were transferred to a 96-well plate and a blank consisting of 200 µl TMB and 50 µl sulfuric acid was added. Absorbance at 450 nm was detected with the FLUOstar Omega microplate reader and displayed as OD. If OD values higher than 1 were measured, the protocol was adjusted by shortening TMB incubation time.

5.10 Water soluble tetrazolium 1 (WST-1) assay

WST-1 is the sodium salt of 4-[3-(4iodophenyl)-2-(4-nitrophenyl)-2H-5-tetrazolio]-1,3-benzene disulfonate and is a dye that can be used in quantitative cell viability assays or cytotoxicity assays. The assay is based on the ability of mitochondrial dehydrogenases from living cells to cleave tetrazolium salt to formazan [366]. The resulting amount of formazan dye is directly proportional to the number of metabolically active cells and absorption of the dye can be measured at 440 nm.

2,000 cells were seeded into 96-well plates and incubated for 24 h. Then, cells were stimulated in 100 µl for 72 h and WST-1 assay was performed. 10 µl of WST-1 reagent were added to each well, thereby achieving a 1:10 dilution of WST-1 reagent. After 1 h at 37 °C, plates were shaken on a shaker for min and absorbance at 440 nm was measured.

5.11 Quantitative real-time reverse transcriptase polymerase chain reaction

Quantitative real-time reverse transcriptase polymerase chain reaction (qRT-PCR) is used to analyze gene expression. In addition to DNA multiplication as in conventional PCR, qRT-PCR allows for quantification of DNA and therefore to conclude on RNA expression. Quantification is achieved by measuring fluorescence of a DNA-intercalating fluorescent dye which is directly proportional to the amount of PCR products. Before starting qRT-PCR, RNA was extracted from cells and transcribed into DNA via reverse transcription.

5.11.1 RNA Isolation

Cells were seeded onto 6-well plates (150,000 cells per well) and stimulated for the desired time periods. After stimulation, cells were lysed with 1 ml Trizol reagent from Sigma containing phenol and guanidinium thiocyanate. Phenol serves as RNA solvent whereas guanidinium thiocyanate is used for cell lysis by protein denaturation and enzyme deactivation. Lysis was performed by pipetting up and down for 5 min at room temperature and transferring samples to Eppendorf tubes. Samples were stored at -80 °C or directly processed. 200 µl chloroform was added,

incubated for 2 min and tubes were centrifuged at 12,000 x g for 15 min at 4 °C. This step resulted in the formation of 3 phases: a lower, organic phase containing proteins, an interphase containing DNA and the upper, transparent and aqueous phase containing RNA which was carefully transferred to a new tube. 500 µl 100 % isopropanol were added to RNA solution to precipitate RNA, incubated for 10 min at room temperature and centrifuged at 21,000 x g for 10 min at 4 °C. Supernatant was removed, the pellet was washed with 1 ml 70 % RNAse free ethanol and tubes were centrifuged at 21,000 x g for 10 min at 4 °C. Supernatant was carefully removed and pellets were air dried for approximately 15 min. RNA pellets were then resuspended in 20 µl RNAse-free water at 60 °C for 10 min. RNA concentration was determined photometrically by measuring absorbance at 260 nm. 1µl of RNA solution was added to the "TrayCell" extension on the BioPhotometer® from Eppendorf. Additionally, absorbance at 280 nm was measured to check for RNA purity. RNA purity is sufficient when the 260/280 ratio is above 1.8. RNA was stored at -80 °C.

5.11.2 Reverse transcription

RNA was transcribed into complementary DNA (cDNA) before using it in qRT-PCR by the enzyme reverse transcriptase. All steps were performed on ice and all used solutions were provided by the RevertAid first strand cDNA-synthesis kit from ThermoFischer. In a first step, 1 µl random hexamer primer (100 µM) was mixed with the equivalent volume of 1 µg RNA solution and RNAse-free water was added to the tube to reach a final volume of 12 µl. Components were mixed thoroughly and incubated for 5 min at 65 °C. In the next step, the following components were added to each tube:

- 4 µl 5 x reaction buffer
- 1 µl RNAse inhibitor (20 U/µl)
- 2 µl DNTP mix (10 mM)
- 1 µl RevertAid reverse transcriptase (200 U/µl)

Tube content was mixed thoroughly, incubated at 25 °C for 5 min, at 42 °C for 60 min and finally for 5 min at 70 °C to stop enzyme function. Samples containing cDNA were stored at -20 °C until further use.

5.11.3 Realtime Polymerase chain reaction

The LightCycler® 480 II from Roche used in this work combines thermocycler and fluorimeter and measures fluorescence after every elongation cycle. SYBR™ green is a dye which intercalates into DNA and resulting DNA-dye complex can be excited at 494 nm. Emitted light at 521 nm is detected and correlates with the amount of DNA in the sample. The crossing point (Cp) value displays the cycle at which fluorescence is crosses the background fluorescence level to measure amplification in the early exponential phase (fig 12).
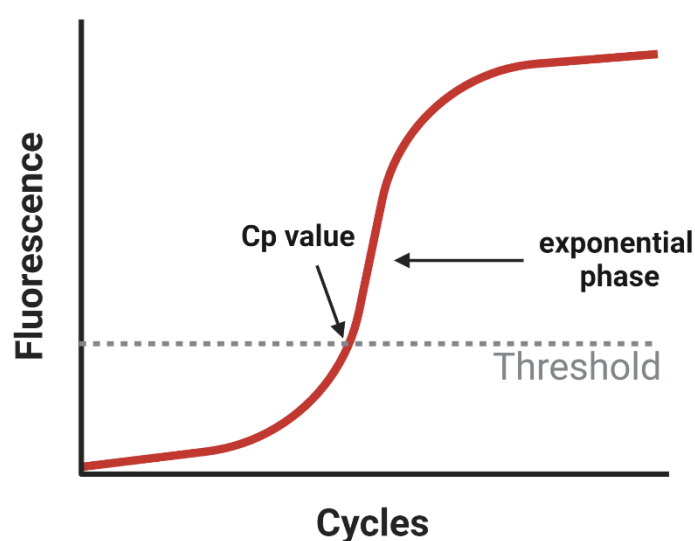
Figure 12: Graphical representation of qRT-PCR

Fluorescence is measured after every elongation cycle. Cp value is measured in the early exponential phase and defined as the cycle at which fluorescence first crosses the threshold.

Primers were designed using the "universal probe library assay design center" by Roche. To prevent amplification of genomic DNA, intron-spanning primers were designed. An overview of the used primer sequences is shown in table 4.

To ensure the formation of a specific PCR product, a melting curve analysis was performed with each experiment. Samples were heated continuously to 95 °C while measuring fluorescence. Upon heating, double strands were separated and dye dissociated from DNA leading to a change in fluorescence counts. Since the SYBR green can also bind unspecifically to primer dimers and PCR products and is

released from these unspecific bindings at considerably lower temperatures, each sample could be tested for unwanted side products.

All pipetting steps were performed on ice. cDNAs were prediluted 1:50 in nuclease-free water and added to 96-well qPCR micro well plates. To check for contamination, a negative control was added consisting of water instead of cDNA. To each well, the following solutions were added:

- 10 µl 2 x SYBR™ green mastermix
- 1 µl forward primer (10 µM)
- 1 µl reverse primer (10 µM)

SYBR™ green mastermix consists of SYBR green, DNA polymerase and nucleotide in a buffered solution. Plates were sealed with adhesive film and centrifuged at 200 x g for 1 min. The following protocol was then started at the thermocycler:

- 95 °C 5 min
- 95 °C 15 s ⎤
- 60°C 15 s ⎬ **40 cycles**
- 72 °C 30 s ⎦
- Melting curve: continuous heating from 60 °C to 95 °C

Table 4: Primer sequences designed with the "universal probe library assay design center" by Roche

Target gene	RefSeq	forward primer 5 '- 3'	reverse primer 5 '- 3'
actin beta	NM_001101.5	ccaaccgcgagaagatga	ccagaggcgtacagggatag
SERPINE1	NM_000602.5	aaggcacctctgagaacttca	cccaggactaggcaggtg
FN1	NM_212482.4	ccgaccagaagtttgggttct	caatgcggtacatgacccct
Col1A1	NM_000088.4	tacagaacggcctcaggtacca	acagatcacgtcatcgcacaac
PLAU	NM_002658.6	agtgtcagcagccccact	ccccctgagtctccctgg
PLAUR	NM_002659.4	gcccaatcctggagcttga	tccccttgcagctgtaacact
SPINT2	NM_021102.4	gcatccacgagaatgccacg	ctgccttctgggagcacttg
TRPM7	NM_017672.5	ttgacattgccaaaaatcatgt	cttgttccaaggatccaacc

Quantification was performed by calculating the difference of Cp values (ΔCp) of target and housekeeping gene. Cp of housekeeping gene was subtracted from Cp of the target gene to calculate the ΔCp value. Since target genes were expressed higher than housekeeping gene, the negative ΔCp (- ΔCp) was calculated and displayed for better understanding. ΔCp of unstimulated condition was subtracted from ΔCp of stimulated condition to calculate ΔΔCp. As mentioned before, a negative ΔΔCp (- ΔΔCp) was calculated and displayed. To convert ΔΔCp values into x-fold of basal values, the following formula was used:

$$\text{x-fold} = 2^{-\Delta\Delta Cp}$$

An overview of qRT-PCR analysis is shown in figure 13.
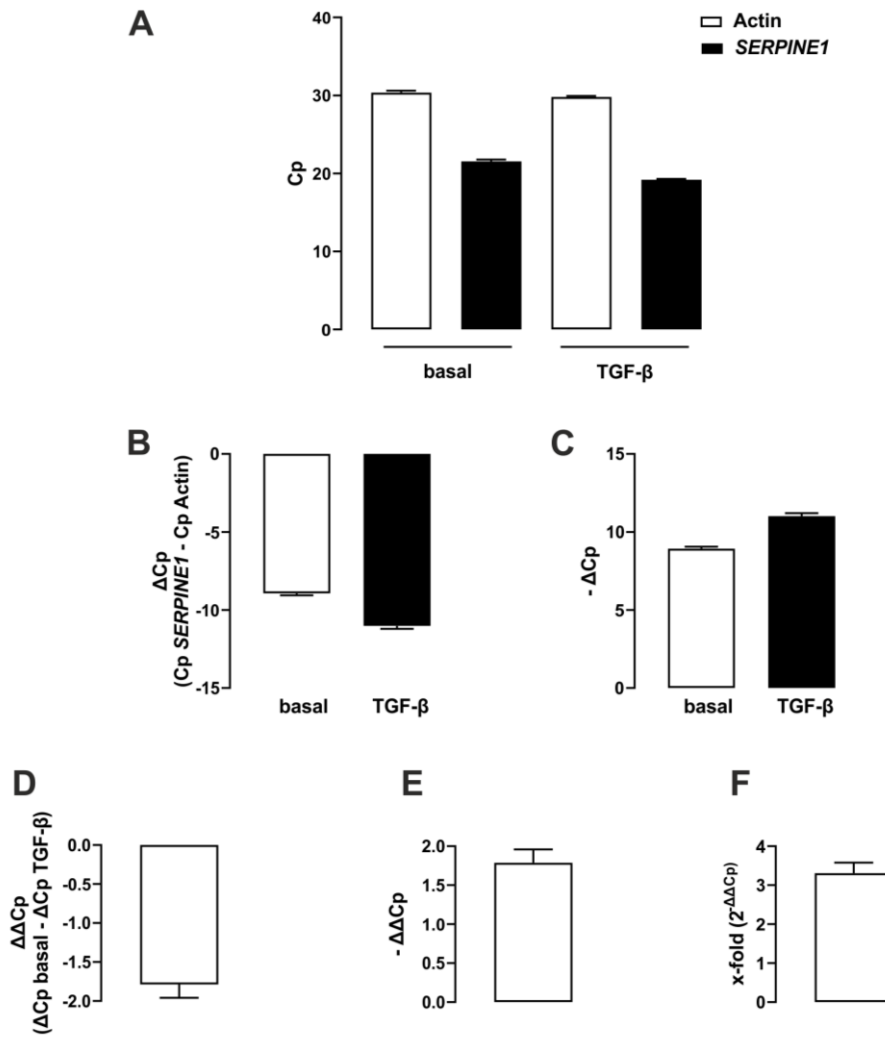
Figure 13: Exemplary analysis of *SERPINE1* mRNA levels in pHPF

SERPINE1 mRNA levels in pHPF were determined by qRT-PCR after 24 h TGF-β stimulation. mRNA levels of *SERPINE1* and β-actin are displayed as cp values (**A**). ΔCp (**B**) was calculated by subtracting Cp Actin from Cp *SERPINE1*. ΔCp are displayed as negative ΔCp for better visualization (**C**). ΔCp basal was subtracted from ΔCp TGF- β to calculate ΔΔCp (**D**) and values are displayed as negative ΔΔCp (**E**). ΔΔCp values were converted into x-fold of basal values (**F**).

5.12 Migration assay

Migratory properties of cells were monitored by a boyden chamber migration assay. A membrane with 5 µM pore size was used to identify cells that are able to change their cytoskeleton to actively migrate through these pores. Migratory cells were then dyed, dye was dissolved and absorption was measured to quantify migratory cells. Dying of the cells was performed with sulforhodamine B (SRB), which determines total protein amount. The principle of SRB staining is described in chapter 5.2.2.

250,000 cells were placed in cell culture inserts in 100 µl growth medium and inserts were placed in 24- well plates containing 500 µl growth medium. A part of the inserts was submerged in the medium from the lower chamber and incubated for 24 h. Medium in upper and lower chambers was then replaced with medium containing the desired reagent. Basal migration was monitored by using the same FCS concentration in upper and lower chamber. Serum-induced migration was monitored by adding low FCS concentration to the upper chamber and high FCS concentration to the lower chamber, thus cells were migrating within a serum-gradient. Effects of TGF-β or NS8593 were measured by adding the reagents to the upper chamber. After 24 h stimulation, medium within the inserts was aspirated and inserts were placed in a new well containing 400 µl SRB dye. After 1 h, inserts were dipped in 1 % acetic acid to remove unbound dye and cells on top of the membrane were removed thoroughly with cotton buds. Migrated cells remained dyed on the bottom of the membrane. The insert was then placed in a new well containing 200 µl TRIS-base (pH 10.5) and incubated on a shaker for 20 min until dye was completely dissolved. Samples were transferred to a 96-well plate and absorbance at 510 nm was measured with the FLUOstar Omega microplate reader and displayed as OD. An overview of the protocol is shown in figure 14.
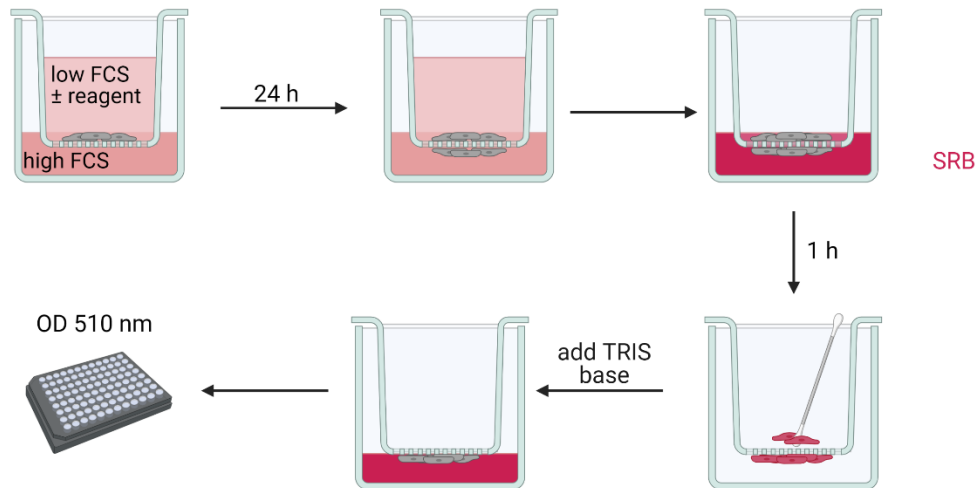
Figure 14: Exemplary workflow of cell migration assay

After 24 h in growth medium, medium in both chambers were replaced with medium of different FCS concentrations to measure FCS-induced migration. Reagents were added to medium in upper chamber to monitor effects on migration. After 24 h, medium was removed and inserts were incubated in SRB solution for 1 h to dye cells. Cells in upper chamber were removed with a cotton swab, SRB was dissolved in TRIS/HCl base (pH 10.5) and absorption was measured at 510 nm.

5.13   Statistical methods

Experiments were conducted at least 3 times independently and the actual number of experiments is stated in the corresponding figure legends. In each experiment, different conditions were measured at least twice and data are shown as mean with standard error of the mean (SEM). GraphPad Prism 9.0 was used to conduct distinct statistical hypothesis testing. Three levels of significance were defined (* $p<0.05$, ** $p<0.01$, *** $p<0.001$). One-sample t-test was used to test for significant differences between a mean value and a hypothetical value (0, 1 or 100). Differences of two mean values were tested with two-sample t-test. Multiple mean values were compared using one-way analysis of variance (one-way ANOVA) followed by Tukey's post-hoc-test. Mean values depending on two independent variables were analyzed using two-way analysis of variance (two-way ANOVA) followed by Tukey's post-hoc-test. Statistic tests on normalized data were only performed after checking for statistical significance of raw data.

6. Results

6.1 Fluorescence-based live cell measurements of plasmin activity in lung cells

Increased levels of plasminogen activator and plasmin and subsequent activation of the plasmin system are crucial for the degradation of ECM proteins, like collagens or fibronectin. This process is linked to diseases in which ECM remodeling is dysfunctional, especially in tissue fibrosis or tumor progression [12-16]. Despite its importance, enzymatic activity of plasmin has rarely been measured directly. Instead, previous studies mostly focused on PAI1 or uPA expression as dynamic regulators of plasmin activity in fibrotic or tumorigenic tissues and concluded on possible changes in plasmin activity [13, 43, 261, 289, 290, 367]. Wu et al. correlated plasmin activity in lung tumor cells to metastasis. Horowitz et al. described a pro-apoptotic effect of plasmin on the IMR-90 fibroblast cell line [14, 367]. Interestingly, both studies used exogenous plasminogen (PLG) in order to detect endogenous plasmin activity. With pulmonary fibroblasts being the main drivers of fibrosis by producing ECM proteins and since plasmin activity has never been measured directly in primary human lung fibroblasts, the first aim of this work was to establish a protocol to monitor plasmin activity in living pHPF [103, 140].
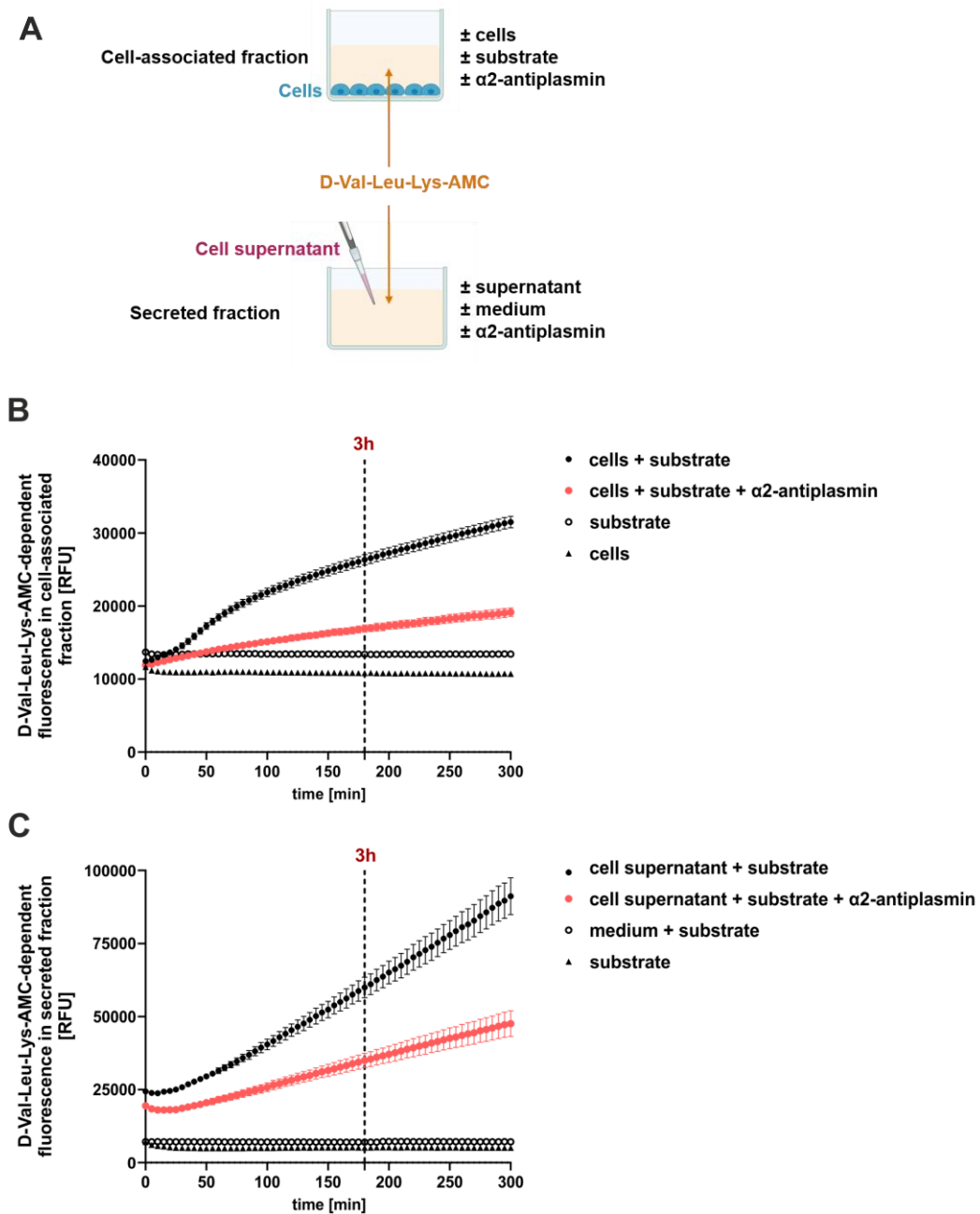
Figure 15: Effects of α2-antiplasmin on D-Val-Leu-Lys-AMC-dependent fluorescence in pHPF

A: Schematic overview of the plasmin activity assay. Cells were seeded into 96-well plates and after 24 h, supernatant and cells were incubated with the plasmin substrate (D-Val-Leu-Lys-AMC, 50 μM) at 37 °C for 5 h. As controls, cells or medium was either incubated alone or along with the substrate. Fluorescence intensity of the cell-associated fraction (**B**) and of the secreted fraction (**C**) was measured in 5 min intervals. Data of one exemplary experiment measured in octuplicates are shown as SEM of RFU. The line at 180 min indicates the standard incubation time used in further experiments. α2-antiplasmin (500 nM) was added 1 min before starting the measurement.

Since plasmin acts both in solution and cell-associated when bound to its surface receptors, the synthetic plasmin substrate D-Val-Leu-Lys-AMC was incubated directly with pHPF or their corresponding supernatant, as depicted in fig 15 a. D-Val-Leu-Lys-AMC-dependent fluorescence is thought to be dramatically increased after the AMC fluorophore has been released by cleavage via plasmin. To assess the specificity of the substrate, controls were added, where either substrate or cells were not included. Fig 15 b shows live measurement of D-Val-Leu-Lys-AMC-dependent fluorescence of the cell-associated fraction of pHPF over 300 min. When pHPF were incubated with the plasmin-specific substrate, a clear increase in fluorescence was detected. In cells that were not incubated with substrate, no increase in fluorescence was measured. Similarly, substrate that was not in contact with cells showed no increase in fluorescence over time, but signals were higher than in the control without substrate.

Substrate with no cell contact was therefore used as control for plasmin measurements to eliminate background (plasmin-independent) fluorescence. Co-stimulation with the plasmin inhibitor α2-antiplasmin decreased fluorescence signals, suggesting that fluorescence is indeed dependent on plasmin activity. D-Val-Leu-Lys-AMC-dependent fluorescence of the secreted fraction is shown in Fig 15 c. When pHPF supernatant was incubated with the substrate, fluorescence counts increased over time and this increase was again dampened by α2-antiplasmin. Substrate alone was added as control as well as substrate incubated with medium that was never in contact with cells. Both controls did not show an increase in fluorescence. Of note, in contrast to previous studies using other cells than pHPF, no addition of exogenous PLG to pHPF was required in order to detect endogenous plasmin activity of pHPF. However, to further attribute D-Val-Leu-Lys-AMC-dependent fluorescence to plasmin activity, cells were also stimulated with the plasmin-precursor plasminogen. As expected, a dramatic increase in fluorescence in both fractions was observed when plasminogen was added compared to basal conditions (Fig 16 a and b).
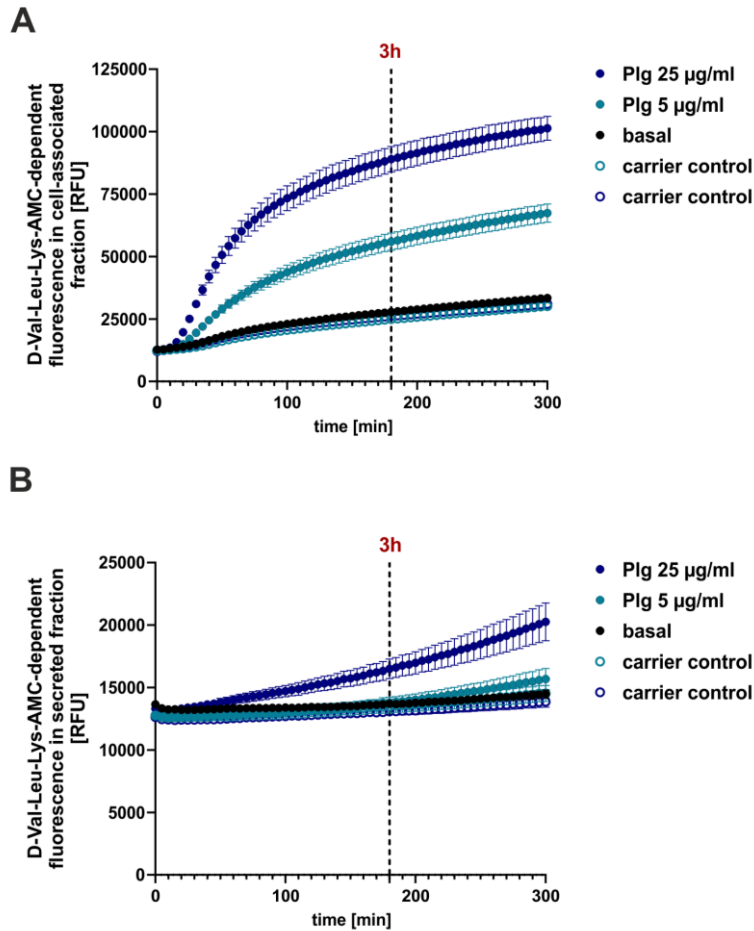
Figure 16: Effects of plasminogen on D-Val-Leu-Lys-AMC-dependent fluorescence in pHPF

Cells were incubated for 24 h with plasminogen (Plg; 5 µg/ml or 25 µg/ml) or glycerol as carrier control. Fluorescence intensity of the cell-associated fraction (**A**) and of the secreted fraction (**B**) was measured in 5 min intervals during incubation with D-Val-Leu-Lys-AMC (50 µM) at 37 °C for 5 h. Data of one exemplary experiment measured in octuplicates are shown as SEM of RFU. The line at 180 min indicates the standard incubation time used in further experiments.

Effects of α2-antiplasmin and plasminogen on D-Val-Leu-Lys-AMC-dependent fluorescence are summarized in fig 17 b. α2-antiplasmin reduced fluorescence to 0.39 ± 0.05 fold of basal in the cell-associated fraction and to 0.59 ± 0.02 fold under basal in the secreted fraction. When 5 µg/ml plasminogen was added, effects on both fractions were similar with an increase of 2.66 ± 0.13 fold over basal in the cell-associated and of 2.05 ± 0.21 fold over basal in the secreted fraction. Increasing plasminogen concentration to 25 µg/ml resulted in a stronger increase of fluorescence in the cell-associated fraction (5.41 ± 0.26 fold over basal) compared to the secreted fraction (3.30 ± 0.43 fold over basal).
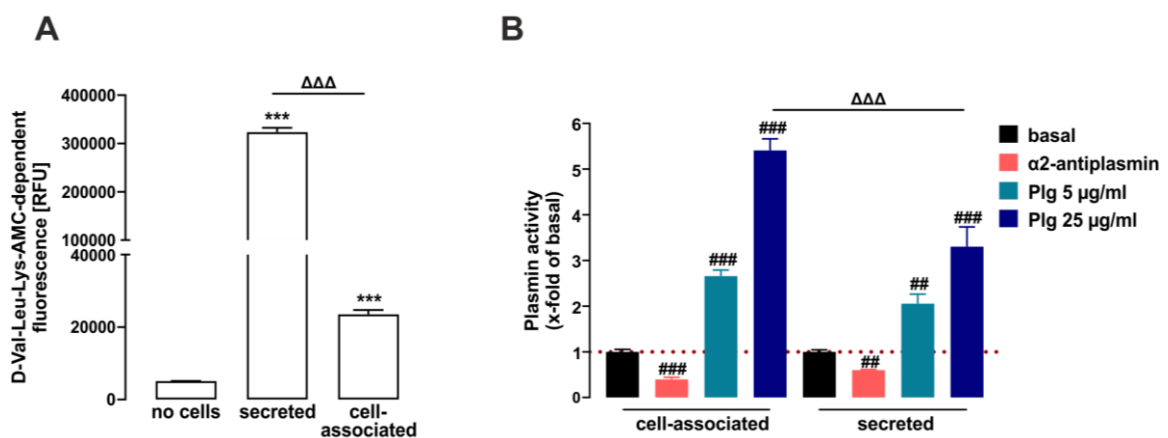
Figure 17: Analysis of D-Val-Leu-Lys-AMC-dependent fluorescence in pHPF

In **A**, RFU of secreted and cell-associated fraction after 3 h incubation with D-Val-Leu-Lys-AMC are compared, n = 3. In **B**, cells were incubated for 24 h with plasminogen (Plg; 5 µg/ml or 25 µg/ml) or α2-antiplasmin (500 nM) was added 1 min before starting 3 h incubation with D-Val-Leu-Lys-AMC. Results are displayed as SEM of x-fold of basal, n = 3-5. Statistical analysis was performed using one-way ANOVA (A) or two-way ANOVA (B) followed by Tukey´s post-test. Asterisks indicate significant differences to "no cells", hash signs indicate significant differences to basal, deltas indicate significant differences between the fractions, ## $p < 0.01$, ***/###/ΔΔΔ $p < 0.001$.

In summary, data shown so far led to the conclusion that the obtained fluorescence signal can be correlated to a specific D-Val-Leu-Lys-AMC turnover by plasmin, thus providing a tool to reliably measure plasmin activity in living pHPF. D-Val-Leu-Lys-AMC dependent fluorescence was therefore defined as indicator of plasmin activity. Of note, fluorescence of the secreted fraction was significantly higher than

of the cell-associated fraction, suggesting a different relevance of plasmin that is secreted or bound to its cell surface receptors. (Fig 17 a).

Finally, plasmin activity was measured in additional human lung cells to validate functionality of the plasmin activity assay in distinct lung cells. As shown in fig 18, plasmin activity of a lung epithelial cell line (16-HBE) and of primary human pulmonary artery endothelial cells (HPAEC) was determined (Fig 18). Plasmin activity could be measured reliably and plasmin activity was higher in the secreted fraction than in the cell-associated fraction in these cells, similar to the finding in pHPF. Thus, the established assay provided a tool for measuring plasmin activity in human lung cell lines as well as primary cells, independent of the used cell types.
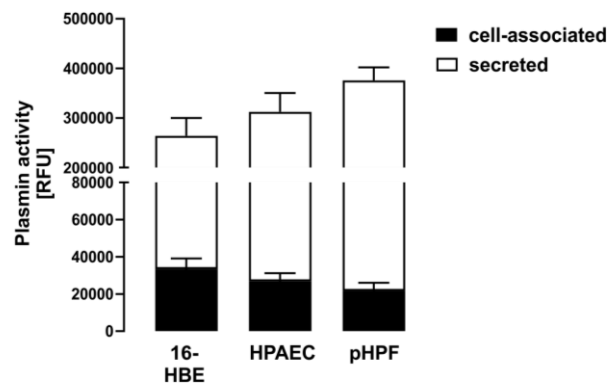
Figure 18: Comparison of plasmin activity of human lung cells

16-HBE, HPAEC and pHPF were seeded into 96-well plates and after 24 h, fluorescence intensity of the secreted and cell-associated fraction was measured after incubation with D-Val-Leu-Lys-AMC (50 µM) for 3 h at 37 °C. Bars represent SEM of basal plasmin activity displayed as RFU/SRB n = 10.

6.2 TGF-β affects the plasmin activation system in human lung cells

6.2.1 TGF-β activates SMAD signaling in pHPF

TGF-β is a central mediator of lung fibrosis by activating SMAD signaling, which triggers expression of SMAD-dependent genes and leads to enhanced ECM accumulation [368-370]. Of note, SMAD-dependent ECM accumulation could stem from direct induction of ECM proteins like collagen1 or fibronectin or from reduced ECM degradation via induction of PAI1 and consequent reduction of plasmin activity (see chapter 3.4.2.1). Second aim of this work was to study whether the previously described effects of TGF-β on SMAD signaling and expression of SMAD-dependent genes are also found in cultivated pHPF.

SMAD activation was examined using the pCAGA reporter plasmid, which contains the SMAD3/4 sensitive part of the human *SERPINE1* promotor [179]. Since no protocol for transfection of pHPF was available, an electroporation protocol was optimized in this work in order to achieve sufficient transfection of pHPF. Electroporation settings of 1650 V and 3 pulses for 10 ms were acquired from a fibroblast electroporation protocol obtained from the manufacturer of the electroporation system [371]. In previous experiments using epithelial cell lines, 500.000 cells and 5 µg DNA were used per electroporation step. In fig 19 a, data of unsuccessful electroporation is shown. 500.000 cells were electroporated with 5 or 10 µg plasmid DNA, but no reporter activity was detectable. Since electroporation settings need to fit perfectly to the targeted cell type, in order to ensure successful transfection, and cell number is one factor that influences the electric field in the sample, different cell numbers were tested. Taking into account that fibroblasts are considerably larger in size than epithelial cells, reduction of cell number seemed a reasonable possibility to optimize the electric field. Indeed, when using 250,000 cells per electroporation step, the best transfection was achieved and stimulation with TGF-β increased SMAD3/4 reporter activity as expected (fig 19 b). A summary of SMAD3/4 reporter activity after TGF-β stimulation is shown in fig 20 a. Reporter activity shown as RLU rose from 80,358 ± 7,262 to 394,769 ± 25,818 upon TGF-β stimulation. Since phosphorylation of SMAD2 is

crucial for TGF-β signaling, a phospho-SMAD2 ELISA Kit was used and a significant TGF-β-induced increase of SMAD2 phosphorylation was detected (fig 20 b).
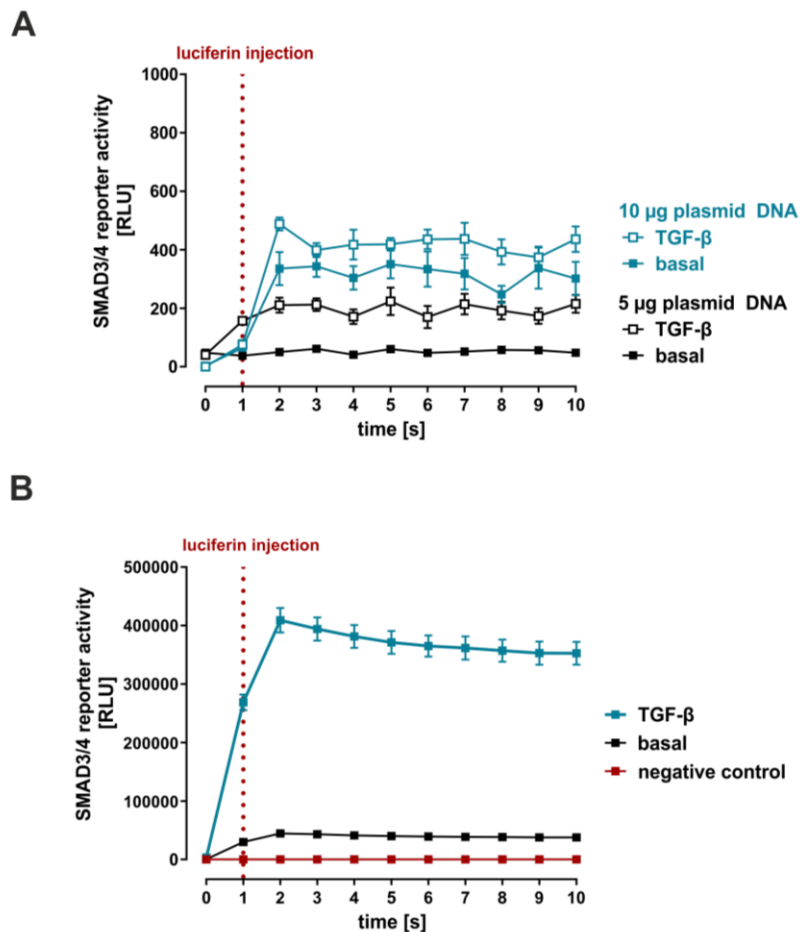
Figure 19: Optimization of the electroporation protocol for pHPF

pHPF were electroporated with the SMAD3/4 reporter plasmid. After 24 h, cells were stimulated with TGF-β (2 ng/ml) and luciferase activity determined. In **A**, 500.000 cells were transfected with the indicated amount of plasmid DNA. In **B**, 250.000 cells were electroporated with 5 µg plasmid DNA. Data are shown as triplicates from one representative experiment, n = 1. Light emission was measured for 10 s with luciferin being injected at 2 s. Results are displayed as SEM of random light units (RLU).
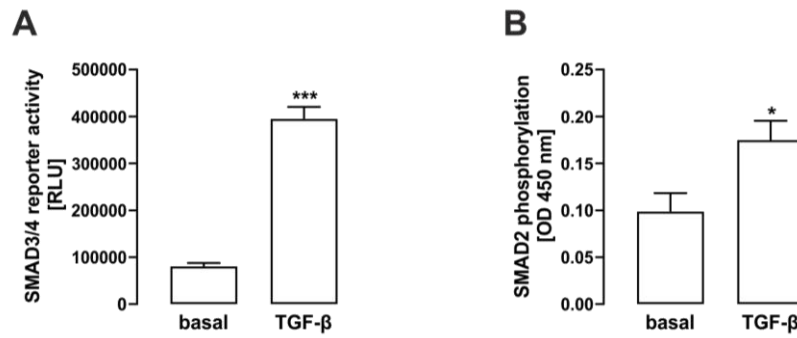
Figure 20: TGF-β induces SMAD activity in pHPF

In **A**, the PathScan® Phospho-Smad2 Sandwich ELISA Kit was used to determine SMAD2 phosphorylation after 40 min stimulation with TGF-β (2 ng/ml). Bars represent SEM of OD 450 values, n = 3. In **B**, pHPF were electroporated with the SMAD3/4 reporter plasmid. After 24 h, cells were stimulated with TGF-β (2 ng/ml) for 24 h and luciferase activity was determined. Bars represent SEM of x-fold over basal values, n = 3. Statistical analysis was performed using two-sample t-test. Asterisks indicate significant differences to DMSO, * $p<0.5$, *** $p<0.001$.
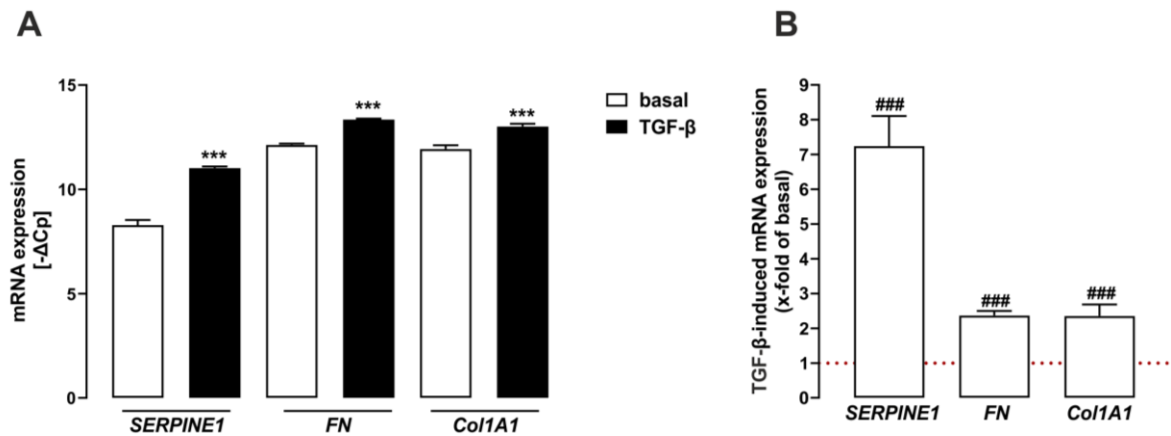
Figure 21: TGF-β induces *SERPINE1*, *FN1* and *Col1A1* mRNA expression in pHPF

SERPINE1, FN1 and *Col1A1* mRNA amounts of pHPF were determined by qRT-PCR after 24 stimulation with TGF-β (2 ng/ml). Bars represent SEM of –ΔCp or x-fold over basal values, n = 3-5. Statistical analysis was performed using two-way ANOVA (**A**) or one-way ANOVA (**B**) followed by Tukey´s post-test or one-sample t-test. Asterisks indicate significant differences to basal, hash signs indicate significant differences to one, ***/### $p<0.001$.

91

As stated before, TGF-β-induced SMAD signaling induces transcription of several genes. Therefore, mRNA levels of *SERPINE1*, *FN1* and *Col1* were tested. Accordingly, mRNA levels of all 3 genes were significantly enhanced after stimulation with TGF-β, however *SERPINE1* induction (7.24 ± 0.87 fold of basal) was considerably higher than *FN1* (2.37 ± 0.13 fold of basal) or *Col1* (2.35 ± 0.33 fold of basal) induction (fig 21 a and b). *SERPINE1* expression leads to PAI1 protein formation. Indeed, when stimulated with TGF-β, PAI1 protein levels increased in both cell-associated and secreted fraction (fig 22 a). When normalized to the basal PAI1 protein levels, TGF-β induced PAI1 protein levels by 2.37 ± 0.22 fold of basal in the cell-associated fraction and by 2.81 ± 0.45 fold of basal in the secreted fraction (fig 22 b).

It could therefore be concluded that TGF-β affected SMAD signaling and SMAD-dependent gene expression in cultivated pHPF as expected and that pHPF could thus be used as cellular model to study pulmonary fibrosis on the cellular level. Further, the higher induction of *SERPINE1* compared to *Col1A1* and *FN1* could indicate that TGF-β-induced SMAD signaling promotes ECM accumulation mainly via promoting the inhibitor of plasmin activity PAI1, rather than directly inducing expression of ECM genes.
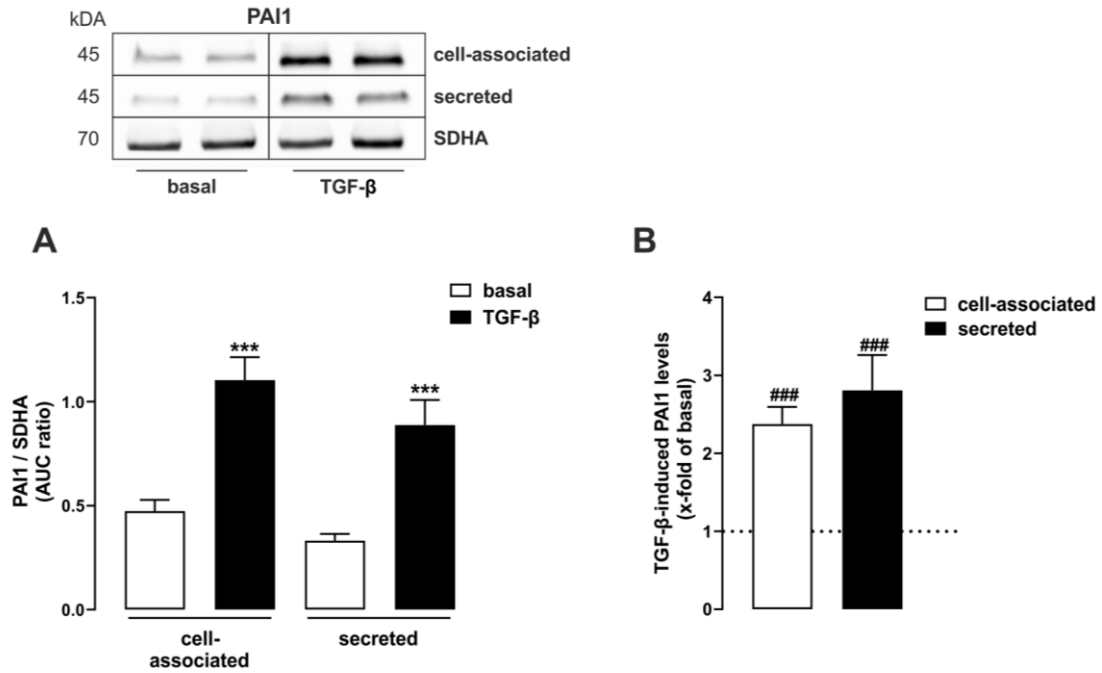
Figure 22: TGF-β increases PAI1 protein levels in pHPF

pHPF were stimulated with TGF-β (2 ng/ml) for 24 h. Protein amounts of PAI1 were determined in the cell-associated and secreted fraction via Western Blot and normalized to the loading control (SDHA) of the cell-associated fraction. Blots with the cell-associated fraction were cut in half to detect PAI1 (45 kDa) and SDHA (70 kDa). One set of representative blots is shown. Bars represent SEM of AUC ratios (**A**) or x-fold of basal (**B**), n = 3-4. Statistical analysis was performed using two-way ANOVA (A) or one-way ANOVA (B) followed by Tukey´s post-test. Asterisks indicate significant differences to basal, hash signs indicate significant differences to one, ***/### $p < 0.001$.

6.2.2 TGF-β reduces plasmin activity of pHPF

TGF-β-induced SMAD signaling resulted in increased expression of PAI1 (*SERPINE1*), a major regulator of the plasminogen activation system. Due to its inhibitory effects on plasminogen activators, increased levels of PAI1 should negatively affect plasmin activity. Thus, effects of TGF-β on plasmin activity were investigated in pHPF. TGF-β significantly reduced plasmin activity of pHPF in both fractions, however with 0.52 ± 0.04 fold compared to 0.30 ± 0.04 fold under basal, this effect was higher in the secreted fraction than in the cell-associated fraction (fig 23 a and b).
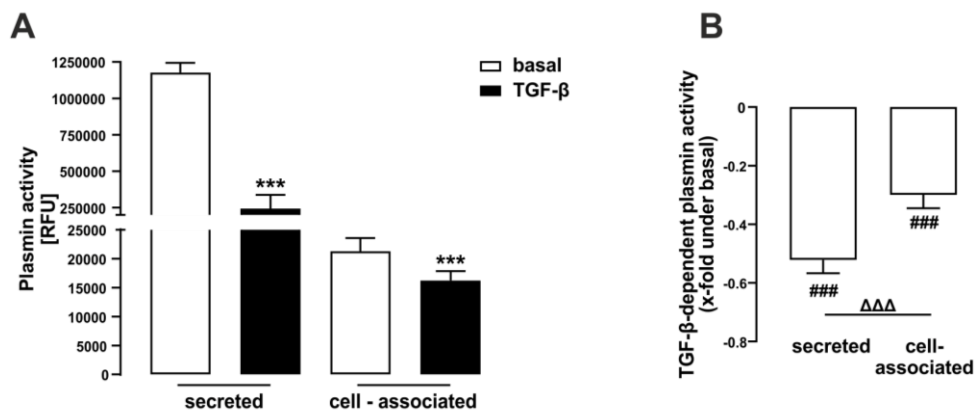
Figure 23: TGF-β reduces plasmin activity of pHPF

pHPF were stimulated with TGF-β (2 ng/ml) for 24 h and fluorescence intensity of the secreted and cell-associated fraction was measured after incubation with D-Val-Leu-Lys-AMC (50 µM) for 3 h at 37 °C. **A**: Bars represent SEM of RFU, n = 10. **B**: Bars represent SEM of % under basal values, n = 10. Statistical analysis was performed using two-way ANOVA (A) followed by Tukey´s post-test or one-sample t-test (B). Asterisks indicate significant differences to basal, hash signs indicate significant differences to zero, deltas indicate significant differences between fractions ***/###/ΔΔΔ $p<0.001$.
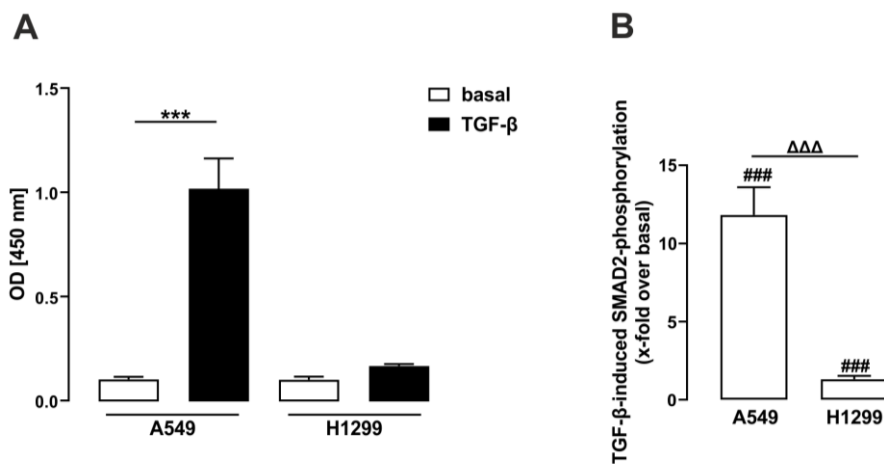
Observed increased PAI1 protein levels after TGF-β treatment therefore affected plasmin activity as expected. In a previous study with the IMR-90 fibroblast cell line, it was necessary to increase basal plasmin with exogenous plasminogen addition in order to monitor inhibitory effects of TGF-β [367]. Since the plasmin

inhibition by TGF-β was clearly detectable in lung fibroblasts used in this work, it was refrained from adding exogenous plasminogen.

To evaluate a possible cellular consequence of TGF-β-mediated decrease in plasmin activity, migration of pHPF was studied. Cell migration requires degradation of extracellular matrix and activation of the plasmin system has been linked to cell migration in previous studies [372, 373].

First, migration at high FCS was monitored to mimic the exact experimental settings of the plasmin activity assay. In accordance to the reduction in plasmin activity, TGF-β significantly decreased migration of pHPF in this protocol (fig 24 a). Additionally, cells were allowed to migrate with or without a serum-gradient. It could be shown that pHPF migration increases to 0.41 ± 0.09 fold over basal within a serum-gradient (fig 24 b and c). Interestingly, serum-induced migration was abolished when cells were stimulated with TGF-β (fig 24 b and c). Since these changes in migration could mistakenly be attributed to changes in proliferation, effects of TGF-β on cell number and viability were studied using the SRB or WST-1 assay (fig 24 d). Because TGF-β did not affect cell number or viability, inhibitory actions of TGF-β in the migration assay can most likely be attributed to direct effects on migratory features of pHPF via the observed depression of plasmin activity.
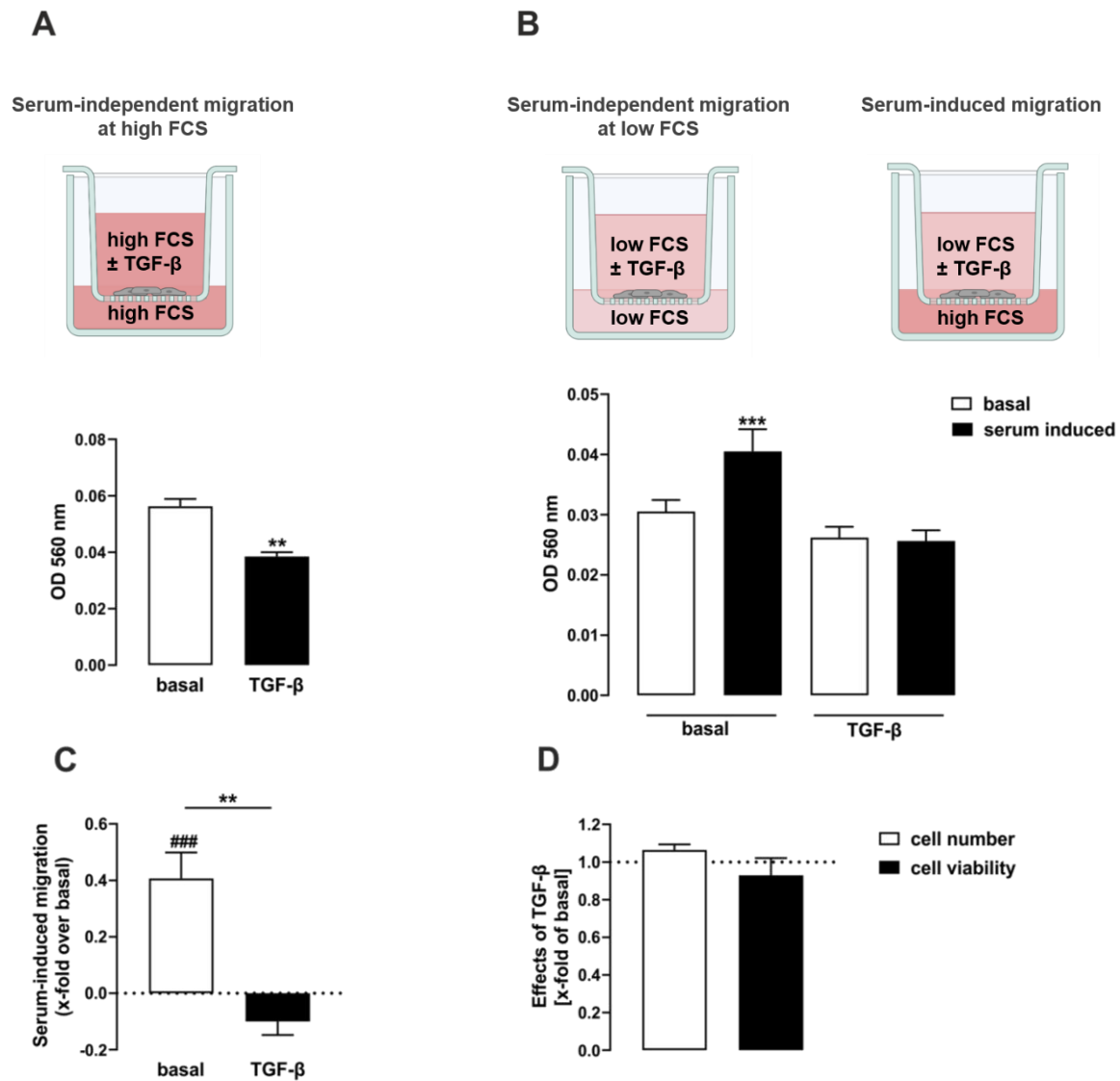
Figure 24: TGF-β reduces migration of pHPF

pHPF were added to the top compartment of Boyden chambers. After 24 h stimulation with TGF-β (2 ng/ml) cells located at the bottom side of the membrane were quantified. In **A**, serum-independent migration at 5% FCS was detected. In **B** and **C**, serum-induced (5 % FCS) was compared to serum-independent (0.5 % FCS) migration. Bars represent SEM of OD 560 values or x-fold over basal values, n = 3-5. In **D**, cell number was determined via SRB assay and cell viability was determined via WST-1 assay. Bars represent SEM of x-fold of basal, n= 3-6. Statistical analysis was performed using two-way ANOVA followed by Tukey´s post-test (B), two-sample t-test (A, C) or one-sample t-test (C). Asterisks indicate significant differences to basal, hash signs indicate significant differences to zero, ** $p < 0.01$, ***/### $p < 0.001$.

6.2.3 TGF-β signaling in lung tumor cells

After successfully analyzing effects of TGF-β on the plasmin system in pHPF, TGF-β-promoted regulation of the plasmin system was also investigated in the context of lung cancer. TGF-β signaling via SMAD proteins has previously been linked to ECM remodeling and consequent migration of tumor cells [374, 375]. Besides, targeting plasmin activation as modulator of ECM has been shown to affect tumorigenesis [14, 374, 376-378]. The role of TGF-β in tumorigenesis is complex, as in early stage cancer cells, TGF-β acts as a tumor suppressor, but promotes cell invasion and metastasis in late stages. This is commonly referred to as the "TGF-β-paradox" [272-274]. In this work, TGF-β signaling was compared in a stationary lung tumor cell line (A549) and in a highly invasive and metastatic tumor cell line derived from the lymph node (H1299). Interestingly, SMAD6, an inhibitor of TGF-β-induced SMAD signaling, is overexpressed in H1299 cells [293]. Thus, activity of SMAD proteins in A549 and H1299 cells was monitored. In fig 25, kinetics of SMAD2 phosphorylation were analyzed via western blot. While phosphorylation of SMAD2 peaked at 40 min in both cell lines, it was significantly lower in H1299 cells compared to A549 cells (fig 25). The same finding was discovered in fig 26 b using an ELISA specifically detecting pSMAD2. Here, TGF-β-induced SMAD2 phosphorylation was also dramatically higher in A549 (11.82 ± 1.77 fold of basal) compared to H1299 cells (1.30 ± 0.23 fold of basal). In line with these data, TGF-β induced SMAD3/4-dependent reporter activity significantly higher in A549 than in H1299 cells (fig 27 b). Interestingly, basal H1299 reporter activity was dramatically lower than in A549 (fig 27 a). To investigate if alternative signaling pathways are induced in H1299 cells, activity of YAP/TAZ was measured, which has been suggested as target of SMAD-independent TGF-β signaling in cancer cells [379]. While basal YAP/TAZ reporter activity did not differ between the cell lines, induction by TGF-β was significantly higher in A549 than in H1299 cells (fig 27 a and b). It could thus be concluded that TGF-β signaling via SMAD and also via YAP/TAZ was reduced in H1299 cells.
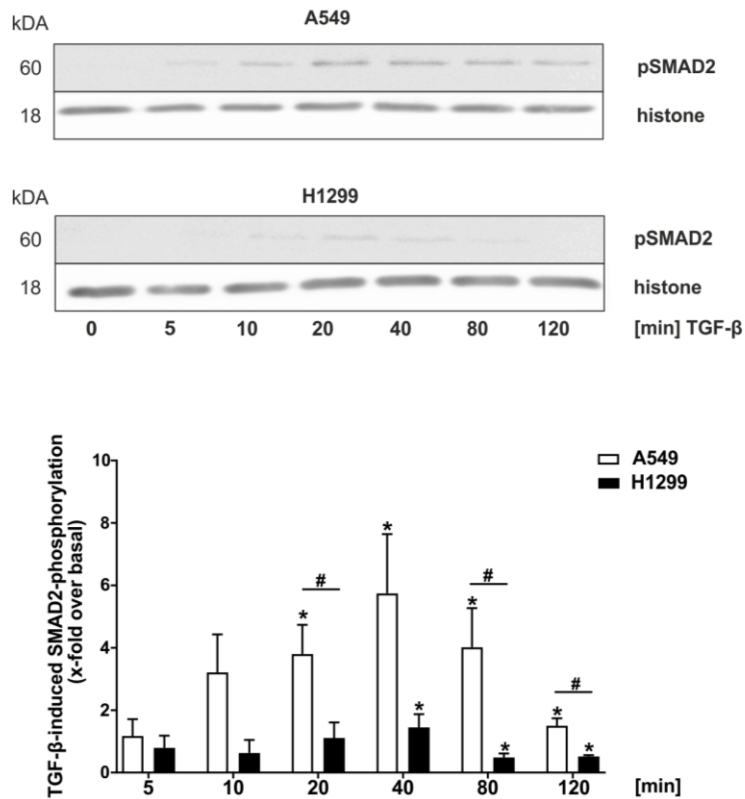
Figure 25: Kinetics of TGF-β-induced SMAD2-phosphorylation in human lung tumor cells

Cells were stimulated with TGF-β (2 ng/ml) for the indicated time periods and protein amount of pSMAD2 and histone (loading control) were determined via Western Blot. Blots were cut in half to detect pSMAD2 (60 kDa) together with the loading control histone (18 kDa). One set of representative blots is shown. Bars represent SEM of x-fold over basal, n = 3. Statistical analysis was performed using one-sample t-test or two-way ANOVA followed by Tukey´s post-test. Asterisks indicate significant differences to zero and hash signs indicate significant differences between cell lines, */# p<0.05.

Figure 26: TGF-β-induced SMAD2-phosphorylation in human lung tumor cells

Cells were stimulated with TGF-β (2 ng/ml) for 40 min and SMAD2-phosphorylation was determined using the PathScan® Phospho-Smad2 Sandwich ELISA Kit. Bars represent SEM of OD 450 values (**A**) or x-fold over basal (**B**), n = 4. Statistical analysis was performed using two-way ANOVA followed by Tukey´s post-test (A), two-sample t-test (B) or one-sample t-test (B). Asterisks indicate significant differences to basal, hash signs indicate significant differences to zero, deltas indicate significant differences between cells, ***/###/ΔΔΔ $p < 0.001$.
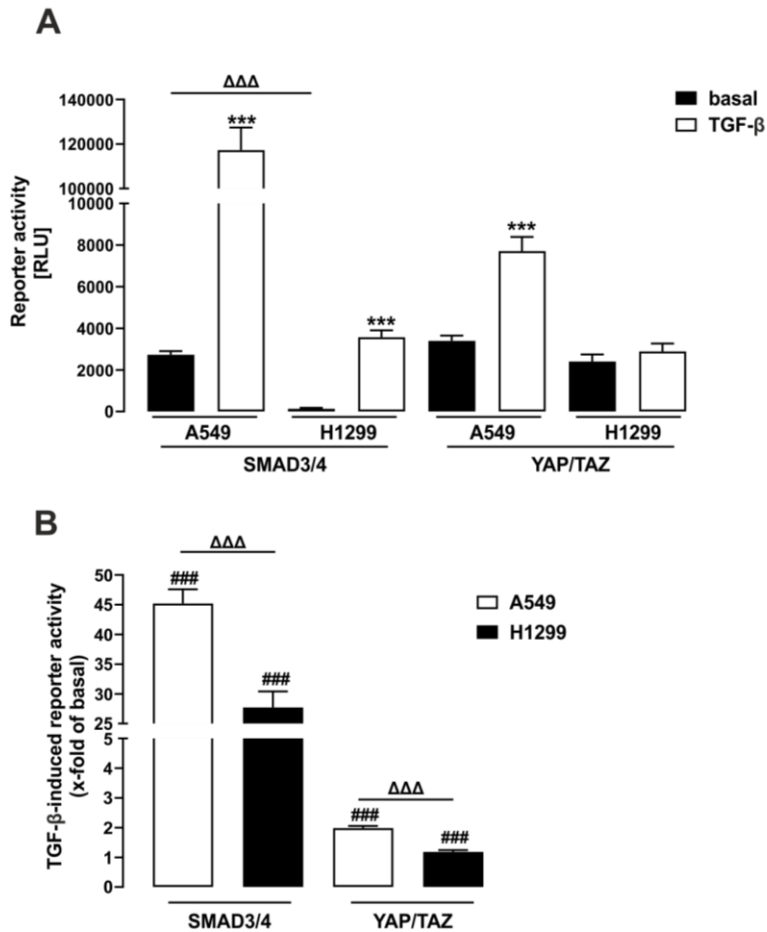
Figure 27: Effects of TGF-β on SMAD3/4 or YAP/TAZ activity in human lung tumor cells

Cells were transfected with the SMAD3/4 reporter plasmid or with the YAP/TAZ reporter plasmid. After 24 h, cells were stimulated with TGF (2 ng/ml) for 24 h and luciferase activity was determined. Bars represent SEM of RLU (**A**) or x-fold of basal (**B**), n = 10. Statistical analysis was performed using one-sample t-test or two-way ANOVA followed by Tukey´s post-test. Asterisks indicate significant differences to basal, hash signs indicate significant differences to one, deltas indicate significant differences between cells, ***/###/ΔΔΔ $p < 0.001$.

PAI1 expression is regulated by TGF-β/SMAD signaling. Due to the above mentioned upregulation of the inhibitory SMAD6 in H1299 cells and the observed reduction in SMAD activity in these cells, a weakened TGF-β–induced SMAD-dependent gene expression was proposed. Thus, PAI1 protein levels were compared in A549 and H1299 cells after TGF-β treatment. While TGF-β induced PAI1 protein levels in both fractions of both cell lines, induction was dramatically lower in H1299 compared to A549 cells (fig 28). In the cell-associated fraction of H1299 cells, TGF-β induced PAI1 protein levels only by 1.82 ± 0.42 compared to 11.78 ± 2.13 fold over basal in A549 cells. Similarly, induction in the secreted fraction was only 1.08 ± 0.29 in H1299 cells in comparison to 3.68 ± 1.00 fold over basal in A549 (fig 28). These data are in accordance with the diminished SMAD activity in H1299 cells and confirm weakened SMAD-dependent gene expression in these cells. In accordance to the increased PAI1 induction in A549 compared to H1299 cells, TGF-βinduced expression of the plasmin substrate fibronectin exclusively in A549, highlighting the distinct effects of TGF-β in solid or metastatic tumor cells based on alterations in SMAD signaling (fig 28).

Increased plasmin activity has previously been linked to tumor progression, however plasmin activity has rarely been measured directly, but assumptions on plasmin activity have been made based on the effects observed on PAI1 or uPA expression. To analyze, whether the observed differences in TGF-β-induced PAI1 and fibronectin expression were reflected on the level of plasmin activity, a plasmin activity assay was performed with A549 and H1299 cells. Interestingly, basal plasmin activity of both tumor cell lines A549 and H1299 was significantly lower compared to 16-HBE, HPAEC and pHPF (fig 18 and fig 29 b). This finding is unexpected, since increased activation of the plasmin system has been attributed to tumor cells, as described above. Surprisingly, the metastatic tumor cell line H1299 showed significant lower basal plasmin activity than the non-metastatic cell line A549 (fig 29 a and b). This result is contrary to previously postulated pro-metastatic effects of plasmin activity [14].

In A549 cells, TGF-β significantly decreased plasmin activity in both fractions (fig 29 a). Showing a reduction of -0.60 ± 0.03 in the cell-associated and -42 ± 0.04 fold under basal in the secreted fraction (fig 29 c and 23 b). Surprisingly and in

contrast to the reduction of plasmin activity observed in pHPF and A549, TGF-β stimulation in H1299 cells led to a strong increase in plasmin activity in both fractions (fig 29 a). In the secreted fraction, an increase of 0.93 ± 0.16 fold over basal was detected, TGF-β therefore nearly doubled basal plasmin activity (fig 29 c). The effect was smaller in the cell-associated fraction, but still a significant increase of 0.41 ± 0.07 fold over basal was observed (fig 29 c). This data show for the first time a direct correlation of PAI1 expression and plasmin activity in tumor cells and suggest that altered TGF-β signaling in distinct tumor cells affects plasmin activity differently.
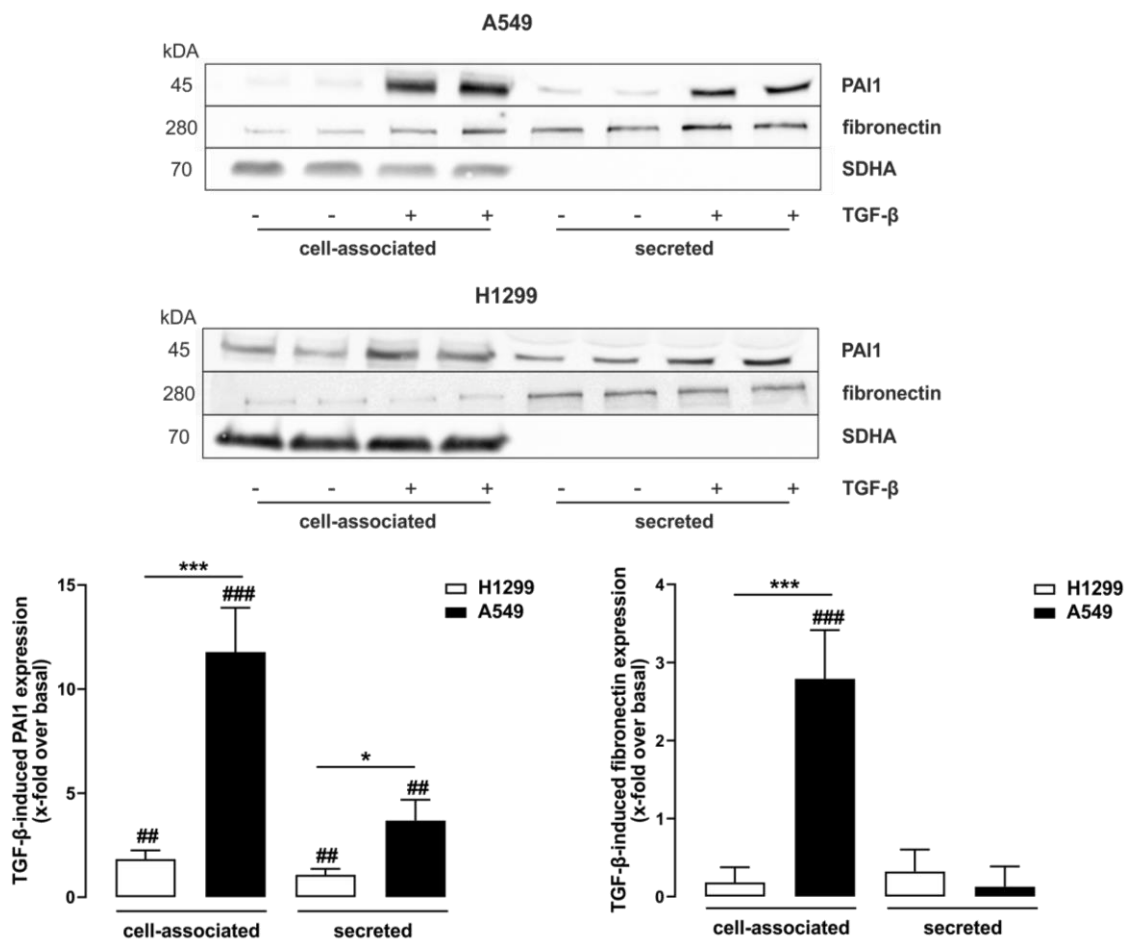
Figure 28: TGF-β-induced PAI1 or fibronectin protein levels in human lung tumor cells

A549 and H1299 cells were stimulated with TGF-β (2 ng/ml) for 24 h and protein amounts of PAI1, fibronectin and SDHA (loading control) were determined via Western Blot. Blots of the cell-associated fraction were cut in half to detect PAI1 (45 kDa) or fibronectin (280 kDa) together with SDHA (70 kDa). The loading control of the cell-associated fraction was also used for the secreted fraction. One set of representative blots is shown. Bars represent SEM of x-fold over basal, n = 4-7. Statistical analysis was performed using two-way ANOVA followed by Tukey´s post-test or one-sample t-test. Asterisks indicate significant differences between A549 and H1299 cells and hash signs indicate significant differences to zero, * $p<0.05$, ## $p<0.01$, ***/### $p<0.001$.
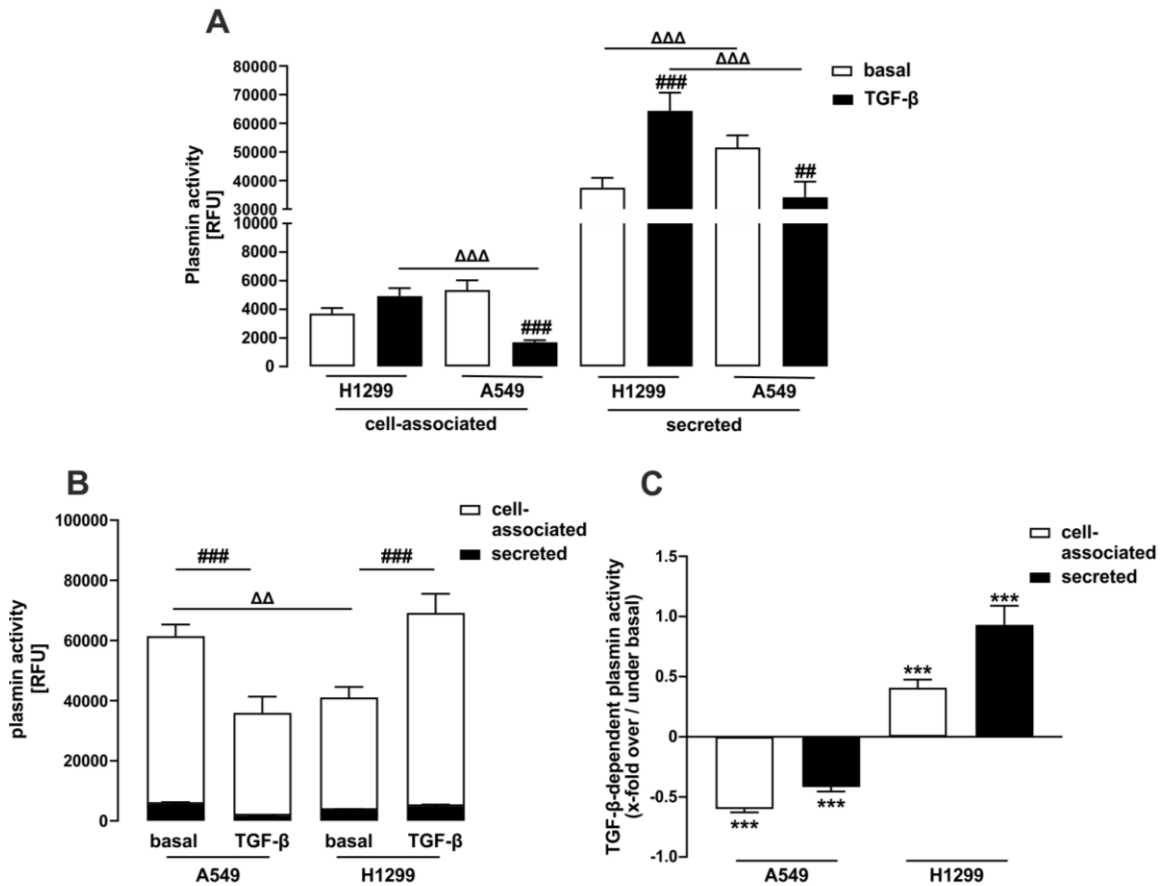
Figure 29: Effects of TGF-β on plasmin activity in human lung tumor cells

Cells were stimulated with TGF-β (2 ng/ml) for 24 h and fluorescence intensity of the secreted and cell-associated fraction was measured after incubation with D-Val-Leu-Lys-AMC (50 µM) for 3 h at 37 °C. **A**, **B**: Bars represent SEM of plasmin activity, n = 14. **C**: Bars represent SEM of % over/under basal values, n = 14. Statistical analysis was performed using two-way ANOVA (A) followed by Tukey´s post-test, two-sample t-test (B) or one-sample t-test (C). Asterisks indicate significant differences to zero, hash signs indicate significant differences to basal, deltas indicate significant differences between the two cell lines, ## $p<0.01$, ***/###/ΔΔΔ $p<0.001$.

6.2.4 Altered TGF-β signaling in lung tumor cells

Since the increase in plasmin activity in H1299 cells after stimulation with TGF-β was entirely unexpected, mRNA levels of modulators regulating plasmin activity were analyzed in A549 and H1299 cells.

First, mRNA levels of the *SERPINE1* (PAI1, fig 30 a) and *SPINT2* (HAI2, fig 30 b) gene were compared after TGF-β treatment. Interestingly, H1299 cells have been shown to express lower levels of HAI2 protein and *SPINT2* mRNA compared to A549 cells [14]. However, effects of TGF-β on *SPINT2* expression have not yet been described. H1299 cells showed higher basal *SERPINE1* expression than A549 cells (fig 30 a). TGF-β increased mRNA expression to 5.67 ± 0.46 in A549, but only to 1.93 ± 0.41 fold of basal in H1299 cells (fig 30 a and e). This finding correlates with the previously shown effects on PAI1 protein levels (fig 28). Expression of the *SPINT2* gene leads to production of the HAI2 protein, a direct plasmin inhibitor [14]. H1299 showed significantly lower *SPINT2* expression compared to A549 cells, as expected from the previous study. Interestingly, TGF-β decreased *SPINT2* expression to 0.34 ± 0.04 fold of basal in A549 (fig 30 b and e), but had no effects in H1299 cells. Thus, regulation of HAI2 levels does not account for the plasmin induction by TGF-β in H1299 cells. Further, mRNA levels of *PLAU*, the gene encoding for uPA and *PLAUR*, which encodes the uPA receptor were analyzed. While no differences in basal *PLAU* or *PLAUR* expression were detected, TGF-β led to a significant decrease of *PLAU* and *PLAUR* in A549 and to an increase of *PLAU* in H1299 cells (fig 30 c, d and e). With plasmin being the product of plasminogen cleavage by uPA, the effects of TGF-β on *PLAU* expression could count for the distinct effects of TGF-β on plasmin activity in A549 and H1299 cells.
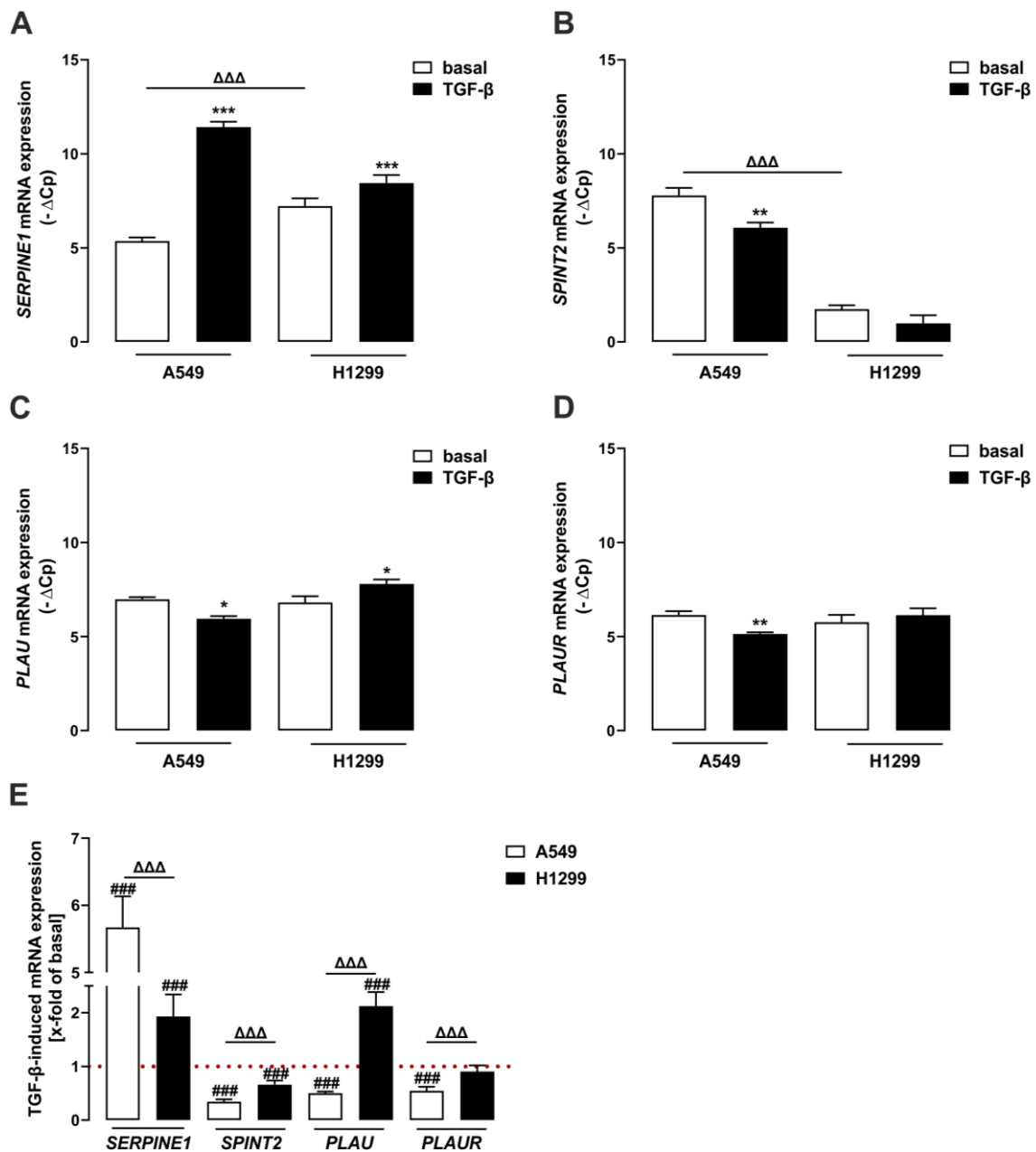
Figure 30: TGF-β-induced mRNA expression in human lung tumor cells

A549 and H1299 cells were stimulated with TGF-β (2 ng/ml) for 24 h and *SERPINE1* (**A**)*, SPINT2* (**B**)*, PLAU* (**C**) *and PLAUR* (**D**) mRNA was determined by qRT-PCR. Bars represent SEM of –Δcp (A-D) or x-fold of basal (**E**), n = 3-4. Statistical analysis was performed using two-way ANOVA followed by Tukey´s post-test (A-D), one-sample t-test (E) or two-sample t-test (E). Asterisks indicate significant differences to basal, hash signs indicate significant differences to one, deltas indicate significant differences between the two cell types, * $p<0.05$, ** $p<0.01$, ***/###/ΔΔΔ $p<0.001$.

To study a cellular consequence of the distinct effects observed of TGF-β on plasmin activity and to see how this affects solid tumor cells in comparison to metastatic tumor cells, A549 and H1299 cells were tested in a migration assay. Firstly, serum-independent migration was measured, thereby simulating conditions of the plasmin activity assay. The solid tumor cell line A549 showed increased basal migration compared to the metastatic cell line H1299 (fig 31 d). TGF-β affected migration of both cells accordingly to its effects on plasmin activity: TGF-β increased migration of H1299, but decreased migration of A549 (fig 31 d). When migrating within a serum gradient, migration of H1299 cells was reduced by TGF-β, whereas migration of A549 cells was enhanced by the cytokine (fig 31 c). These effects however could also be attributed to the changes on basal serum-independent migration after TGF-β stimulation (fig 31 a and b). These data suggest that TGF-β signaling is crucial for migratory features of cancer cells and that directly targeting TGF-β-signaling may be a means to modulate migration of cancer cells.
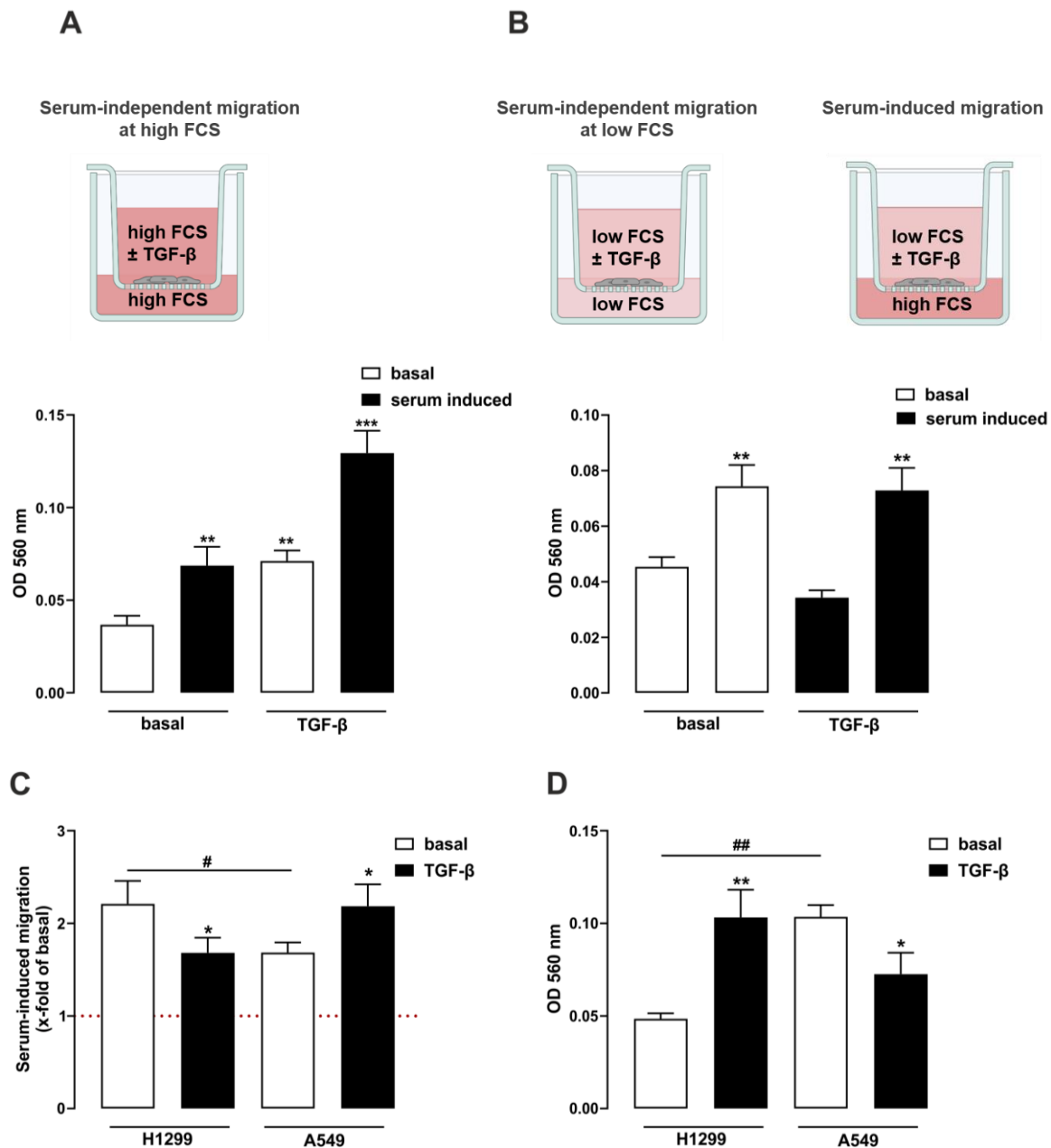
Figure 31: Effects of TGF-β on migration of human lung tumor cells

H1299 (**A**) or A549 (**B**) cells were added to the top compartment of a Boyden chamber. After 24 h stimulation with TGF-β (2 ng/ml) cells located at the bottom side of the membrane were quantified In **A**, **B** and **C**, serum-induced (10 % FCS) was compared to serum-independent (0.5 % FCS) migration. In **D**, serum-independent migration at 10 % FCS was detected. Bars represent SEM of OD 560 values or % of basal values n = 3-6. Statistical analysis was performed using two-way ANOVA followed by Tukey´s post-test. Asterisks indicate significant differences to basal, hash signs indicate significant differences between A549 and H1299, */# $p<0.05$, **/## $p<0.01$, *** $p<0.001$.

6.2.5 Activity of extracellular-regulated kinases-1/2 (ERK-1/2) affects TGF-β signaling in lung tumor cells

A549 and H1299 cells carry a mutation in the proto-oncogenes K-ras or N-ras, respectively, which both activate the MEK/ERK signaling pathway [297-299]. Additionally, MEK/ERK signaling has been shown to interact with TGF-β/SMAD signaling and the plasmin system [304-306, 380]. Therefore, in order to obtain first data about the underlying signaling events responsible for the unusual effects of TGF-β on plasmin activity in H1299 cells, basal and TGF-β-induced ERK1/2 phosphorylation was studied in A549 and H1299 cells. As shown in fig 32 a, basal ERK1/2 phosphorylation was significantly higher in H1299 cells compared to A549 cells, while total levels of ERK1 were comparable (fig 32 b). After stimulation with TGF-β for 24 h, ER1/2 phosphorylation levels were significantly increased in both cell lines (fig 32 c). With 2.18 ± 0.09 fold of basal, induction of ERK1/2 phosphorylation was, however, significantly higher in H1299 compared to 1.46 ± 0.15 fold of basal in A549 cells. Since increased levels of phosphorylated ERK1/2 could also be explained by an increase in expression of the protein, ERK1 levels were studied. Levels of ERK1 remained unchanged after stimulation with TGF-β, thus effects of TGF-β on ERK1 expression could be excluded (fig 32 d). These data thus give a first hint at a distinct importance of ERK1/2 activation in A549 and H1299.

To further decipher whether ERK1/2 plays a role in the effects observed on plasmin activity in H1299 cells, the ERK-inhibitor PD184352 was tested. Firstly, basal plasmin activity significantly increased in H1299 upon ERK inhibition, but not in A549 cells (fig 33 a and b). While TGF-β effects in A549 cells remained unchanged during co-stimulation with PD184352, the enhancing effect of TGF-β on plasmin in H1299 cells was no longer detectable, instead a significant decrease in plasmin activity was observed (fig 33 a and b). When normalized to basal values, the TGF-β-induced increase in plasmin activity of 0.96 ± 0.26 over basal was reversed to an inhibition of plasmin activity of 0.36 ± 0.11 under basal upon PD184352 incubation (fig 33 c). This reduction of plasmin activity was similar to the TGF-β-induced reduction in A549 with 0.45 ± 0.03 fold under basal (fig 33 c). These data

strongly indicate that ERK1/2 activity is responsible for the unexpected effect of TGF-β on plasmin activity.

ERK1/2-inhibition has previously been linked to the YAP/TAZ signaling pathway and SMAD signaling in lung cells [177, 252]. Thus, SMAD3/4 and YAP/TAZ reporter activity upon ERK1/2-inhibition was also studied. As shown in fig 34 a, PD184352 increased basal SMAD3/4 reporter activity of H1299, but not of A549 cells. In contrast, no effect of PD184352 on basal YAP/TAZ activity was detected (fig 34 b). In A549, TGF-β-induced SMAD3/4 and YAP/TAZ reporter activity was significantly reduced with PD184352, but not in H1299 (fig 34 c and d). These data indicate distinct effects of ERK1/2 signaling on SMAD or YAP/TAZ signaling in A549 and H1299 cells.
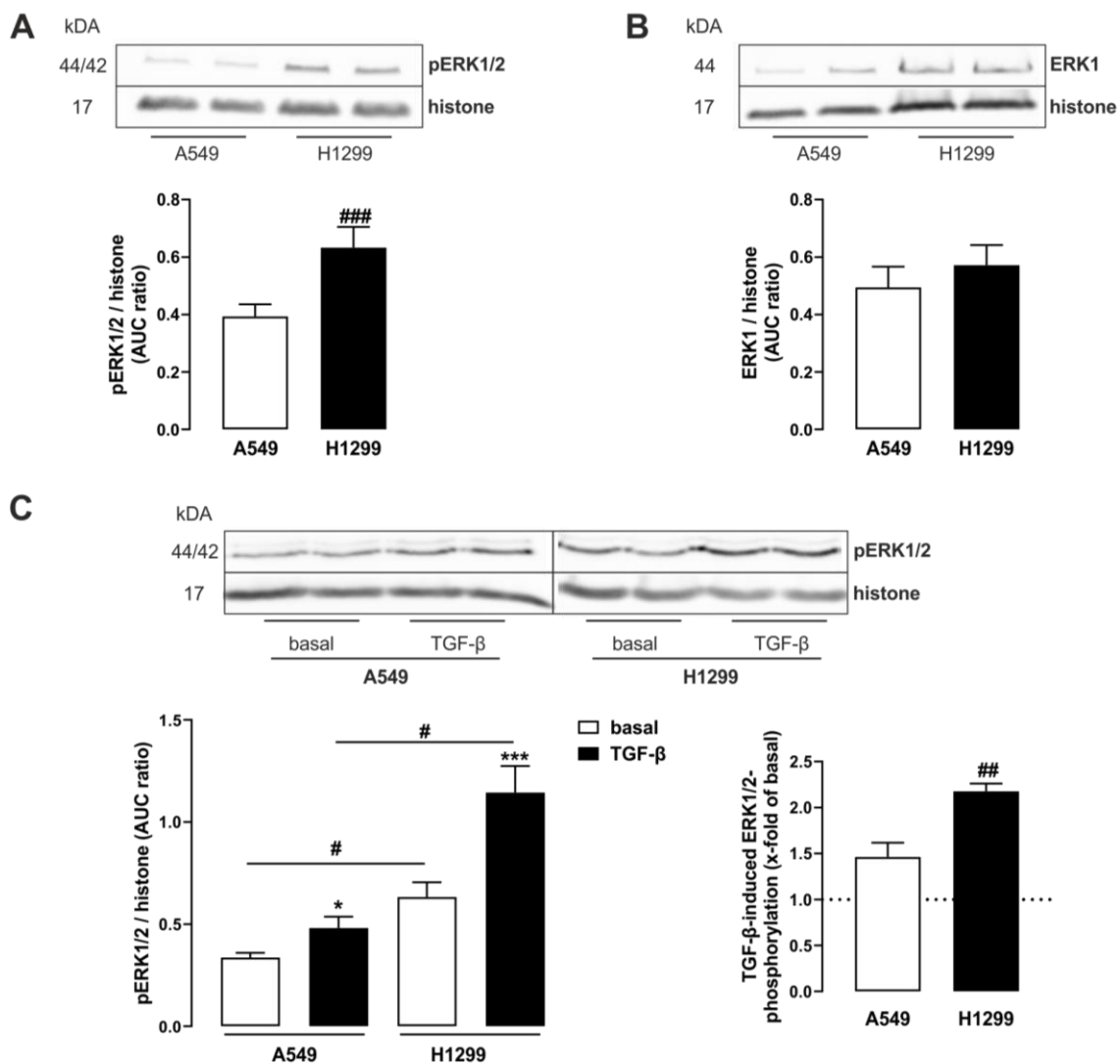
D
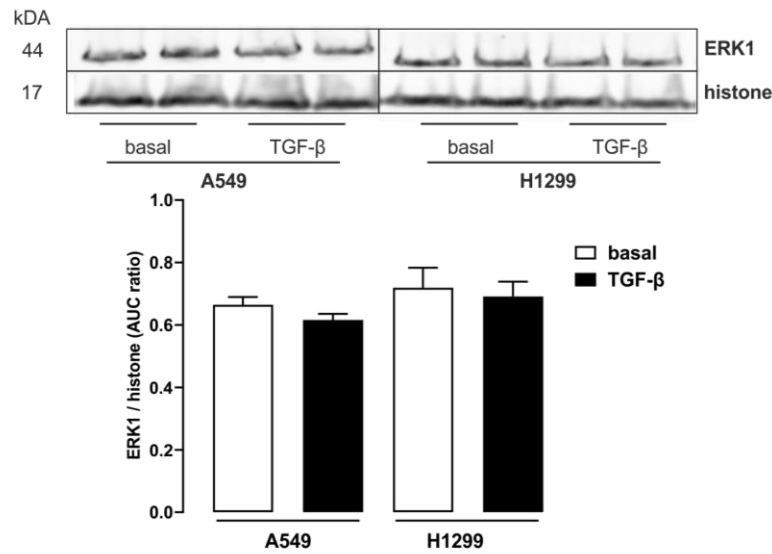
Figure 32: Basal and TGF-β-induced ERK1/2 phosphorylation and ERK1 levels in A549 and H1299 cells

A549 and H1299 cells were stimulated with TGF-β (2 ng/ml) for 24 h and protein amounts of pERK1/2, ERK1 and histone (loading control) were determined via Western Blot. Blots were cut in half to detect pERK1/2 (44/42 kDa), ERK1 (44 kDa) and the loading control histone (18 kDa). Basal levels of pERK1/2 (**A**) and ERK1 (**B**) or effects of TGF-β on pERK1/2 (**C**) or ERK1 (**D**) are displayed. One set of representative blots is shown. Bars represent SEM of AUC ratios or x-fold of basal, n = 3. Statistical analysis was performed using two-way ANOVA followed by Tukey´s post-test or two-sample t-test. Asterisks indicate significant differences to basal, hash signs indicate significant differences between A549 and H1299 cells, */# $p < 0.05$, ## $p < 0.01$, ***/### $p < 0.001$.

C
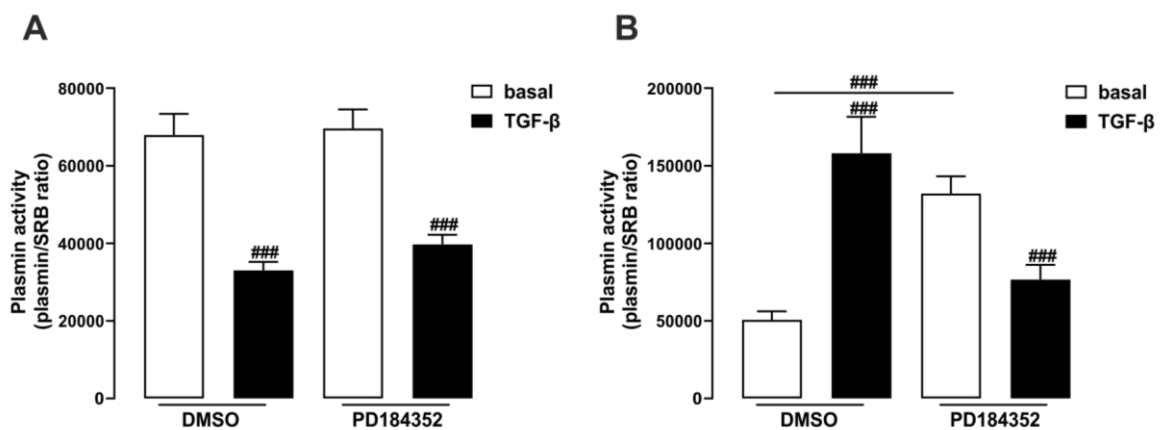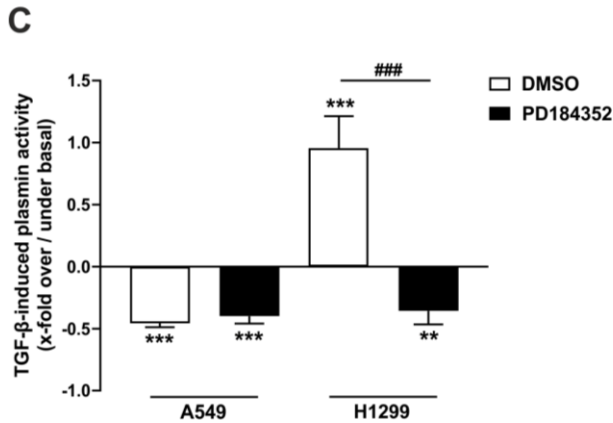
Figure 33: Effects of PD184352 on plasmin activity in human lung tumor cells

A549 (**A**) or H1299 cells (**B**) were stimulated with PD184352 (10 µM), TGF-β (2 ng/ml) or co-stimulated for 24 h and fluorescence intensity of the secreted fraction measured after incubation with D-Val-Leu-Lys-AMC (50 µM) for 3 h at 37 °C. Bars represent SEM of RFU/SRB ratios (A, B) or x-fold over/under basal (**C**), n = 3. Statistical analysis was performed using two-way ANOVA followed by Tukey´s post-test or one-sample t-test. Asterisks indicate significant differences to zero and hash signs indicate significant differences to basal or DMSO, ** $p<0.01$, ***/### $p<0.001$.
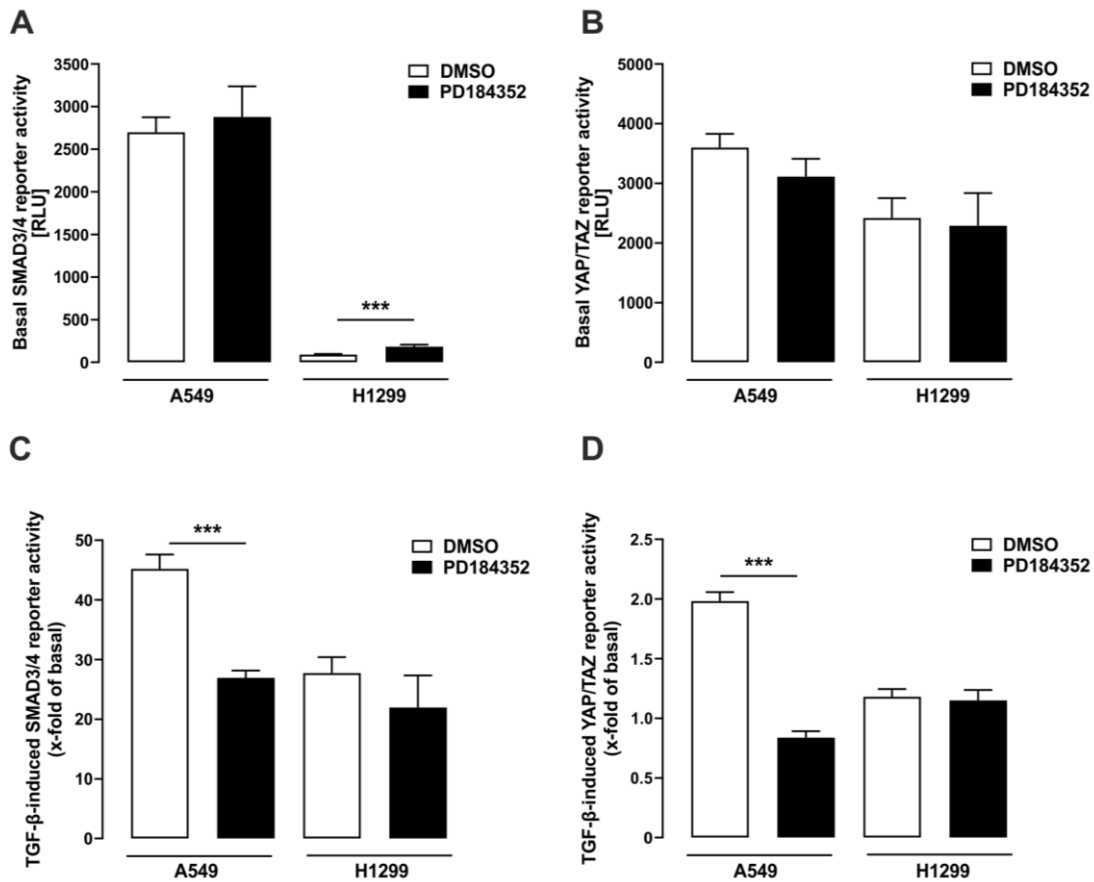
Figure 34: Effects of PD184352 on SMAD3/4 or YAP/TAZ activity in human lung tumor cells

Cells were transfected with the SMAD3/4 reporter plasmid (**A**, **C**) or with the YAP/TAZ reporter plasmid (**B**, **D**). After 24 h, cells were stimulated with TGF-β (2 ng/ml) or PD184352 (10 µM) or co-stimulated for 24 h and luciferase activity was determined. Bars represent SEM of RLU (A, B) or % of basal (C, D) n = 5. Statistical analysis was performed using two-way ANOVA followed by Tukey´s post-test. Asterisks indicate significant differences to basal, *** $p<0.001$.

Since ERK1/2 activity is crucial for cell proliferation and survival, possible cytotoxic effects of PD184352 were assessed using SRB assay. After 24h incubation, no effects on cell proliferation were visible in both cell lines, indicating that the abovementioned effects of PD184352 are independent of cytotoxic effects (fig 35 a). After 5 d of stimulation, PD184352 significantly reduced cell number in both cell lines (fig 35 b). Interestingly, after five days, TGF-β was highly cytotoxic for A549 cells, but not for H1299 cells (fig 35 b and d). TGF-β-induced cell toxicity was also tested after 24 h, in order to exclude that TGF-β effects on plasmin activity in A549 cells (see chapter 6.2.3) relied on cytotoxic effects, but no effects could be detected (fig 35 c). Finally, during co-stimulation of TGF-β and PD184352 for 5 d, TGF-β-induced cell toxicity was completely reversed in A549, while no effects where visible in H1299 (fig 35 d).
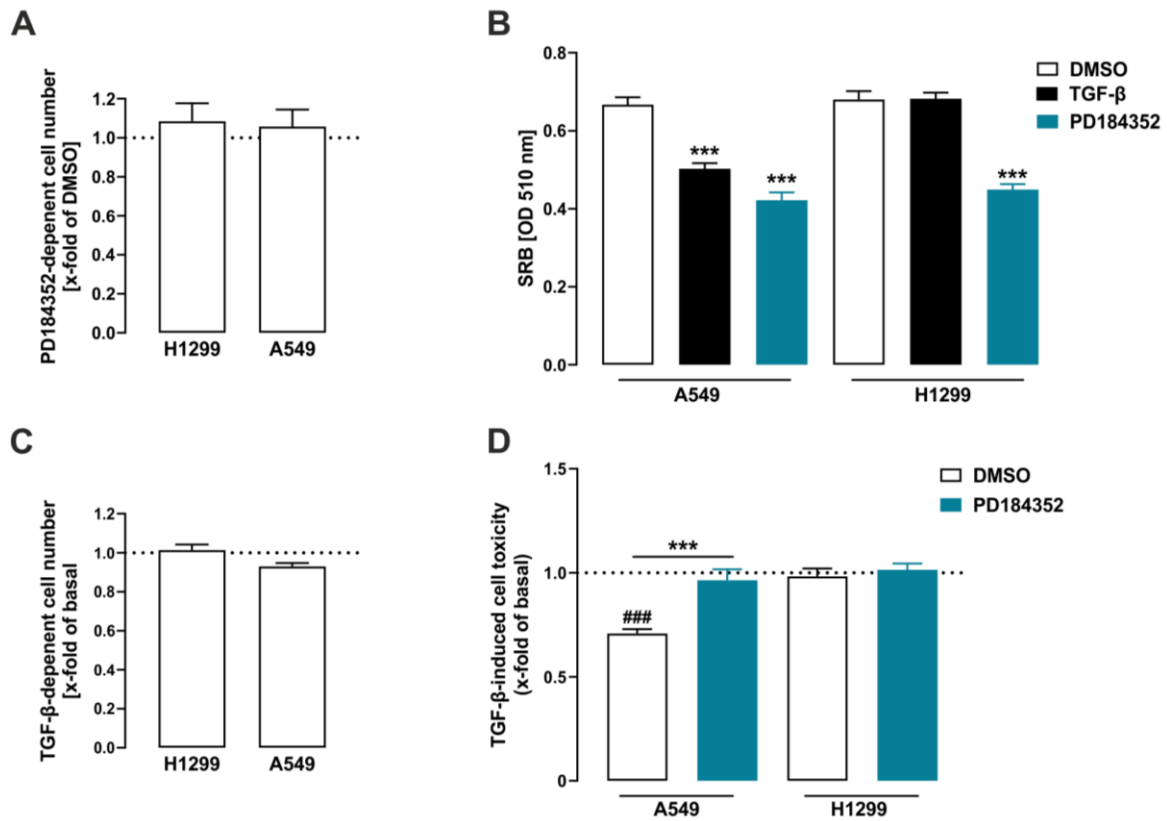
Figure 35: Effects of TGF-β or PD184352 on cell number in human lung tumor cells

Cells were stimulated with TGF-β (2 ng/ml) or PD184352 (10 µM) or co-stimulated for or 24 h (**A**, **C**) or 5 d (**B**, **D**) and cell number determined with the SRB assay. B Bars represent SEM of OD 510 values, n = 6-8. A, C, D Bars represent SEM of x-fold of DMSO values, n = 6. Statistical analysis was performed using two-way ANOVA (B, D) followed by Tukey´s post-test or one-sample t-test (D). Asterisks indicate significant differences to DMSO and hash signs indicate significant differences to 1, ***/### $p<0.001$.

6.3 TRPM7 activity affects the plasmin activation system in human lung cells

### 6.3.1 Blockade of TRPM7 activity enhances plasmin activity in pHPF

TRPM7 has recently been proposed as potential drug target in fibrotic diseases due to its association with the development of heart and kidney fibrosis [312, 330, 331]. Downregulation of TRPM7 in MRC5 cells, a fetal human lung fibroblast cell line, led to reduction of TGF-β-induced collagen1 expression, a substrate of active plasmin [333]. Interestingly, TRPM7 has been shown to directly phosphorylate SMAD2 via its kinase domain in T-cells [329]. Apart from changes in uPA expression in lung cancer cells, TRPM7 activity has however not been linked to the plasmin system before [345]. Likewise, effects of TRPM7 in pHPF are unknown. Thus, it was proposed that SMAD2 could be a possible target of TRPM7 to affect the plasmin system and consequently ECM in pHPF.

To assess a possible link between TRPM7 and plasmin activity, the small molecule TRPM7 blocker NS8593 was used [324]. pHPF were treated with different concentrations of NS8593 and plasmin activity in the secreted or cell-associated fraction was measured. After 24 h stimulation, a concentration dependent increase of plasmin activity was found in the cell-associated fraction of pHPF (fig 36 a and e). A significant increase of 1.10 ± 0.12 fold over basal with 50 µM NS8593, of 0.63 ± 0.09 for 25 µM and of 0.30 ± 0.06 for 12.5 µM was found (fig 36 e). Increased plasmin activity was also observed in the secreted fraction, with 0.28 ± 0.06 for 50 µM and 0.02 ± 0.05 for 25 µM, the effect was noticeable smaller than in the cell-associated fraction (fig 36 b and f). No increase in plasmin activity in both fractions was found after 4 h stimulation with NS8593, indicating that immediate blockade of TRPM7 has no effects on the plasmin system (fig 36 c-f). As NS8593 not only blocks TRPM7 but also SK channels, the selective SK blocker apamin was used as control [325, 326, 381]. No significant effects of apamin on plasmin activity were observed in both fractions, indicating that TRPM7 but not SK channels are linked to the plasmin system (fig 37 a-c).
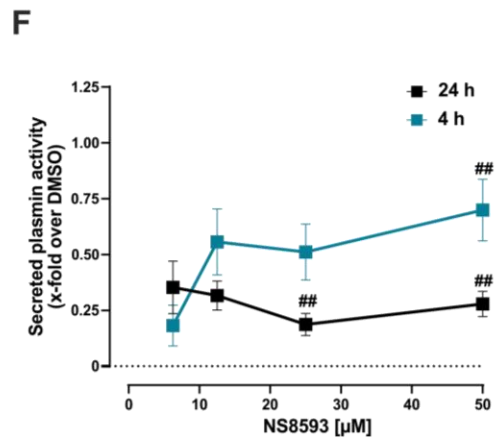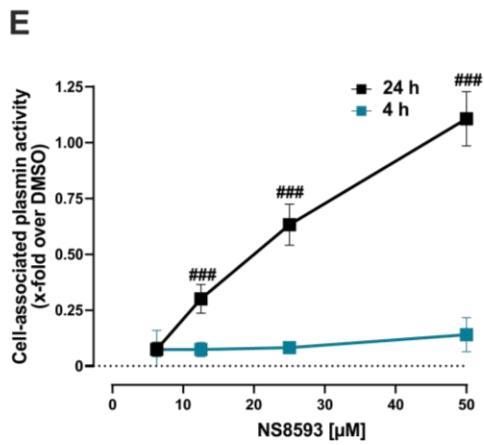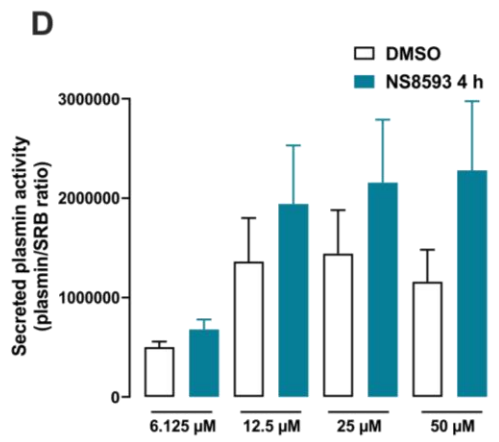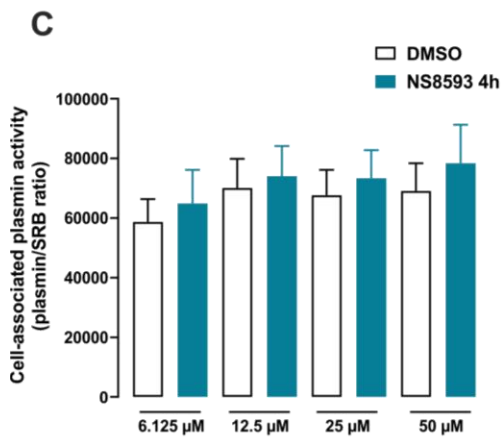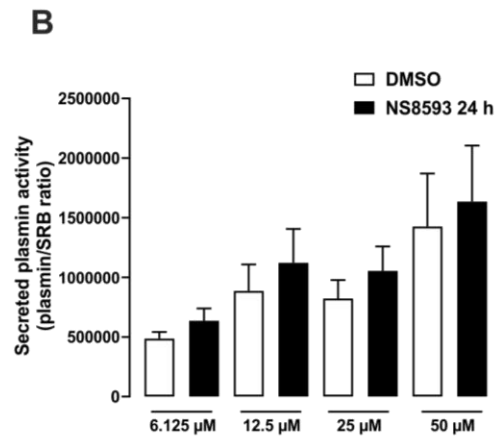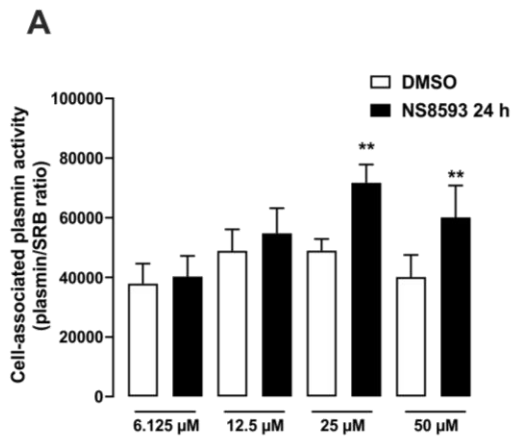
Figure 36: NS8593 enhances plasmin activity of pHPF

pHPF were stimulated with the indicated concentrations of NS8593 for 24 h (**A**, **B**) or 4 h (**C**, **D**) and fluorescence intensity of the cell-associated (**A**, **C**, **E**) and secreted (**B**, **D**, **F**) fraction measured after incubation with D-Val-Leu-Lys-AMC (50 µM) for 3 h at 37 °C. Plasmin activity is displayed as SEM of RFU/SRB ratios (A-D) or x-fold over DMSO (E, F), n = 3-8. Statistical analysis was performed using two-way ANOVA followed by Tukey´s post-test (A) or one-sample t-test (E, F). Asterisks indicate significant differences to DMSO, hash signs indicate significant differences to zero, * $p<0.05$, **/## $p<0.01$, ***/### $p<0.001$.
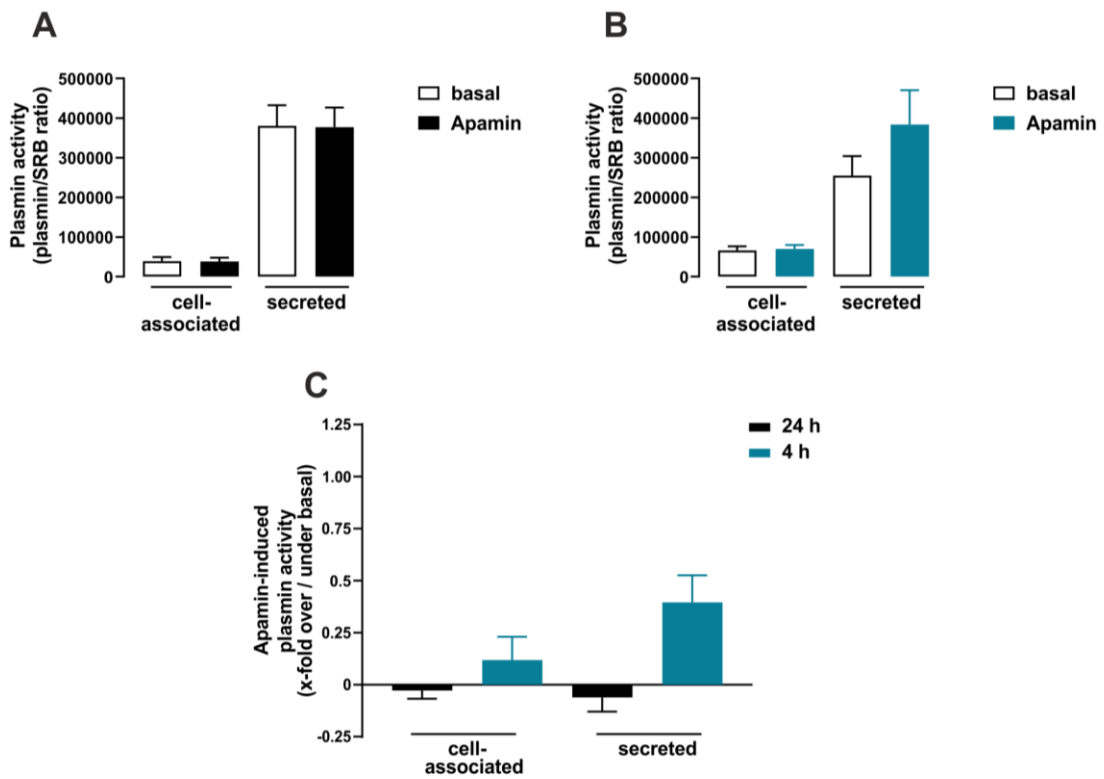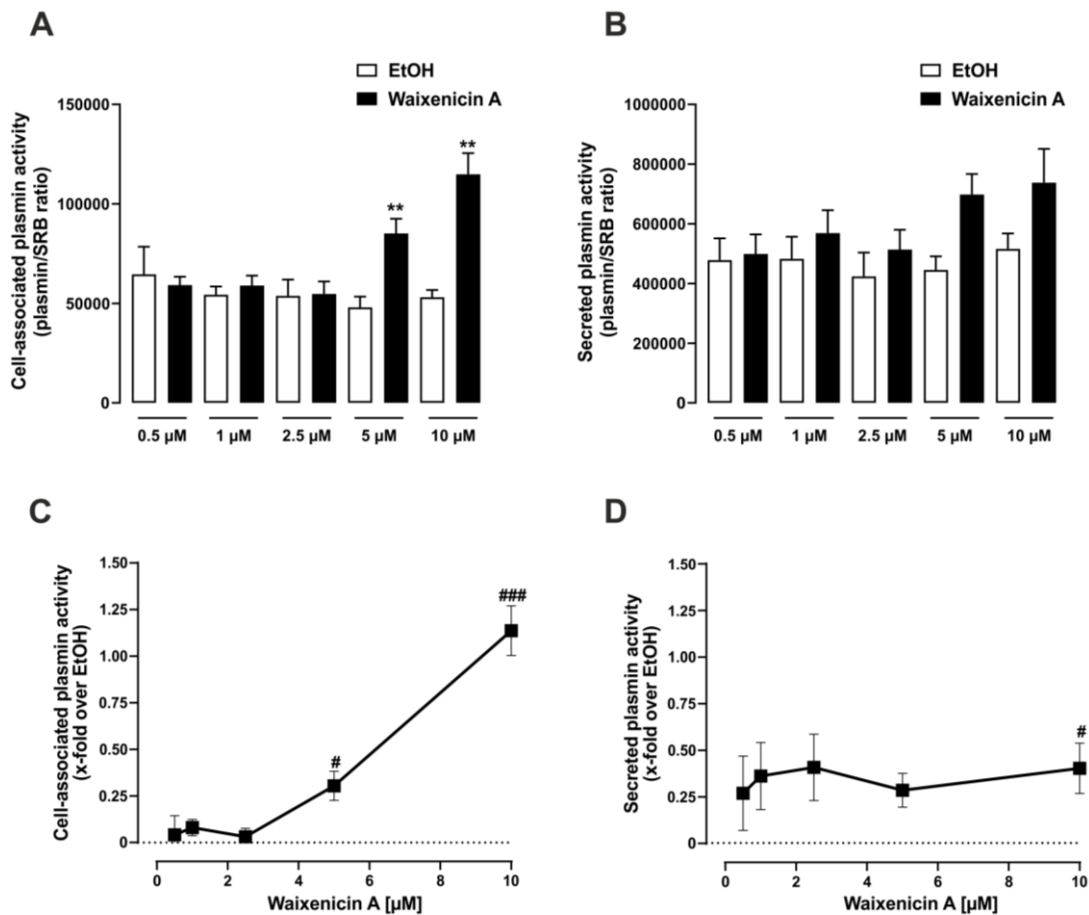

Figure 37: Apamin does not affect plasmin activity of pHPF

pHPF were stimulated with Apamin (100 nM) for 24 h (**A**) or 4 h (**B**) and fluorescence intensity of the secreted and cell-associated fraction was measured after incubation with D-Val-Leu-Lys-AMC (50 µM) for 3 h at 37 °C. Plasmin activity is displayed as SEM of RFU/SRB ratio (A, B) or % over/ under basal (**C**), n = 3-4.

To confirm the effects of TRPM7 blockade on plasmin activity, a second TRPM7 blocker was used. The xenicane diterpenoid Waixenicin A was isolated from the Hawaiian soft coral *Sarcothelia edmondsoni* and is a, to NS8593 structurally unrelated blocker of TRPM7 activity [323]. Waixenicin A increased plasmin activity

in a dose-dependent manner in the cell-associated fraction of pHPF (fig 38 a and c). With an increase of 1.13 ± 0.13 fold over basal at 10 µM and 0.30 ± 0.08 at 5 µM, these effects were similar to those observed with NS8593 (fig 38 c). In the secreted fraction, a slight increase of plasmin activity of 0.40 ± 0.13 fold over basal was detected with the highest concentration of Waixenicin A (fig 38 b and d).

Figure 38: Waixenicin A enhances plasmin activity of pHPF

pHPF were stimulated with indicated concentrations of Waixenicin A for 24 h and fluorescence intensity of the secreted (**B**, **D**) and cell-associated (**A**, **C**) fraction was measured after incubation with D-Val-Leu-Lys-AMC (50 µM) for 3 h at 37 °C. Plasmin activity is displayed as SEM of RFU/SRB ratio (A, B) or % over EtOH (C, D), n = 4. Statistical analysis was performed using two-way ANOVA followed by Tukey´s post-test (A) or one-sample t-test (C, D). Asterisks indicate significant differences to EtOH, hash signs indicate significant differences to zero, [#] $p < 0.05$, ** $p < 0.01$, ***/### $p < 0.001$.
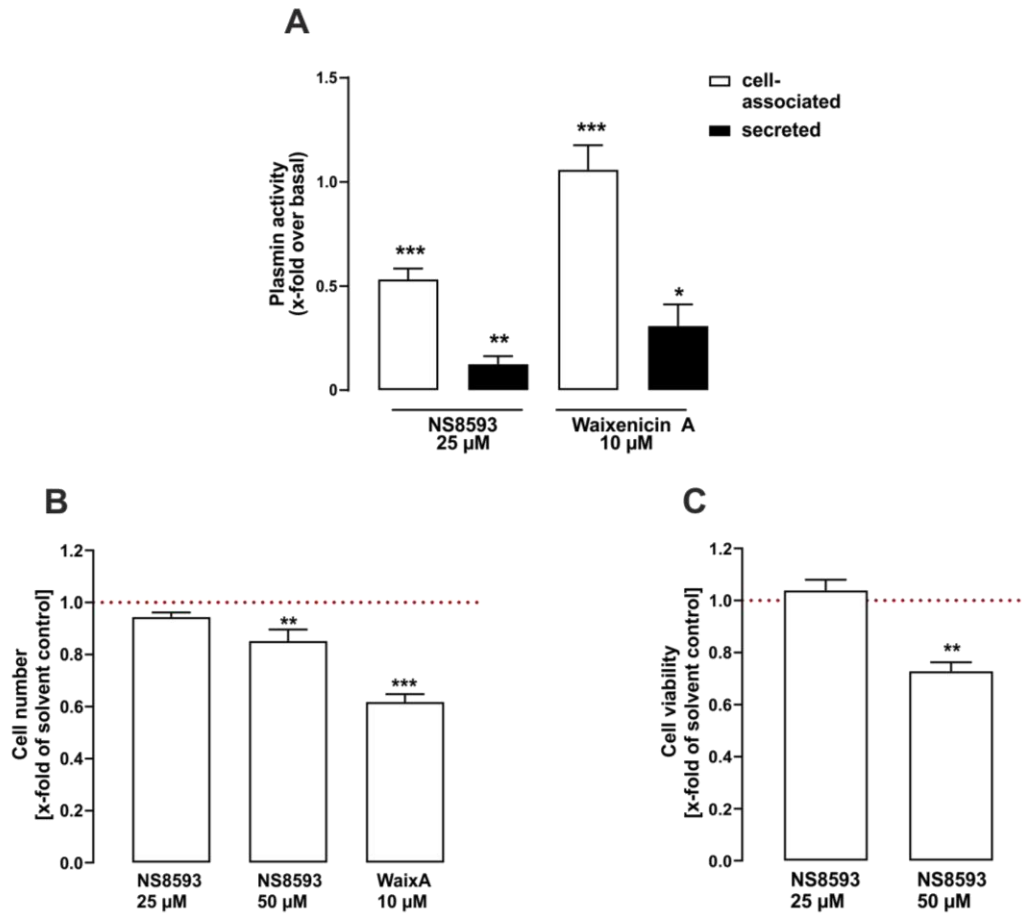
Figure 39: TRPM7 blockade enhances plasmin activity of pHPF

pHPF were stimulated with NS8593 (25 µM) or Waixenicin A (10 µM) for 24 h. In **A**, fluorescence intensity of the secreted and cell-associated fraction was measured after incubation with D-Val-Leu-Lys-AMC (50 µM) for 3 h at 37 °C. Plasmin activity is displayed as SEM of x-fold over the corresponding carrier control, n = 3-8. In **B**, cell number was determined via SRB assay and cell viability was measured using the WST-1 assay in **C**. Bars represent SEM of x-fold of the carrier control, n = 3-6. Statistical analysis was performed with one-sample t-test. Asterisks indicate significant differences to zero, * $p<0.05$, ** $p<0.01$, *** $p<0.001$.

Since TRPM7 function is crucial for cell survival, both NS8593 and Waixenicin A have been reported to inhibit proliferation in other cell types than pHPF [323, 324]. Thus, effects on cell number and cell viability at those concentrations that showed the highest effects on plasmin activity in pHPF were tested and plasmin activity was normalized to the cell number. While 25 µM NS8593 did not have a significant effect, 50 µM NS8593 significantly reduced cell number to 0.85 ± 0.04 fold under basal and cell viability to 0.73 ± 0.03 fold under basal (fig 39 b and c). 10 µM Waixenicin A reduced cell number to 0.62 ± 0.03 fold under basal, therefore clearly showing higher cytotoxicity than NS8593 (fig 39 b). The effects of 25 µM NS8593 and 10 µM Waixenicin A on plasmin activity are summarized in fig 39 a. In the cell-associated fraction, NS8593 increased plasmin activity by 0.53 ± 0.05 fold over basal and Waixenicin A by 1.05 ± 0.12 fold over basal. Only minor effects of both blockers were detected in the secreted fraction (fig 39 a).

To confirm that TRPM7 is the target of NS8593, siRNAs against TRPM7 were introduced into pHPF. TRPM7 siRNAs significantly decreased TRPM7 mRNA levels to 0.54 ± 0.05 fold of control siRNA (fig 40 a and b), while cell number remained unaffected (fig 40 c). Besides, TRPM7 siRNA increased basal cell-associated plasmin activity to 1.27 ± 0.10 fold compared to the control siRNA, confirming that TRPM7 activity restrains plasmin activity in pHPF (fig 40 d). Further, TRPM7 siRNAs reduced effects of NS8593 but not of TGF-β on plasmin activity, strengthening the theory that TRPM7 is the cellular target of NS8593 linking it to plasmin activity (fig 40 e).
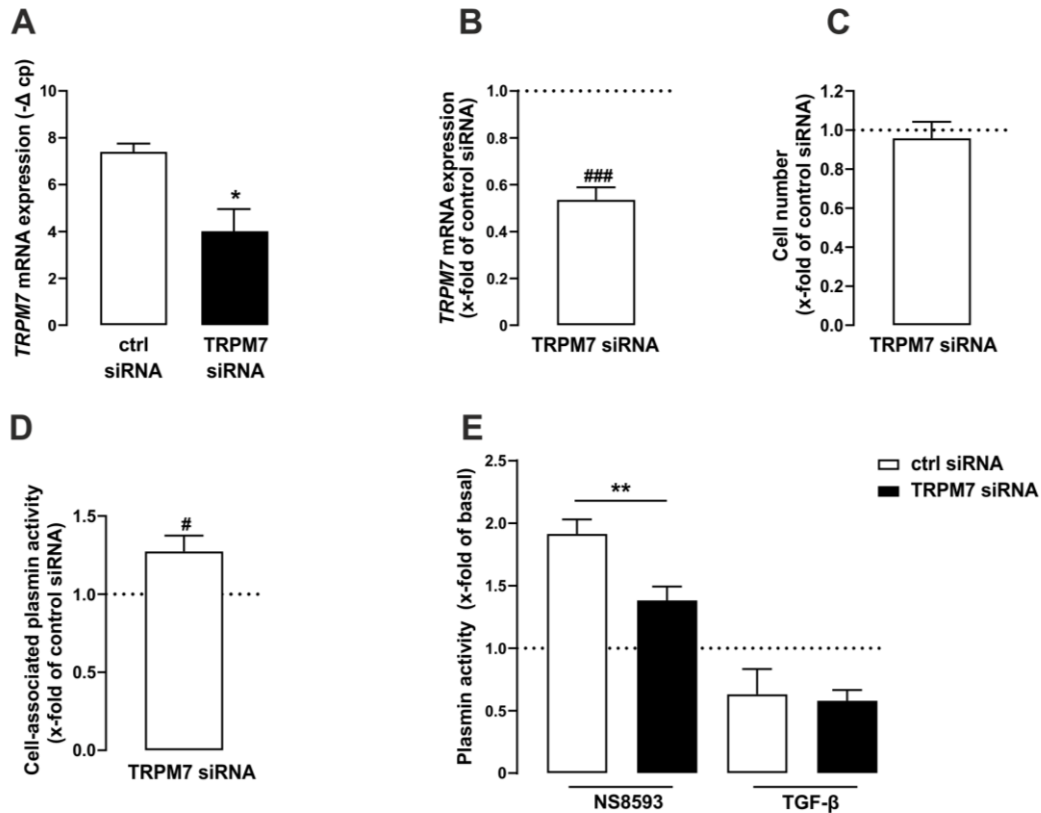
Figure 40: TRPM7 siRNA reduces *TRPM7* mRNA levels and enhances plasmin activity in pHPF

pHPF were transfected with TRPM7 or control siRNA. 72 h post transfection cells were stimulated with NS8593 (25 µM) or TGF-β (2 ng/ml) for 24 h. *TRPM7* mRNA amounts were determined by qRT-PCR 72 h post-transfection and are displayed as -Δcp (**A**) or x-fold of control siRNA (**B**), n = 4. In **C**, cell number was determined via SRB assay. Bars represent SEM of x-fold of control siRNA, n = 4. Fluorescence intensity of the secreted (TGF-β) and cell-associated (NS8593) fraction was measured after incubation with D-Val-Leu-Lys-AMC (50 µM) for 3 h at 37 °C. The effect of TRPM7 siRNA on basal plasmin activity as x-fold of control siRNA is displayed in **D**. Plasmin activity is displayed as SEM of x-fold of basal, n = 4 in **E**. Statistical analysis was performed using two-way ANOVA (E) followed by Tukey´s post-test, two-sample t-test (A) or one-sample t-test (B, D). Asterisks indicate significant differences to control siRNA, hash signs indicate significant differences zero, */# $p<0.05$, ** $p<0.01$, ### $p<0.001$

6.3.2 Blockade of TRPM7 activity reduces PAI1 and fibronectin protein levels and PAI1 mRNA expression in pHPF

Since direct effects of NS8593 on plasmin activity in pHPF were excluded by the data obtained after stimulation for 4 h (fig 36 c-f), it seemed likely that NS8593 indirectly affects plasmin activity via modulation of gene expression. Because PAI1 is a major modulator of plasmin activity, effects of TRPM7 on PAI1 protein levels were monitored in a first step. For this purpose, pHPF were stimulated with 25 μM NS8593 or 10 μM Waixenicin A. Indeed, both NS8593 and Waixenicin significantly reduced basal PAI1 protein levels in the cell-associated fraction (fig 41 a and b). NS8593 additionally reduced PAI1 protein levels in the secreted fraction (fig 41 a).
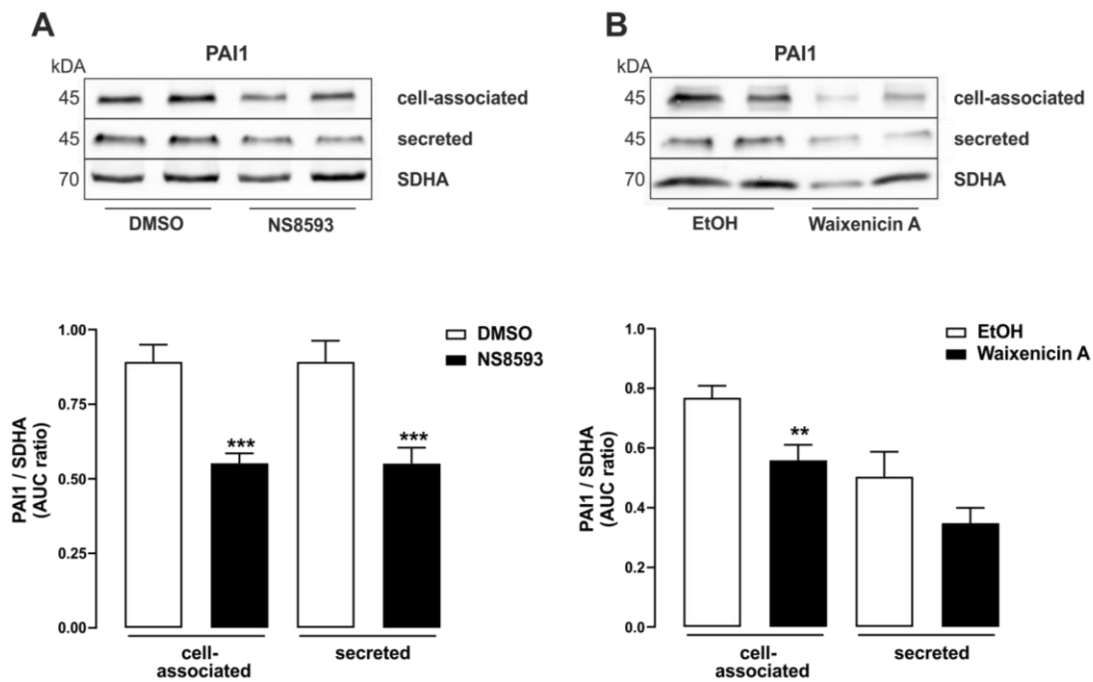
Figure 41: TRPM7 blockade reduces PAI1 protein levels in pHPF

Cells were stimulated with NS8593 (25 μM, **A**) or Waixenicin A (10 μM, **B**) for 24 h. Protein amounts of PAI-1 were determined in the cell-associated and secreted fraction via Western Blot and normalized to the loading control (SDHA) of the cell-associated fraction. Blots with the cell-associated fraction were cut in half to detect PAI-1 (45 kDa) and SDHA (70 kDa). One set of representative blots is shown. Bars represent SEM of AUC ratios, n = 4. Statistical analysis was performed using two-way ANOVA followed by Tukey´s post-test. Asterisks indicate significant differences between the TRPM7 blocker and the corresponding carrier control, ** $p < 0.01$, *** $p < 0.001$.

It was then tested, if the increase in plasmin activity affects plasmin substrates such as fibronectin. Again, both TRPM7 blockers significantly reduced fibronectin protein levels in the cell-associated fraction (fig 42 a and b).
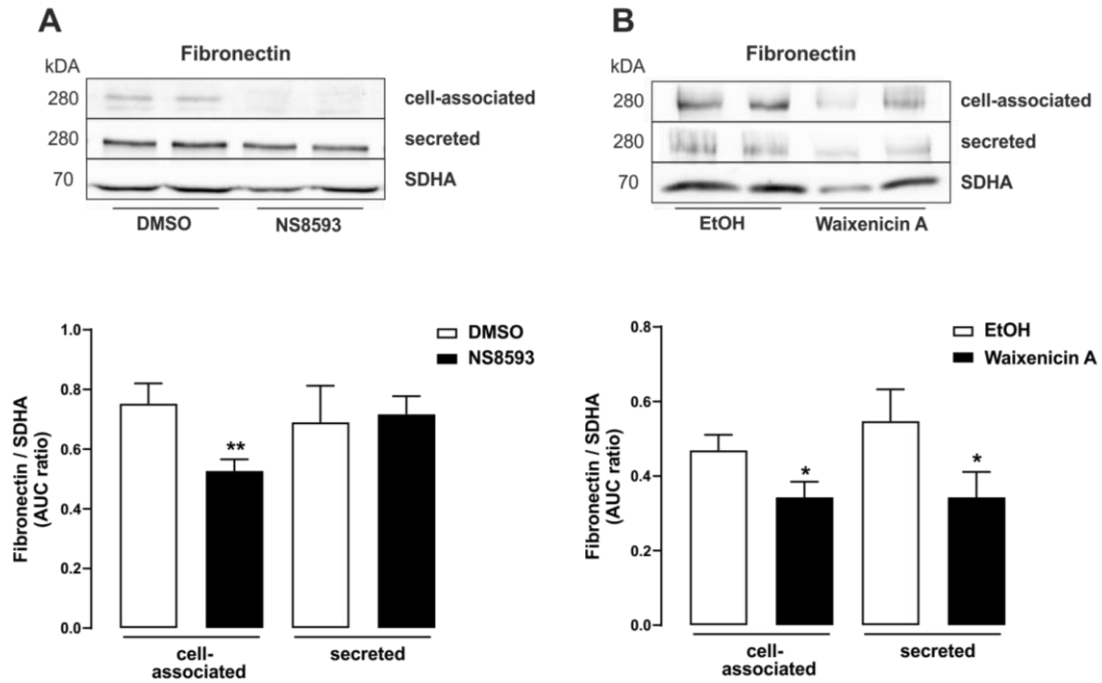
Figure 42: TRPM7 blockade reduces fibronectin protein levels in pHPF

Cells were stimulated with NS8593 (25 µM, **A**) or Waixenicin A (10 µM, **B**) for 24 h. Protein amounts of fibronectin were determined in the cell-associated and secreted fraction via Western Blot and normalized to the loading control (SDHA) of the cell-associated fraction. Blots of the cell-associated fraction were cut in half to detect fibronectin (280 kDa) and SDHA (70 kDa). One set of representative blots is shown. Bars represent SEM of AUC ratios, n = 3. Statistical analysis was performed using two-way ANOVA followed by Tukey´s post-test. Asterisks indicate significant differences between the TRPM7 blocker and the corresponding carrier control, * $p<0.05$, ** $p<0.01$.

To examine if TRPM7 blockade affects mRNA levels of proteins dependent on TGF-β signaling, *SERPINE1*, *FN1* and *Col1A1* mRNA expression was measured after co-stimulation with NS8593 and TGF-β. Interestingly, *SERPINE1* levels were significantly reduced from 7.24 ± 0.87 fold of basal to 4.87 ± 0.33 fold of basal, while *FN1* and *Col1A1* mRNA remained unchanged (fig 43), indicating that TRPM7 blockade specifically interferes with *SERPINE1* expression.
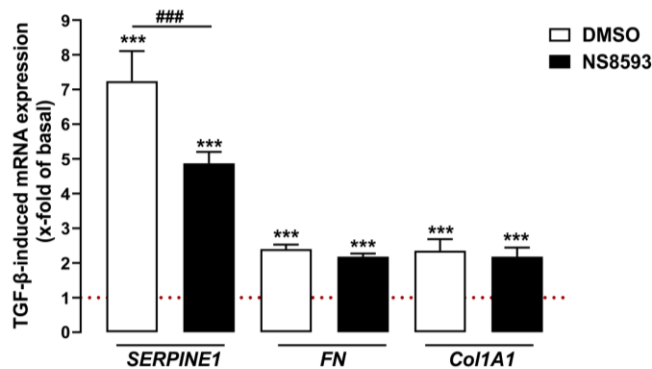
Figure 43: TRPM7 blockade reduces *SERPINE1*, but not *FN1* and *Col1A1* mRNA expression in pHPF

SERPINE1, FN1 and *Col1A1* mRNA amounts of pHPF were determined by qRT-PCR after 24 stimulation with TGF-β (2 ng/ml) or NS8593 (25 µM) or co-stimulation. Bars represent SEM of x-fold over basal values, n = 4. Statistical analysis was performed using two-way ANOVA followed by Tukey´s post-test or one-sample t-test. Asterisks indicate significant differences to basal, hash signs indicate significant differences to one, ***/### $p < 0.001$.

Finally, to assess a possible cellular consequence for pHPF, NS8593 was tested in a cell migration assay. When migrating at high FCS, therefore mimicking the experimental conditions of the plasmin assay, pHPF showed significantly enhanced cell migration with NS8593 (fig 44 a). Furthermore, when migrating within a serum gradient, NS8593 significantly enhanced migration of pHPF from 0.28 ± 0.04 to 0.56 ± 0.13 fold over basal (fig 44 b and c). Thus, modulating plasmin activity by TRPM7 blockade possibly affects migration of pHPF.

122
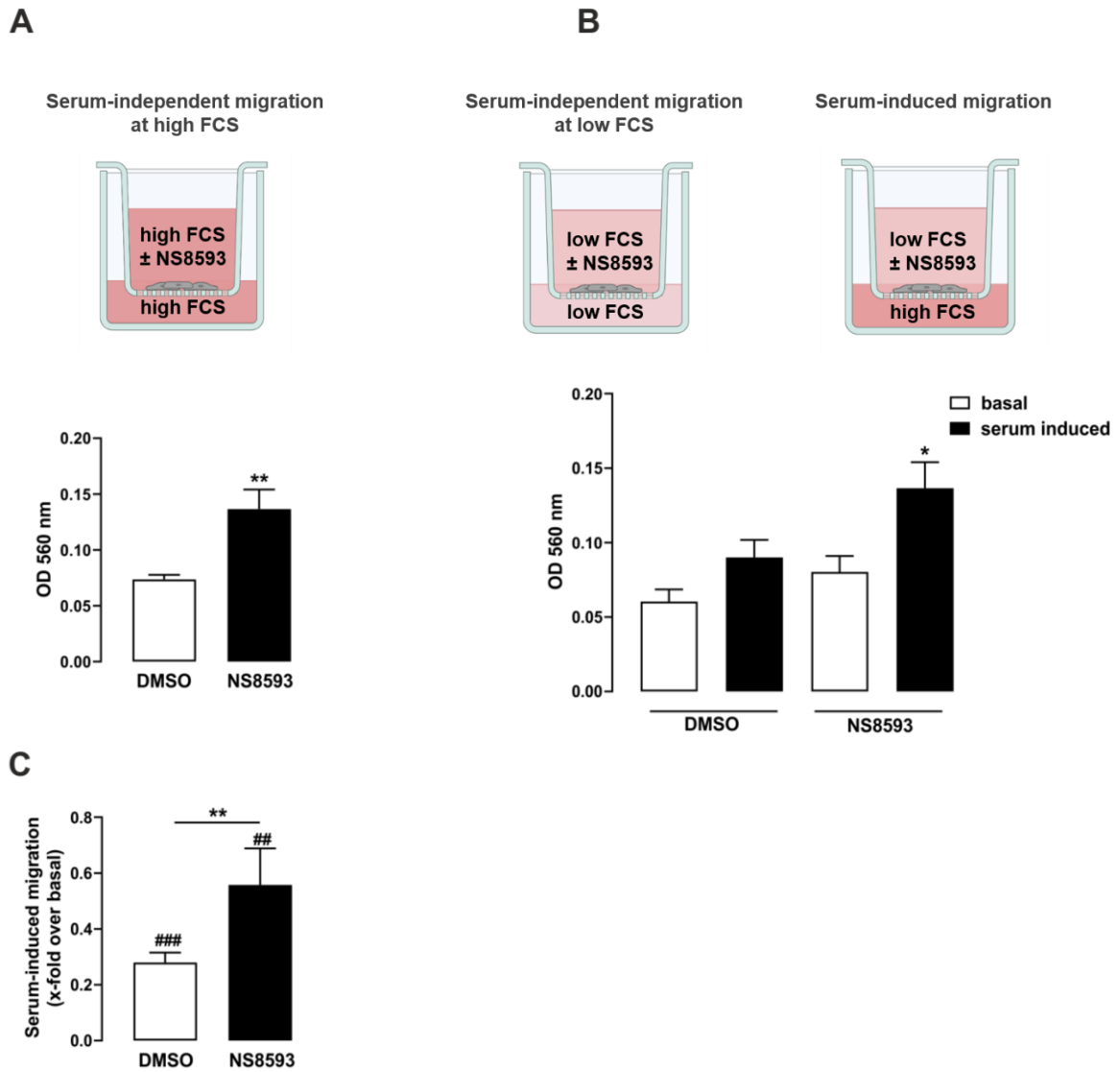
Figure 44: TRPM7 blockade increases migration of pHPF

pHPF were added to the top compartment of a Boyden chamber. After 24 h stimulation with NS5893 (10 μM) cells located at the bottom side of the membrane were quantified. In **A**, serum-independent migration at 5 % FCS was detected. In **B** and **C**, serum-induced (5 % FCS) was compared to serum-independent (0.5 % FCS) migration. Bars represent SEM of OD 560 values or x-fold over basal values, n = 3-5. Statistical analysis was performed using two-way ANOVA followed by Tukey´s post-test (B), one-sample t-test (C) or two-sample t-test (A, C). Asterisks indicate significant differences to basal, hash signs indicate significant differences to zero, * $p<0.05$, **/## $p<0.01$, ### $p<0.001$.

### 6.3.3 Comparison of plasmin activity in pHPF from healthy or PF donors

Data shown until now originated from pHPF which were provided by 2 donors and purchased from PromoCell. To confirm that the observed effects of NS8593 are comparable in pHPF from different suppliers and in different culture media, pHPF from a third, healthy donor were purchased from Lonza together with pHPF from a donor diagnosed with pulmonary fibrosis. First, basal plasmin activity of both donors were compared, expecting a lower plasmin activity in the PF donor due to excessive ECM accumulation in fibrotic tissue. Indeed, pHPF from a PF donor showed significantly lower basal plasmin activity. Basal plasmin activity in the cell-associated fraction was 0.19 ± 0.03 fold lower compared to the healthy donor and even 0.51 ± 0.04 fold lower in the secreted fraction (fig 45).
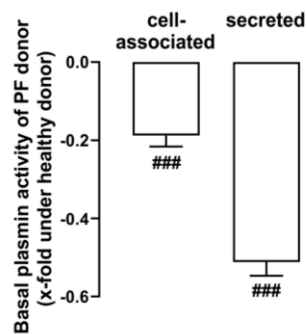
Figure 45: Comparison of plasmin activity in pHPF derived from a healthy or a PF donor
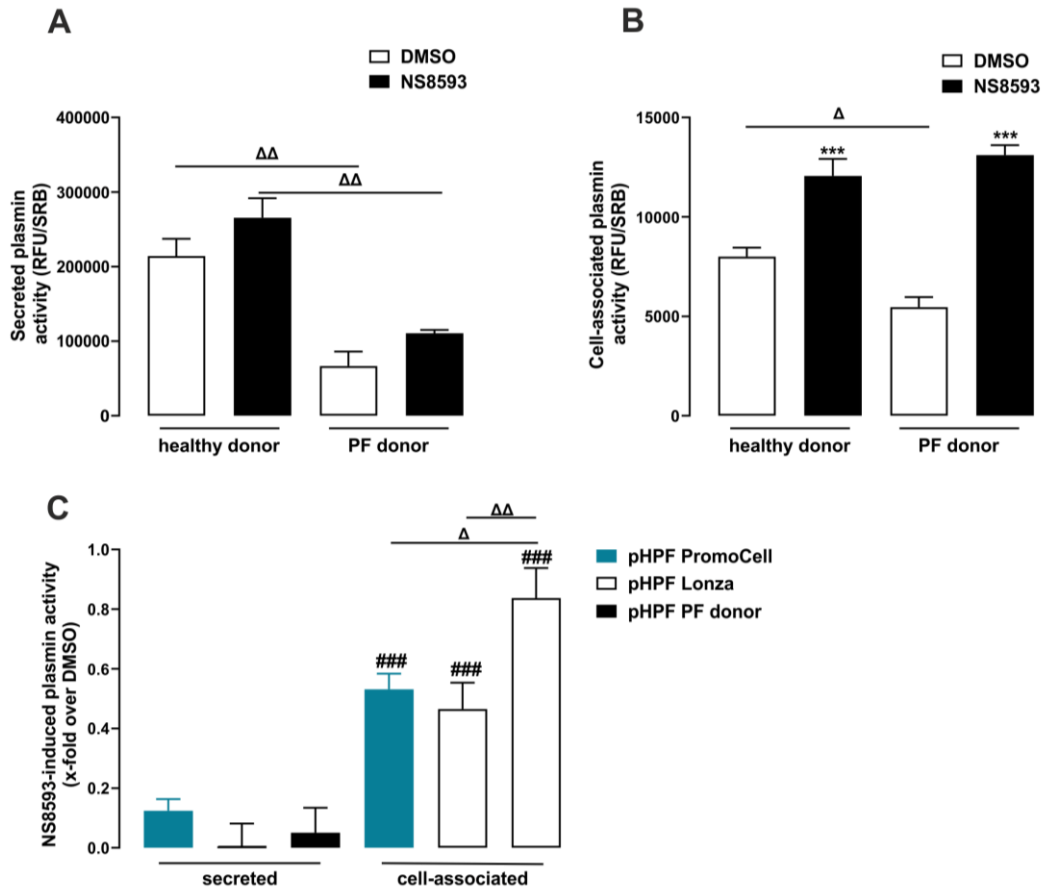
pHPF from a healthy donor (Lonza: CC-2512) or a donor with pulmonary fibrosis (PF) (Lonza: CC-7231) were cultivated for 24 h and fluorescence intensity of the secreted and cell-associated fraction was measured after incubation with D-Val-Leu-Lys-AMC (50 µM) for 3 h at 37 °C . Bars represent SEM x-fold under basal values, n = 12. Statistical analysis was performed using one-sample t-test. Hash signs indicate significant differences to zero, ### $p < 0.001$.

Next, effects of TGF-β were compared. As shown in fig 46 a-c, TGF-β reduced plasmin activity similarly in all three pHPF pools and no difference was detected, indicating that TGF-β signaling is not altered in fibroblasts from fibrotic tissue. NS8593 increased plasmin activity in the cell-associated fraction in all 3 pHPF pools and no significant difference was observed in healthy pHPF from PromoCell or Lonza, thus confirming that the effects of NS8593 can be transferred to pHPF from different suppliers (fig 47 a-c). However with 0.83 ± 0.10 fold over basal, the enhancing effect of NS8593 was significantly higher in pHPF from a PF donor compared to both healthy pHPF from PromoCell or Lonza with 0.47 ± 0.09 and 0.53 ± 0.05 fold over basal, respectively (fig 47 a-c). In summary, these data indicate that the plasmin system plays an important role in the context of pulmonary fibrosis and show an increased sensitivity towards TRPM7 blockade in pHPF from a PF donor. Thus, TRPM7 blockers could be used to selectively target the plasmin system of fibrotic tissue.
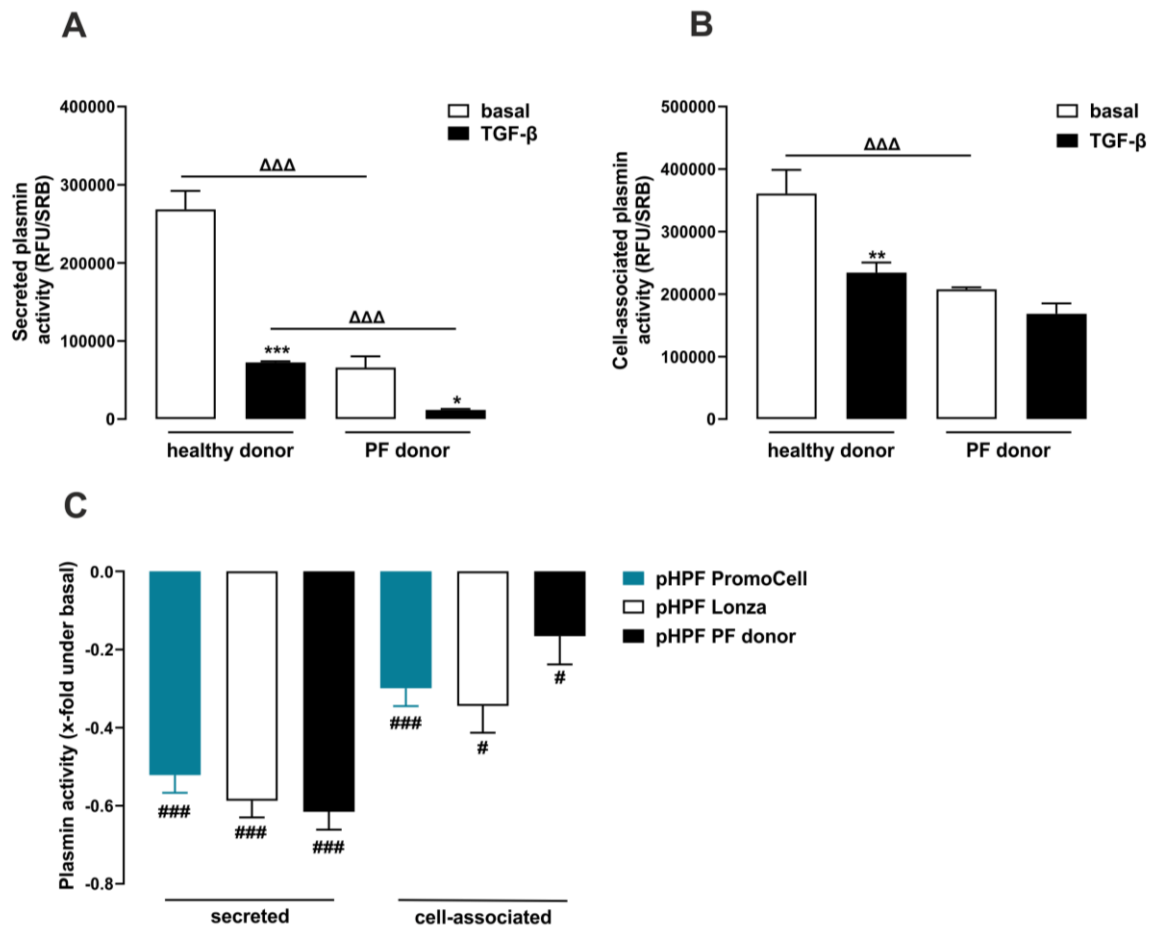
Figure 46: Effects of TGF-β on plasmin activity in pHPF derived from a donor with pulmonary fibrosis

pHPF from a healthy donor (Lonza: CC-2512) or a donor with pulmonary fibrosis (PF) (Lonza: CC-7231) or pHPF from PromoCell were stimulated with TGF-β (2 ng/ ml) for 24 h and fluorescence intensity of the secreted and cell-associated fraction was measured after incubation with D-Val-Leu-Lys-AMC (50 µM) for 3 h at 37 °C . Bars represent SEM of RFU/SRB ratios of one exemplary experiment (**A**, **B**) or x-fold under basal values (**C**), n = 6. Statistical analysis was performed using two-way ANOVA followed by Tukey´s post-test (A, B) or one-sample t-test (C). Asterisks indicate significant differences to basal, hash signs indicate significant differences to zero, deltas indicate significant differences between distinct cell pools, */# $p < 0.05$, ** $p < 0.01$, ***/###/ΔΔΔ $p < 0.001$.

Figure 47: Effects of NS8593 on plasmin activity in pHPF derived from a donor with pulmonary fibrosis

pHPF from a healthy donor (Lonza: CC-2512) or a donor with pulmonary fibrosis (PF) (Lonza: CC-7231) or pHPF from PromoCell were stimulated with NS8593 (25 µM) for 24 h and fluorescence intensity of the secreted and cell-associated fraction was measured after incubation with D-Val-Leu-Lys-AMC (50 µM) for 3 h at 37 °C. Bars represent SEM of RFU/SRB ratios of one exemplary experiment (**A**, **B**) or x-fold over basal values (**C**), n = 6. Statistical analysis was performed using two-way ANOVA followed by Tukey´s post-test (A, B, C) or one-sample t-test (C). Asterisks indicate significant differences to DMSO, hash signs indicate significant differences to zero, deltas indicate significant differences between distinct cell pools, $^{\Delta}$ $p<0.05$, $^{\Delta\Delta}$ $p<0.01$, ***/### $p<0.001$.

6.3.4 Blockade of TRPM7 activity enhances plasmin activity in human lung cells

Considering that effects of TRPM7 blockade on plasmin activity in pHPF have not been reported before, data presented in this work is unique. In order to clarify whether the effects of TRPM7 blockade were specific for pHPF, effects of NS8593 stimulation were tested in two additional lung cell types, 16-HBE cells and primary HPAEC. Since activation of the plasmin system has not only been associated with pulmonary fibrosis but also as an important factor to modulate tumor cell migration, effects of TRPM7 blockade on plasmin activity were also monitored in the lung tumor cell lines A549 and H1299.
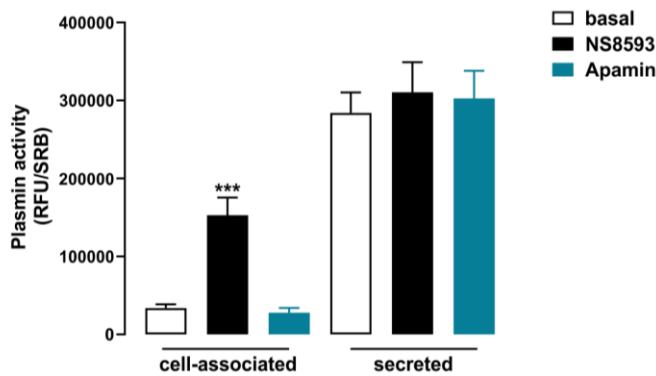
Figure 48: TRPM7 blockade enhances plasmin activity in 16-HBE cells

16-HBE cells were stimulated with NS8593 (25 µM) or Apamin (100 nM) for 24 h and fluorescence intensity of the secreted and cell-associated fraction was measured after incubation with D-Val-Leu-Lys-AMC (50 µM) for 3 h at 37 °C. Bars represent SEM of RFU/SRB ratios, n = 4-10. Statistical analysis was performed using two-way ANOVA followed by Tukey´s post-test. Asterisks indicate significant differences to basal, *** $p < 0.001$.

In the non-tumor epithelial 16-HBE cells, TRPM7 blockade significantly increased plasmin activity in the cell-associated fraction and the apamin control showed no effects (fig 48). In primary human pulmonary artery endothelial cells (HPAEC), NS8593 did not lead to an increase in plasmin activity in the cell-associated fraction, but it did so in the secreted fraction (fig 49). However, the increase was relatively small and the apamin control showed a slight increase as well, indicating that in these cells, effects of NS8593 did not originate from specifically targeting TRPM7 (fig 49).
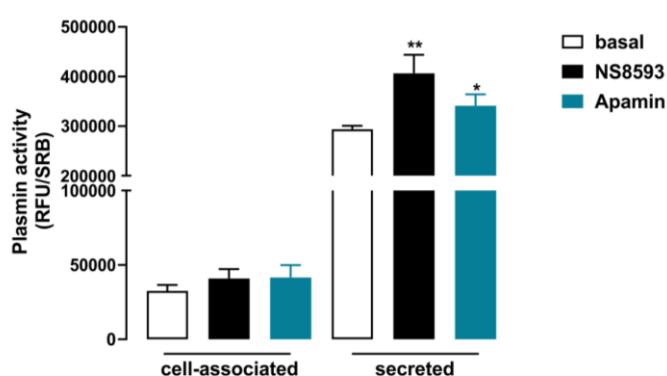
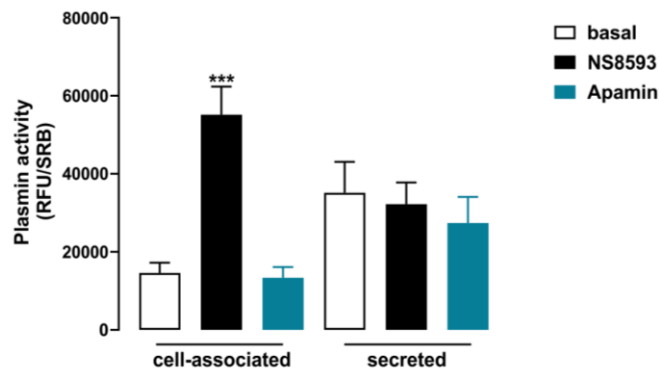**Figure 49: Effects of TRPM7 on plasmin activity in HPAEC**

HPAEC were stimulated with NS8593 (25 µM) or Apamin (100 nM) for 24 h and fluorescence intensity of the secreted and cell-associated fraction was measured after incubation with D-Val-Leu-Lys-AMC (50 µM) for 3 h at 37 °C. Bars represent SEM of RFU/SRB ratios, n = 4-10. Statistical analysis was performed using two-way ANOVA followed by Tukey´s post-test. Asterisks indicate significant differences to basal, *** $p < 0.001$.

In the human lung tumor cell lines A549 and H1299, TRPM7 blockade resulted in a significant increase in plasmin activity in the cell-associated fraction, similar to the effect in pHPF (fig 50 and 51). No effects were detected in the secreted fractions. Additionally, no changes in plasmin activity were detected with apamin, indicating that NS8593-induced plasmin activity was due to blocking of TRPM7 function (fig 48, 50 and 51).
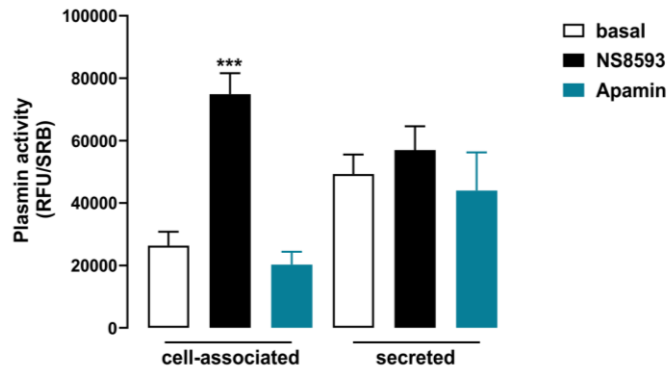
**Figure 50: TRPM7 blockade enhances plasmin activity in A549 cells**

A549 cells were stimulated with NS8593 (25 µM) or Apamin (100 nM) for 24 h and fluorescence intensity of the secreted and cell-associated fraction was measured after incubation with D-Val-Leu-Lys-AMC (50 µM) for 3 h at 37 °C. Bars represent SEM of RFU/SRB, n = 4-10. Statistical analysis was performed using two-way ANOVA followed by Tukey´s post-test. Asterisks indicate significant differences to basal, *** $p<0.001$.

Figure 51: TRPM7 blockade enhances plasmin activity in H1299 cells

H1299 cells were stimulated with NS8593 (25 µM) or Apamin (100 nM) for 24 h and fluorescence intensity of the secreted and cell-associated fraction was measured after incubation with D-Val-Leu-Lys-AMC (50 µM) for 3 h at 37 °C. Bars represent SEM of RFU/SRB ratios, n = 4-10. Statistical analysis was performed using two-way ANOVA followed by Tukey´s post-test. Asterisks indicate significant differences to basal, *** $p<0.001$.

These data indicate that TRPM7 blockers could be used as selective tools to target plasmin activity in different types of lung cells. As previously described, TRPM7 blockade has been shown to inhibit cell proliferation. In fig 52, effects of NS8593 on cell number and viability on the used lung cells are summarized, but no effects on cell number or viability were detected in the distinct cells.
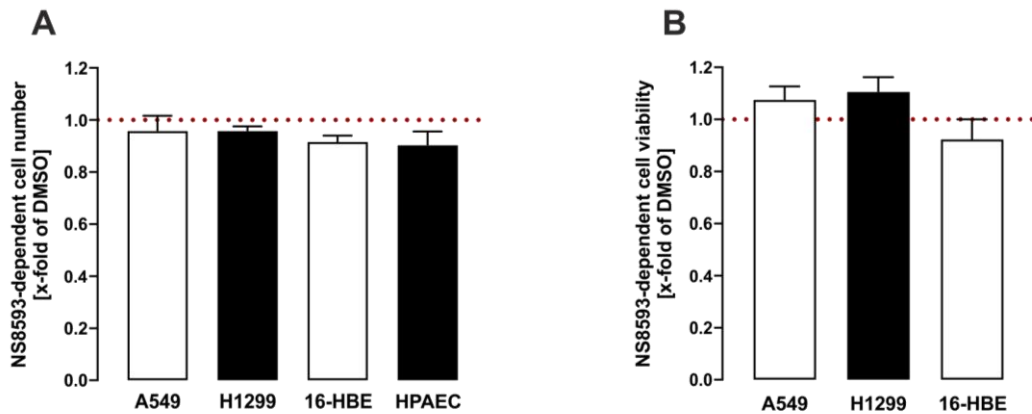
Figure 52: Effects of NS8593 on cell number and cell viability

A549, H1299, 16-HBE or HPAEC cells were stimulated with 25 µM NS8593 for 24 h. Cell number was determined via SRB assay (**A**) and cell viability via WST-1 assay (**B**). Bars represent SEM of x-fold of DMSO, n = 3-6.

6.4 TRPM7 affects plasminogen activation system in human lung cells after sustained TGF-β stimulation

### 6.4.1 TGF-β induces differentiation of fibroblasts to myofibroblasts

The next aim of this work was to induce fibroblast to myofibroblast differentiation in cultured pHPF in order to analyze a potential role of TRPM7 blockers in this process. TGF-β treatment for 48 h at low serum concentrations is an established protocol to induce differentiation of pulmonary fibroblasts to myofibroblasts which is characterized by secretion of ECM proteins like collagen1 and fibronectin as well as increased levels of PAI1 and α-SMA [175, 353, 354].

First, effects of TGF-β on the protein levels of fibrotic markers were analyzed. TGF-β significantly enhanced protein levels of α-SMA in the cell-associated fraction and PAI1 in cell-associated and secreted fraction, indicating the successful differentiation to myofibroblasts (fig 53 a and b). Consequently, fibronectin and collagen1 protein levels were significantly increased in both fractions by TGF-β stimulation, displaying the ability of generated myofibroblasts to deposit ECM proteins (fig 53 c and d). In line with this notion, TGF-β was shown to significantly enhance mRNA levels of *SERPINE1* to 3.42 ± 0.32, of *FN1* to 2.68 ± 0.15 and of *Col1A1* to 3.38 ± 0.32 fold of basal (fig 54). Summarized, the applied protocol was suitable for successful fibroblast to myofibroblasts differentiation in cultivated pHPF.
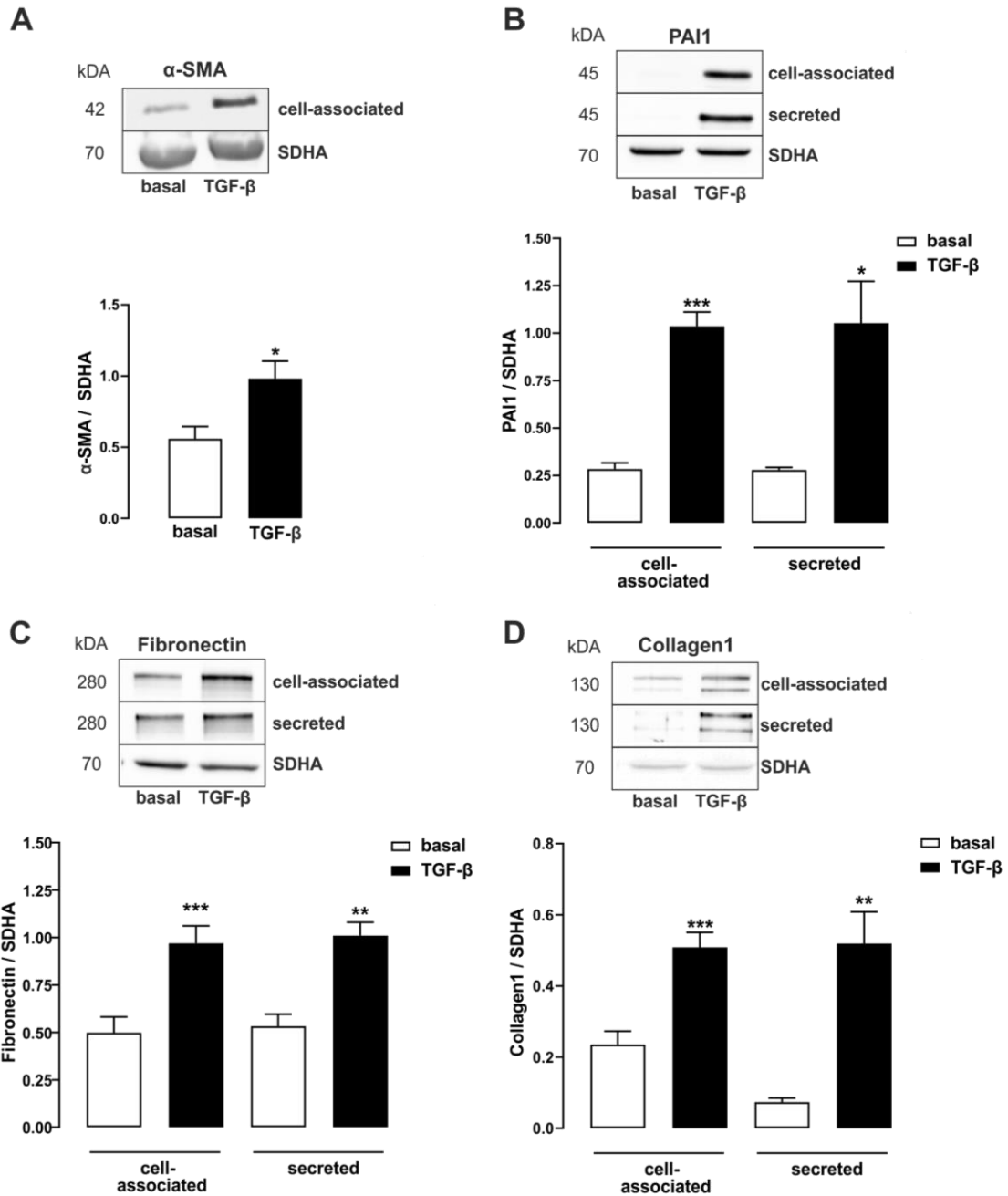
Figure 53: Sustained TGF-β-exposure elevates levels of fibrotic markers in pHPF

Cells were stimulated with TGF-β (2 ng/ml) for 48h, protein amounts of α-SMA (**A**), PAI1 (**B**), fibronectin (**C**), collagen1 (**D**) were determined in the cell-associated and secreted fraction via Western Blot and normalized to the loading control (SDHA) of the cell-associated fraction. Blots of the cell-associated fraction were cut in half to detect α-SMA (42 kDa), PAI1 (45 kDa), fibronectin (280 kDa) or collagen1 (130 kDa) together with SDHA (70 kDa). One set of representative blots is shown. Bars represent SEM of AUC ratios, n = 3-5. Statistical analysis was performed using two-way ANOVA (B, C, D) followed by Tukey´s post-test or two-sample t-test (A). Asterisks indicate significant differences to basal, * $p<0.05$, ** $p<0.01$, *** $p<0.001$.
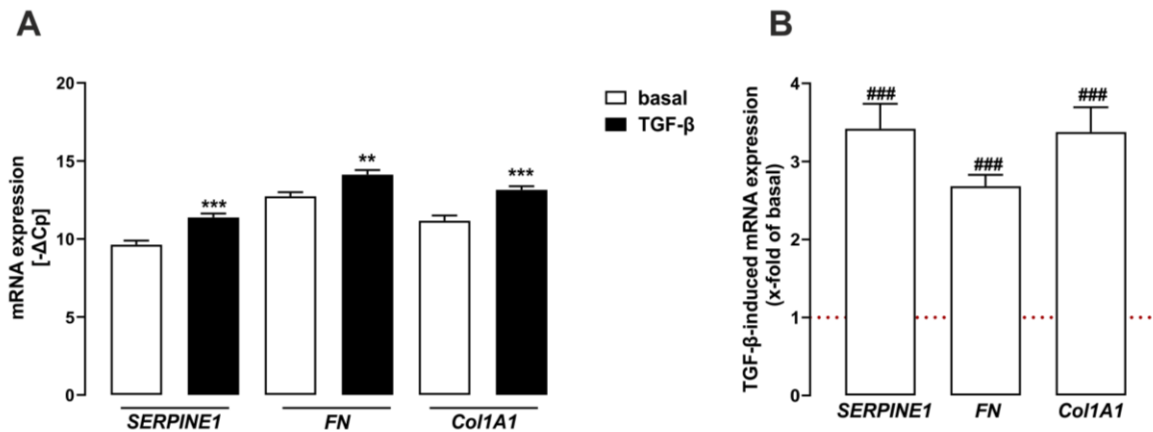
Figure 54: TGF-β induces mRNA expression of *SERPINE1, FN1* and *Col1A1* in pHPF

SERPINE1, FN1 and *Col1A1* mRNA amounts of pHPF were determined by qRT-PCR after 48 h stimulation with TGF-β (2 ng/ml). In **A**, bars represent SEM of −Δcp and in **B,** x-fold over basal values, n = 4. Statistical analysis was performed using two-way ANOVA followed by Tukey´s post-test (A) or one-sample t-test (B). Asterisks indicate significant differences to basal, hash signs indicate significant differences to one, ** p<0.01, ***/### p<0.001.

6.4.2 Blockade of TRPM7 activity inhibits TGF-β induced differentiation of fibroblasts to myofibroblasts

Stimulating pHPF with TGF-β for 48 h results in the differentiation of fibroblasts to myofibroblasts which produce excessive amounts of ECM, thereby imitating fibrosis on a cellular level. Since therapeutic options for fibrosis are insufficient, especially in late stages of the disease, modulating plasmin activity to counteract ECM production seems a promising approach. To investigate if effects of TRPM7 blockade on plasmin activity in the differentiation protocol were comparable to the effects described above, effects of NS8593 on plasmin activity were measured after 48 h stimulation with NS8593. As shown in fig 55, NS8593 induced plasmin activity in the same manner, with an increase of 0.89 ± 0.13 fold over DMSO (fig 55). Enhancing effects on plasmin activity of the secreted fraction were noticeable smaller. Thus, TRPM7 blockade was investigated in TGF-β-mediated effect on plasmin activity.

134
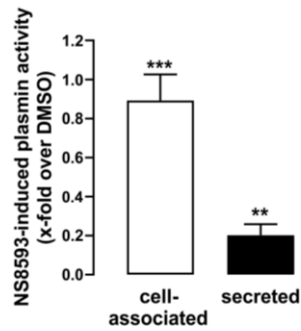
Figure 55: NS8593-induced plasmin activity after 48 h

pHPF were stimulated with NS8593 (25 µM) for 48 h in medium supplied with 0.5% FCS and fluorescence intensity of the secreted and cell-associated fraction was measured after incubation with D-Val-Leu-Lys-AMC (50 µM) for 3 h at 37 °C. Plasmin activity is displayed as SEM of x-fold over corresponding carrier control, n = 3. Statistical analysis was performed with one-sample t-test. Asterisks indicate significant differences to zero, ** $p<0.01$, *** $p<0.001$.

Incubation with TGF-β led to a significant reduction of plasmin activity in the secreted fraction but not in the cell-associated fraction, similar to the data obtained after 24 h (fig 56 a and b). When normalized to basal values, NS8593 was able to counteract TGF-β-induced inhibition of plasmin activity by elevating it from 0.86 ± 0.03 to 0.68 ± 0.06 fold under basal (fig 56 c). Possible antiproliferative effects of NS8593 in the 48 h stimulation protocol were investigated, but no effects on cell number or cell viability could be detected (fig 56 d).

135
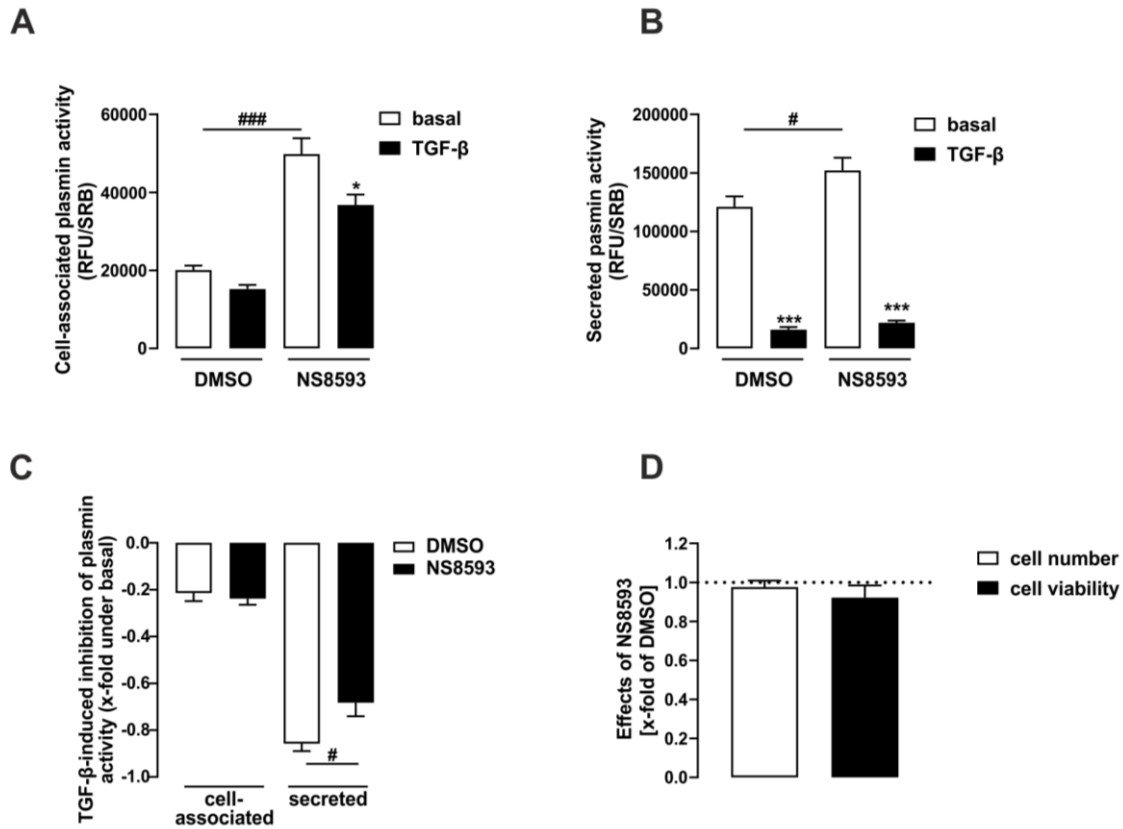
Figure 56: TRPM7 blockade increases basal plasmin activity and counteracts effects after sustained TGF-β exposure in pHPF.

pHPF were stimulated with NS8593 (25 µM) or TGF-β (2 ng/ml) or co-stimulated for 48 h and fluorescence intensity of the secreted and cell-associated fraction was measured after incubation with D-Val-Leu-Lys-AMC (50 µM) for 3 h at 37 °C. Plasmin activity is displayed as SEM of RFU/SRB ratio (**A**, **B**) or x-fold under basal (**C**), n = 5. In **D**, Cell number was determined via SRB assay and cell viability was measured using the WST-1 assay. Bars represent SEM of x-fold of DMSO, n = 3-6. Statistical analysis was performed using two-way ANOVA followed by Tukey´s post-test. Asterisks indicate significant differences to basal and hash signs indicate significant differences to DMSO, */# $p < 0.05$, ***/### $p < 0.001$.
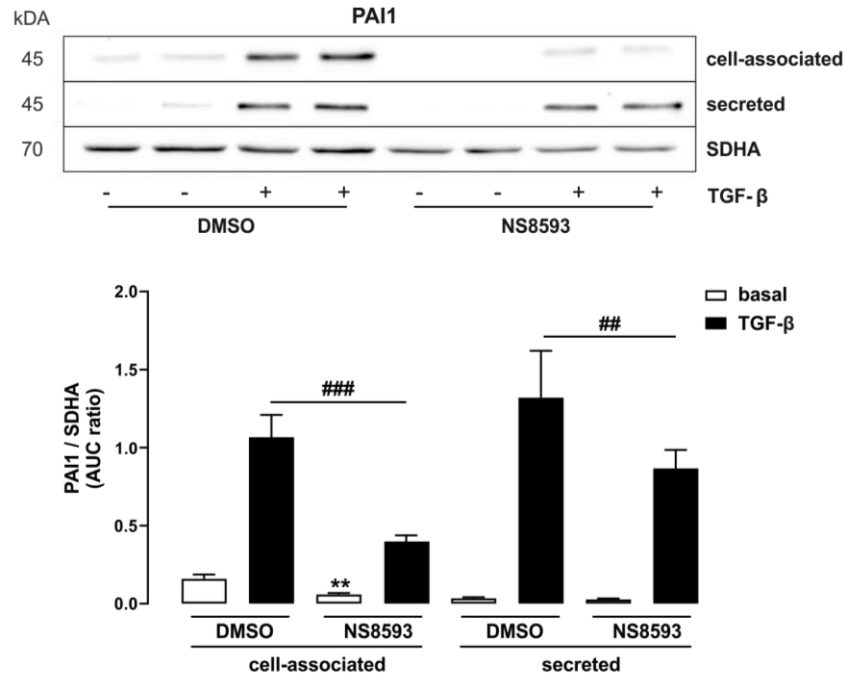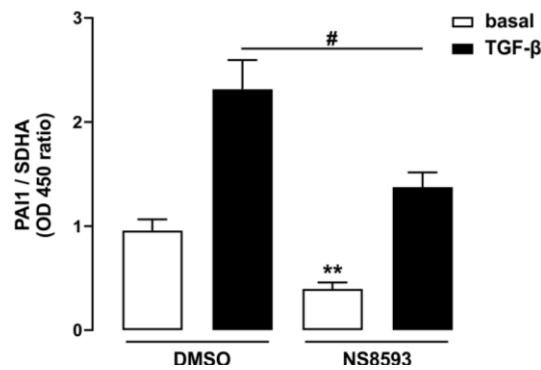
Figure 57: TRPM7 blockade inhibits basal and TGF-β-induced PAI1 protein levels in pHPF

Cells were stimulated with TGF-β (2 ng/ml), NS8593 (25 µM) or co-stimulated for 48 h. Protein amounts of PAI1 were determined in the cell-associated and secreted fraction via Western Blot and normalized to the loading control (SDHA) of the cell-associated fraction. Blots of the cell-associated fraction were cut in half to detect PAI1 (45 kDa) and SDHA (70 kDa). One set of representative blots is shown. Bars represent SEM of AUC ratios, n = 4. Statistical analysis was performed using two-way ANOVA followed by Tukey´s post-test. Asterisks indicate significant differences to basal PAI1 expression and hash signs indicate significant differences to TGF-β-induced PAI1 expression, **/## $p<0.01$, ### $p<0.001$.

To strengthen the hypothesis that TRPM7 blockade affects the plasmin system after sustained TGF-β stimulation, PAI1 protein levels were investigated. Indeed, co-stimulation of NS8593 and TGF-β significantly reduced TGF-β-induced PAI1 protein levels in both fractions (fig 57). Additionally, basal PAI1 protein levels were significantly inhibited from 0.16 ± 0.03 to 0.06 ± 0.01 (AUC ratio) by NS8593 in the cell-associated fraction (fig 57). Considering the small AUC values for basal PAI1 protein levels obtained by western blot, PAI1 ELISA was used as a second method to confirm this finding. As shown in fig 58, TRPM7 blockade with NS8593 inhibited basal and TGF-β-induced PAI1 protein levels. To show that NS8593 affects PAI1 protein levels specifically via targeting TRPM7, the effects of apamin were studied.

137

As shown in fig 59, apamin did not affect basal or TGF-β-induced PAI1 protein levels. Thus, a connection of TRPM7 and plasmin activity after TGF-β stimulation was found.

Figure 58: TRPM7 blockade inhibits basal and TGF-β-induced PAI1 protein levels in pHPF

Cells were stimulated with TGF-β (2 ng/ml), NS8593 (25 µM) or co-stimulated for 48 h and protein amounts of PAI1 and SDHA were determined via whole-cell ELISA. Bars represent SEM of OD 450 ratios detected via ELISA, n = 3. Statistical analysis was performed using two-way ANOVA followed by Tukey´s post-test. Asterisks indicate significant differences to basal PAI1 expression and hash signs indicate significant differences to TGF-β-induced PAI1 expression, [#] $p < 0.05$, ** $p < 0.01$.

Further, effects of TRPM7 on the fibrotic marker α-SMA and on the ECM proteins fibronectin and collagen1 were studied. Protein levels of fibronectin were significantly inhibited by NS8593 in the cell-associated fraction under basal or TGF-β-stimulated conditions (fig 60). Similarly, basal α-SMA proteins levels were reduced from 0.56 ± 0.08 to 0.13 ± 0.02 (AUC ratio) and induction by TGF-β was lowered from 0.98 ± 0.12 to 0.18 ± 0.03 fold over basal (fig 61). Finally, basal collagen1 protein levels were significantly inhibited by NS8593, however no significant effect was seen on TGF-β-induced protein levels (fig 62). Since Western Blot failed to reproduce the results, a second approach was used for measuring collagen in pHPF. Sircol™ assay measures secreted collagens and TGF-β-induced secretion of collagens was significantly inhibited by NS8593 (fig 63).
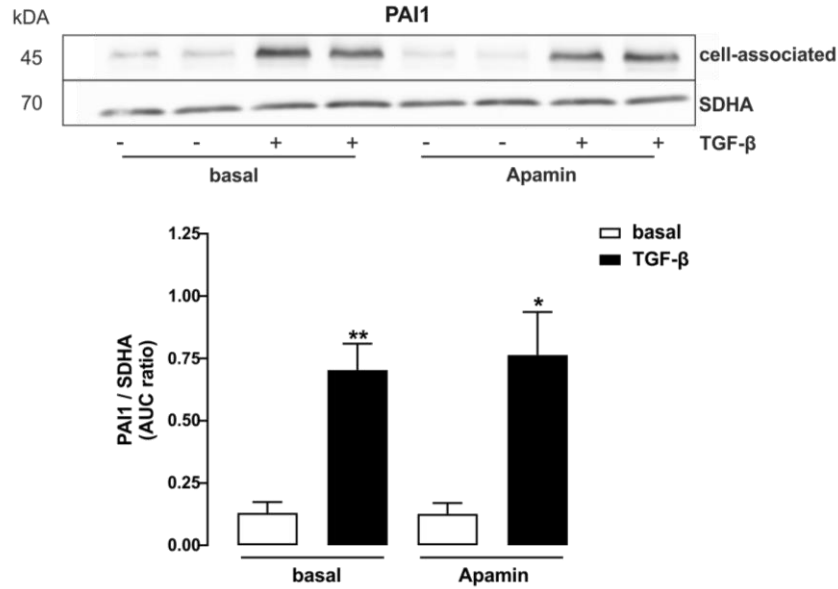
Figure 59: Apamin does not affect TGF-β-induced PAI1 protein levels in pHPF

Cells were stimulated with TGF-β (2 ng/ml), Apamin (100 nM, C) or co-stimulated for 48 h and protein amounts of PAI1 and SDHA (loading control) were determined in the cell-associated fraction via Western Blot. Blots were cut in half to detect PAI1 (45 kDa) and SDHA (70 kDa). One set of representative blots is shown. Bars represent SEM of AUC ratios, n = 3. Statistical analysis was performed using two-way ANOVA followed by Tukey´s post-test. Asterisks indicate significant differences to basal PAI1 expression, * $p<0.05$, ** $p<0.01$.
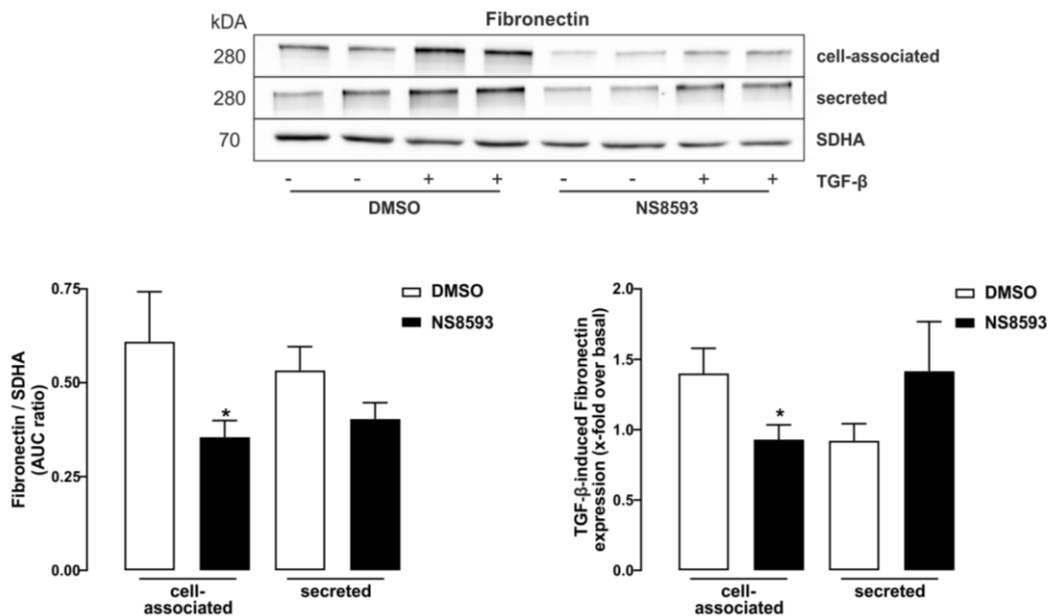
Figure 60: TRPM7 blockade inhibits basal and TGF-β-induced fibronectin protein levels in pHPF

Cells were stimulated with TGF-β (2 ng/ml) or NS8593 (25 µM) or co-stimulated for 48 h. Protein amounts of fibronectin and SDHA (loading control) were determined in the cell-associated and secreted fraction via Western Blot and normalized to the loading control (SDHA) of the cell-associated fraction. Blots of the cell-associated fraction were cut in half to detect fibronectin (280 kDa) and SDHA (70 kDa). The loading control of the cell-associated fraction was also used for the secreted fraction. One set of representative blots is shown. Bars represent SEM of AUC ratios or x-fold over basal, n = 4. Statistical analysis was performed using two-way ANOVA followed by Tukey´s post-test. Asterisks indicate significant differences to the carrier control, * $p<0.05$.

Figure 61: TRPM7 blockade inhibits basal and TGF-β-induced α-SMA protein levels in pHPF

Cells were stimulated with TGF-β (2 ng/ml) or NS8593 (25 µM) or co-stimulated for 48 h and protein amounts of α-SMA and SDHA (loading control) were determined in the cell-associated fraction via Western Blot. Blots of the cell-associated fraction were cut in half to detect α-SMA (42 kDa) and SDHA (70 kDa). One set of representative blots is shown. Bars represent SEM of AUC ratios or x-fold over basal, n = 4. Statistical analysis was performed using two-sample t-test (A). Asterisks indicate significant differences to the carrier control, *** $p<0.001$.
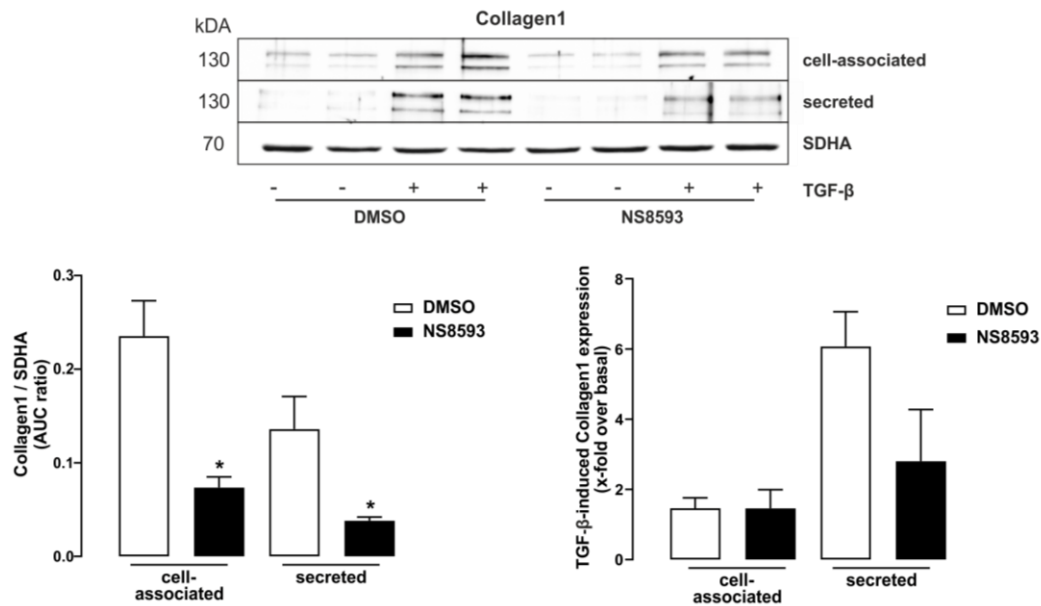
Figure 62: TRPM7 blockade inhibits basal collagen1 protein levels in pHPF

Cells were stimulated with TGF-β (2 ng/ml) or NS8593 (25 µM) or co-stimulated for 48 h. Protein amounts of collagen1 and SDHA (loading control) were determined in the cell-associated and secreted fraction via Western Blot and normalized to SDHA of the cell-associated fraction. Blots of the cell-associated fraction were cut in half to detect collagen1 (130 kDa) and SDHA (70 kDa). The loading control of the cell-associated fraction was also used for the secreted fraction. One set of representative blots is shown. Bars represent SEM of AUC ratios or x-fold over basal, n = 4. Statistical analysis was performed using two-way ANOVA followed by Tukey´s post-test. Asterisks indicate significant differences to the carrier control, * $p < 0.05$.
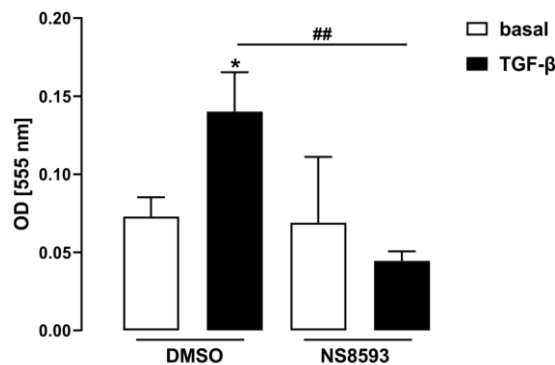

Figure 63: TRPM7 blockade inhibits TGF-β-induced collagen secretion from pHPF

pHPF were stimulated with TGF-β (2 ng/ml) or NS8593 (25 µM) or co-stimulated for 48 h and secreted collagen amounts were determined using Sircol™-soluble collagen assay. Bars represent SEM of OD 555 values, n = 5. Statistical analysis was performed using two-way ANOVA followed by Tukey´s post-test. Asterisks indicate significant differences to basal, hash signs indicate significant differences between DMSO and NS8593, * $p < 0.05$, ## $p < 0.01$.

Importantly, two possibilities for SMADs to enhance ECM production have been reported. Firstly, by directly inducing transcription of fibronectin and collagen and secondly via modulation of the plasmin system. Thus, to evaluate whether the effects of NS8593 on ECM proteins were due to direct effects of SMAD on these proteins or via modulation of the plasmin system, mRNA levels of *FN1*, *COL1A1* and *SERPINE1* after stimulation with TGF-β and NS8593 were detected. On the mRNA level, NS8593 inhibited TGF-β-induced expression *of SERPINE1* from 3.42 ±0.32 to 2.37 ± 0.19 fold over basal, but not of *FN1* or *Col1A1*, indicating that TRPM7 blockade selectively targets TGF-β-mediated induction of *SERPINE1* (fig 64).
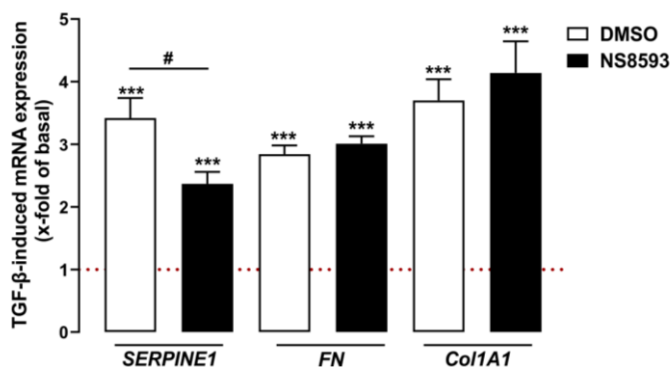
Figure 64: TRPM7 blockade reduces *SERPINE1*, but not *FN1* and *Col1A1* mRNA levels in pHPF

SERPINE1, *FN1* and *Col1A1* mRNA amounts of pHPF were determined by qRT-PCR after 48 stimulation with TGF-β (2 ng/ml) or NS8593 (25 μM) or co-stimulation. Bars represent SEM of x-fold over basal values, n = 4. Statistical analysis was performed using two-way ANOVA followed by Tukey´s post-16test or one-sample t-test. Asterisks indicate significant differences to basal, hash signs indicate significant differences to one, # $p < 0.05$, ***/### $p < 0.001$.

TGF-β induces fibroblast to myofibroblast differentiation via phosphorylation of the transcription factor SMAD2. Two assays were used to monitor SMAD2 phosphorylation in this work. Firstly, a pSMAD2 ELISA was used and TGF-β was shown to significantly induce SMAD2 phosphorylation (fig 65 a). Stimulation with NS8593 reduced TGF-β induction from 2.02 ± 0.31 to 0.74 ± 0.12 fold over basal (fig 65 a). Western blot data of pSMAD2 confirmed these findings: TGF-β induction of 3.76 ± 1.09 was decreased to 0.25 ± 0.23 fold over basal after stimulation with

NS8593 (fig 65 b). Importantly, total SMAD2 protein levels remained unchanged after TGF-β or NS8593 stimulation, indicating that TRPM7 blockade targets phosphorylation rather than expression of SMAD2 (fig 66 a).
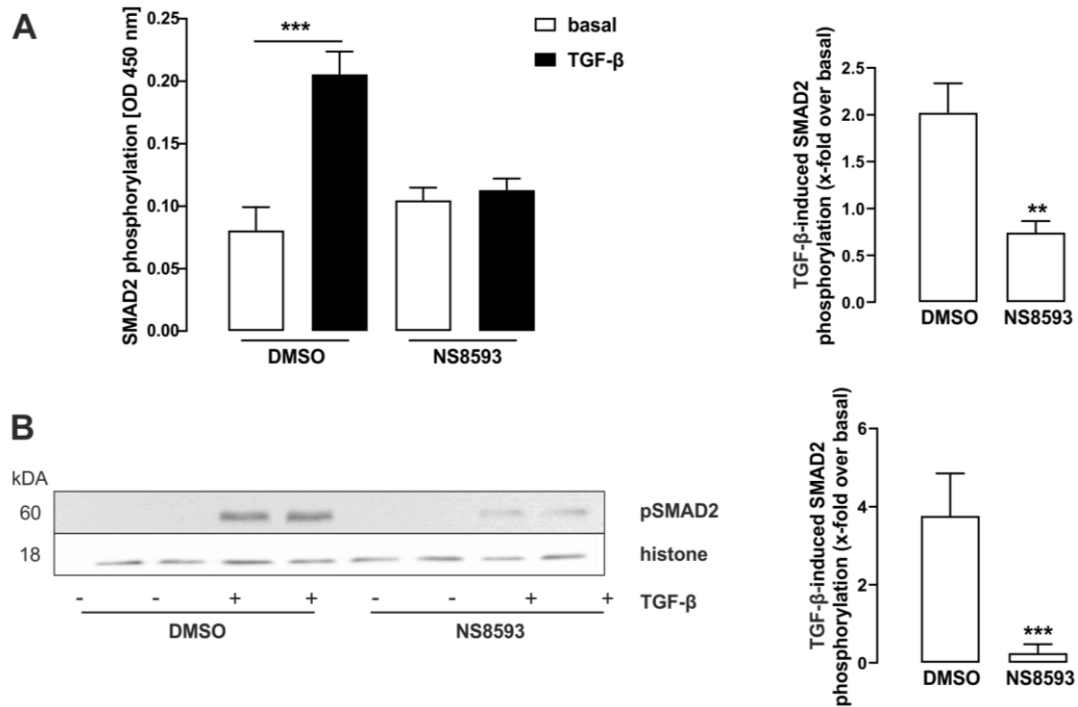
Figure 65: Effects of TRPM7 blockade on SMAD2 phosphorylation in pHPF

In **A**, the PathScan® Phospho-Smad2 Sandwich ELISA Kit was used to determine SMAD2phosphorylation after 40 min stimulation with TGF-β (2 ng/ml) and/or NS8593 (25 µM). Bars represent SEM of OD 450 values or x-fold over basal, n = 3. In **B**, cells were stimulated with TGF-β (2 ng/ml) or NS8593 (25 µM) or co-stimulated for 48 h and amount of pSMAD2 and histone (loading control) were determined via Western Blot. Blots were cut in half to detect pSMAD2 (60 kDa) and histone (18 kDa). One set of representative blots is shown. Bars represent SEM of or x-fold over basal, n = 4. Statistical analysis was performed using two-sample t-test (A, B) or two-way ANOVA (A) followed by Tukey´s post-test. Asterisks indicate significant differences to DMSO, ** $p<0.01$, *** $p<0.001$.
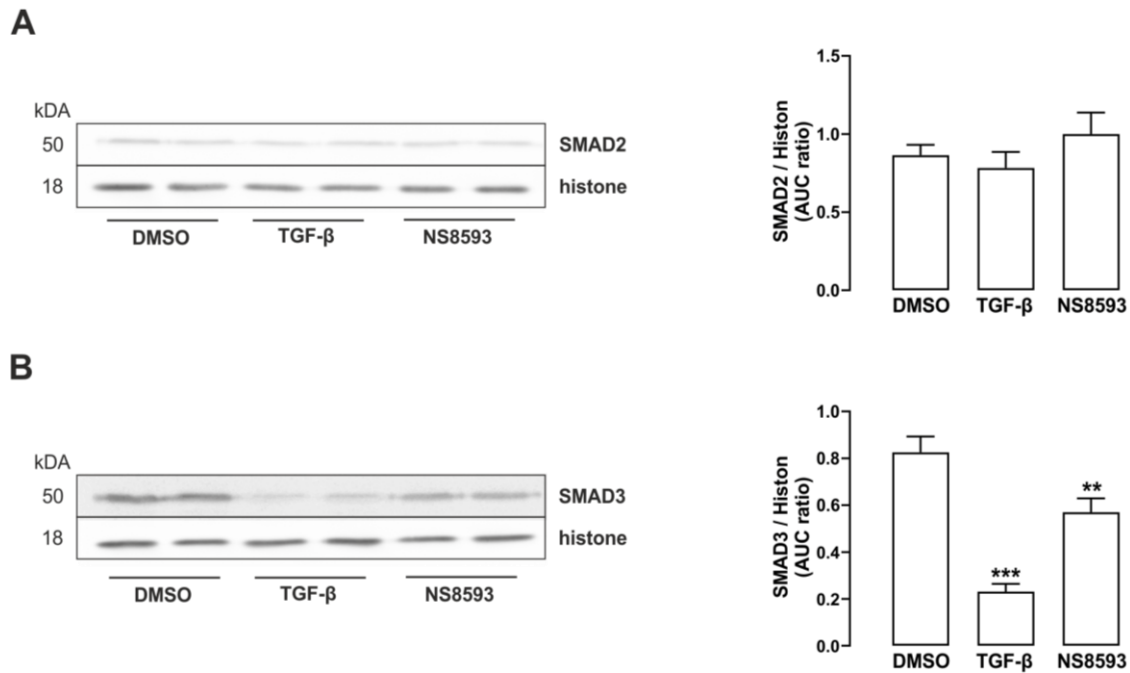
Figure 66: Effects of TRPM7 blockade on SMAD protein levels in pHPF

Cells were stimulated with TGF-β (2 ng/ml) or NS8593 (25 µM) for 48 h and protein amounts of SMAD2 (**A**), SMAD3 (**B**) and histone (loading control) were determined via Western Blot. Blots were cut in half to detect SMAD2 (60 kDa) or SMAD3 (50 kDa) together with their loading control histone (18 kDa). One set of representative blots is shown. Bars represent SEM of AUC ratios, n = 3-8. Statistical analysis was performed using one-way ANOVA followed by Tukey´s post-test. Asterisks indicate significant differences to DMSO, ** $p < 0.01$, *** $p < 0.001$.

SMAD3 has been reported to be reduced upon TGF-β stimulation in human pulmonary fibroblasts [173, 175]. Consistently, TGF-β was found to reduce SMAD3 protein levels in this work (fig 66 b). Interestingly, TRPM7 blockade with NS8593 also led to a reduction of SMAD3 protein levels (fig 66 b). To finally confirm the role of TRPM7 in TGF-β signaling in lung fibrosis, TGF-β-induced SMAD3/4 activation was studied. As shown in fig 67 a, NS8593 inhibited TGF-β induced SMAD3/4 activity from 10.65 ± 2.06 to 4.65 ± 0.46 fold over basal, while the apamin control showed no effects. TGF-β-induced YAP/TAZ activation remained unchanged with NS8593, indicating that TRPM7 blockade specifically targets TGF-β signaling at the level of SMAD activity (fig 67 b).
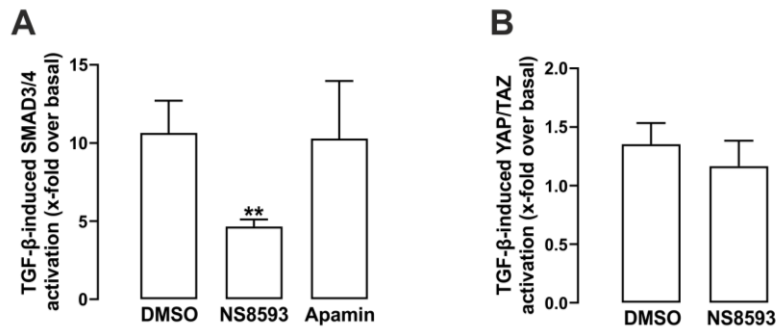
Figure 67: Effects of TRPM7 blockade on SMAD3/4 and YAP/TAZ activity in pHPF

pHPF were electroporated with the SMAD3/4 reporter plasmid (**A**) or with the YAP/TAZ reporter plasmid (**B**). After 24 h, cells were stimulated with TGF-β (2 ng/ml), NS8593 (25 µM) or Apamin (100 nM) or co-stimulated for 48 h and luciferase activity was determined. Bars represent SEM of x-fold over basal values, n = 5. Statistical analysis was performed using one-way ANOVA followed by Tukey´s post-test. Asterisks indicate significant differences to the carrier control, ** p<0.01.

In summary, these data propose TRPM7 blockade as a promising approach to selectively modulate the plasmin system in pHPF by interfering with TGF-β/SMAD signaling, resulting in enhanced plasmin activity and consequent degradation of ECM proteins.

6.4.3 Assessing the TRPM7 function linked to the plasmin system

TRPM7 consists of an ion channel permeable for bivalent cations and a kinase domain that phosphorylates TRPM7 itself or other substrates. Romagnani et al. could show that SMAD2 is a direct substrate of the TRPM7 kinase, therefore TRPM7 kinase has been proposed as the link to the plasmin system in this work [329]. The TRPM7 blockers NS8593 and Waixenicin A do not distinguish between these functions [323, 324]. In fact, TG100-115 is the only compound available that has been proposed to selectively inhibit TRPM7 kinase but not channel function in breast cancer cells [327]. Kinase inhibition has however only been reported under defined conditions and has never been reported after 24 or 48 h. Initially introduced as inhibitor of phosphoinositide 3-kinase isoforms gamma and delta, selective inhibition of TRPM7 remains however rather questionable [328]. As shown in fig 68a, incubation with TG100-115 did not affect plasmin activity. In line with this

notion, no effects of TG100-115 were detected on basal as well as TGF-β-induced PAI1 protein levels (fig 68 b).
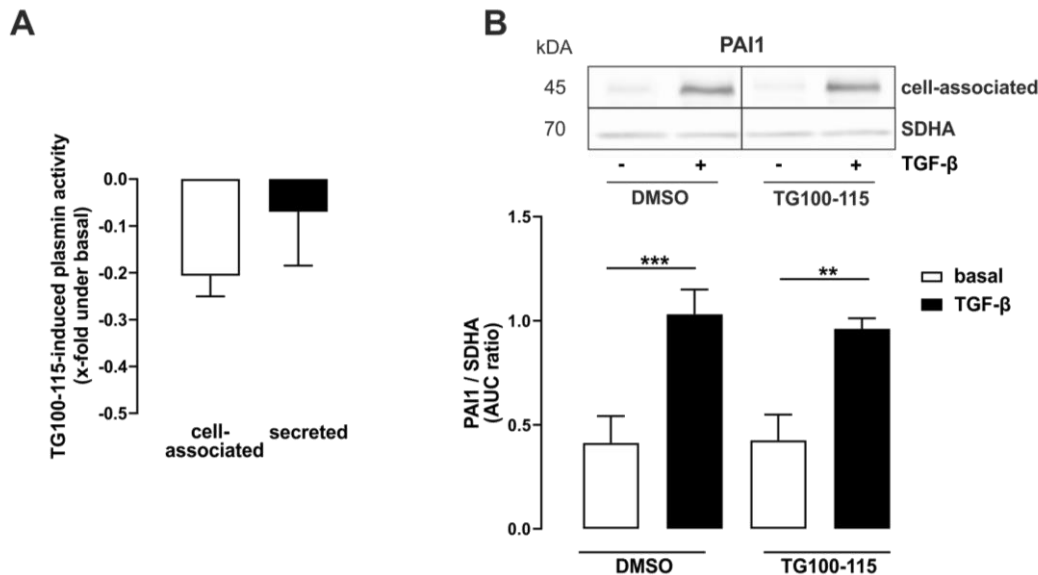
Figure 68: Effects of TG100-115 on plasmin activity or PAI protein levels

pHPF were stimulated with TGF-β (2 ng/ml) or TG100-115 (10 µM) or co-stimulated for 48 h. In **A**, fluorescence intensity of the secreted and cell-associated fraction was measured after incubation with D-Val-Leu-Lys-AMC (50 µM) for 3 h at 37 °C. Bars represent SEM of x-fold under basal values, n = 3. In **B**, protein amounts of PAI1 and SDHA (loading control) were determined via Western Blot. Blots were cut in half to detect PAI1 (45 kDa) and SDHA (70 kDa). One set of representative blots is shown. Bars represent SEM of AUC ratios, n = 3. Statistical analysis was performed using two-way ANOVA followed by Tukey´s post-test. Asterisks indicate significant differences to DMSO, ** $p<0.01$, *** $p<0.001$.

In order to discriminate between the two TRPM7 functions independently of pharmacological tools, a genetically modified mouse model was used, where lysine at position 1646 was replaced by arginine, therefore eliminating kinase activity [329, 382]. Basal protein levels of fibrotic markers from pulmonary fibroblast isolated from wild type or TRPM7-K1646R mice were compared in fig 69. Basal protein levels of PAI1, fibronectin and α-SMA were not distinguishable between murine and human pulmonary fibroblasts, and kinase deficiency did not affect basal protein levels of these fibrotic markers.
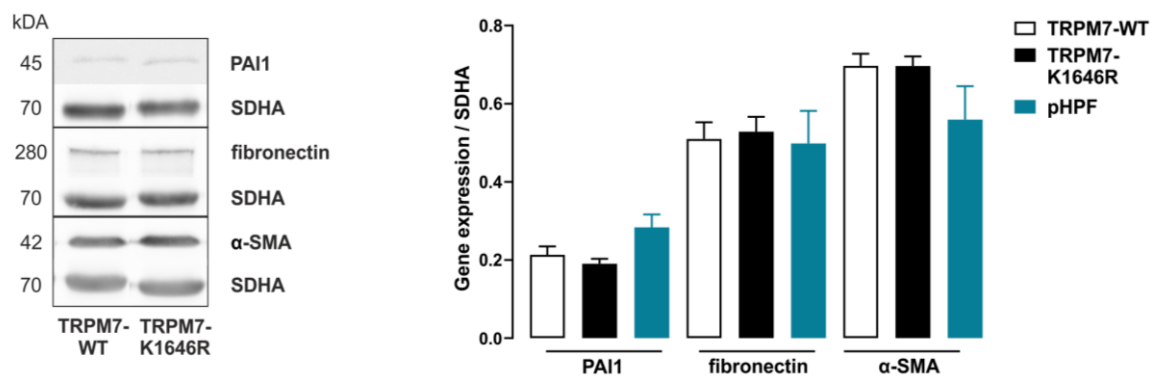
Figure 69: Comparison of fibrotic markers in TRPM7-WT and TRPM7-K1646R primary mouse pulmonary fibroblasts

Basal protein levels of fibrotic markers in pMPF isolated from TRPM7-WT or TRPM7-K1646R mice were determined by Western Blot. Blots were cut in half to detect α-SMA (42 kDa), PAI1 (45 kDa) or fibronectin (280 kDa) together with their loading control SDHA (70 kDa). One set of representative blots is shown. Results are compared to data from pHPF (fig 15). Bars represent SEM of AUC ratios, n = 4-5.

To investigate if TGF-β affects primary mouse pulmonary fibroblasts (pMPF) comparably to pHPF, SMAD signaling was studied. Indeed, SMAD3/4 reporter activity and pSMAD2 protein levels detected by Western blot were significantly increased after TGF-β stimulation of pMPF derived from both mouse genotypes (fig 70 a and b). Yet, no differences were detected between pMFP from wild type or TRPM7-K1646R mice. Further, induction of fibrotic markers by TGF-β was examined. Fig 71 a-c show TGF-β-induced elevation of α-SMA, PAI1 and fibronectin. While TGF-β significantly induced all of the above-mentioned fibrotic markers, no difference was seen when cells from wild type or TRPM7-K1646R mice were compared (fig 71 a-c).

Figure 70: TGF-β enhances SMAD activity in pMPF

pMPF isolated from TRPM7-WT or TRPM7-K1646R mice were stimulated with TGF-β (2 ng/ml) for 48 h. In **A**, pMPF were electroporated with the SMAD3/4 reporter plasmid 24 h before stimulation and luciferase activity was determined. Bars represent RLU, n=4. In **B**, protein amounts of pSMAD2 and histone (loading control) were determined via Western Blot. Blots were cut in half to detect pSMAD2 (60 kDa) and histone (18 kDa). One set of representative blots is shown. Bars represent SEM of AUC ratios, n = 5. Statistical analysis was performed using two-way ANOVA followed by Tukey´s post-test. Asterisks indicate significant differences to basal, *** $p < 0.001$.
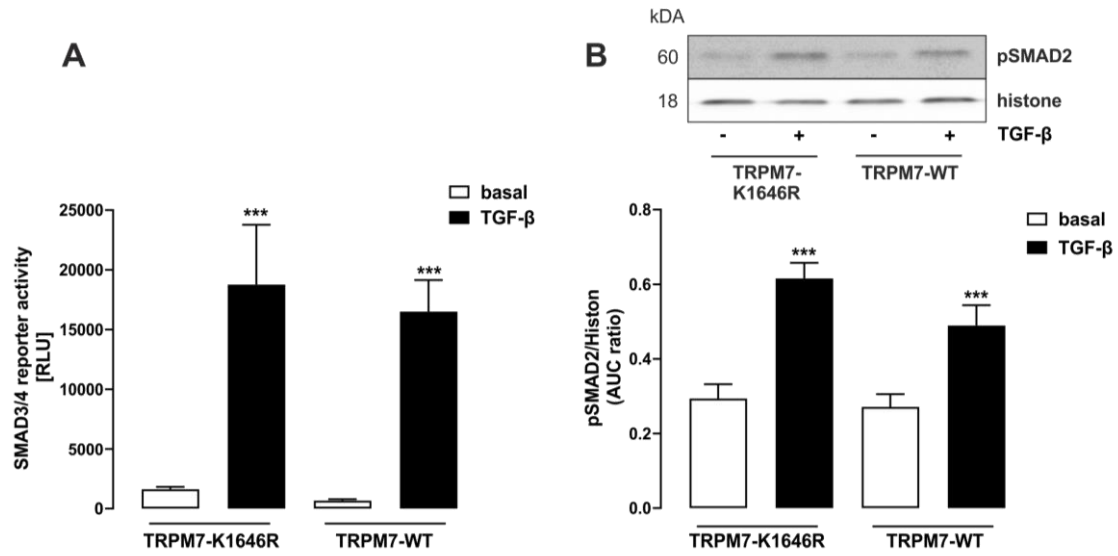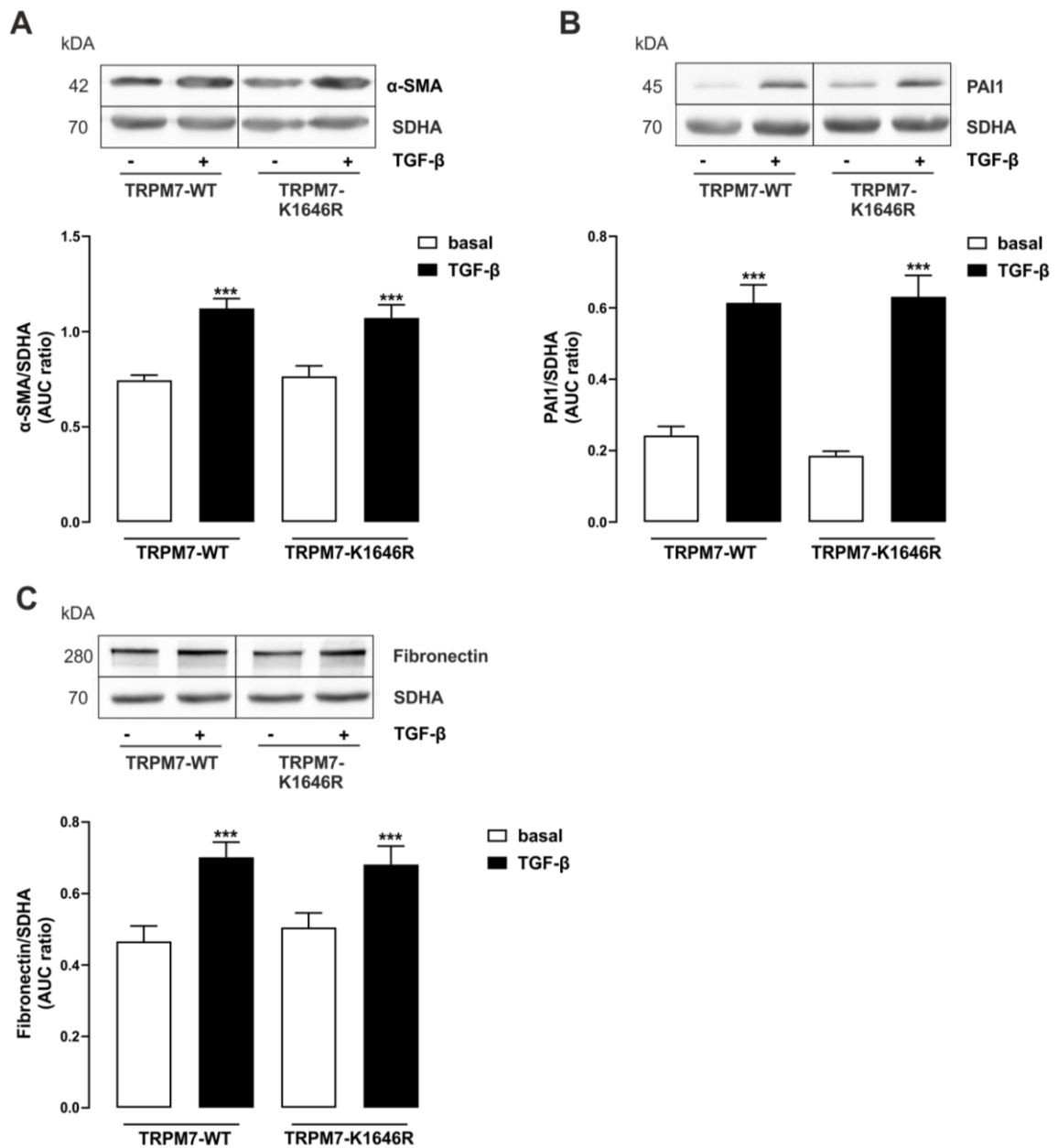
Figure 71: TGF-β enhances protein levels of fibrotic markers in pMPF

pMPF isolated from TRPM7-WT or TRPM7-K1646R mice were stimulated with TGF-β (2 ng/ml) for 48 h. Protein amounts of α-SMA (**A**), PAI1 (**B**), Fibronectin (**C**) and SDHA (loading control) were determined via Western Blot. Blots were cut in half to detect α-SMA (42 kDa), PAI1 (45 kDa) or fibronectin (280 kDa) together with their loading control SDHA (70 kDa). One set of representative blots is shown. Bars represent SEM of AUC ratios, n = 4-5. Statistical analysis was performed using two-way ANOVA followed by Tukey´s post-test. Asterisks indicate significant differences to basal, *** $p < 0.001$.

In pMPF, TGF-β enhanced SMAD activity and protein levels of fibrotic markers comparably to pHPF, thus, the next step was to analyze effects of NS8593. However, neither SMAD3/4 activity nor PAI1 protein levels were affected by TRPM7 blockade in pMPF from wild type mice, in contrast to the strong effects in pHPF, pointing at species-specific effects of TRPM7 activity (fig 72 a and b). SMAD3/4-dependent reporter activation was also measured after stimulation with TG100-115, however no effects were detected (fig 72 a). In addition to pMPF, the mouse fibroblast cell line L929 was tested in the plasmin assay in order to analyze whether the lack of effects after TRPM7 blockade was specific for the isolated pMPF or a common feature of mouse-derived cells. Interestingly, TGF-β did not affect plasmin activity in pMPF or L929 cells. Similarly, NS8593 showed no effects on plasmin activity in pMPF or L929, implying that the entire plasmin system in mice may be regulated via different signaling pathways compared to the human system (fig 72 c-f).

Further, effects of TGF-β on SMAD3 protein levels appeared to be completely different compared to pHPF. When stimulated with TGF-β, no changes in SMAD3 expression in pMPF were detected, in contrast to the strong inhibition observed in pHPF (fig 73). In summary, several species-specific differences were detected concerning TGF-β signaling and actions of NS8593.
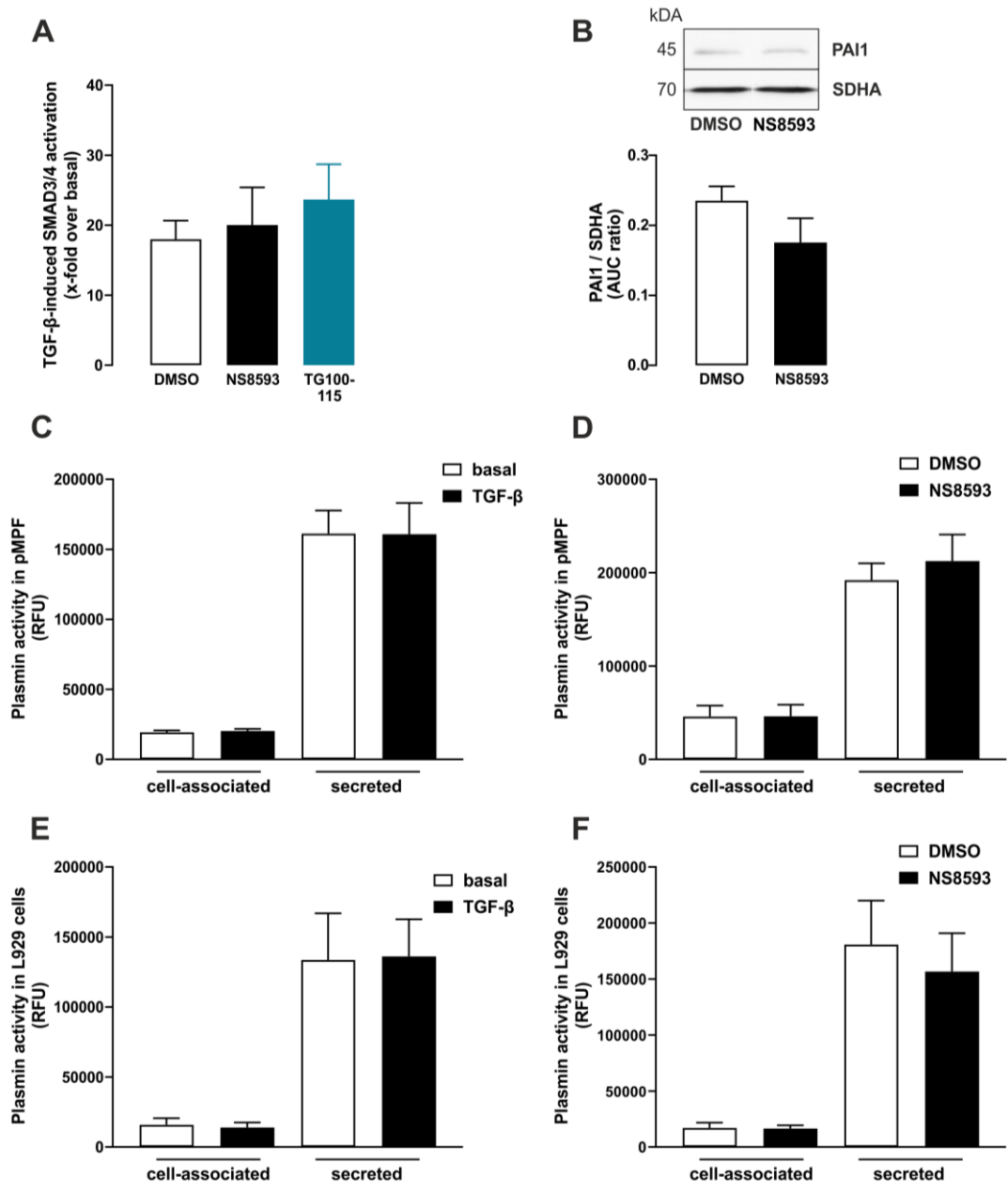
Figure 72: NS8593 does not affect SMAD3/4, PAI1 protein levels or plasmin activity in pMPF or L929 cells

WT pMPF or L929 cells were stimulated with TGF-β (2 ng/ml), NS8593 (25 µM) or TG100-115 (10 µM) for 48 h. In **A**, pMPF were electroporated with the SMAD3/4 reporter plasmid 24 h before stimulation and luciferase activity was determined. Bars represent RLU, n=3. Protein amounts of PAI1 and histone or SDHA (loading control) were determined via Western Blot in **B**. Blots were cut in half to detect PAI1 (45 kDa) and SDHA (70 kDa). One set of representative blots is shown. Bars represent SEM of AUC ratios, n = 3. In **C-F**, plasmin activity of pMPF or L929 cells was determined. Bars represent x-fold over/under basal, n=4-8.
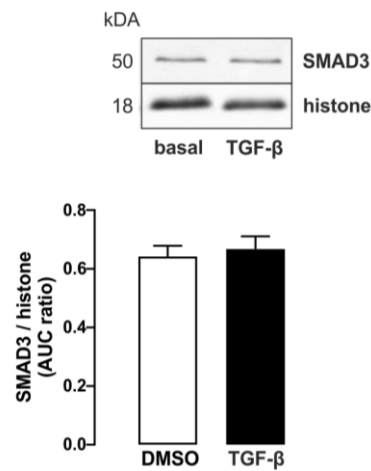
Figure 73: Effects of TGF-β on SMAD3 protein levels in pMPF

WT pMPF were stimulated with TGF-β (2 ng/ml) for 48 and protein amounts of SMAD3 and histone (loading control) were determined via Western Blot. Blots were cut in half to detect SMAD3 (50 kDa) or histone (18 kDa). One set of representative blots is shown. Bars represent SEM of AUC ratios, n = 6.

6.4.4 TRPM7 blockade counteracts epithelial to mesenchymal transition in human lung tumor cell lines

TGF-β has been shown to induce epithelial to mesenchymal transition relevant for tumor progression during 48 h stimulation [284]. Therefore, the relevance of TGF-β and NS8593 mediated effects on the plasmin system in the context of lung tumor was studied in this work. Indeed, when human lung cancer cell lines A549 and H1299 were stimulated with TGF-β, EMT markers PAI1 and fibronectin significantly increased (fig 74 a and 75 a). Of note, TGF-β induction of PAI1 and fibronectin in

H1299 was dramatically lower compared to A549 cells, which stands in accordance with the findings shown in fig 28. To assess a possible role of TRPM7 on TGF-β-induced EMT, cells were stimulated with NS8593 or co-stimulated with NS8593 and TGF-β. NS8593 reduced TGF-β-induced PAI1 protein levels from 18.31 ± 1.08 to 12.39 ± 1.51 fold over basal and fibronectin protein levels from 7.21 ± 1.77 to 1.15 ± 0.19 fold over basal in A549 cells (fig 74 a).
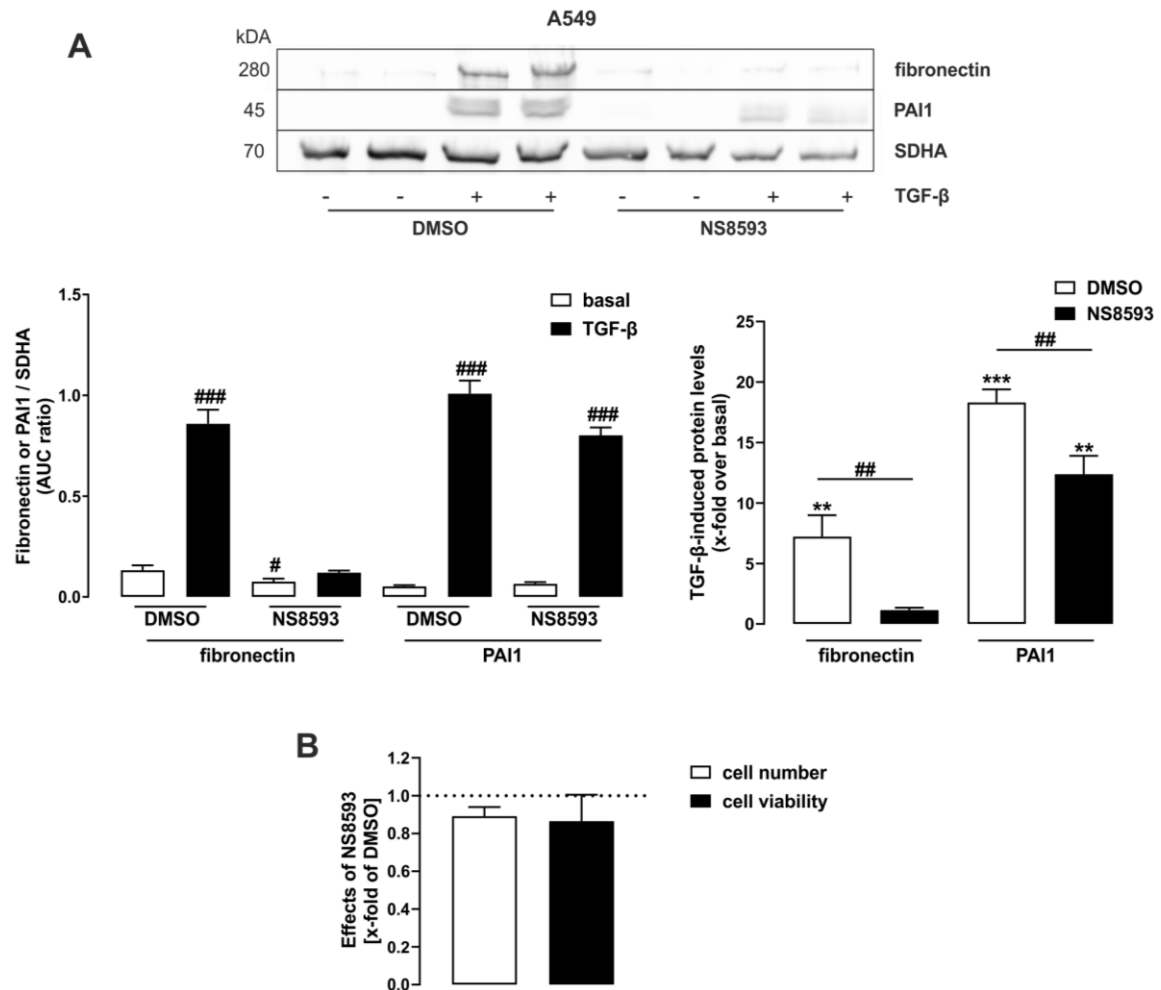
Figure 74: Effects of TRPM7 blockade on TGF-dependent PAI1 or fibronectin protein levels in A549 cells

A: A549 cells were stimulated with TGF-β (2 ng/ml) or NS8593 (25 μM) or co-stimulated for 48 h and protein amounts of PAI1, fibronectin and SDHA (loading control) were determined via Western Blot. Blots were cut in half to detect PAI1 (45 kDa) or fibronectin (280 kDa) together with their loading control SDHA (70 kDa). One set of representative blots is shown. Bars represent SEM of AUC ratios or x-fold over basal, n = 3-5. In **B**, cell number was determined via SRB and cell viability via WST-1 assay. Bars represent SEM of x-fold of DMSO, n = 3-6. Statistical analysis was performed using one-sample t-test or two-way ANOVA followed by Tukey´s post-test. Hash signs indicate significant differences to the carrier control and asterisks indicate significant differences to zero, $^{\#}$ $p<0.05$, **/$^{\#\#}$ $p<0.01$, *** $p<0.001$.

Additionally, a reduction of basal fibronectin expression in A549 cells was observed (fig 74 a). In H1299 cells, NS8593 significantly reduced TGF-β-induced PAI1 protein levels to 0.51 ± 0.06 fold compared to 0.85 ± 0.10 fold over basal and fibronectin protein levels to 0.39 ± 0.16 compared to 0.70 ± 0.18 fold over basal (fig 75 a). Besides, NS8593 inhibited basal PAI1 and fibronectin protein levels in H1299 cells (fig 75 a). Of note, no adverse effects of NS8593 on cell number or cell viability were observed with this stimulation protocol in either of the cell lines (fig 74 b and 75 b). This data suggests a role of TRPM7 in TGF-β-induced EMT of lung tumor cells.
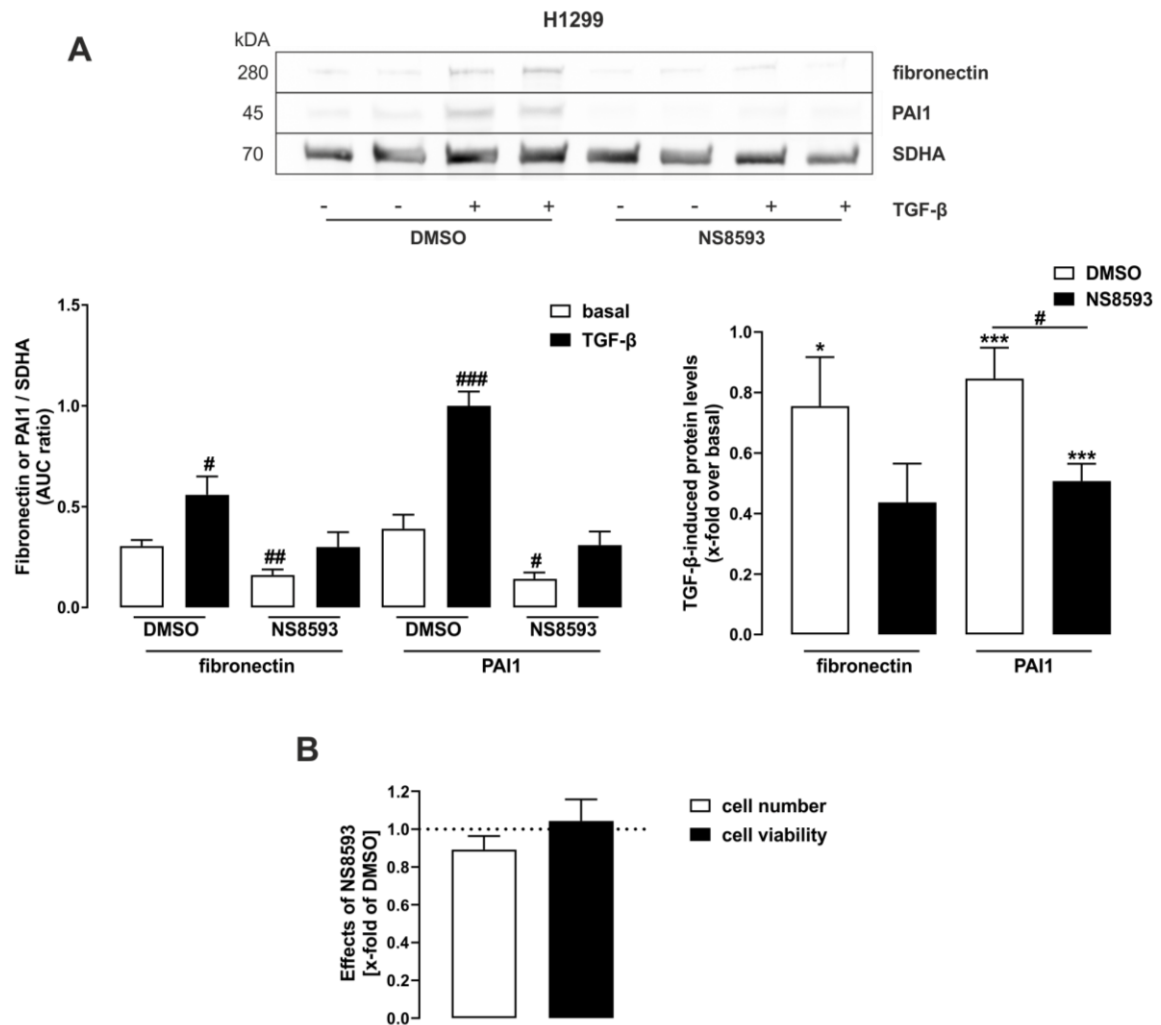
Figure 75: Effects of TRPM7 blockade on TGF-dependent PAI1 or fibronectin protein levels in H1299 cells

A: H1299 cells were stimulated with TGF-β (2 ng/ml) or NS8593 (25 µM) or co-stimulated for 48 h and protein amounts of PAI1, fibronectin and SDHA (loading control) were determined via Western Blot. Blots were cut in half to detect PAI1 (45 kDa) or fibronectin (280 kDa) together with their loading control SDHA (70 kDa). One set of representative blots is shown. Bars represent SEM of AUC ratios or x-fold over basal, n = 3-5. In **B**, cell number was determined via SRB and cell viability via WST-1 assay. Bars represent SEM of x-fold of DMSO, n = 3-6. Statistical analysis was performed using one-sample t-test or two-way ANOVA followed by Tukey´s post-test. Hash signs indicate significant differences to the carrier control and asterisks indicate significant differences to zero, *'# p<0.05, ## p<0.01, ***/### p<0.001.

7.   Discussion

This work established a protocol for reliable measurements of plasmin activity in distinct lung cells. Data provided in this study revealed a correlation between plasmin activity, TGF-β/SMAD signaling and PAI1 expression in pHPF. Further, unique effects of TGF-β on plasmin activity in a late stage compared to an early stage tumor cell line were found. In addition, small molecule inhibitors of TRPM7 were found to increase plasmin activity, thus being the first description of a link between plasmin activity and an ion channel. TRPM7 was found to restrain plasmin activity by supporting TGF-β-mediated PAI1 expression, thus reducing degradation of ECM proteins in distinct lung cells. TRPM7 blockers are thus presented as valuable tools to increase plasmin activity and to target ECM accumulations.

7.1   Measurement of plasmin activity

Plasmin activity is key in degrading ECM proteins and thus linked to diseases with aberrant ECM remodeling like fibrosis or cancer. Increased plasmin activity has previously been attributed to tumor cells in advanced stages by promoting migration of cells and invasion into other tissues. Surprisingly, plasmin activity has rarely been measured directly, instead conclusions on plasmin activity were drawn from analyzing modulators of plasmin activity like uPA or PAI1. Thus, the first aim of this work was to establish a plasmin activity assay using a synthetic substrate.

As previously described, the synthetic substrate D-Val-Leu-Lys-AMC is cleaved by active plasmin [356]. While the substrate is not cleaved by other proteases like factor Xa, α-thrombin or uPA, it is cleaved by kallikrein, however to a far lesser extent compared to plasmin, as explained in detail in chapter 5.2 [356, 357]. In this work, several controls were added to live-measurements of both cellular fractions to ensure specific detection of plasmin activity (see chapter 6.1). That way, unspecific interactions between the substrate and the cell culture medium were excluded. Further, by adding the plasmin inhibitor α2-antiplasmin, fluorescence signals significantly decreased [45]. Accordingly, addition of the plasmin precursor plasminogen significantly increased fluorescence [18]. Thus, changes in

fluorescence were defined as plasmin-dependent turnover of D-Val-Leu-Lys-AMC to reliably monitor plasmin activity.

Plasmin acts when bound to its receptor or when in solution, however previous studies exclusively used cell supernatant to measure plasmin activity [30, 31]. In this work, plasmin activity was measured in the cell-associated and in the secreted fraction of cells and thus provides data of cell-bound plasmin activity for the first time. Basal plasmin activity was significantly higher in the secreted fraction of all tested cells, suggesting an increased activity of plasmin when released from its receptor (fig 18). However, it should be noted that due to the experimental setup, the volume of the supernatant was considerably larger than the volume of the cell-associated fraction. Fibroblasts have a volume of 2000 μm^3 per cell and epithelial cells only have around half of that volume, thus the total volume of the cells within one well of the plate used in the experiments is around 0.01 – 0.02 µl [383, 384]. The volume of the secreted fraction was 50 µl per well, thus the actual plasmin concentration might be even higher in the cell-associated fraction.

As mentioned above, only a few studies measured plasmin activity directly. In these studies, exogenous plasmin was added to measure plasmin activity. Exogenous plasminogen was most likely added because the studies aimed at measuring inhibitory effects of TGF-β and thus saw a need to artificially increase the basal level of plasmin activity. In contrast to that, the results presented in this work clearly show basal plasmin activity as well as the inhibition of plasmin activity by TGF-β in pHPF without the addition of exogenous plasminogen (fig 23). It is possible that distinct cell types differ in their basal plasmin activity and thus determine whether exogenous plasminogen is needed. However, pHPF used in this work show no need for that and are comparable to the embryonic lung fibroblast cell line IMR-90 used in a previous study. Further, plasmin activity without exogenous plasminogen was successfully measured in several cell types, including primary cells pHPF and HPAEC as well as the epithelial lung cell line 16-HBE and two lung tumor cell lines, A549 and H1299. It thus seems likely that previous studies had to artificially increase plasmin activity due to restriction in sensitivity of their detection device. Data presented clearly demonstrates that this approach is not necessary with the experimental setup used in this work, since a

significant and stable decrease of plasmin activity after TGF-β stimulation was observed without the addition of exogenous plasminogen. A positive side effect of not having to add exogenous plasminogen is the representation of native cellular conditions, since binding of plasminogen to its receptor is known to activate various signaling pathways relevant for cellular processes and inflammatory responses [3, 385, 386].

In summary, this work provides a valuable and reliable tool for future studies to decipher the role of plasmin activity in various lung cell types.

7.2   TGF-β-dependent regulation of plasmin activity in pHPF

The canonical TGF-β signaling pathway via SMAD proteins regulates expression of a variety of genes, including *SERPINE1*, which encodes the negative modulator of plasmin activation PAI1. It is a well described pathway and correlates with enhanced ECM deposition in fibrotic diseases. Aim of this work was to confirm the functionality of TGF-β signaling in pHPF. Since no protocol for transfection of pHPF was available, a new protocol for successful electroporation of pHPF was established to study SMAD3/4 activity. It could be confirmed that TGF-β signaling promotes SMAD3/4 activity and SMAD2 phosphorylation in pHPF (fig 20). Further, mRNA expression and protein levels of the known TGF-β-dependent genes *SERPINE1* (PAI1), *Col1A1* (collagen1) and *FN1* (fibronectin) were tested. Indeed, all three genes were induced by TGF-β stimulation on the mRNA and on the protein level. Interestingly, mRNA induction of these three genes seem to follow distinct kinetics (fig 78).

In line with the measurement of plasmin activity in both cellular fractions, protein levels were also assessed in the cell-associated and in the secreted fraction. PAI1, fibronectin and collagen1 protein levels were increased in both fractions to a similar extent by TGF-β (fig 22).

In summary, TGF-β affects SMAD signaling and expression of SMAD dependent genes as expected in pHPF. TGF-β signaling via SMAD proteins is not only important in the context of the plasminogen activation system, but is also known to be of utmost importance in the differentiation of fibroblasts to myofibroblasts and

the concomitant upregulation of fibrotic markers. As expected, an increase of fibrotic markers like α-SMA, fibronectin and collagen1 was found after prolonged TGF-β stimulation of pHPF (see chapter 6.4.1).

Despite the importance of TGF-β on modulators of the plasminogen activation system like PAI1 and on proteins of the ECM, direct effects of TGF-β on plasmin activity have rarely been measured in tumor cells or pHPF. As expected and in line with the effects of TGF-β on PAI1, a decrease of plasmin activity after TGF-β stimulation was found in the secreted fraction of pHPF. This result is in line with previously published results that measured inhibition of plasmin activity after TGF-β stimulation in the cell supernatant [358, 367]. Additionally, inhibition of plasmin activity was measured in the cell-associated fraction in this work, therefore providing first data for the effects of TGF-β in distinct cellular fractions. Interestingly, the inhibitory effect of TGF-β on plasmin activity was notably stronger in the secreted fraction compared to the cell-associated fraction. Plasmin activity in these distinct fractions could have different effects. While cell-associated plasmin activity might primarily affect the cell itself or the cells nearby, cells might secrete plasmin to affect cells farther away within the tissue or the lung. Thus, TGF-β would mainly reduce the cells ability to secrete plasmin. Of note, the effects of TGF-β on plasmin activity correlated with a decreased cell migration, thus providing a possible link between plasmin and migration of cells. In summary, this work describes for the first time an inhibitory effect of TGF-β on plasmin activity in pHPF.

7.3 Differences in the regulation of plasmin activity in lung tumor cells

In accordance with the statements postulated in the literature, increased basal plasmin activity was expected in the tumor cell lines A549 and H1299 compared to non-tumor cell lines [14, 82]. However, the opposite was true and tumor cell lines exhibited lower basal plasmin activity than all other tested cells. It could be discussed that cell lines in culture lose certain cellular features or undergo changes in key characteristics upon passaging, thus future studies should include testing of primary lung cancer cells in this assay [387]. Further, migratory and invasive features of lung cancer cells might not be determined by basal levels of plasmin activity, but rather by responses to certain stimuli and consequent regulation of the plasmin system.

Further, as described in chapter 3.4.4, it has yet to be clarified whether and how basal plasmin activity differs between an early stage tumor cell line (A549) and a metastatic tumor cell line (H1299). Surprisingly, this work demonstrates that plasmin activity of invasive H1299 cells was significantly lower than of A549 cells (fig 29). Possible explanations for this unexpected finding are described in the following paragraph. In view of the data provided in this work and the complex regulation of the plasmin system, the necessity arises to directly measure plasmin activity rather than concluding from plasmin modulators. Thus, the establishment of the plasmin activity assay in this work provides a valuable tool for future studies to decipher the role of plasmin in the tumor environment.

TGF-β signaling via SMAD proteins has been linked to increased migration of tumor cells, however the role of TGF-β in tumor progression is complex and is thought to depend on the stage of the tumor. Thus, SMAD activity and PAI1 expression of A549 and H1299 cells was tested in this work.

SMAD2 phosphorylation and SMAD3/4 activation were significantly increased in both cell lines after TGF-β stimulation, with SMAD2 phosphorylation peaking at 40 min. Accordingly, PAI1 protein levels were induced by TGF-β in both cell lines. The plasmin substrate fibronectin was, however, only induced in A549 cells after TGF-β stimulation. Of note, TGF-β-induced SMAD2 phosphorylation, SMAD3/4 activity

and PAI1 expression were significantly lower in H1299 cells, suggesting a different regulation or importance of this pathway in these cell lines (see chapter 6.2.3). Inhibitory SMADs like SMAD6 inhibit TGF-β signaling by competing with R-SMADs or Co-SMAD4, thereby preventing SMAD2 activation by the receptor or nuclear translocation of the SMAD complex [168, 169].The overexpression of SMAD6 in H1299 cells mentioned in chapter 3.4.4 could thus possibly explain reduced SMAD2 phosphorylation as well as lower SMAD3/4 activity observed in these cells. In line with that finding, basal SMAD3/4 activity was dramatically lower in H1299 cells. Measurement of YAP/TAZ activity as SMAD-independent TGF-β signaling target revealed further differences between the two cell lines. YAP/TAZ is known to promote EMT of cancer cells, thus a higher YAP/TAZ activity is assumed in the invasive H1299 cells [237]. However, no differences in basal YAP/TAZ activity and even a higher induction by TGF-β in A549 cells were observed (fig 27). This result is in line with the assumption that A549 cells exhibit higher RhoA activity due to their loss of DLC1, since YAP/TAZ is a prominent target of RhoA signaling. TGF-β has however been shown to induce YAP/TAZ signaling via ERK1/2, thus increased ERK1/2 postulated in H1299 cells due to their N-ras mutation should manifest in a higher YAP/TAZ activation [252]. Thus, more research is needed to decipher the role of YAP/TAZ in these cell lines. In summary, data on SMAD and YAP/TAZ activity in A549 and H1299 cells further undermine the possibility of distinct effects of TGF-β.

To assess a possible consequence of lower TGF-β-induced SMAD signaling and PAI1 expression in H1299 cells compared to A549 cells, plasmin activity after TGF-β stimulation was compared in the two cell lines. Similar to the effects observed in pHPF, TGF-β decreased plasmin activity in A549 cells. However, an entirely unexpected observation in contrast to that was found in H1299 cells, where TGF-β stimulation led to a strong increase of plasmin activity (fig 29). This finding is unique and was followed by extensive research to decipher the differences of TGF-β on plasmin activity in early and late stage lung tumor cells. As mentioned before, H1299 cells showed significant lower SMAD activation and PAI1 protein levels after TGF-β stimulation, however these findings cannot explain the dramatic difference observed in plasmin activity. Thus, it appears that not only SMAD-

mediated PAI1 levels account for the modulation of plasmin activity and that the complexity of the plasminogen activation system in tumor cells has previously been underestimated. Therefore, mRNA levels of several possible modulators of plasmin activity were analyzed (fig 30). In accordance with the reduced PAI1 protein induction by TGF-β in H1299, TGF-β-induced *SERPINE1* mRNA expression levels were also significantly lower in H1299 cells. Basal expression of the direct plasmin inhibitor *SPINT2* (HAI2) was lower in H1299, as expected from the literature [14]. Interestingly, TGF-β decreased *SPINT2* expression in A549, which stands in contrast to its decreasing effects on plasmin activity, thus suggesting that *SERPINE1* is the major modulator of plasmin activity in these cells. In H1299 cells, *SPINT2* expression was not affected by TGF-β, thus regulation of *SPINT2* does not provide an explanation for the increase in plasmin activity in H1299 cells. Further, *PLAU* (uPA) and *PLAUR* (uPA receptor) mRNA levels were analyzed. Interestingly, TGF-β decreased *PLAU* and *PLAUR* in A549, which stands in contrast to a previously reported increase in uPAR expression by TGF-β in these cells [388]. One explanation for these different findings could be the stimulation procedure, since cells were stimulated in medium containing FCS in this work, but experiments from previously published results were conducted in the absence of FCS. The additional FCS, containing a variety of growth factors and hormones, might affect the plasmin activation system via various signaling pathways. ERK1/2 for example, which has been reported to be activated by FCS, induces uPAR expression and might explain the aberrant effects of TGF-β on uPAR expression observed in this work [389, 390]. Further studies are required to decipher the effects of serum on uPAR expression in distinct cells. However, TGF-β increased *PLAU* mRNA levels in H1299, thereby providing a first possible explanation for increased plasmin activity by TGF-β in these cells. Indeed, increased levels of uPA are established biomarkers for invasive tumors and downregulation of uPA has been shown to reduce invasion of breast cancer cells [285, 391]. A previous study reported that TGF-β-induced uPA expression is dependent on ERK1/2 signaling in keratinocytes, thus increased ERK1/2 activity postulated in H1299 cells due to their N-ras mutation may explain the high levels of uPA [299, 300, 389].

In summary, it seems likely that distinct pathways are activated depending on the presence or absence of TGF-β: The possible pathways for basal (fig 76) and TGF-β stimulated (fig 77) conditions are depicted in two schematic overviews. Under basal conditions, H1299 show decreased SMAD activity, which can be explained by the SMAD6 overexpression reported in these cells. Despite that, basal PAI1 protein levels are higher than those observed in A549 cells, pointing to distinct regulation of PAI1 expression, independently of SMAD signaling. An explanation might be the increased ERK1/2 activity in H1299 cells due to their N-ras mutation, which leads to increased AP-1 induction, consequent PAI1 expression and plasmin inhibition. Importantly, YAP/TAZ does not seem to have a function in the regulation of basal plasmin activity in H1299 cells. As depicted in chapter 3.4.4, higher RhoA activity postulated in A549 may result in increased AP-1 and SMAD7 activity, in this case dependent on YAP/TAZ signaling, and consequent SMAD inhibition, thus explaining higher plasmin activity in A549 cells under basal conditions. However, data presented in this work does not support this theory, since basal SMAD2 phosphorylation and SMAD3/4 were not found to be lower in A549 cells compared to H1299 cells. Despite that, these differences in RhoA activity might account for the strongly diminished YAP/TAZ activity observed in H1299 cells. To test the importance of RhoA signaling in this context, future studies could determine levels of AP-1 and SMAD7 under basal conditions.
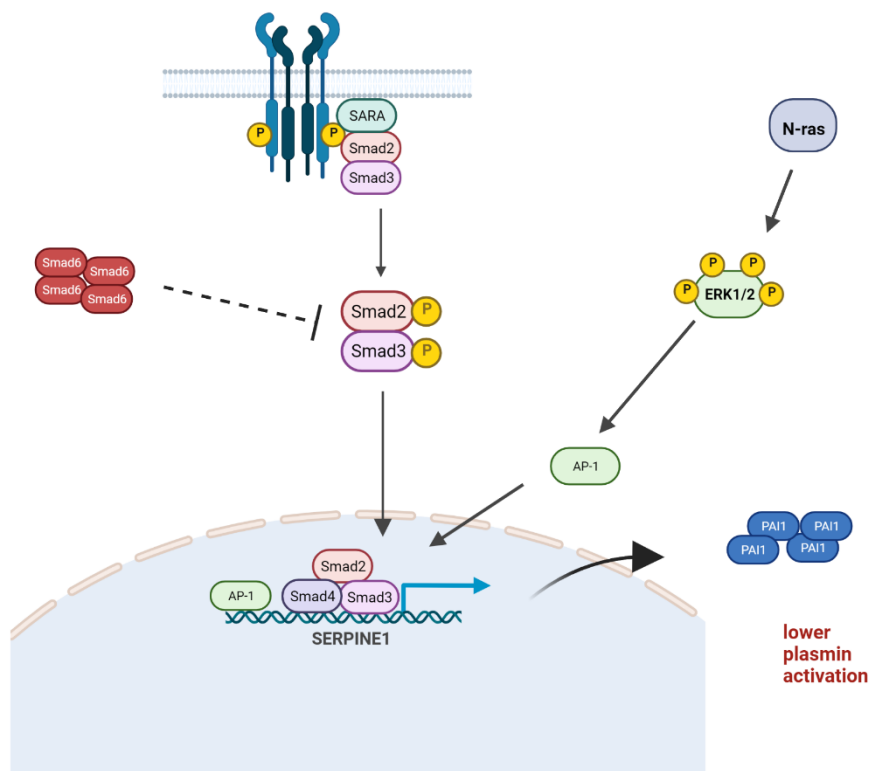
Figure 76: Schematic overview of a possible mechanism explaining lower basal plasmin activity in H1299 cells

AP-1: activator protein 1, PAI1: plasminogen activator inhibitor 1, SARA: SMAD anchor for receptor activation, P in yellow circle indicates phosphorylation.
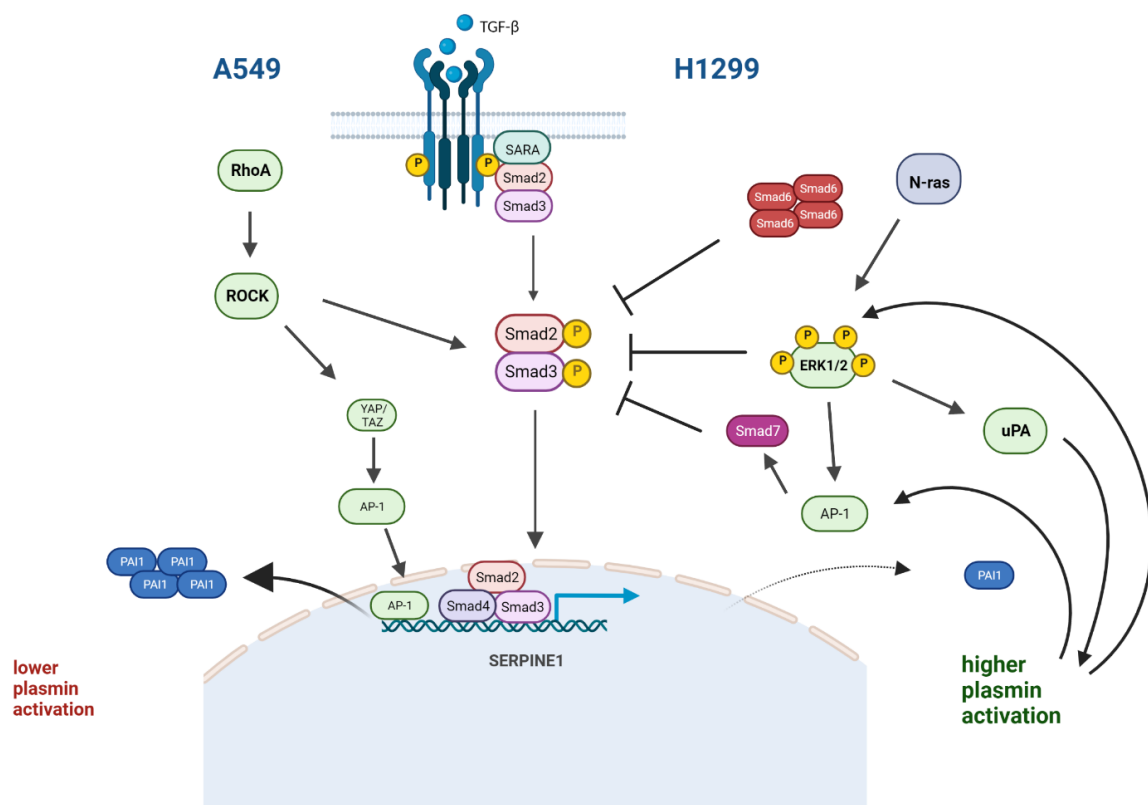
Figure 77: Schematic overview of a possible mechanism explaining the dramatic increase in plasmin activity in H1299 cells after TGF-β stimulation

AP-1: activator protein 1, PAI1: plasminogen activator inhibitor 1, ROCK: Rho-kinase, SARA: SMAD anchor for receptor activation, uPA: urokinase plasminogen activator, P in yellow circle indicates phosphorylation

In the presence of TGF-β, SMAD6 overexpression in H1299 cells could possibly explain lower SMAD and PAI1 induction by inhibiting SMAD signaling. Moreover, lower RhoA activity compared to A549 cells might also account for reduced SMAD, YAP/TAZ and AP-1 activity, resulting in reduced PAI1 expression. In compliance with this concept, lower YAP/TAZ induction by TGF-β was observed in H1299 cells. However, while these differences may explain why TGF-β does not reduce plasmin activity as observed in A549 cells, it seems unlikely that these differences account for the strong increasing effects on plasmin activity in H1299 cells. Increased ERK1/2 activity due to the N-ras mutation leading to inhibition of SMAD signaling

and PAI1 expression might additionally explain the increase in plasmin activity in H1299 cells. Most interestingly, plasmin-dependent activation of ERK1/2 and AP-1 has been reported, thus proposing a positive feedback loop [392, 393]. As plasmin promotes ERK1/2 activity as well as AP-1 transcriptional activity, SMAD signaling and PAI1 expression would be even further decreased, thereby eliminating TGF-β-induced PAI1 expression via SMAD signaling. This mode of action combined with induction of uPA by TGF-β may give a possible explanation for the increase in plasmin activity in H1299 cells upon TGF-β stimulation. Besides, uPA induction by TGF-β has been shown to be dependent on ERK1/2 signaling, thus increased ERK1/2 activity may further increase plasmin activity in these cells [389]. Accordingly, TGF-β-induced ERK1/2 phosphorylation was found to be higher in H1299 cells compared to A549 cells (fig 32 c). To support this theory, future studies should determine whether uPA induction by TGF-β is dependent on ERK1/2 activity in these cells.

To decipher cellular consequences of distinct TGF-β-mediated plasmin activity, cell migration was measured (fig 31). Interestingly, the metastatic cell line H1299 showed lower basal (not serum-induced) migration than the early stage A549 cells. While unexpected and not in line with the postulated stages of disease of these cell lines, this result still fits to the observed lower basal plasmin activity in H1299 cells. Considering the importance of YAP/TAZ and RhoA for cellular migration, it seems plausible that H1299 cells, who are thought to exhibit lower RhoA activity and who display significantly lower YAP/TAZ activity than A549 cells, also show reduced migration. When performed at the same conditions as the plasmin activity assay, TGF-β affected cell migration of both cell lines according to its distinct effects on plasmin activity in these cells, by increasing migration of H1299 cells and decreasing migration of A549 cells. It thus seems that basal features of lung tumor cells do not decide about the invasiveness of the cells, but rather the different responses to TGF-β. This finding stands in contrast to previously described increase in migration after TGF-β stimulation in A549 cells [394-396]. However, previous studies performed migration assays within a serum-gradient, thus measuring chemotaxis induced migration. When the protocol was changed and cells were allowed to migrate within a serum gradient, TGF-β reduced migration of

H1299 cells but increased migration of A549 cells, thus showing opposite effects compared to the basal migration assay. Increased migration of A549 after TGF-β stimulation in this protocol fits to previously reported effects. However, these effects were considerably smaller than those observed under basal, non-gradient conditions and could also stem from the effects of TGF-β on basal migration at low serum concentration. It thus appears that the well-established and widely used protocol for assessing migration with a chemoattractant is reliable and suitable to address defined scientific questions. However, measurement of serum-independent migration as a so far unattended opportunity to monitor cellular migration is revealed as suitable means to decipher the consequences of plasmin activity in this work. In summary, effects of TGF-β on plasmin activity seem to correlate with migratory features in both cell lines and targeting TGF-β signaling might affect migration of cancer cells.

7.4 Role of ERK1/2 in TGF-β signaling in lung tumor cells

The observed increase in plasmin activity in H1299 cells after TGF-β stimulation is unexpected and unique. While several factors, like reduced SMAD signaling and PAI1 expression compared to A549 offer a hint at different signaling pathways in these cell lines leading to stronger reduction of plasmin activity in A549 cells, they do not provide an explanation for the observed increase in plasmin activity. Thus, this work aimed at determining the difference in signaling pathways upon TGF-β stimulation in these cells. A549 cells carry a K-ras mutation, while H1299 cells carry a N-ras mutation, thus A549 and H1299 cell possibly differ in ERK1/2 activity. As shown in this work, H1299 display higher basal ERK1/2 phosphorylation levels than A549 cells, fitting to the assumption that the N-ras mutation in these cells leads to activation of ERK1/2 (fig 32a). With the above-mentioned positive feedback loop of plasmin and ERK1/2 activity and the dependency of uPA induction by TGF-β on ERK1/2 signaling, the next logical step was to look at the consequences of ERK1/2 inhibition on plasmin activity in these cells. To further decipher the differences of TGF-β on plasmin activity in distinct tumor cell lines, a MEK1/2 inhibitor was used to determine the role of ERK1/2 activity. ERK1/2 inhibition increased basal plasmin activity in H1299 cells, but not in A549 cells, thus

implying greater relevance of ERK1/2 signaling in H1299 cells (fig 32). Most interestingly, upon ERK1/2 inhibition, the increase in plasmin activity observed in H1299 after TGF-β stimulation was completely eliminated and even inverted to a decrease in plasmin activity, just as observed in A549 cells (fig 32). Thus, ERK1/2 seems to be responsible for the unique effects of TGF-β observed in H1299 cells, and blockade of ERK1/2 seems to adjust the effects of TGF-β in H1299 to those observed in A549 cells. Accordingly, basal SMAD3/4 activity increased in H1299 after ERK1/2 blockade, thereby resembling the effect observed in A549 cells (fig 33). Further, ERK1/2 blockade reduced TGF-β-induced SMAD3/4 and YAP/TAZ activity in A549, but not in H1299 cells, supporting the assumption of differences in the effects of ERK1/2 signaling on SMAD or YAP/TAZ signaling in these cells (fig 34). In summary, ERK1/2 signaling alone and in combination with TGF-β signaling seems to be of utmost importance in conferring differences in tumor cell lines from early or late stages of the disease. Further, inhibition of ERK1/2 seems to break the above-mentioned positive feedback loop in invasive lung cancer cells to a great extent, thus being able to restore TGF-β signaling to its normal state. Of note, mutations in K-ras are predominantly found in NSCLC while N-ras mutations are not frequently found, thus this work provides novel insight into cellular mechanisms for lung tumor cells with a specific N-ras mutation [296].

Interestingly, TGF-β seemed to be highly toxic to A549 cells after 5 days of stimulation, which was completely reversed with simultaneous ERK1/2 blockade. H1299 cells were unaffected by both protocols (fig 35). In view of this data, testing ERK1/2 blockade in migration and invasion assays seems a promising approach for future studies to assess the consequence of ERK1/2 and TGF-β interactions in tumor cell lines. Interestingly, growth inhibition of H1299 cells has previously been reported upon MEK1/2 blockade [300].

7.5 TRPM7 restrains plasmin activity in human lung cells

Due to its bifunctionality, TRPM7 could possibly affect cellular mechanisms via its kinase domain or by modulating levels of Ca^{2+}, Mg^{2+} or Zn^{2+} via its channel activity. It has yet to be clarified whether TRPM7 kinase is essential for TRPM7 channel function. Few studies reported that channel activity depends on a functional kinase domain [327, 397, 398]. By contrast, other studies clearly show that kinase activity is not required [329, 399]. Of note, TRPM7 kinase is regulated by Mg^{2+}, thus depending on the channel function [397]. An interdependency of channel function and kinase activity has therefore to be assumed.

As described in chapter 3.5.2, TRPM7-mediated levels of distinct cations are indeed considered as crucial factor influencing fibrotic diseases. Du et al stated that TRPM7-mediated Ca^{2+} levels support atrial fibrosis [330]. However, the methods used in this study could not exclude that the observed effects were dependent on Mg^{2+} levels or kinase function. Of note, they used the TRPM7 blocker 2-APB, which is not considered as selective TRPM7 blocker, as described in chapter 3.5.2. While they confirmed their findings by silencing TRPM7 with a small hairpin RNA, this method can also not distinguish between the cations involved. Besides, knockout of TRPM7 channel function may lead to loss of TRPM7 kinase function, thus effects observed could also be attributed to kinase dependent signaling.

Rios et al discovered antifibrotic effects of TRPM7-mediated Mg^{2+} levels in cardiac fibrosis [312]. However, as they stated in their conclusive remarks, these effects can only be partly attributed to Mg^{2+}, since effects of other cations cannot be excluded. They observed reduced Mg^{2+} in heterozygous kinase-deficient mice and thus correlated TRPM7 kinase and Mg^{2+} levels to the observed fibrotic phenotype. However, hypomagnesemia in these mice might hint at a reduced channel function in addition to the reduced kinase function, as proposed by Romagnani et al [329]. Thus, a clear correlation of a TRPM7 function to the observed effects remains questionable.

As a general remark, there is a tremendous difference concerning the kinetics of usage of TRPM7 blockers. Cation levels determined with the patch clamp technique are commonly measured after blockade of the channel in the range of seconds to a few minutes [325]. Conclusions on expression of fibrotic markers or cellular processes conferring a fibrotic phenotype are however typically drawn after 48 h [175, 353]. Thus, it seems questionable whether prolonged blockade of TRPM7 can still be attributed to a change in specific cation levels, as stated in the above-mentioned studies. Of note, the widely used TRPM7 blockers NS8593 and Waixenicin A cannot distinguish between both functions, thus blockade of TRPM7 leads to blockade of both kinase function and channel activity [324, 342, 343]. Moreover, TRPM7 blockers can also not distinguish between the regulation of distinct cations [325, 337]. In summary, so far, no study achieved to assign the effects observed in fibrotic diseases to a specific TRPM7 function and further studies are required to decipher distinct effects of channel and kinase function.

In addition to the suggested effects of TRPM7 by modulating cation levels, TRPM7 has been shown to promote fibrosis by supporting PI3K/Akt or SMAD signaling pathways [312, 400]. Due to a direct interaction of TRPM7 kinase and SMAD2 in T-cells, regulation of cellular processes via its kinase domain seems likely [329]. While above-mentioned previous studies suggested TRPM7 as crucial modulator of fibrotic diseases, e.g. in supporting kidney and cardiac fibrosis, no involvement of TRPM7 in pulmonary fibrosis has been described yet [330, 331]. Thus, this work aimed at analyzing the effects of TRPM7 blockade under basal and TGF-β-stimulated conditions in pHPF and to decipher the role of the two TRPM7 functions using a genetically modified mouse model with TRPM7-kinase deficiency.

Herein, it could be shown, that two structurally unrelated TRPM7 blockers reduced basal PAI1 and fibronectin protein levels in pHPF (see chapter 6.3.2). On the mRNA level, TRPM7 blockade reduced *SERPINE1* expression, but not *FN1* or *Col1A1*, suggesting that TRPM7 specifically modulates *SERPINE1* expression, which may lead to degradation of fibronectin proteins via plasmin activity (see chapter 6.3.2). To test this hypothesis, plasmin activity after TRPM7 blockade was measured. Both structurally unrelated TRPM7 blockers as well as siRNA against TRPM7 significantly enhanced plasmin activity of pHPF and the elevation was

higher in the cell-associated fraction than in the secreted fraction (see chapter 6.3.1). Importantly, off-target effects of the TRPM7 blocker NS8593 could be excluded by using the apamin control (fig 37). Since effects of TRPM7 blockade on plasmin activity have not been reported before, data shown in this work is unique. This work therefore describes for the first time TRPM7 as plasmin activity inhibitor and provides TRPM7 inhibitors as new small molecules to enhance plasmin activity. Activation of the fibrinolytic system is an emergency treatment for heart attacks or acute pulmonary embolisms, but prominently used thrombolytic drugs to increase plasmin activity are difficult to dose correctly and usage is accompanied by severe side effects. Thus, the results presented in this work provide a new treatment option by targeting TRPM7.

Considering the unique nature of plasmin enhancement after TRPM7 blockade in pHPF reported in this work, it was aimed at monitoring the effects of TRPM7 blockade in additional cell types. Indeed, TRPM7 blockade increased plasmin activity in three additional lung cell lines (fig 48, 50, 51). Thus, effects of TRPM7 blockade were not specific for pHPF but appear to be a general feature in pulmonary cells. Since TRPM7 blocker have been previously reported for their antiproliferative effect, plasmin activity measurements were normalized to the cell number. Further, several concentrations of the blockers have been tested in this work and experiments were conducted using concentrations that did not (in the case of NS8593) or only slightly (in the case of Waixenicin A) reduce overall cell number (fig 39). It should be noted however, that reduced cell number after Waixenicin A stimulation would not result in increased plasmin activity and would even dilute the enhancing effect on plasmin activity. To decipher a cellular consequence of increased plasmin activity after TRPM7 blockade, cellular migration was measured. Indeed, TRPM7 blockade increased serum-independent as well as serum-induced migration, thus revealing TRPM7 as possible target to modulate cell migration
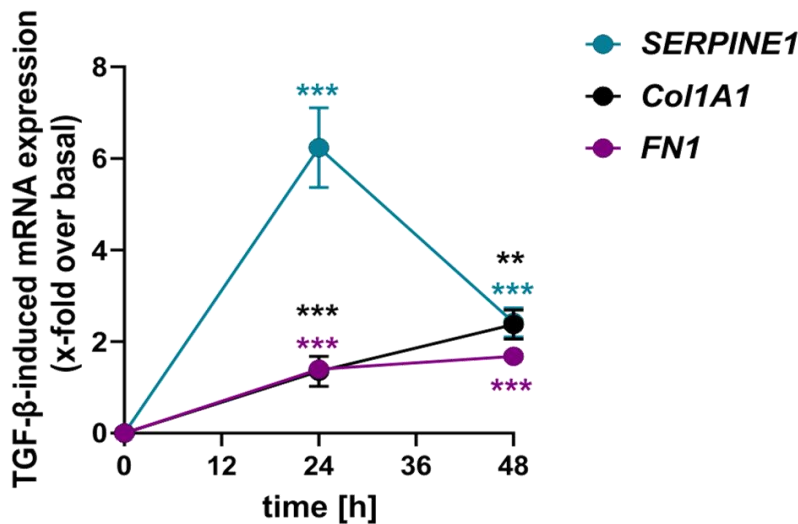
Figure 78: Kinetics of TGF-β-induced *SERPINE1, FN1* and *Col1A1* mRNA expression in pHPF

SERPINE1, FN1 and *Col1A1* mRNA amounts of pHPF were determined by qRT-PCR after 24 h and 48 h stimulation with TGF-β (2 ng/ml). Data is shown as SEM of x-fold over basal values, n = 3-5. Statistical analysis was performed using two-way ANOVA followed by Tukey´s post-test. Asterisks indicate significant differences to zero, ** $p<0.01$, *** $p<0.001$.

TRPM7 blockade enhanced plasmin activity after 24 and 48 h, however it did not so after 4 h (see chapter 6.3.1). Thus, TRPM7 activity likely affects plasmin activity indirectly via regulating gene expression rather than acutely. Therefore, SMAD signaling after TRPM7 blockade was analyzed. SMAD signaling is key in TGF-β conveyed effects on plasmin activity and ECM remodeling. Indeed, TRPM7 blockade decreased TGF-β-induced SMAD2 phosphorylation, *SERPINE1* mRNA expression and PAI1 protein levels (see chapter 6.4.2). Thus, SMAD-dependent signaling and its effects on the PAI1 promoter emerged as a possible link between TRPM7 and plasmin activity. Accordingly, TRPM7 blockade counteracted effects of TGF-β on plasmin activity in the secreted fraction and inhibited TGF-β-induced protein levels of fibrotic markers. Importantly, TRPM7 blockade did not affect mRNA levels of *FN* or *Col1A1*, suggesting that TRPM7 targets ECM protein levels indirectly via modulation of *SERPINE1* and subsequent plasmin activity. This finding is especially important since late stages of fibrosis require degradation of ECM to achieve tissue restoration. Explanations for the selective effect of TRPM7 on TGF-β-induced *SERPINE1* expression can only be speculated. Of note, TGF-β-

172

induced mRNA levels of *FN1* and *Col1A1* rose linearly, but *SERPINE1* expression peaked at 24 h and then declined (fig 78). This could indicate distinct modes of actions of TGF-β/SMAD signaling on these promoters. Besides, all three promoters contain binding sites for several transcription factors other than SMAD, thus the regulation may not be solely dependent on TGF-β/SMAD signaling. These distinct kinetics therefore suggest differences of TGF-β signaling on these SMAD-dependent promoters and thus different effects of TRPM7. However, the promoters of these genes also carry binding sites for transcription factors other than SMADs. According to this, TRPM7 blockade selectively reduced TGF-β-induced SMAD but not YAP/TAZ activity (fig 67). Such specific effects of TRPM7 may explain the selective targeting of *SERPINE1*, but further studies are required to determine why TRPM7 blocker affect *SERPINE1*, but not *FN1* or *Col1A1* expression.

In summary, TRPM7 likely promotes TGF-β signaling via SMAD proteins and thereby modulates plasmin activation. A possible implication of TRPM7 on the fibrinolytic system is summarized in figure 79.

Next goal was to decipher a role of TRPM7 during prolonged TGF-β stimulation. Fibroblast to myofibroblast differentiation was achieved upon TGF-β stimulation of pHPF for 48 h and confirmed by evaluation of mRNA and protein levels of the fibrotic markers α-SMA, collagen1, fibronectin and PAI1 (see chapter 6.4.1). TRPM7 blockade inhibited TGF-β-induced protein levels of all tested fibrotic markers, thus suggesting an inhibition of fibroblast to myofibroblast differentiation (see chapter 6.4.2). Importantly, TGF-β-induced mRNA levels of *FN1* and *Col1A1* were not affected, but *SERPINE1* levels were strongly inhibited by TRPM7 blockade (fig 64). Effects on fibrotic markers could further be correlated to plasmin activity, since inhibitory effects of TGF-β on plasmin activity were reduced by TRPM7 blockade, suggesting that reduced protein levels of collagen1 and fibronectin stem from increased degradation by plasmin and not from direct modulation of these genes (fig 56). Interestingly, TRPM7 siRNA did not affect the inhibitory effect of TGF-β on plasmin activity (fig 40). One possible explanation for this finding could be that downregulation of TRPM7 via siRNA was not as efficient as its blockade using NS8593. Besides, TRPM7 mRNA levels may not linearly correlate with protein levels, thus the effects of siRNA could be even smaller.

Finally, TRPM7 blockade reduced SMAD signaling, thus confirming the involvement of TGF-β-signaling via SMAD signaling in this context.
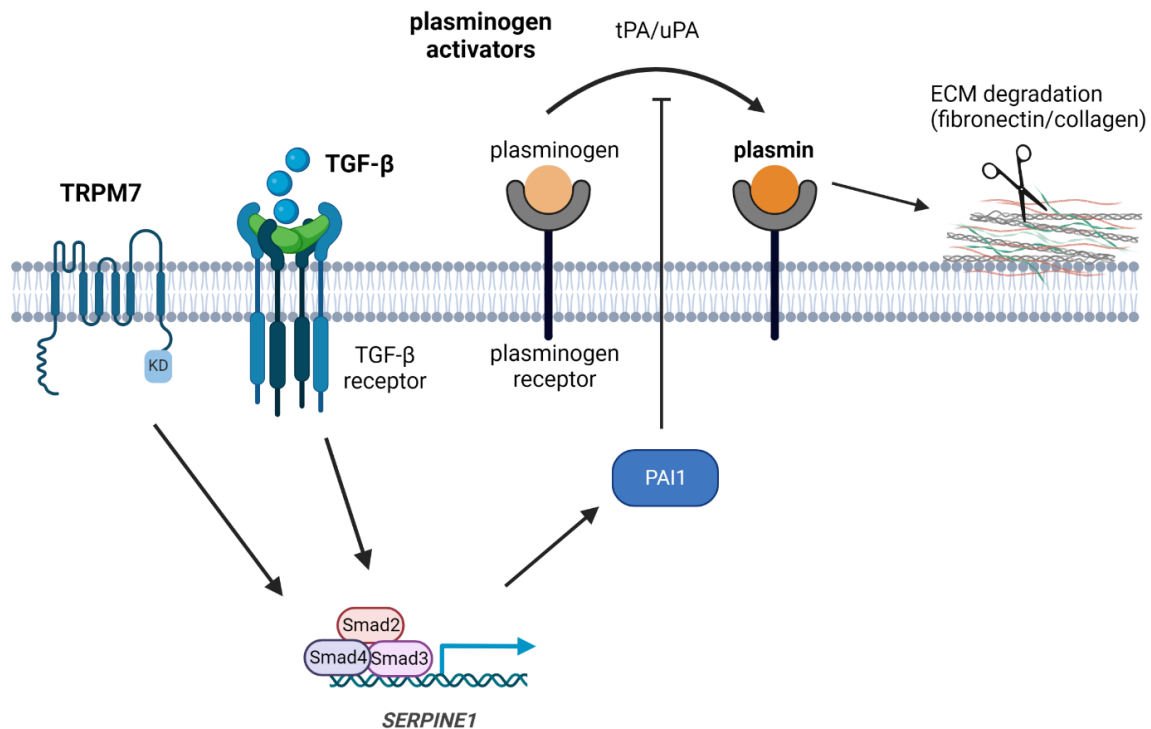
Figure 79: Schematic overview of the proposed implication of TRPM7 on the fibrinolytic system

Plasminogen to plasmin activation is mediated by plasminogen activators tPA and uPA. Active plasmin degrades components of the extracellular matrix (ECM) like fibronectin and collagens. TGF-β-signaling via SMAD proteins induces expression of plasminogen-activator-inhibitor 1 (PAI1), thereby inhibiting plasmin activation. TRPM7 supports TGF-β signaling and thereby restrains plasmin activation.

The finding that TRPM7 blockade mostly affects plasmin activity in the cell-associated fraction stands in contrast to the effects of TGF-β, which acts mostly on the secreted fraction. One possible explanation could be that different kinetics lead to activation or inhibition of plasmin activity. Besides, enhanced plasmin activity due to TRPM7 blockade probably depends on protein levels of PAI1. Since PAI1 levels are higher in the cell-associated fraction than in the secreted fraction,

inhibitory effects on basal PAI1 levels can be stronger in the cell-associated fraction and thus affect plasmin activity to a greater extent.

In accordance, pHPF from a healthy donor and a donor with PF were compared (see chapter 6.3.3). Due to the pathophysiological appearance of PF which includes excessive accumulation of ECM, lower plasmin activity was expected in the PF donor. Indeed, plasmin activity of both fractions was significantly lower compared to pHPF from the healthy donor. Importantly, TGF-β reduced plasmin activity similarly in both cell pools, but TRPM7 blockade led to a significantly higher increase in plasmin activity in cells from the PF donor. Thus, while TGF-β signaling leading to plasmin activity seems unaltered in fibroblasts from fibrotic tissues, they may be more susceptible to agents modulating TRPM7 activity. Thereby, this work reveals TRPM7 as promising target to selectively modulate ECM accumulation in fibrotic tissues and achieve tissue restoration even in late stages of the disease.

Besides its role in fibrotic diseases, plasmin has also been reported to degrade fibronectin among other ECM components to facilitate invasion of tumor cells to surrounding tissues. Thus, TRPM7 blockade leading to increased plasmin activity and reduced fibronectin levels may actually be fatal and support tumor progression. It therefore seems promising to test TRPM7 agonists on the effects of plasmin activity and ECM degradation. However, TRPM7 overexpression is reported for several cancer types and associated with enhanced migration and tumor growth. One possible explanation could be that TRPM7 channel function and kinase activity possess distinct cellular functions regarding tumor cell migration and invasion. Thus, further studies are required to decipher the role of TRPM7 functions on tumor progression.

While fibronectin is a prominent part of the ECM, it is also considered a marker of EMT. Similar to the differentiation of fibroblasts, sustained TGF-β exposure has been shown to induce EMT of tumor cells, which is a relevant step in the progression of the disease. Data provided in this work confirmed induction of EMT markers PAI1 and fibronectin after 48 h TGF-β stimulation and TRPM7 blockade significantly reduced both markers in both cell lines (see chapter 6.4.4). These findings suggest an additional role for TRPM7 as potential target to modulate EMT

of lung tumor cells. In summary, this work provides evidence for TRPM7 as potential target for fibrotic and malignant diseases.

As mentioned before, TRPM7 consists of an ion channel and a kinase domain, which phosphorylates serines and threonines of TRPM7 itself or of other substrates. SMAD signaling is key in TGF-β-conveyed effects on plasmin activity and ECM remodeling. As TRPM7 kinase is known to phosphorylate SMAD2 in T-lymphocytes, it seemed a promising target for modulation of TGF-β signaling [329]. One aim of this work was to assess which function of TRPM7 is involved in SMAD signaling and plasmin activity. However, no pharmacological tools are available to selectively inhibit one of the TRPM7 functions. Thus, a mouse model was used with a point mutation at Lysine 1646, which is essential for kinase function [329]. Using these TRPM7-K1646R and TRPM7-WT mice, discrimination between kinase and ion channel function of TRPM7 is possible. Basal expression of fibrotic markers in pMPF from both genotypes were comparable to those observed in pHPF, suggesting that neither the isolation procedure nor the different cell culture media affected these protein levels (fig 69). Fibrotic markers, SMAD2 phosphorylation and SMAD3/4 activity were induced by TGF-β in the same manner as reported for pHPF, thus TGF-β signaling seemed comparable in murine and human primary pulmonary fibroblasts (fig 70-71). However, in pulmonary fibroblasts isolated from mice, TRPM7 blockade did not affect TGF-β-induced SMAD3/4 activity, PAI1 protein levels and plasmin activity (fig 72). It was thus concluded that interactions between TRPM7 and TGF-β in lung fibroblasts are species specific. Interestingly, SMAD3 protein expression was not decreased after TGF-β stimulation in the murine cells and no effects on plasmin activity were observed after TGF-β stimulation (fig 72, 73). These findings hint at further species-specific differences of TGF-β signaling, independently of TRPM7.

Plasmin activity was additionally measured in another murine fibroblast cell line, which was entirely unaffected by TRPM7 blockade or TGF-β stimulation, suggesting that the entire plasminogen activation system may be regulated differently in mice compared to the human system (fig 72). Of note, it is known that the sequence of the promoter region of the PAI1 gene in rats is different than in

humans and that PAI1 from mice and human have structural and sequence differences, thus a different regulation of PAI1 and subsequent plasmin activity seems likely in different species [231]. It was thus refrained to further use the murine fibroblasts to analyze effects of TRPM7 on TGF-β signaling and plasmin activation. Further, no statement could be made regarding the TRPM7 function involved in the modulation of TGF-β signaling and plasmin activity in pulmonary fibroblasts.

As stated previously, TRPM7 could affect cellular processes via modulating cation levels or via its kinase domain. Ca^{2+} signaling via calmodulin has been reported to reduce SMAD signaling in HEK-293 cells and R-SMADs have been shown to bind to calmodulin in a calcium dependent way [401, 402]. Further, the SMAD2/3 phosphatase PPM1a inhibits TGF/SMAD signaling dependent on Mg^{2+} in MRC5 cells [403]. Inhibition of channel function and reduced Ca^{2+} and Mg^{2+} levels in the cell would therefore increase SMAD activity, however no such effect was observed in this work. Since specific effects of TRPM7 kinase on SMAD2 phosphorylation have been reported before, it thus seems more likely that TRPM7 affects cellular processes leading to its effect on plasmin activity via its kinase domain [329]. However, these effects were observed after 10 min stimulation with TGF-β and therefore display fully distinct kinetics than the experiments performed in this work. It should also be noted, that cellular processes may vary hugely when using a blocker for 48 h comparing to using a genetically deficient mouse, which never possessed a kinase function.

Due to the unavailability of suitable tools to specifically target one function of TRPM7, this work thus faced the same problems as previous works and only assumptions on the function involved can be made. Just recently, a study identified small molecules that selectively inhibit the channel function of TRPM7, thus a selective effect of the channel moiety could be targeted in future studies [404].

Despite that, TRPM7 blocker emerge as possible treatment option to target plasmin activation and ECM degradation in pulmonary fibroblasts. TRPM7 supports TGF-β-induced ECM accumulation by inhibiting the proteolytic degradation by plasmin. It selectively affects TGF-β-induced PAI1 expression and

not directly affects expression of ECM proteins. Thus, plasmin activation after TRPM7 blockade leading to degradation of proteins of the ECM might be crucial for targeting accumulated ECM in late stages of pulmonary fibrosis and reveal a possibility for tissue restoration.

8. List of references

1. Dastre, A., *Fibrinolyse dans le sang.* Arch Norm Pathol, 1893. **5**: p. 661-73.

2. Lasne, D., B. Jude, and S. Susen, *From normal to pathological hemostasis.* Can J Anaesth, 2006. **53**(6 Suppl): p. S2-11.

3. Miles, L.A. and R.J. Parmer, *Plasminogen receptors: the first quarter century.* Seminars in thrombosis and hemostasis, 2013. **39**(4): p. 329-337.

4. Rinder, H.M., *Hemostasis and coagulation.* Clin Lab Med, 2009. **29**(2): p. xi.

5. Sierra, C., M. Moreno, and J.C. García-Ruiz, *The physiology of hemostasis.* Blood Coagul Fibrinolysis, 2022. **33**(Suppl 1): p. S1-s2.

6. Horan, J.T. and C.W. Francis, *Fibrin degradation products, fibrin monomer and soluble fibrin in disseminated intravascular coagulation.* Semin Thromb Hemost, 2001. **27**(6): p. 657-66.

7. Fukuda, I. and K. Daitoku, *Surgical Embolectomy for Acute Pulmonary Thromboembolism.* Ann Vasc Dis, 2017. **10**(2): p. 107-114.

8. Duffett, L., L.A. Castellucci, and M.A. Forgie, *Pulmonary embolism: update on management and controversies.* Bmj, 2020. **370**: p. m2177.

9. Martinez Licha, C.R., C.M. McCurdy, S.M. Maldonado, and L.S. Lee, *Current Management of Acute Pulmonary Embolism.* Ann Thorac Cardiovasc Surg, 2020. **26**(2): p. 65-71.

10. Levi, M. and T. van der Poll, *Inflammation and coagulation.* Crit Care Med, 2010. **38**(2 Suppl): p. S26-34.

11. Henkin, J., P. Marcotte, and H.C. Yang, *The plasminogen-plasmin system.* Prog Cardiovasc Dis, 1991. **34**(2): p. 135-64.

12. Brassart-Pasco, S., S. Brézillon, B. Brassart, L. Ramont, J.-B. Oudart, and J.C. Monboisse, *Tumor Microenvironment: Extracellular Matrix Alterations Influence Tumor Progression.* Frontiers in Oncology, 2020. **10**.

13. Hattori, N., S. Mizuno, Y. Yoshida, K. Chin, M. Mishima, T.H. Sisson, R.H. Simon, T. Nakamura, and M. Miyake, *The plasminogen activation system reduces fibrosis in the lung by a hepatocyte growth factor-dependent mechanism.* Am J Pathol, 2004. **164**(3): p. 1091-8.

14. Wu, S.-R., C.-H. Lin, H.-P. Shih, C.-J. Ko, H.-Y. Lin, S.-W. Lan, H.-H. Lin, H.-F. Tu, C.-C. Ho, H.-P. Huang, and M.-S. Lee, *HAI-2 as a novel inhibitor of plasmin represses lung cancer cell invasion and metastasis.* British Journal of Cancer, 2019. **120**(5): p. 499-511.

15. Berres, M.L., B. Schlosser, T. Berg, C. Trautwein, and H.E. Wasmuth, *Soluble urokinase plasminogen activator receptor is associated with progressive liver fibrosis in hepatitis C infection.* J Clin Gastroenterol, 2012. **46**(4): p. 334-8.

16. Carl, P.L., P.K. Chakravarty, J.A. Katzenellenbogen, and M.J. Weber, *Protease-activated "prodrugs" for cancer chemotherapy.* Proceedings of the National Academy of Sciences, 1980. **77**(4): p. 2224-2228.

17.   Hochschwender, S.M. and R.A. Laursen, *The lysine binding sites of human plasminogen. Evidence for a critical tryptophan in the binding site of kringle 4.* J Biol Chem, 1981. **256**(21): p. 11172-6.

18.   Plow, E.F., T. Herren, A. Redlitz, L. Miles, and J.L. Hoover-Plow, *The cell biology of the plasminogen system.* FASEB journal : official publication of the Federation of American Societies for Experimental Biology, 1995. **9**: p. 939-45.

19.   Zhang, L., D. Seiffert, B.J. Fowler, G.R. Jenkins, T.C. Thinnes, D.J. Loskutoff, R.J. Parmer, and L.A. Miles, *Plasminogen has a broad extrahepatic distribution.* Thromb Haemost, 2002. **87**(3): p. 493-501.

20.   Saito, H., S.M. Hamilton, A.S. Tavill, L. Louis, and O.D. Ratnoff, *Production and release of plasminogen by isolated perfused rat liver.* Proc Natl Acad Sci U S A, 1980. **77**(11): p. 6837-40.

21.   Bohmfalk, J.F. and G.M. Fuller, *Plaminogen is synthesized by primary cultures of rat hepatocytes.* Science, 1980. **209**(4454): p. 408-10.

22.   Forsgren, M., B. Råden, M. Israelsson, K. Larsson, and L.O. Hedén, *Molecular cloning and characterization of a full-length cDNA clone for human plasminogen.* FEBS Lett, 1987. **213**(2): p. 254-60.

23.   Robbins, K.C., L. Summaria, B. Hsieh, and R.J. Shah, *The peptide chains of human plasmin. Mechanism of activation of human plasminogen to plasmin.* J Biol Chem, 1967. **242**(10): p. 2333-42.

24.   Horrevoets, A.J., H. Pannekoek, and M.E. Nesheim, *A steady-state template model that describes the kinetics of fibrin-stimulated [Glu1]- and [Lys78]plasminogen activation by native tissue-type plasminogen activator and variants that lack either the finger or kringle-2 domain.* J Biol Chem, 1997. **272**(4): p. 2183-91.

25.   Whyte, C.S. and N.J. Mutch, *uPA-mediated plasminogen activation is enhanced by polyphosphate.* Haematologica, 2021. **106**(2): p. 522-531.

26.   Andreasen, P.A., R. Egelund, and H.H. Petersen, *The plasminogen activation system in tumor growth, invasion, and metastasis.* Cellular and Molecular Life Sciences CMLS, 2000. **57**(1): p. 25-40.

27.   Plow, E.F., L. Doeuvre, and R. Das, *So many plasminogen receptors: why?* J Biomed Biotechnol, 2012. **2012**: p. 141806.

28.   Felez, J., C.J. Chanquia, E.G. Levin, L.A. Miles, and E.F. Plow, *Binding of tissue plasminogen activator to human monocytes and monocytoid cells.* Blood, 1991. **78**(9): p. 2318-27.

29.   Miles, L.A., C.M. Dahlberg, J. Plescia, J. Felez, K. Kato, and E.F. Plow, *Role of cell-surface lysines in plasminogen binding to cells: identification of alpha-enolase as a candidate plasminogen receptor.* Biochemistry, 1991. **30**(6): p. 1682-91.

30.   Deryugina, E.I. and J.P. Quigley, *Cell surface remodeling by plasmin: a new function for an old enzyme.* J Biomed Biotechnol, 2012. **2012**: p. 564259.

31. Irigoyen, J.P., P. Muñoz-Cánoves, L. Montero, M. Koziczak, and Y. Nagamine, *The plasminogen activator system: biology and regulation.* Cell Mol Life Sci, 1999. **56**(1-2): p. 104-32.

32. Miles, L.A., S.B. Hawley, N. Baik, N.M. Andronicos, F.J. Castellino, and R.J. Parmer, *Plasminogen receptors: the sine qua non of cell surface plasminogen activation.* Front Biosci, 2005. **10**: p. 1754-62.

33. De Taeye, B., L.H. Smith, and D.E. Vaughan, *Plasminogen activator inhibitor-1: a common denominator in obesity, diabetes and cardiovascular disease.* Curr Opin Pharmacol, 2005. **5**(2): p. 149-54.

34. Gorlatova, N.V., J.M. Cale, H. Elokdah, D. Li, K. Fan, M. Warnock, D.L. Crandall, and D.A. Lawrence, *Mechanism of inactivation of plasminogen activator inhibitor-1 by a small molecule inhibitor.* J Biol Chem, 2007. **282**(12): p. 9288-96.

35. Irving, J.A., R.N. Pike, A.M. Lesk, and J.C. Whisstock, *Phylogeny of the serpin superfamily: implications of patterns of amino acid conservation for structure and function.* Genome Res, 2000. **10**(12): p. 1845-64.

36. Bharadwaj, A.G., R.W. Holloway, V.A. Miller, and D.M. Waisman, *Plasmin and Plasminogen System in the Tumor Microenvironment: Implications for Cancer Diagnosis, Prognosis, and Therapy.* Cancers, 2021. **13**(8): p. 1838.

37. Kruithof, E., M. Baker, and C. Bunn, *Biological and clinical aspects of plasminogen activator inhibitor type 2.* Blood, 1995. **86**(11): p. 4007-4024.

38. España, F., A. Estellés, P.J. Fernández, J. Gilabert, J. Sánchez-Cuenca, and J.H. Griffin, *Evidence for the regulation of urokinase and tissue type plasminogen activators by the serpin, protein C inhibitor, in semen and blood plasma.* Thromb Haemost, 1993. **70**(6): p. 989-94.

39. Diéval, J., G. Nguyen, S. Gross, J. Delobel, and E.K. Kruithof, *A lifelong bleeding disorder associated with a deficiency of plasminogen activator inhibitor type 1.* Blood, 1991. **77**(3): p. 528-32.

40. Fay, W.P., A.C. Parker, L.R. Condrey, and A.D. Shapiro, *Human plasminogen activator inhibitor-1 (PAI-1) deficiency: characterization of a large kindred with a null mutation in the PAI-1 gene.* Blood, 1997. **90**(1): p. 204-8.

41. Lee, M.H., E. Vosburgh, K. Anderson, and J. McDonagh, *Deficiency of plasma plasminogen activator inhibitor 1 results in hyperfibrinolytic bleeding.* Blood, 1993. **81**(9): p. 2357-62.

42. Margaglione, M., G. Cappucci, D. Colaizzo, N. Giuliani, G. Vecchione, E. Grandone, O. Pennelli, and G. Di Minno, *The PAI-1 gene locus 4G/5G polymorphism is associated with a family history of coronary artery disease.* Arterioscler Thromb Vasc Biol, 1998. **18**(2): p. 152-6.

43. Omori, K., N. Hattori, T. Senoo, Y. Takayama, T. Masuda, T. Nakashima, H. Iwamoto, K. Fujitaka, H. Hamada, and N. Kohno, *Inhibition of Plasminogen Activator Inhibitor-1 Attenuates Transforming Growth Factor-β-Dependent Epithelial Mesenchymal Transition and Differentiation of Fibroblasts to Myofibroblasts.* PLOS ONE, 2016. **11**(2): p. e0148969.

44. Takayama, Y., N. Hattori, H. Hamada, T. Masuda, K. Omori, S. Akita, H. Iwamoto, K. Fujitaka, and N. Kohno, *Inhibition of PAI-1 Limits Tumor Angiogenesis Regardless of Angiogenic Stimuli in Malignant Pleural Mesothelioma.* Cancer Research, 2016. **76**(11): p. 3285-3294.

45. Wiman, B. and D. Collen, *On the mechanism of the reaction between human alpha 2-antiplasmin and plasmin.* J Biol Chem, 1979. **254**(18): p. 9291-7.

46. Shieh, B.H. and J. Travis, *The reactive site of human alpha 2-antiplasmin.* J Biol Chem, 1987. **262**(13): p. 6055-9.

47. Nakamura, K., A. Hongo, J. Kodama, and Y. Hiramatsu, *The role of hepatocyte growth factor activator inhibitor (HAI)-1 and HAI-2 in endometrial cancer.* Int J Cancer, 2011. **128**(11): p. 2613-24.

48. Tsai, C.H., C.H. Teng, Y.T. Tu, T.S. Cheng, S.R. Wu, C.J. Ko, H.Y. Shyu, S.W. Lan, H.P. Huang, S.F. Tzeng, M.D. Johnson, C.Y. Lin, P.W. Hsiao, and M.S. Lee, *HAI-2 suppresses the invasive growth and metastasis of prostate cancer through regulation of matriptase.* Oncogene, 2014. **33**(38): p. 4643-52.

49. Tung, E.K., C.M. Wong, T.O. Yau, J.M. Lee, Y.P. Ching, and I.O. Ng, *HAI-2 is epigenetically downregulated in human hepatocellular carcinoma, and its Kunitz domain type 1 is critical for anti-invasive functions.* Int J Cancer, 2009. **124**(8): p. 1811-9.

50. Hughes, A.L., *Modes of evolution in the protease and kringle domains of the plasminogen-prothrombin family.* Mol Phylogenet Evol, 2000. **14**(3): p. 469-78.

51. Patthy, L., *Evolution of the proteases of blood coagulation and fibrinolysis by assembly from modules.* Cell, 1985. **41**(3): p. 657-63.

52. Miyazawa, K., Y. Wang, S. Minoshima, N. Shimizu, and N. Kitamura, *Structural organization and chromosomal localization of the human hepatocyte growth factor activator gene--phylogenetic and functional relationship with blood coagulation factor XII, urokinase, and tissue-type plasminogen activator.* Eur J Biochem, 1998. **258**(2): p. 355-61.

53. Jendroszek, A., M.S. Sønnichsen, A.C. Muñoz, K. Leyman, A. Christensen, S.V. Petersen, T. Wang, C. Bendixen, F. Panitz, P.A. Andreasen, and J.K. Jensen, *Latency transition of plasminogen activator inhibitor type 1 is evolutionarily conserved.* Thromb Haemost, 2017. **117**(9): p. 1688-1699.

54. Madureira, P.A., P.A. O'Connell, A.P. Surette, V.A. Miller, and D.M. Waisman, *The Biochemistry and Regulation of S100A10: A Multifunctional Plasminogen Receptor Involved in Oncogenesis.* Journal of Biomedicine and Biotechnology, 2012. **2012**: p. 353687.

55. Nanbu, R., P.A. Menoud, and Y. Nagamine, *Multiple instability-regulating sites in the 3' untranslated region of the urokinase-type plasminogen activator mRNA.* Molecular and Cellular Biology, 1994. **14**(7): p. 4920-4928.

56. Sharma, S., S.S. Shinde, L. Teekas, and N. Vijay, *Evidence for the loss of plasminogen receptor KT gene in chicken.* Immunogenetics, 2020. **72**(9): p. 507-515.

57.   Prendergast, G.C., L.E. Diamond, D. Dahl, and M.D. Cole, *The c-myc-regulated gene mrl encodes plasminogen activator inhibitor 1.* Mol Cell Biol, 1990. **10**(3): p. 1265-9.

58.   Declerck, P.J., A. Gils, and B. De Taeye, *Chapter five - Use of Mouse Models to Study Plasminogen Activator Inhibitor-1*, in *Methods in Enzymology*, J.C. Whisstock and P.I. Bird, Editors. 2011, Academic Press. p. 77-104.

59.   Dewilde, M., B. Van De Craen, G. Compernolle, J.B. Madsen, S. Strelkov, A. Gils, and P.J. Declerck, *Subtle structural differences between human and mouse PAI-1 reveal the basis for biochemical differences.* Journal of Structural Biology, 2010. **171**(1): p. 95-101.

60.   Lijnen, H.R., B. Van Hoef, V. Beelen, and D. Collen, *Characterization of the Murine Plasma Fibrinolytic System.* European Journal of Biochemistry, 1994. **224**(3): p. 863-871.

61.   Haddadin, A.S. and N. Faraday, *Chapter 10 - Hemostasis, Coagulopathy, and Tamponade*, in *The Johns Hopkins Manual of Cardiac Surgical Care (Second Edition)*, J.V. Conte, et al., Editors. 2008, Mosby: Philadelphia. p. 237-256.

62.   Griffin, J.D. and L. Ellman, *Epsilon-aminocaproic acid (EACA).* Semin Thromb Hemost, 1978. **5**(1): p. 27-40.

63.   Dhir, A., *Antifibrinolytics in cardiac surgery.* Ann Card Anaesth, 2013. **16**(2): p. 117-25.

64.   Francis, R.B., Jr., *Clinical disorders of fibrinolysis: a critical review.* Blut, 1989. **59**(1): p. 1-14.

65.   Holbrook, A.M., J.A. Pereira, R. Labiris, H. McDonald, J.D. Douketis, M. Crowther, and P.S. Wells, *Systematic overview of warfarin and its drug and food interactions.* Arch Intern Med, 2005. **165**(10): p. 1095-106.

66.   Levy, J.H., W. Ageno, N.C. Chan, M. Crowther, P. Verhamme, and J.I. Weitz, *When and how to use antidotes for the reversal of direct oral anticoagulants: guidance from the SSC of the ISTH.* J Thromb Haemost, 2016. **14**(3): p. 623-7.

67.   Hurd, M.D., I. Goel, Y. Sakai, and Y. Teramura, *Current status of ischemic stroke treatment: From thrombolysis to potential regenerative medicine.* Regen Ther, 2021. **18**: p. 408-417.

68.   Liaw, N. and D. Liebeskind, *Emerging therapies in acute ischemic stroke.* F1000Res, 2020. **9**.

69.   Chevilley, A., F. Lesept, S. Lenoir, C. Ali, J. Parcq, and D. Vivien, *Impacts of tissue-type plasminogen activator (tPA) on neuronal survival.* Front Cell Neurosci, 2015. **9**: p. 415.

70.   Singh, S., A. Houng, and G.L. Reed, *Releasing the Brakes on the Fibrinolytic System in Pulmonary Emboli: Unique Effects of Plasminogen Activation and α2-Antiplasmin Inactivation.* Circulation, 2017. **135**(11): p. 1011-1020.

71. Mackay, A.R., R.H. Corbitt, J.L. Hartzler, and U.P. Thorgeirsson, *Basement membrane type IV collagen degradation: evidence for the involvement of a proteolytic cascade independent of metalloproteinases.* Cancer Res, 1990. **50**(18): p. 5997-6001.

72. Moser, T.L., J.J. Enghild, S.V. Pizzo, and M.S. Stack, *The extracellular matrix proteins laminin and fibronectin contain binding domains for human plasminogen and tissue plasminogen activator.* J Biol Chem, 1993. **268**(25): p. 18917-23.

73. Hattori, N., J.L. Degen, T.H. Sisson, H. Liu, B.B. Moore, R.G. Pandrangi, R.H. Simon, and A.F. Drew, *Bleomycin-induced pulmonary fibrosis in fibrinogen-null mice.* J Clin Invest, 2000. **106**(11): p. 1341-50.

74. Sisson, T.H., N. Hattori, Y. Xu, and R.H. Simon, *Treatment of bleomycin-induced pulmonary fibrosis by transfer of urokinase-type plasminogen activator genes.* Hum Gene Ther, 1999. **10**(14): p. 2315-23.

75. Swaisgood, C.M., E.L. French, C. Noga, R.H. Simon, and V.A. Ploplis, *The development of bleomycin-induced pulmonary fibrosis in mice deficient for components of the fibrinolytic system.* Am J Pathol, 2000. **157**(1): p. 177-87.

76. Senoo, T., N. Hattori, T. Tanimoto, M. Furonaka, N. Ishikawa, K. Fujitaka, Y. Haruta, H. Murai, A. Yokoyama, and N. Kohno, *Suppression of plasminogen activator inhibitor-1 by RNA interference attenuates pulmonary fibrosis.* Thorax, 2010. **65**(4): p. 334-40.

77. Higgins, P.J., J.K. Slack, R.F. Diegelmann, and L. Staiano-Coico, *Differential regulation of PAI-1 gene expression in human fibroblasts predisposed to a fibrotic phenotype.* Exp Cell Res, 1999. **248**(2): p. 634-42.

78. Tuan, T.L., P. Hwu, W. Ho, P. Yiu, R. Chang, A. Wysocki, and P.D. Benya, *Adenoviral overexpression and small interfering RNA suppression demonstrate that plasminogen activator inhibitor-1 produces elevated collagen accumulation in normal and keloid fibroblasts.* Am J Pathol, 2008. **173**(5): p. 1311-25.

79. Chuang-Tsai, S., T.H. Sisson, N. Hattori, C.G. Tsai, N.M. Subbotina, K.E. Hanson, and R.H. Simon, *Reduction in fibrotic tissue formation in mice genetically deficient in plasminogen activator inhibitor-1.* Am J Pathol, 2003. **163**(2): p. 445-52.

80. Oda, T., Y.O. Jung, H.S. Kim, X. Cai, J.M. López-Guisa, Y. Ikeda, and A.A. Eddy, *PAI-1 deficiency attenuates the fibrogenic response to ureteral obstruction.* Kidney Int, 2001. **60**(2): p. 587-96.

81. Wang, H., Y. Zhang, and R.O. Heuckeroth, *PAI-1 deficiency reduces liver fibrosis after bile duct ligation in mice through activation of tPA.* FEBS Lett, 2007. **581**(16): p. 3098-104.

82. Gouri, A., A. Dekaken, K. El Bairi, A. Aissaoui, N. Laabed, M. Chefrour, J. Ciccolini, G. Milano, and S. Benharkat, *Plasminogen Activator System and Breast Cancer: Potential Role in Therapy Decision Making and Precision Medicine.* Biomark Insights, 2016. **11**: p. 105-11.

83.   Kaul, B., V. Cottin, H.R. Collard, and C. Valenzuela, *Variability in Global Prevalence of Interstitial Lung Disease.* Front Med (Lausanne), 2021. **8**: p. 751181.

84.   Albera, C., G. Verri, F. Sciarrone, E. Sitia, M. Mangiapia, and P. Solidoro, *Progressive Fibrosing Interstitial Lung Diseases: A Current Perspective.* Biomedicines, 2021. **9**(9).

85.   Maher, T.M., E. Bendstrup, L. Dron, J. Langley, G. Smith, J.M. Khalid, H. Patel, and M. Kreuter, *Global incidence and prevalence of idiopathic pulmonary fibrosis.* Respir Res, 2021. **22**(1): p. 197.

86.   Boag, A.H., T.V. Colby, A.E. Fraire, C. Kuhn, 3rd, V.L. Roggli, W.D. Travis, and V. Vallyathan, *The pathology of interstitial lung disease in nylon flock workers.* Am J Surg Pathol, 1999. **23**(12): p. 1539-45.

87.   Cordasco, E.M., S.L. Demeter, J. Kerkay, H.S. Van Ordstrand, E.V. Lucas, T. Chen, and J.A. Golish, *Pulmonary manifestations of vinyl and polyvinyl chloride (interstitial lung disease). Newer aspects.* Chest, 1980. **78**(6): p. 828-34.

88.   Mossman, B.T. and A. Churg, *Mechanisms in the pathogenesis of asbestosis and silicosis.* Am J Respir Crit Care Med, 1998. **157**(5 Pt 1): p. 1666-80.

89.   Kelleher, P., K. Pacheco, and L.S. Newman, *Inorganic dust pneumonias: the metal-related parenchymal disorders.* Environ Health Perspect, 2000. **108 Suppl 4**(Suppl 4): p. 685-96.

90.   Della Latta, V., A. Cecchettini, S. Del Ry, and M.A. Morales, *Bleomycin in the setting of lung fibrosis induction: From biological mechanisms to counteractions.* Pharmacol Res, 2015. **97**: p. 122-30.

91.   Giuranno, L., J. Ient, D. De Ruysscher, and M.A. Vooijs, *Radiation-Induced Lung Injury (RILI).* Front Oncol, 2019. **9**: p. 877.

92.   Morse, D. and I.O. Rosas, *Tobacco smoke-induced lung fibrosis and emphysema.* Annu Rev Physiol, 2014. **76**: p. 493-513.

93.   George, P.M., A.U. Wells, and R.G. Jenkins, *Pulmonary fibrosis and COVID-19: the potential role for antifibrotic therapy.* Lancet Respir Med, 2020. **8**(8): p. 807-815.

94.   Ojo, A.S., S.A. Balogun, O.T. Williams, and O.S. Ojo, *Pulmonary Fibrosis in COVID-19 Survivors: Predictive Factors and Risk Reduction Strategies.* Pulm Med, 2020. **2020**: p. 6175964.

95.   Tale, S., S. Ghosh, S.P. Meitei, M. Kolli, A.K. Garbhapu, and S. Pudi, *Post-COVID-19 pneumonia pulmonary fibrosis.* Qjm, 2020. **113**(11): p. 837-838.

96.   Meyer, K.C., *Diagnosis and management of interstitial lung disease.* Transl Respir Med, 2014. **2**: p. 4.

97.   Raghu, G., K.J. Anstrom, T.E. King, Jr., J.A. Lasky, and F.J. Martinez, *Prednisone, azathioprine, and N-acetylcysteine for pulmonary fibrosis.* N Engl J Med, 2012. **366**(21): p. 1968-77.

98.   Funke, M. and T. Geiser, *Idiopathic pulmonary fibrosis: the turning point is now!* Swiss Med Wkly, 2015. **145**: p. w14139.

99.   Richeldi, L., H.R. Collard, and M.G. Jones, *Idiopathic pulmonary fibrosis.* Lancet, 2017. **389**(10082): p. 1941-1952.

100.   Behr, J., A. Prasse, M. Kreuter, J. Johow, K.F. Rabe, F. Bonella, R. Bonnet, C. Grohe, M. Held, H. Wilkens, P. Hammerl, D. Koschel, S. Blaas, H. Wirtz, J.H. Ficker, W. Neumeister, N. Schönfeld, M. Claussen, N. Kneidinger, M. Frankenberger, S. Hummler, N. Kahn, S. Tello, J. Freise, T. Welte, P. Neuser, and A. Günther, *Pirfenidone in patients with progressive fibrotic interstitial lung diseases other than idiopathic pulmonary fibrosis (RELIEF): a double-blind, randomised, placebo-controlled, phase 2b trial.* Lancet Respir Med, 2021. **9**(5): p. 476-486.

101.   Laporta Hernandez, R., M. Aguilar Perez, M.T. Lázaro Carrasco, and P. Ussetti Gil, *Lung Transplantation in Idiopathic Pulmonary Fibrosis.* Med Sci (Basel), 2018. **6**(3).

102.   Staab-Weijnitz, C.A., *Fighting the Fiber: Targeting Collagen in Lung Fibrosis.* Am J Respir Cell Mol Biol, 2022. **66**(4): p. 363-381.

103.   Pardo, A. and M. Selman, *Molecular mechanisms of pulmonary fibrosis.* Front Biosci, 2002. **7**: p. d1743-61.

104.   Wilson, M.S. and T.A. Wynn, *Pulmonary fibrosis: pathogenesis, etiology and regulation.* Mucosal Immunol, 2009. **2**(2): p. 103-21.

105.   Chanda, D., E. Otoupalova, S.R. Smith, T. Volckaert, S.P. De Langhe, and V.J. Thannickal, *Developmental pathways in the pathogenesis of lung fibrosis.* Molecular Aspects of Medicine, 2019. **65**: p. 56-69.

106.   Lekkerkerker, A.N., J. Aarbiou, T. van Es, and R.A. Janssen, *Cellular players in lung fibrosis.* Curr Pharm Des, 2012. **18**(27): p. 4093-102.

107.   Habiel, D.M. and C.M. Hogaboam, *Heterogeneity of Fibroblasts and Myofibroblasts in Pulmonary Fibrosis.* Curr Pathobiol Rep, 2017. **5**(2): p. 101-110.

108.   Kristensen, J.H., M.A. Karsdal, F. Genovese, S. Johnson, B. Svensson, S. Jacobsen, P. Hägglund, and D.J. Leeming, *The role of extracellular matrix quality in pulmonary fibrosis.* Respiration, 2014. **88**(6): p. 487-99.

109.   Chen, W., J.B. Rock, M.M. Yearsley, L.D. Ferrell, and W.L. Frankel, *Different collagen types show distinct rates of increase from early to late stages of hepatitis C-related liver fibrosis.* Hum Pathol, 2014. **45**(1): p. 160-5.

110.   Bateman, E.D., M. Turner-Warwick, and B.C. Adelmann-Grill, *Immunohistochemical study of collagen types in human foetal lung and fibrotic lung disease.* Thorax, 1981. **36**(9): p. 645-653.

111.   Reich, A., M. Meurer, B. Eckes, J. Friedrichs, and D.J. Muller, *Surface morphology and mechanical properties of fibroblasts from scleroderma patients.* J Cell Mol Med, 2009. **13**(8b): p. 1644-1652.

112. Liu, F., J.D. Mih, B.S. Shea, A.T. Kho, A.S. Sharif, A.M. Tager, and D.J. Tschumperlin, *Feedback amplification of fibrosis through matrix stiffening and COX-2 suppression.* J Cell Biol, 2010. **190**(4): p. 693-706.

113. Eitzman, D.T., R.D. McCoy, X. Zheng, W.P. Fay, T. Shen, D. Ginsburg, and R.H. Simon, *Bleomycin-induced pulmonary fibrosis in transgenic mice that either lack or overexpress the murine plasminogen activator inhibitor-1 gene.* J Clin Invest, 1996. **97**(1): p. 232-7.

114. Bauman, K.A., S.H. Wettlaufer, K. Okunishi, K.M. Vannella, J.S. Stoolman, S.K. Huang, A.J. Courey, E.S. White, C.M. Hogaboam, R.H. Simon, G.B. Toews, T.H. Sisson, B.B. Moore, and M. Peters-Golden, *The antifibrotic effects of plasminogen activation occur via prostaglandin E2 synthesis in humans and mice.* J Clin Invest, 2010. **120**(6): p. 1950-60.

115. Sung, H., J. Ferlay, R.L. Siegel, M. Laversanne, I. Soerjomataram, A. Jemal, and F. Bray, *Global Cancer Statistics 2020: GLOBOCAN Estimates of Incidence and Mortality Worldwide for 36 Cancers in 185 Countries.* CA: A Cancer Journal for Clinicians, 2021. **71**(3): p. 209-249.

116. Allemani, C., T. Matsuda, V. Di Carlo, R. Harewood, M. Matz, M. Nikšić, A. Bonaventure, M. Valkov, C.J. Johnson, J. Estève, O.J. Ogunbiyi, E.S.G. Azevedo, W.Q. Chen, S. Eser, G. Engholm, C.A. Stiller, A. Monnereau, R.R. Woods, O. Visser, G.H. Lim, J. Aitken, H.K. Weir, and M.P. Coleman, *Global surveillance of trends in cancer survival 2000-14 (CONCORD-3): analysis of individual records for 37 513 025 patients diagnosed with one of 18 cancers from 322 population-based registries in 71 countries.* Lancet, 2018. **391**(10125): p. 1023-1075.

117. Molina, J.R., P. Yang, S.D. Cassivi, S.E. Schild, and A.A. Adjei, *Non-small cell lung cancer: epidemiology, risk factors, treatment, and survivorship.* Mayo Clin Proc, 2008. **83**(5): p. 584-94.

118. Hirsch, F.R., G.V. Scagliotti, J.L. Mulshine, R. Kwon, W.J. Curran, Jr., Y.L. Wu, and L. Paz-Ares, *Lung cancer: current therapies and new targeted treatments.* Lancet, 2017. **389**(10066): p. 299-311.

119. Kinoshita, T. and T. Goto, *Molecular Mechanisms of Pulmonary Fibrogenesis and Its Progression to Lung Cancer: A Review.* Int J Mol Sci, 2019. **20**(6).

120. Rodriguez-Canales, J., E. Parra-Cuentas, and Wistuba, II, *Diagnosis and Molecular Classification of Lung Cancer.* Cancer Treat Res, 2016. **170**: p. 25-46.

121. Zheng, M., *Classification and Pathology of Lung Cancer.* Surg Oncol Clin N Am, 2016. **25**(3): p. 447-68.

122. Mok, T.S., Y.L. Wu, S. Thongprasert, C.H. Yang, D.T. Chu, N. Saijo, P. Sunpaweravong, B. Han, B. Margono, Y. Ichinose, Y. Nishiwaki, Y. Ohe, J.J. Yang, B. Chewaskulyong, H. Jiang, E.L. Duffield, C.L. Watkins, A.A. Armour, and M. Fukuoka, *Gefitinib or carboplatin-paclitaxel in pulmonary adenocarcinoma.* N Engl J Med, 2009. **361**(10): p. 947-57.

123. Zhou, C., Y.L. Wu, G. Chen, J. Feng, X.Q. Liu, C. Wang, S. Zhang, J. Wang, S. Zhou, S. Ren, S. Lu, L. Zhang, C. Hu, C. Hu, Y. Luo, L. Chen, M. Ye, J. Huang, X. Zhi, Y. Zhang, Q. Xiu, J. Ma, L. Zhang, and C. You, *Erlotinib versus chemotherapy as first-line treatment for patients with advanced EGFR mutation-positive non-small-cell lung cancer (OPTIMAL, CTONG-0802): a multicentre, open-label, randomised, phase 3 study.* Lancet Oncol, 2011. **12**(8): p. 735-42.

124. Hay, E.D., *An overview of epithelio-mesenchymal transformation.* Acta Anat (Basel), 1995. **154**(1): p. 8-20.

125. Thiery, J.P. and J.P. Sleeman, *Complex networks orchestrate epithelial-mesenchymal transitions.* Nat Rev Mol Cell Biol, 2006. **7**(2): p. 131-42.

126. Park, J. and J.E. Schwarzbauer, *Mammary epithelial cell interactions with fibronectin stimulate epithelial-mesenchymal transition.* Oncogene, 2014. **33**(13): p. 1649-1657.

127. Lee, J.M., S. Dedhar, R. Kalluri, and E.W. Thompson, *The epithelial-mesenchymal transition: new insights in signaling, development, and disease.* J Cell Biol, 2006. **172**(7): p. 973-81.

128. Schwager, S.C., P.V. Taufalele, and C.A. Reinhart-King, *Cell-Cell Mechanical Communication in Cancer.* Cell Mol Bioeng, 2019. **12**(1): p. 1-14.

129. Muñoz-Galván, S., M. Rivero, J. Peinado-Serrano, J. Martinez-Pérez, M.C. Fernández-Fernández, M.J. Ortiz, J.M. García-Heredia, and A. Carnero, *PAI1 is a Marker of Bad Prognosis in Rectal Cancer but Predicts a Better Response to Treatment with PIM Inhibitor AZD1208.* Cells, 2020. **9**(5).

130. Chen, H., H. Peng, W. Liu, Y. Sun, N. Su, W. Tang, X. Zhang, J. Wang, L. Cui, P. Hu, and S. Liu, *Silencing of plasminogen activator inhibitor-1 suppresses colorectal cancer progression and liver metastasis.* Surgery, 2015. **158**(6): p. 1704-13.

131. Li, S., X. Wei, J. He, X. Tian, S. Yuan, and L. Sun, *Plasminogen activator inhibitor-1 in cancer research.* Biomed Pharmacother, 2018. **105**: p. 83-94.

132. Humphries, B.A., J.M. Buschhaus, Y.C. Chen, H.R. Haley, T. Qyli, B. Chiang, N. Shen, S. Rajendran, A. Cutter, Y.H. Cheng, Y.T. Chen, J. Cong, P.C. Spinosa, E. Yoon, K.E. Luker, and G.D. Luker, *Plasminogen Activator Inhibitor 1 (PAI1) Promotes Actin Cytoskeleton Reorganization and Glycolytic Metabolism in Triple-Negative Breast Cancer.* Mol Cancer Res, 2019. **17**(5): p. 1142-1154.

133. Kwaan, H.C., J. Wang, K. Svoboda, and P.J. Declerck, *Plasminogen activator inhibitor 1 may promote tumour growth through inhibition of apoptosis.* Br J Cancer, 2000. **82**(10): p. 1702-8.

134. Alexander, C.M. and Z. Werb, *Proteinases and extracellular matrix remodeling.* Curr Opin Cell Biol, 1989. **1**(5): p. 974-82.

135. Juban, G., M. Saclier, H. Yacoub-Youssef, A. Kernou, L. Arnold, C. Boisson, S. Ben Larbi, M. Magnan, S. Cuvellier, M. Théret, B.J. Petrof, I. Desguerre, J. Gondin, R. Mounier, and B. Chazaud, *AMPK Activation Regulates*

LTBP4-Dependent TGF-β1 Secretion by Pro-inflammatory Macrophages and Controls Fibrosis in Duchenne Muscular Dystrophy. Cell Rep, 2018. **25**(8): p. 2163-2176.e6.

136. Nevers, T., A.M. Salvador, F. Velazquez, N. Ngwenyama, F.J. Carrillo-Salinas, M. Aronovitz, R.M. Blanton, and P. Alcaide, *Th1 effector T cells selectively orchestrate cardiac fibrosis in nonischemic heart failure.* J Exp Med, 2017. **214**(11): p. 3311-3329.

137. To, W.S. and K.S. Midwood, *Plasma and cellular fibronectin: distinct and independent functions during tissue repair.* Fibrogenesis & Tissue Repair, 2011. **4**(1): p. 21.

138. Schultz, G.S. and A. Wysocki, *Interactions between extracellular matrix and growth factors in wound healing.* Wound Repair and Regeneration, 2009. **17**(2): p. 153-162.

139. Danen, E.H.J., P. Sonneveld , C. Brakebusch , R. Fässler , and A. Sonnenberg *The fibronectin-binding integrins α5β1 and αvβ3 differentially modulate RhoA–GTP loading, organization of cell matrix adhesions, and fibronectin fibrillogenesis.* Journal of Cell Biology, 2002. **159**(6): p. 1071-1086.

140. White, E.S., *Lung extracellular matrix and fibroblast function.* Annals of the American Thoracic Society, 2015. **12 Suppl 1**(Suppl 1): p. S30-S33.

141. Werb, Z., C.L. Mainardi, C.A. Vater, and E.D. Harris, Jr., *Endogenous activation of latent collagenase by rheumatoid synovial cells. Evidence for a role of plasminogen activator.* N Engl J Med, 1977. **296**(18): p. 1017-23.

142. Pins, G.D., M.E. Collins-Pavao, L. Van De Water, M.L. Yarmush, and J.R. Morgan, *Plasmin Triggers Rapid Contraction and Degradation of Fibroblast-Populated Collagen Lattices.* Journal of Investigative Dermatology, 2000. **114**(4): p. 647-653.

143. Baba, A.B., B. Rah, G.R. Bhat, I. Mushtaq, S. Parveen, R. Hassan, M. Hameed Zargar, and D. Afroze, *Transforming Growth Factor-Beta (TGF-β) Signaling in Cancer-A Betrayal Within.* Front Pharmacol, 2022. **13**: p. 791272.

144. Clark, D.A. and R. Coker, *Transforming growth factor-beta (TGF-beta).* Int J Biochem Cell Biol, 1998. **30**(3): p. 293-8.

145. Derynck, R., J.A. Jarrett, E.Y. Chen, D.H. Eaton, J.R. Bell, R.K. Assoian, A.B. Roberts, M.B. Sporn, and D.V. Goeddel, *Human transforming growth factor-beta complementary DNA sequence and expression in normal and transformed cells.* Nature, 1985. **316**(6030): p. 701-5.

146. Aashaq, S., A. Batool, S.A. Mir, M.A. Beigh, K.I. Andrabi, and Z.A. Shah, *TGF-β signaling: A recap of SMAD-independent and SMAD-dependent pathways.* J Cell Physiol, 2022. **237**(1): p. 59-85.

147. Kulkarni, A.B., C.G. Huh, D. Becker, A. Geiser, M. Lyght, K.C. Flanders, A.B. Roberts, M.B. Sporn, J.M. Ward, and S. Karlsson, *Transforming growth factor beta 1 null mutation in mice causes excessive inflammatory response and early death.* Proc Natl Acad Sci U S A, 1993. **90**(2): p. 770-4.

148. Li, M.O. and R.A. Flavell, *TGF-beta: a master of all T cell trades.* Cell, 2008. **134**(3): p. 392-404.

149. Li, M.O., Y.Y. Wan, S. Sanjabi, A.K. Robertson, and R.A. Flavell, *Transforming growth factor-beta regulation of immune responses.* Annu Rev Immunol, 2006. **24**: p. 99-146.

150. Mirshafiey, A. and M. Mohsenzadegan, *TGF-beta as a promising option in the treatment of multiple sclerosis.* Neuropharmacology, 2009. **56**(6-7): p. 929-36.

151. Hannon, G.J. and D. Beach, *p15INK4B is a potential effector of TGF-beta-induced cell cycle arrest.* Nature, 1994. **371**(6494): p. 257-61.

152. Chen, C.L., S.S. Huang, and J.S. Huang, *Cholesterol modulates cellular TGF-beta responsiveness by altering TGF-beta binding to TGF-beta receptors.* J Cell Physiol, 2008. **215**(1): p. 223-33.

153. Gabitova-Cornell, L., A. Surumbayeva, S. Peri, J. Franco-Barraza, D. Restifo, N. Weitz, C. Ogier, A.R. Goldman, T.R. Hartman, R. Francescone, Y. Tan, E. Nicolas, N. Shah, E.A. Handorf, K.Q. Cai, A.M. O'Reilly, I. Sloma, R. Chiaverelli, R.A. Moffitt, V. Khazak, C.Y. Fang, E.A. Golemis, E. Cukierman, and I. Astsaturov, *Cholesterol Pathway Inhibition Induces TGF-β Signaling to Promote Basal Differentiation in Pancreatic Cancer.* Cancer Cell, 2020. **38**(4): p. 567-583.e11.

154. Grainger, D.J., P.R. Kemp, J.C. Metcalfe, A.C. Liu, R.M. Lawn, N.R. Williams, A.A. Grace, P.M. Schofield, and A. Chauhan, *The serum concentration of active transforming growth factor-beta is severely depressed in advanced atherosclerosis.* Nat Med, 1995. **1**(1): p. 74-9.

155. Wang, H.L., L. Wang, C.Y. Zhao, and H.Y. Lan, *Role of TGF-Beta Signaling in Beta Cell Proliferation and Function in Diabetes.* Biomolecules, 2022. **12**(3).

156. Das, P. and T. Golde, *Dysfunction of TGF-beta signaling in Alzheimer's disease.* J Clin Invest, 2006. **116**(11): p. 2855-7.

157. Loeys, B.L. and H.C. Dietz, *Loeys-Dietz Syndrome*, in *GeneReviews(®)*, M.P. Adam, et al., Editors. 1993, University of Washington, Seattle

158. Singh, M., C. Vaughn, K. Sasaninia, C. Yeh, D. Mehta, I. Khieran, and V. Venketaraman, *Understanding the Relationship between Glutathione, TGF-β, and Vitamin D in Combating Mycobacterium tuberculosis Infections.* J Clin Med, 2020. **9**(9).

159. Saito, A., M. Horie, and T. Nagase, *TGF-β Signaling in Lung Health and Disease.* International Journal of Molecular Sciences, 2018. **19**(8): p. 2460.

160. Hata, A. and Y.G. Chen, *TGF-β Signaling from Receptors to Smads.* Cold Spring Harb Perspect Biol, 2016. **8**(9).

161. Tzavlaki, K. and A. Moustakas, *TGF-β Signaling.* Biomolecules, 2020. **10**(3).

162. Sekelsky, J.J., S.J. Newfeld, L.A. Raftery, E.H. Chartoff, and W.M. Gelbart, *Genetic characterization and cloning of mothers against dpp, a gene*

required for decapentaplegic function in Drosophila melanogaster. Genetics, 1995. **139**(3): p. 1347-58.

163. Savage, C., P. Das, A.L. Finelli, S.R. Townsend, C.Y. Sun, S.E. Baird, and R.W. Padgett, *Caenorhabditis elegans genes sma-2, sma-3, and sma-4 define a conserved family of transforming growth factor beta pathway components.* Proc Natl Acad Sci U S A, 1996. **93**(2): p. 790-4.

164. Liu, F., A. Hata, J.C. Baker, J. Doody, J. Cárcamo, R.M. Harland, and J. Massagué, *A human Mad protein acting as a BMP-regulated transcriptional activator.* Nature, 1996. **381**(6583): p. 620-3.

165. Moustakas, A., S. Souchelnytskyi, and C.H. Heldin, *Smad regulation in TGF-beta signal transduction.* J Cell Sci, 2001. **114**(Pt 24): p. 4359-69.

166. Abdollah, S., M. Macías-Silva, T. Tsukazaki, H. Hayashi, L. Attisano, and J.L. Wrana, *TbetaRI phosphorylation of Smad2 on Ser465 and Ser467 is required for Smad2-Smad4 complex formation and signaling.* J Biol Chem, 1997. **272**(44): p. 27678-85.

167. Souchelnytskyi, S., K. Tamaki, U. Engström, C. Wernstedt, P. ten Dijke, and C.H. Heldin, *Phosphorylation of Ser465 and Ser467 in the C terminus of Smad2 mediates interaction with Smad4 and is required for transforming growth factor-beta signaling.* J Biol Chem, 1997. **272**(44): p. 28107-15.

168. Hata, A., G. Lagna, J. Massagué, and A. Hemmati-Brivanlou, *Smad6 inhibits BMP/Smad1 signaling by specifically competing with the Smad4 tumor suppressor.* Genes Dev, 1998. **12**(2): p. 186-97.

169. Imamura, T., M. Takase, A. Nishihara, E. Oeda, J. Hanai, M. Kawabata, and K. Miyazono, *Smad6 inhibits signalling by the TGF-beta superfamily.* Nature, 1997. **389**(6651): p. 622-6.

170. Nakao, A., M. Afrakhte, A. Morén, T. Nakayama, J.L. Christian, R. Heuchel, S. Itoh, M. Kawabata, N.E. Heldin, C.H. Heldin, and P. ten Dijke, *Identification of Smad7, a TGFbeta-inducible antagonist of TGF-beta signalling.* Nature, 1997. **389**(6651): p. 631-5.

171. Hayashi, H., S. Abdollah, Y. Qiu, J. Cai, Y.Y. Xu, B.W. Grinnell, M.A. Richardson, J.N. Topper, M.A. Gimbrone, Jr., J.L. Wrana, and D. Falb, *The MAD-related protein Smad7 associates with the TGFbeta receptor and functions as an antagonist of TGFbeta signaling.* Cell, 1997. **89**(7): p. 1165-73.

172. Macias, M.J., P. Martin-Malpartida, and J. Massagué, *Structural determinants of Smad function in TGF-β signaling.* Trends Biochem Sci, 2015. **40**(6): p. 296-308.

173. Breton, J.-D., D. Heydet, L.M. Starrs, T. Veldre, and R. Ghildyal, *Molecular changes during TGFβ -mediated lung fibroblast-myofibroblast differentiation: implication for glucocorticoid resistance.* Physiological Reports, 2018. **6**(7): p. e13669.

174. Hu, B., Z. Wu, and S.H. Phan, *Smad3 mediates transforming growth factor-beta-induced alpha-smooth muscle actin expression.* Am J Respir Cell Mol Biol, 2003. **29**(3 Pt 1): p. 397-404.

175. Staab-Weijnitz, C.A., I.E. Fernandez, L. Knüppel, J. Maul, K. Heinzelmann, B.M. Juan-Guardela, E. Hennen, G. Preissler, H. Winter, C. Neurohr, R. Hatz, M. Lindner, J. Behr, N. Kaminski, and O. Eickelberg, *FK506-Binding Protein 10, a Potential Novel Drug Target for Idiopathic Pulmonary Fibrosis.* American Journal of Respiratory and Critical Care Medicine, 2015. **192**(4): p. 455-467.

176. Kretzschmar, M., J. Doody, and J. Massagué, *Opposing BMP and EGF signalling pathways converge on the TGF-beta family mediator Smad1.* Nature, 1997. **389**(6651): p. 618-22.

177. Kretzschmar, M., J. Doody, I. Timokhina, and J. Massagué, *A mechanism of repression of TGFbeta/ Smad signaling by oncogenic Ras.* Genes & development, 1999. **13**(7): p. 804-816.

178. Kamato, D. and P.J. Little, *Smad2 linker region phosphorylation is an autonomous cell signalling pathway: Implications for multiple disease pathologies.* Biomed Pharmacother, 2020. **124**: p. 109854.

179. Dennler, S., S. Itoh, D. Vivien, P. ten Dijke, S. Huet, and J.M. Gauthier, *Direct binding of Smad3 and Smad4 to critical TGF beta-inducible elements in the promoter of human plasminogen activator inhibitor-type 1 gene.* Embo j, 1998. **17**(11): p. 3091-100.

180. Song, C.Z., T.E. Siok, and T.D. Gelehrter, *Smad4/DPC4 and Smad3 mediate transforming growth factor-beta (TGF-beta) signaling through direct binding to a novel TGF-beta-responsive element in the human plasminogen activator inhibitor-1 promoter.* J Biol Chem, 1998. **273**(45): p. 29287-90.

181. Hua, X., Z.A. Miller, G. Wu, Y. Shi, and H.F. Lodish, *Specificity in transforming growth factor beta-induced transcription of the plasminogen activator inhibitor-1 gene: interactions of promoter DNA, transcription factor muE3, and Smad proteins.* Proc Natl Acad Sci U S A, 1999. **96**(23): p. 13130-5.

182. Verrecchia, F., M.L. Chu, and A. Mauviel, *Identification of novel TGF-beta /Smad gene targets in dermal fibroblasts using a combined cDNA microarray/promoter transactivation approach.* J Biol Chem, 2001. **276**(20): p. 17058-62.

183. Zhao, J., W. Shi, Y.L. Wang, H. Chen, P. Bringas, Jr., M.B. Datto, J.P. Frederick, X.F. Wang, and D. Warburton, *Smad3 deficiency attenuates bleomycin-induced pulmonary fibrosis in mice.* Am J Physiol Lung Cell Mol Physiol, 2002. **282**(3): p. L585-93.

184. Isono, M., S. Chen, S.W. Hong, M.C. Iglesias-de la Cruz, and F.N. Ziyadeh, *Smad pathway is activated in the diabetic mouse kidney and Smad3 mediates TGF-beta-induced fibronectin in mesangial cells.* Biochem Biophys Res Commun, 2002. **296**(5): p. 1356-65.

185. Jaffe, A.B. and A. Hall, *Rho GTPases: biochemistry and biology.* Annu Rev Cell Dev Biol, 2005. **21**: p. 247-69.

186. Ihara, K., S. Muraguchi, M. Kato, T. Shimizu, M. Shirakawa, S. Kuroda, K. Kaibuchi, and T. Hakoshima, *Crystal structure of human RhoA in a*

dominantly active form complexed with a GTP analogue. J Biol Chem, 1998. **273**(16): p. 9656-66.

187. Peng, F., B. Zhang, D. Wu, A.J. Ingram, B. Gao, and J.C. Krepinsky, *TGFbeta-induced RhoA activation and fibronectin production in mesangial cells require caveolae.* Am J Physiol Renal Physiol, 2008. **295**(1): p. F153-64.

188. Bhowmick, N.A., M. Ghiassi, A. Bakin, M. Aakre, C.A. Lundquist, M.E. Engel, C.L. Arteaga, and H.L. Moses, *Transforming Growth Factor-β1 Mediates Epithelial to Mesenchymal Transdifferentiation through a RhoA-dependent Mechanism.* Molecular Biology of the Cell, 2001. **12**(1): p. 27-36.

189. Shen, X., J. Li, P.P. Hu, D. Waddell, J. Zhang, and X.F. Wang, *The activity of guanine exchange factor NET1 is essential for transforming growth factor-beta-mediated stress fiber formation.* J Biol Chem, 2001. **276**(18): p. 15362-8.

190. Lee, J., H.-J. Moon, J.-M. Lee, and C.-K. Joo, *Smad3 Regulates Rho Signaling via NET1 in the Transforming Growth Factor-β-induced Epithelial-Mesenchymal Transition of Human Retinal Pigment Epithelial Cells*.* Journal of Biological Chemistry, 2010. **285**(34): p. 26618-26627.

191. Voorneveld, P.W., L.L. Kodach, R.J. Jacobs, N. Liv, A.C. Zonnevylle, J.P. Hoogenboom, I. Biemond, H.W. Verspaget, D.W. Hommes, K. de Rooij, C.J.M. van Noesel, H. Morreau, T. van Wezel, G.J.A. Offerhaus, G.R. van den Brink, M.P. Peppelenbosch, P. ten Dijke, and J.C.H. Hardwick, *Loss of SMAD4 Alters BMP Signaling to Promote Colorectal Cancer Cell Metastasis via Activation of Rho and ROCK.* Gastroenterology, 2014. **147**(1): p. 196-208.e13.

192. Gao, L., G. Joberty, and I.G. Macara, *Assembly of epithelial tight junctions is negatively regulated by Par6.* Curr Biol, 2002. **12**(3): p. 221-5.

193. Ozdamar, B., R. Bose, M. Barrios-Rodiles, H.R. Wang, Y. Zhang, and J.L. Wrana, *Regulation of the polarity protein Par6 by TGFbeta receptors controls epithelial cell plasticity.* Science, 2005. **307**(5715): p. 1603-9.

194. Zhang, Y.E., *Non-Smad pathways in TGF-β signaling.* Cell Research, 2009. **19**(1): p. 128-139.

195. Wang, D., X. Qian, M. Rajaram, M.E. Durkin, and D.R. Lowy, *DLC1 is the principal biologically-relevant down-regulated DLC family member in several cancers.* Oncotarget, 2016. **7**(29): p. 45144-45157.

196. Zhou, H., Y.-j. Li, M. Wang, L.-h. Zhang, B.-y. Guo, Z.-s. Zhao, F.-l. Meng, Y.-g. Deng, and R.-y. Wang, *Involvement of RhoA/ROCK in myocardial fibrosis in a rat model of type 2 diabetes.* Acta Pharmacologica Sinica, 2011. **32**(8): p. 999-1008.

197. Gao, H.C., H. Zhao, W.Q. Zhang, Y.Q. Li, and L.Q. Ren, *The role of the Rho/Rock signaling pathway in the pathogenesis of acute ischemic myocardial fibrosis in rat models.* Exp Ther Med, 2013. **5**(4): p. 1123-1128.

198. Chen, S., M. Crawford, R.M. Day, V.R. Briones, J.E. Leader, P.A. Jose, and R.J. Lechleider, *RhoA modulates Smad signaling during transforming*

growth factor-beta-induced smooth muscle differentiation. J Biol Chem, 2006. **281**(3): p. 1765-70.

199. Ji, H., H. Tang, H. Lin, J. Mao, L. Gao, J. Liu, and T. Wu, *Rho/Rock cross-talks with transforming growth factor-β/Smad pathway participates in lung fibroblast-myofibroblast differentiation.* Biomed Rep, 2014. **2**(6): p. 787-792.

200. Lee, S.J., J.H. Kang, S.Y. Choi, and O.S. Kwon, *PKCδ as a regulator for TGF-β-stimulated connective tissue growth factor production in human hepatocarcinoma (HepG2) cells.* Biochem J, 2013. **456**(1): p. 109-18.

201. Lin, X., X. Duan, Y.Y. Liang, Y. Su, K.H. Wrighton, J. Long, M. Hu, C.M. Davis, J. Wang, F.C. Brunicardi, Y. Shi, Y.G. Chen, A. Meng, and X.H. Feng, *PPM1A functions as a Smad phosphatase to terminate TGFbeta signaling.* Cell, 2006. **125**(5): p. 915-28.

202. Bhowmick, N.A., R. Zent, M. Ghiassi, M. McDonnell, and H.L. Moses, *Integrin beta 1 signaling is necessary for transforming growth factor-beta activation of p38MAPK and epithelial plasticity.* J Biol Chem, 2001. **276**(50): p. 46707-13.

203. Yu, L., M.C. Hébert, and Y.E. Zhang, *TGF-β receptor-activated p38 MAP kinase mediates Smad-independent TGF-β responses.* The EMBO Journal, 2002. **21**(14): p. 3749-3759.

204. Frey, R.S. and K.M. Mulder, *Involvement of extracellular signal-regulated kinase 2 and stress-activated protein kinase/Jun N-terminal kinase activation by transforming growth factor beta in the negative growth control of breast cancer cells.* Cancer Res, 1997. **57**(4): p. 628-33.

205. Hocevar, B.A., T.L. Brown, and P.H. Howe, *TGF-β induces fibronectin synthesis through a c-Jun N-terminal kinase-dependent, Smad4-independent pathway.* The EMBO Journal, 1999. **18**(5): p. 1345-1356.

206. Zhang, J., N. Jiang, J. Ping, and L. Xu, *TGF-β1-induced autophagy activates hepatic stellate cells via the ERK and JNK signaling pathways.* Int J Mol Med, 2021. **47**(1): p. 256-266.

207. Nie, D., X. Liu, Y. Wang, W. He, M. Li, Y. Peng, J. Zhang, L. Sun, Z. Yan, and L. Ye, *Involvement of the JNK signaling in granular corneal dystrophy by modulating TGF-β-induced TGFBI expression and corneal fibroblast apoptosis.* In Vitro Cell Dev Biol Anim, 2020. **56**(3): p. 234-242.

208. Xiao, L., Y. Du, Y. Shen, Y. He, H. Zhao, and Z. Li, *TGF-beta 1 induced fibroblast proliferation is mediated by the FGF-2/ERK pathway.* Front Biosci (Landmark Ed), 2012. **17**(7): p. 2667-74.

209. Zhao, Y., J. Ma, Y. Fan, Z. Wang, R. Tian, W. Ji, F. Zhang, and R. Niu, *TGF-β transactivates EGFR and facilitates breast cancer migration and invasion through canonical Smad3 and ERK/Sp1 signaling pathways.* Mol Oncol, 2018. **12**(3): p. 305-321.

210. Hammaker, D.R., D.L. Boyle, T. Inoue, and G.S. Firestein, *Regulation of the JNK pathway by TGF-beta activated kinase 1 in rheumatoid arthritis synoviocytes.* Arthritis Res Ther, 2007. **9**(3): p. R57.

211. Kim, S.I., J.H. Kwak, H.J. Na, J.K. Kim, Y. Ding, and M.E. Choi, *Transforming growth factor-beta (TGF-beta1) activates TAK1 via TAB1-mediated autophosphorylation, independent of TGF-beta receptor kinase activity in mesangial cells.* J Biol Chem, 2009. **284**(33): p. 22285-22296.

212. Okada, M., A. Matsuzawa, A. Yoshimura, and H. Ichijo, *The lysosome rupture-activated TAK1-JNK pathway regulates NLRP3 inflammasome activation.* J Biol Chem, 2014. **289**(47): p. 32926-36.

213. Zhou, J., Y. Fan, J. Zhong, Z. Huang, T. Huang, S. Lin, and H. Chen, *TAK1 mediates excessive autophagy via p38 and ERK in cisplatin-induced acute kidney injury.* J Cell Mol Med, 2018. **22**(5): p. 2908-2921.

214. Grynberg, K., F.Y. Ma, and D.J. Nikolic-Paterson, *The JNK Signaling Pathway in Renal Fibrosis.* Front Physiol, 2017. **8**: p. 829.

215. Dowdy, S.C., A. Mariani, and R. Janknecht, *HER2/Neu- and TAK1-mediated up-regulation of the transforming growth factor beta inhibitor Smad7 via the ETS protein ER81.* J Biol Chem, 2003. **278**(45): p. 44377-84.

216. Hocevar, B.A., C. Prunier, and P.H. Howe, *Disabled-2 (Dab2) mediates transforming growth factor beta (TGFbeta)-stimulated fibronectin synthesis through TGFbeta-activated kinase 1 and activation of the JNK pathway.* J Biol Chem, 2005. **280**(27): p. 25920-7.

217. Flanc, R.S., F.Y. Ma, G.H. Tesch, Y. Han, R.C. Atkins, B.L. Bennett, G.C. Friedman, J.H. Fan, and D.J. Nikolic-Paterson, *A pathogenic role for JNK signaling in experimental anti-GBM glomerulonephritis.* Kidney Int, 2007. **72**(6): p. 698-708.

218. Mulder, K.M. and S.L. Morris, *Activation of p21ras by transforming growth factor beta in epithelial cells.* J Biol Chem, 1992. **267**(8): p. 5029-31.

219. Lawler, S., X.H. Feng, R.H. Chen, E.M. Maruoka, C.W. Turck, I. Griswold-Prenner, and R. Derynck, *The type II transforming growth factor-beta receptor autophosphorylates not only on serine and threonine but also on tyrosine residues.* J Biol Chem, 1997. **272**(23): p. 14850-9.

220. Lee, M.K., C. Pardoux, M.C. Hall, P.S. Lee, D. Warburton, J. Qing, S.M. Smith, and R. Derynck, *TGF-β activates Erk MAP kinase signalling through direct phosphorylation of ShcA.* The EMBO Journal, 2007. **26**(17): p. 3957-3967.

221. McKay, M.M. and D.K. Morrison, *Integrating signals from RTKs to ERK/MAPK.* Oncogene, 2007. **26**(22): p. 3113-21.

222. van der Geer, P., S. Wiley, G.D. Gish, and T. Pawson, *The Shc adaptor protein is highly phosphorylated at conserved, twin tyrosine residues (Y239/240) that mediate protein-protein interactions.* Curr Biol, 1996. **6**(11): p. 1435-44.

223. Quilliam, L.A., R. Khosravi-Far, S.Y. Huff, and C.J. Der, *Guanine nucleotide exchange factors: activators of the Ras superfamily of proteins.* Bioessays, 1995. **17**(5): p. 395-404.

224. Marshall, C.J., *Ras effectors.* Curr Opin Cell Biol, 1996. **8**(2): p. 197-204.

225. Frey, R.S. and K.M. Mulder, *TGFbeta regulation of mitogen-activated protein kinases in human breast cancer cells.* Cancer Lett, 1997. **117**(1): p. 41-50.

226. Mucsi, I., K.L. Skorecki, and H.J. Goldberg, *Extracellular signal-regulated kinase and the small GTP-binding protein, Rac, contribute to the effects of transforming growth factor-beta1 on gene expression.* J Biol Chem, 1996. **271**(28): p. 16567-72.

227. Vicent, S., J.M. López-Picazo, G. Toledo, M.D. Lozano, W. Torre, C. Garcia-Corchón, C. Quero, J.C. Soria, S. Martín-Algarra, R.G. Manzano, and L.M. Montuenga, *ERK1/2 is activated in non-small-cell lung cancer and associated with advanced tumours.* Br J Cancer, 2004. **90**(5): p. 1047-52.

228. Ku, B., J. Heo, J. Kim, J.-M. Sun, S.-H. Lee, J.S. Ahn, K.-S. Park, and M.-J. Ahn, *ERK inhibitor ASN007 effectively overcomes acquired resistance to EGFR inhibitor in non-small cell lung cancer.* Investigational New Drugs, 2022. **40**.

229. Zavadil, J., M. Bitzer, D. Liang, Y.C. Yang, A. Massimi, S. Kneitz, E. Piek, and E.P. Bottinger, *Genetic programs of epithelial cell plasticity directed by transforming growth factor-beta.* Proc Natl Acad Sci U S A, 2001. **98**(12): p. 6686-91.

230. Zou, M., G. Zhang, J. Zou, Y. Liu, B. Liu, X. Hu, and Z. Cheng, *Inhibition of the ERK1/2-ubiquitous calpains pathway attenuates experimental pulmonary fibrosis in vivo and in vitro.* Experimental Cell Research, 2020. **391**(1): p. 111886.

231. Guo, B., K. Inoki, M. Isono, H. Mori, K. Kanasaki, T. Sugimoto, S. Akiba, T. Sato, B. Yang, R. Kikkawa, A. Kashiwagi, M. Haneda, and D. Koya, *MAPK/AP-1-dependent regulation of PAI-1 gene expression by TGF-beta in rat mesangial cells.* Kidney Int, 2005. **68**(3): p. 972-84.

232. Koo, J.H., S.W. Plouffe, Z. Meng, D.H. Lee, D. Yang, D.S. Lim, C.Y. Wang, and K.L. Guan, *Induction of AP-1 by YAP/TAZ contributes to cell proliferation and organ growth.* Genes Dev, 2020. **34**(1-2): p. 72-86.

233. Monje, P., J. Hernández-Losa, R.J. Lyons, M.D. Castellone, and J.S. Gutkind, *Regulation of the transcriptional activity of c-Fos by ERK. A novel role for the prolyl isomerase PIN1.* J Biol Chem, 2005. **280**(42): p. 35081-4.

234. Pulverer, B.J., J.M. Kyriakis, J. Avruch, E. Nikolakaki, and J.R. Woodgett, *Phosphorylation of c-jun mediated by MAP kinases.* Nature, 1991. **353**(6345): p. 670-4.

235. Reddy, C.E., L. Albanito, P. De Marco, D. Aiello, M. Maggiolini, A. Napoli, and A.M. Musti, *Multisite phosphorylation of c-Jun at threonine 91/93/95 triggers the onset of c-Jun pro-apoptotic activity in cerebellar granule neurons.* Cell Death & Disease, 2013. **4**(10): p. e852-e852.

236. Justice, R.W., O. Zilian, D.F. Woods, M. Noll, and P.J. Bryant, *The Drosophila tumor suppressor gene warts encodes a homolog of human*

myotonic dystrophy kinase and is required for the control of cell shape and proliferation. Genes Dev, 1995. **9**(5): p. 534-46.

237. Pan, D., *The hippo signaling pathway in development and cancer.* Dev Cell, 2010. **19**(4): p. 491-505.

238. Chan, E.H., M. Nousiainen, R.B. Chalamalasetty, A. Schäfer, E.A. Nigg, and H.H. Silljé, *The Ste20-like kinase Mst2 activates the human large tumor suppressor kinase Lats1.* Oncogene, 2005. **24**(12): p. 2076-86.

239. Chan, S.W., C.J. Lim, K. Guo, C.P. Ng, I. Lee, W. Hunziker, Q. Zeng, and W. Hong, *A role for TAZ in migration, invasion, and tumorigenesis of breast cancer cells.* Cancer Res, 2008. **68**(8): p. 2592-8.

240. Varelas, X., R. Sakuma, P. Samavarchi-Tehrani, R. Peerani, B.M. Rao, J. Dembowy, M.B. Yaffe, P.W. Zandstra, and J.L. Wrana, *TAZ controls Smad nucleocytoplasmic shuttling and regulates human embryonic stem-cell self-renewal.* Nat Cell Biol, 2008. **10**(7): p. 837-48.

241. Lei, Q.Y., H. Zhang, B. Zhao, Z.Y. Zha, F. Bai, X.H. Pei, S. Zhao, Y. Xiong, and K.L. Guan, *TAZ promotes cell proliferation and epithelial-mesenchymal transition and is inhibited by the hippo pathway.* Mol Cell Biol, 2008. **28**(7): p. 2426-36.

242. Liu, F., D. Lagares, K.M. Choi, L. Stopfer, A. Marinković, V. Vrbanac, C.K. Probst, S.E. Hiemer, T.H. Sisson, J.C. Horowitz, I.O. Rosas, L.E. Fredenburgh, C. Feghali-Bostwick, X. Varelas, A.M. Tager, and D.J. Tschumperlin, *Mechanosignaling through YAP and TAZ drives fibroblast activation and fibrosis.* Am J Physiol Lung Cell Mol Physiol, 2015. **308**(4): p. L344-57.

243. Noguchi, S., A. Saito, Y. Mikami, H. Urushiyama, M. Horie, H. Matsuzaki, H. Takeshima, K. Makita, N. Miyashita, A. Mitani, T. Jo, Y. Yamauchi, Y. Terasaki, and T. Nagase, *TAZ contributes to pulmonary fibrosis by activating profibrotic functions of lung fibroblasts.* Sci Rep, 2017. **7**: p. 42595.

244. Nakamura, R., N. Hiwatashi, R. Bing, C. Doyle, and R. Branski, *Concurrent YAP/TAZ and SMAD signaling mediate vocal fold fibrosis.* Scientific Reports, 2021. **11**.

245. Yingling, J.M., M.B. Datto, C. Wong, J.P. Frederick, N.T. Liberati, and X.F. Wang, *Tumor suppressor Smad4 is a transforming growth factor beta-inducible DNA binding protein.* Mol Cell Biol, 1997. **17**(12): p. 7019-28.

246. Chung, K.Y., A. Agarwal, J. Uitto, and A. Mauviel, *An AP-1 binding sequence is essential for regulation of the human alpha2(I) collagen (COL1A2) promoter activity by transforming growth factor-beta.* J Biol Chem, 1996. **271**(6): p. 3272-8.

247. Kaneko-Kawano, T. and K. Suzuki, *Mechanical stress regulates gene expression via Rho/Rho-kinase signaling pathway.* The Journal of Physical Fitness and Sports Medicine, 2015. **4**: p. 53-61.

248. Haak, A.J., M.T. Ducharme, A.M. Diaz Espinosa, and D.J. Tschumperlin, *Targeting GPCR Signaling for Idiopathic Pulmonary Fibrosis Therapies.* Trends in Pharmacological Sciences, 2020. **41**(3): p. 172-182.

249. Mo, J.S., F.X. Yu, R. Gong, J.H. Brown, and K.L. Guan, *Regulation of the Hippo-YAP pathway by protease-activated receptors (PARs).* Genes Dev, 2012. **26**(19): p. 2138-43.

250. Zhao, B., L. Li, L. Wang, C.Y. Wang, J. Yu, and K.L. Guan, *Cell detachment activates the Hippo pathway via cytoskeleton reorganization to induce anoikis.* Genes Dev, 2012. **26**(1): p. 54-68.

251. Reddy, B.V. and K.D. Irvine, *Regulation of Hippo signaling by EGFR-MAPK signaling through Ajuba family proteins.* Dev Cell, 2013. **24**(5): p. 459-71.

252. You, B., Y.-L. Yang, Z. Xu, Y. Dai, S. Liu, J.-H. Mao, O. Tetsu, H. Li, D.M. Jablons, and L. You, *Inhibition of ERK1/2 down-regulates the Hippo/YAP signaling pathway in human NSCLC cells.* Oncotarget, 2015. **6**(6): p. 4357-4368.

253. Noguchi, S., A. Saito, and T. Nagase, *YAP/TAZ Signaling as a Molecular Link between Fibrosis and Cancer.* Int J Mol Sci, 2018. **19**(11).

254. Yao, M., J. Li, S. Yuan, X. Zhu, Z. Hu, Q. Li, R. Cao, W. Wang, and C. Fang, *Role of the arecoline/YAP1/BMP4 pathway in promoting endothelial-mesenchymal transition in oral submucous fibrosis.* J Oral Pathol Med, 2020. **49**(4): p. 305-310.

255. Wu, P., Z. Liu, T. Zhao, F. Xia, L. Gong, Z. Zheng, Z. Chen, T. Yang, and Q. Duan, *Lovastatin attenuates angiotensin II induced cardiovascular fibrosis through the suppression of YAP/TAZ signaling.* Biochem Biophys Res Commun, 2019. **512**(4): p. 736-741.

256. Zhang, Z., J. Du, S. Wang, L. Shao, K. Jin, F. Li, B. Wei, W. Ding, P. Fu, H. van Dam, A. Wang, J. Jin, C. Ding, B. Yang, M. Zheng, X.H. Feng, K.L. Guan, and L. Zhang, *OTUB2 Promotes Cancer Metastasis via Hippo-Independent Activation of YAP and TAZ.* Mol Cell, 2019. **73**(1): p. 7-21.e7.

257. Qin, Z., W. Xia, G.J. Fisher, J.J. Voorhees, and T. Quan, *YAP/TAZ regulates TGF-β/Smad3 signaling by induction of Smad7 via AP-1 in human skin dermal fibroblasts.* Cell Commun Signal, 2018. **16**(1): p. 18.

258. Noguchi, S., A. Saito, M. Horie, Y. Mikami, H.I. Suzuki, Y. Morishita, M. Ohshima, Y. Abiko, J.S. Mattsson, H. König, M. Lohr, K. Edlund, J. Botling, P. Micke, and T. Nagase, *An integrative analysis of the tumorigenic role of TAZ in human non-small cell lung cancer.* Clin Cancer Res, 2014. **20**(17): p. 4660-72.

259. Lin, H., L. Xu, S. Yu, W. Hong, M. Huang, and P. Xu, *Therapeutics targeting the fibrinolytic system.* Exp Mol Med, 2020. **52**(3): p. 367-379.

260. Vindevoghel, L., R.J. Lechleider, A. Kon, M.P. de Caestecker, J. Uitto, A.B. Roberts, and A. Mauviel, *SMAD3/4-dependent transcriptional activation of the human type VII collagen gene (COL7A1) promoter by transforming growth factor beta.* Proc Natl Acad Sci U S A, 1998. **95**(25): p. 14769-74.

261. Binder, B., G. Christ, F. Gruber, N. Grubic, P. Hufnagl, M. Krebs, J. Mihaly-Bison, and G. Prager, *Plasminogen Activator Inhibitor 1: Physiological and Pathophysiological Roles.* News in physiological sciences : an international journal of physiology produced jointly by the International Union of Physiological Sciences and the American Physiological Society, 2002. **17**: p. 56-61.

262. Czekay, R.P., T.M. Simone, and P.J. Higgins, *SerpinE1*, in *Encyclopedia of Signaling Molecules*, S. Choi, Editor. 2017, Springer New York: New York, NY. p. 1-11.

263. Hisatomi, K., H. Mukae, N. Sakamoto, Y. Ishimatsu, T. Kakugawa, S. Hara, H. Fujita, S. Nakamichi, H. Oku, Y. Urata, H. Kubota, K. Nagata, and S. Kohno, *Pirfenidone inhibits TGF-β1-induced over-expression of collagen type I and heat shock protein 47 in A549 cells.* BMC Pulm Med, 2012. **12**: p. 24.

264. Knüppel, L., Y. Ishikawa, M. Aichler, K. Heinzelmann, R. Hatz, J. Behr, A. Walch, H.P. Bächinger, O. Eickelberg, and C.A. Staab-Weijnitz, *A Novel Antifibrotic Mechanism of Nintedanib and Pirfenidone. Inhibition of Collagen Fibril Assembly.* American Journal of Respiratory Cell and Molecular Biology, 2017. **57**(1): p. 77-90.

265. Lin, X., M. Yu, K. Wu, H. Yuan, and H. Zhong, *Effects of pirfenidone on proliferation, migration, and collagen contraction of human Tenon's fibroblasts in vitro.* Invest Ophthalmol Vis Sci, 2009. **50**(8): p. 3763-70.

266. Choi, K., K. Lee, S.W. Ryu, M. Im, K.H. Kook, and C. Choi, *Pirfenidone inhibits transforming growth factor-β1-induced fibrogenesis by blocking nuclear translocation of Smads in human retinal pigment epithelial cell line ARPE-19.* Mol Vis, 2012. **18**: p. 1010-20.

267. Henry, M.T., K. McMahon, A.J. Mackarel, K. Prikk, T. Sorsa, P. Maisi, R. Sepper, M.X. Fitzgerald, and C.M. O'Connor, *Matrix metalloproteinases and tissue inhibitor of metalloproteinase-1 in sarcoidosis and IPF.* Eur Respir J, 2002. **20**(5): p. 1220-7.

268. Mishra, A., P. Bhattacharya, S. Paul, R. Paul, and S. Swarnakar, *An alternative therapy for idiopathic pulmonary fibrosis by doxycycline through matrix metalloproteinase inhibition.* Lung India, 2011. **28**(3): p. 174-9.

269. Shulgina, L., A.P. Cahn, E.R. Chilvers, H. Parfrey, A.B. Clark, E.C.F. Wilson, O.P. Twentyman, A.G. Davison, J.J. Curtin, M.B. Crawford, and A.M. Wilson, *Treating idiopathic pulmonary fibrosis with the addition of co-trimoxazole: a randomised controlled trial.* Thorax, 2013. **68**(2): p. 155-162.

270. Chen, C.-Y., C.-H. Chen, C.-Y. Wang, C.-C. Lai, C.-M. Chao, and Y.-F. Wei, *The effect of additional antimicrobial therapy on the outcomes of patients with idiopathic pulmonary fibrosis: a systematic review and meta-analysis.* Respiratory Research, 2021. **22**(1): p. 243.

271. Antoniou, K.M., A. Pataka, D. Bouros, and N.M. Siafakas, *Pathogenetic pathways and novel pharmacotherapeutic targets in idiopathic pulmonary fibrosis.* Pulm Pharmacol Ther, 2007. **20**(5): p. 453-61.

272. Sritananuwat, P., N. Sueangoen, P. Thummarati, K. Islam, and T. Suthiphongchai, *Blocking ERK1/2 signaling impairs TGF-β1 tumor promoting function but enhances its tumor suppressing role in intrahepatic cholangiocarcinoma cells.* Cancer Cell International, 2017. **17**(1): p. 85.

273. Zhang, Q., N. Yu, and C. Lee, *Mysteries of TGF-β Paradox in Benign and Malignant Cells.* Front Oncol, 2014. **4**: p. 94.

274. Tian, M. and W.P. Schiemann, *The TGF-beta paradox in human cancer: an update.* Future Oncol, 2009. **5**(2): p. 259-71.

275. Kumar, S., R. Guleria, A. Mohan, V. Singh, A.C. Bharti, and B.C. Das, *Efficacy of Plasma TGF-β1 Level in Predicting Therapeutic Efficacy and Prognosis in Patients with Advanced Non-Small Cell Lung Cancer.* Cancer Investigation, 2011. **29**(3): p. 202-207.

276. Ye, Y., S. Liu, C. Wu, and Z. Sun, *TGFβ modulates inflammatory cytokines and growth factors to create premetastatic microenvironment and stimulate lung metastasis.* J Mol Histol, 2015. **46**(4-5): p. 365-75.

277. Colak, S. and P. Ten Dijke, *Targeting TGF-β Signaling in Cancer.* Trends Cancer, 2017. **3**(1): p. 56-71.

278. Li, J., C. Shen, X. Wang, Y. Lai, K. Zhou, P. Li, L. Liu, and G. Che, *Prognostic value of TGF-beta in lung cancer: systematic review and meta-analysis.* BMC Cancer, 2019. **19**(1): p. 691-700.

279. Neuzillet, C., A. Tijeras-Raballand, R. Cohen, J. Cros, S. Faivre, E. Raymond, and A. de Gramont, *Targeting the TGFbeta pathway for cancer therapy.* Pharmacology & Therapeutics, 2015. **147**: p. 22-31.

280. Zhang, Y. and R.A. Weinberg, *Epithelial-to-mesenchymal transition in cancer: complexity and opportunities.* Front Med, 2018. **12**(4): p. 361-373.

281. Thiery, J.P., H. Acloque, R.Y. Huang, and M.A. Nieto, *Epithelial-mesenchymal transitions in development and disease.* Cell, 2009. **139**(5): p. 871-90.

282. Ungefroren, H., D. Witte, and H. Lehnert, *The role of small GTPases of the Rho/Rac family in TGF-β-induced EMT and cell motility in cancer.* Dev Dyn, 2018. **247**(3): p. 451-461.

283. Song, Y., Z. Wang, J. Jiang, Y. Piao, L. Li, C. Xu, H. Piao, L. Li, and G. Yan, *DEK-targeting aptamer DTA-64 attenuates bronchial EMT-mediated airway remodelling by suppressing TGF-β1/Smad, MAPK and PI3K signalling pathway in asthma.* J Cell Mol Med, 2020. **24**(23): p. 13739-13750.

284. Risolino, M., N. Mandia, F. Iavarone, L. Dardaei, E. Longobardi, S. Fernandez, F. Talotta, F. Bianchi, F. Pisati, L. Spaggiari, P.N. Harter, M. Mittelbronn, D. Schulte, M. Incoronato, P.P.D. Fiore, F. Blasi, and P. Verde, *Transcription factor PREP1 induces EMT and metastasis by controlling the TGF-β–SMAD3 pathway in non-small cell lung adenocarcinoma.* Proceedings of the National Academy of Sciences, 2014. **111**(36): p. E3775-E3784.

285. McMahon, B.J. and H.C. Kwaan, *Components of the Plasminogen-Plasmin System as Biologic Markers for Cancer.* Adv Exp Med Biol, 2015. **867**: p. 145-56.

286. Pavey, S.J., G.A. Hawson, and N.A. Marsh, *Impact of the fibrinolytic enzyme system on prognosis and survival associated with non-small cell lung carcinoma.* Blood Coagul Fibrinolysis, 2001. **12**(1): p. 51-8.

287. Ranson, M., N. Andronicos, M. O'Mullane, and M. Baker, *Increased plasminogen binding is associated with metastatic breast cancer cells: differential expression of plasminogen binding proteins.* British Journal of Cancer, 1998. **77**(10): p. 1586-1597.

288. Tantyo, N., A. Karyadi, S. Rasman, M. Salim, A. Devina, and A. Sumarpo, *The prognostic value of S100A10 expression in cancer (Review).* Oncology Letters, 2018.

289. Thummarati, P., S. Wijitburaphat, A. Prasopthum, A. Menakongka, B. Sripa, R. Tohtong, and T. Suthiphongchai, *High level of urokinase plasminogen activator contributes to cholangiocarcinoma invasion and metastasis.* World journal of gastroenterology, 2012. **18**(3): p. 244-250.

290. Urban, P., V. Vuaroqueaux, M. Labuhn, M. Delorenzi, P. Wirapati, E. Wight, H.J. Senn, C. Benz, U. Eppenberger, and S. Eppenberger-Castori, *Increased expression of urokinase-type plasminogen activator mRNA determines adverse prognosis in ErbB2-positive primary breast cancer.* J Clin Oncol, 2006. **24**(26): p. 4245-53.

291. Giard, D.J., S.A. Aaronson, G.J. Todaro, P. Arnstein, J.H. Kersey, H. Dosik, and W.P. Parks, *In Vitro Cultivation of Human Tumors: Establishment of Cell Lines Derived From a Series of Solid Tumors2.* JNCI: Journal of the National Cancer Institute, 1973. **51**(5): p. 1417-1423.

292. Giaccone, G., J. Battey, A.F. Gazdar, H. Oie, M. Draoui, and T.W. Moody, *Neuromedin B is present in lung cancer cell lines.* Cancer Res, 1992. **52**(9 Suppl): p. 2732s-2736s.

293. Jeon, H.-S., T. Dracheva, S.-H. Yang, D. Meerzaman, J. Fukuoka, A. Shakoori, K. Shilo, W.D. Travis, and J. Jen, *SMAD6 contributes to patient survival in non-small cell lung cancer and its knockdown reestablishes TGF-beta homeostasis in lung cancer cells.* Cancer research, 2008. **68**(23): p. 9686-9692.

294. Du, X., X. Qian, A. Papageorge, A.J. Schetter, W.C. Vass, X. Liu, R. Braverman, A.I. Robles, and D.R. Lowy, *Functional interaction of tumor suppressor DLC1 and caveolin-1 in cancer cells.* Cancer Res, 2012. **72**(17): p. 4405-16.

295. Ghosh, A.K. and D.E. Vaughan, *PAI-1 in tissue fibrosis.* Journal of Cellular Physiology, 2012. **227**(2): p. 493-507.

296. Westcott, P.M. and M.D. To, *The genetics and biology of KRAS in lung cancer.* Chin J Cancer, 2013. **32**(2): p. 63-70.

297. Leung, E.L.H., L.X. Luo, Z.Q. Liu, V.K.W. Wong, L.L. Lu, Y. Xie, N. Zhang, Y.Q. Qu, X.X. Fan, Y. Li, M. Huang, D.K. Xiao, J. Huang, Y.L. Zhou, J.X.

He, J. Ding, X.J. Yao, D.C. Ward, and L. Liu, *Inhibition of KRAS-dependent lung cancer cell growth by deltarasin: blockage of autophagy increases its cytotoxicity.* Cell Death Dis, 2018. **9**(2): p. 216.

298. Ryan, M.B., C.J. Der, A. Wang-Gillam, and A.D. Cox, *Targeting RAS-mutant cancers: is ERK the key?* Trends in cancer, 2015. **1**(3): p. 183-198.

299. Ohashi, K., L.V. Sequist, M.E. Arcila, C.M. Lovly, X. Chen, C.M. Rudin, T. Moran, D.R. Camidge, C.L. Vnencak-Jones, L. Berry, Y. Pan, H. Sasaki, J.A. Engelman, E.B. Garon, S.M. Dubinett, W.A. Franklin, G.J. Riely, M.L. Sos, M.G. Kris, D. Dias-Santagata, M. Ladanyi, P.A. Bunn, Jr, and W. Pao, *Characteristics of Lung Cancers Harboring NRAS Mutations.* Clinical Cancer Research, 2013. **19**(9): p. 2584-2591.

300. Ohashi, K., L.V. Sequist, M.E. Arcila, T. Moran, J. Chmielecki, Y.-L. Lin, Y. Pan, L. Wang, E. de Stanchina, K. Shien, K. Aoe, S. Toyooka, K. Kiura, L. Fernandez-Cuesta, P. Fidias, J.C.-H. Yang, V.A. Miller, G.J. Riely, M.G. Kris, J.A. Engelman, C.L. Vnencak-Jones, D. Dias-Santagata, M. Ladanyi, and W. Pao, *Lung cancers with acquired resistance to EGFR inhibitors occasionally harbor <i>BRAF</i> gene mutations but lack mutations in <i>KRAS, NRAS,</i> or <i>MEK1</i>.* Proceedings of the National Academy of Sciences, 2012. **109**(31): p. E2127-E2133.

301. Song, Z., F. Liu, and J. Zhang, *Targeting NRAS(Q61K) mutant delays tumor growth and angiogenesis in non-small cell lung cancer.* Am J Cancer Res, 2017. **7**(4): p. 831-844.

302. Haigis, K.M., K.R. Kendall, Y. Wang, A. Cheung, M.C. Haigis, J.N. Glickman, M. Niwa-Kawakita, A. Sweet-Cordero, J. Sebolt-Leopold, K.M. Shannon, J. Settleman, M. Giovannini, and T. Jacks, *Differential effects of oncogenic K-Ras and N-Ras on proliferation, differentiation and tumor progression in the colon.* Nature Genetics, 2008. **40**(5): p. 600-608.

303. Stas, M., H. Degreef, A. Demunter, C. De Wolf-Peeters, and J.J. van den Oord, *Analysis of N- and K-Ras Mutations in the Distinctive Tumor Progression Phases of Melanoma.* Journal of Investigative Dermatology, 2001. **117**(6): p. 1483-1489.

304. Samarakoon, R. and P.J. Higgins, *Integration of non-SMAD and SMAD signaling in TGF-β1-induced plasminogen activator inhibitor type-1 gene expression in vascular smooth muscle cells.* Thromb Haemost, 2008. **100**(12): p. 976-983.

305. Chang, M.C., H.H. Chang, W.C. Hsieh, W.L. Huang, Y.C. Lian, P.Y. Jeng, Y.L. Wang, S.Y. Yeung, and J.H. Jeng, *Effects of transforming growth factor-β1 on plasminogen activation in stem cells from the apical papilla: role of activating receptor-like kinase 5/Smad2 and mitogen-activated protein kinase kinase (MEK)/extracellular signal-regulated kinase (ERK) signalling.* International Endodontic Journal, 2020. **53**(5): p. 647-659.

306. Chang, M.C., H.H. Chang, P.S. Lin, Y.A. Huang, C.P. Chan, Y.L. Tsai, S.Y. Lee, P.Y. Jeng, H.Y. Kuo, S.Y. Yeung, and J.H. Jeng, *Effects of TGF-β1 on plasminogen activation in human dental pulp cells: Role of ALK5/Smad2,*

TAK1 and MEK/ERK signalling. J Tissue Eng Regen Med, 2018. **12**(4): p. 854-863.

307. Montell, C. and G.M. Rubin, *Molecular characterization of the Drosophila trp locus: a putative integral membrane protein required for phototransduction.* Neuron, 1989. **2**(4): p. 1313-23.

308. Cosens, D.J. and A. Manning, *Abnormal electroretinogram from a Drosophila mutant.* Nature, 1969. **224**(5216): p. 285-7.

309. Li, H., *TRP Channel Classification.* Adv Exp Med Biol, 2017. **976**: p. 1-8.

310. Venkatachalam, K. and C. Montell, *TRP channels.* Annu Rev Biochem, 2007. **76**: p. 387-417.

311. Koivisto, A.P., M.G. Belvisi, R. Gaudet, and A. Szallasi, *Advances in TRP channel drug discovery: from target validation to clinical studies.* Nat Rev Drug Discov, 2022. **21**(1): p. 41-59.

312. Rios, F.J., Z.G. Zou, A.P. Harvey, K.Y. Harvey, R. Nosalski, P. Anyfanti, L.L. Camargo, S. Lacchini, A.G. Ryazanov, L. Ryazanova, S. McGrath, T.J. Guzik, C.S. Goodyear, A.C. Montezano, and R.M. Touyz, *Chanzyme TRPM7 protects against cardiovascular inflammation and fibrosis.* Cardiovasc Res, 2020. **116**(3): p. 721-735.

313. Fleig, A. and V. Chubanov, *TRPM7.* Handb Exp Pharmacol, 2014. **222**: p. 521-46.

314. Franken, G.A.C., M.A. Huynen, L.A. Martínez-Cruz, R.J.M. Bindels, and J.H.F. de Baaij, *Structural and functional comparison of magnesium transporters throughout evolution.* Cell Mol Life Sci, 2022. **79**(8): p. 418.

315. Fonfria, E., P.R. Murdock, F.S. Cusdin, C.D. Benham, R.E. Kelsell, and S. McNulty, *Tissue distribution profiles of the human TRPM cation channel family.* J Recept Signal Transduct Res, 2006. **26**(3): p. 159-78.

316. Kunert-Keil, C., F. Bisping, J. Krüger, and H. Brinkmeier, *Tissue-specific expression of TRP channel genes in the mouse and its variation in three different mouse strains.* BMC Genomics, 2006. **7**: p. 159.

317. Jin, J., B.N. Desai, B. Navarro, A. Donovan, N.C. Andrews, and D.E. Clapham, *Deletion of Trpm7 disrupts embryonic development and thymopoiesis without altering Mg2+ homeostasis.* Science, 2008. **322**(5902): p. 756-60.

318. Matsushita, M., J.A. Kozak, Y. Shimizu, D.T. McLachlin, H. Yamaguchi, F.Y. Wei, K. Tomizawa, H. Matsui, B.T. Chait, M.D. Cahalan, and A.C. Nairn, *Channel function is dissociated from the intrinsic kinase activity and autophosphorylation of TRPM7/ChaK1.* J Biol Chem, 2005. **280**(21): p. 20793-803.

319. Schmitz, C., A.L. Perraud, C.O. Johnson, K. Inabe, M.K. Smith, R. Penner, T. Kurosaki, A. Fleig, and A.M. Scharenberg, *Regulation of vertebrate cellular Mg2+ homeostasis by TRPM7.* Cell, 2003. **114**(2): p. 191-200.

320. Demeuse, P., R. Penner, and A. Fleig, *TRPM7 channel is regulated by magnesium nucleotides via its kinase domain.* J Gen Physiol, 2006. **127**(4): p. 421-34.

321. Monteilh-Zoller, M.K., M.C. Hermosura, M.J. Nadler, A.M. Scharenberg, R. Penner, and A. Fleig, *TRPM7 provides an ion channel mechanism for cellular entry of trace metal ions.* J Gen Physiol, 2003. **121**(1): p. 49-60.

322. Prakriya , M. and R.S. Lewis *Separation and Characterization of Currents through Store-operated CRAC Channels and Mg2+-inhibited Cation (MIC) Channels.* Journal of General Physiology, 2002. **119**(5): p. 487-508.

323. Zierler, S., G. Yao, Z. Zhang, W.C. Kuo, P. Pörzgen, R. Penner, F.D. Horgen, and A. Fleig, *Waixenicin A Inhibits Cell Proliferation through Magnesium-dependent Block of Transient Receptor Potential Melastatin 7 (TRPM7) Channels.* Journal of Biological Chemistry, 2011. **286**(45): p. 39328-39335.

324. Chubanov, V. and T. Gudermann, *Mapping TRPM7 Function by NS8593.* International Journal of Molecular Sciences, 2020. **21**(19): p. 7017.

325. Chubanov, V., M. Mederos Y Schnitzler, M. Meißner, S. Schäfer, K. Abstiens, T. Hofmann, and T. Gudermann, *Natural and synthetic modulators of SK (Kca2) potassium channels inhibit magnesium-dependent activity of the kinase-coupled cation channel TRPM7.* British Journal of Pharmacology, 2012. **166**(4): p. 1357-1376.

326. Strøbæk, D., C. Hougaard, T.H. Johansen, U.S. Sørensen, E.Ø. Nielsen, K.S. Nielsen, R.D.T. Taylor, P. Pedarzani, and P. Christophersen, *Inhibitory Gating Modulation of Small Conductance Ca2+-Activated K+ Channels by the Synthetic Compound (R)-N-(Benzimidazol-2-yl)-1,2,3,4-tetrahydro-1-naphtylamine(NS8593) Reduces Afterhyperpolarizing Current in Hippocampal CA1 Neurons.* Molecular Pharmacology, 2006. **70**(5): p. 1771-1782.

327. Song, C., Y. Bae, J. Jun, H. Lee, N.D. Kim, K.B. Lee, W. Hur, J.Y. Park, and T. Sim, *Identification of TG100-115 as a new and potent TRPM7 kinase inhibitor, which suppresses breast cancer cell migration and invasion.* Biochim Biophys Acta Gen Subj, 2017. **1861**(4): p. 947-957.

328. Doukas, J., W. Wrasidlo, G. Noronha, E. Dneprovskaia, R. Fine, S. Weis, J. Hood, A. DeMaria, R. Soll, and D. Cheresh, *Phosphoinositide 3-kinase gamma/delta inhibition limits infarct size after myocardial ischemia/reperfusion injury.* Proceedings of the National Academy of Sciences, 2006. **103**(52): p. 19866-19871.

329. Romagnani, A., V. Vettore, T. Rezzonico-Jost, S. Hampe, E. Rottoli, W. Nadolni, M. Perotti, M.A. Meier, C. Hermanns, S. Geiger, G. Wennemuth, C. Recordati, M. Matsushita, S. Muehlich, M. Proietti, V. Chubanov, T. Gudermann, F. Grassi, and S. Zierler, *TRPM7 kinase activity is essential for T cell colonization and alloreactivity in the gut.* Nature Communications, 2017. **8**(1).

330. Du, J., J. Xie, Z. Zhang, H. Tsujikawa, D. Fusco, D. Silverman, B. Liang, and L. Yue, *TRPM7-mediated Ca2+ signals confer fibrogenesis in human atrial fibrillation.* Circ Res, 2010. **106**(5): p. 992-1003.

331. Suzuki, S., R. Penner, and A. Fleig, *TRPM7 contributes to progressive nephropathy.* Scientific Reports, 2020. **10**(1): p. 2333.

332. Hu, F., M. Li, F. Han, Q. Zhang, Y. Zeng, W. Zhang, and X. Cheng, *Role of TRPM7 in cardiac fibrosis: A potential therapeutic target (Review).* Exp Ther Med, 2021. **21**(2): p. 173.

333. Yu, M., C. Huang, Y. Huang, X. Wu, X. Li, and J. Li, *Inhibition of TRPM7 channels prevents proliferation and differentiation of human lung fibroblasts.* Inflammation Research, 2013. **62**(11): p. 961-970.

334. Fang, L., C. Huang, X. Meng, B. Wu, T. Ma, X. Liu, Q. Zhu, S. Zhan, and J. Li, *TGF-β1-elevated TRPM7 channel regulates collagen expression in hepatic stellate cells via TGF-β1/Smad pathway.* Toxicol Appl Pharmacol, 2014. **280**(2): p. 335-44.

335. Chokshi, R., P. Fruasaha, and J.A. Kozak, *2-aminoethyl diphenyl borinate (2-APB) inhibits TRPM7 channels through an intracellular acidification mechanism.* Channels (Austin), 2012. **6**(5): p. 362-9.

336. Hermosura, M.C., M.K. Monteilh-Zoller, A.M. Scharenberg, R. Penner, and A. Fleig, *Dissociation of the store-operated calcium current I(CRAC) and the Mg-nucleotide-regulated metal ion current MagNuM.* J Physiol, 2002. **539**(Pt 2): p. 445-58.

337. Faouzi, M., T. Kilch, F.D. Horgen, A. Fleig, and R. Penner, *The TRPM7 channel kinase regulates store-operated calcium entry.* J Physiol, 2017. **595**(10): p. 3165-3180.

338. Yee, N., *Role of TRPM7 in Cancer: Potential as Molecular Biomarker and Therapeutic Target.* Pharmaceuticals, 2017. **10**(4): p. 39.

339. Davis, F.M., I. Azimi, R.A. Faville, A.A. Peters, K. Jalink, J.W. Putney, Jr., G.J. Goodhill, E.W. Thompson, S.J. Roberts-Thomson, and G.R. Monteith, *Induction of epithelial-mesenchymal transition (EMT) in breast cancer cells is calcium signal dependent.* Oncogene, 2014. **33**(18): p. 2307-16.

340. Middelbeek, J., A.J. Kuipers, L. Henneman, D. Visser, I. Eidhof, R. van Horssen, B. Wieringa, S.V. Canisius, W. Zwart, L.F. Wessels, F.C. Sweep, P. Bult, P.N. Span, F.N. van Leeuwen, and K. Jalink, *TRPM7 is required for breast tumor cell metastasis.* Cancer Res, 2012. **72**(16): p. 4250-61.

341. Meng, X., C. Cai, J. Wu, S. Cai, C. Ye, H. Chen, Z. Yang, H. Zeng, Q. Shen, and F. Zou, *TRPM7 mediates breast cancer cell migration and invasion through the MAPK pathway.* Cancer Lett, 2013. **333**(1): p. 96-102.

342. Zierler, S., G. Yao, Z. Zhang, W.C. Kuo, P. Pörzgen, R. Penner, F.D. Horgen, and A. Fleig, *Waixenicin A inhibits cell proliferation through magnesium-dependent block of transient receptor potential melastatin 7 (TRPM7) channels.* J Biol Chem, 2011. **286**(45): p. 39328-35.

343. Voringer, S., L. Schreyer, W. Nadolni, M.A. Meier, K. Woerther, C. Mittermeier, S. Ferioli, S. Singer, K. Holzer, S. Zierler, V. Chubanov, B. Liebl, T. Gudermann, and S. Muehlich, *Inhibition of TRPM7 blocks MRTF/SRF-dependent transcriptional and tumorigenic activity.* Oncogene, 2020. **39**(11): p. 2328-2344.

344. Luanpitpong, S., N. Rodboon, P. Samart, C. Vinayanuwattikun, S. Klamkhlai, P. Chanvorachote, Y. Rojanasakul, and S. Issaragrisil, *A novel TRPM7/O-GlcNAc axis mediates tumour cell motility and metastasis by stabilising c-Myc and caveolin-1 in lung carcinoma.* Br J Cancer, 2020. **123**(8): p. 1289-1301.

345. Liu, K., S.-H. Xu, Z. Chen, Q.-X. Zeng, Z.-J. Li, and Z.-M. Chen, *TRPM7 overexpression enhances the cancer stem cell-like and metastatic phenotypes of lung cancer through modulation of the Hsp90α/uPA/MMP2 signaling pathway.* BMC Cancer, 2018. **18**(1).

346. Gao, H., X. Chen, X. Du, B. Guan, Y. Liu, and H. Zhang, *EGF enhances the migration of cancer cells by up-regulation of TRPM7.* Cell Calcium, 2011. **50**(6): p. 559-68.

347. Rybarczyk, P., A. Vanlaeys, B. Brassart, I. Dhennin-Duthille, D. Chatelain, H. Sevestre, H. Ouadid-Ahidouch, and M. Gautier, *The Transient Receptor Potential Melastatin 7 Channel Regulates Pancreatic Cancer Cell Invasion through the Hsp90α/uPA/MMP2 pathway.* Neoplasia, 2017. **19**(4): p. 288-300.

348. Cozens, A.L., M.J. Yezzi, K. Kunzelmann, T. Ohrui, L. Chin, K. Eng, W.E. Finkbeiner, J.H. Widdicombe, and D.C. Gruenert, *CFTR expression and chloride secretion in polarized immortal human bronchial epithelial cells.* Am J Respir Cell Mol Biol, 1994. **10**(1): p. 38-47.

349. Sanford, K.K., W.R. Earle, and G.D. Likely, *The growth in vitro of single isolated tissue cells.* J Natl Cancer Inst, 1948. **9**(3): p. 229-46.

350. Edelman, B.L. and E.F. Redente, *Isolation and Characterization of Mouse Fibroblasts*, in *Lung Innate Immunity and Inflammation: Methods and Protocols*, S. Alper and W.J. Janssen, Editors. 2018, Springer New York: New York, NY. p. 59-67.

351. Zhang, W., S. Ohno, B. Steer, S. Klee, C.A. Staab-Weijnitz, D. Wagner, M. Lehmann, T. Stoeger, M. Königshoff, and H. Adler, *S100a4 Is Secreted by Alternatively Activated Alveolar Macrophages and Promotes Activation of Lung Fibroblasts in Pulmonary Fibrosis.* Frontiers in Immunology, 2018. **9**.

352. Yokoyama, W.M., M.L. Thompson, and R.O. Ehrhardt, *Cryopreservation and thawing of cells.* Curr Protoc Immunol, 2012. **Appendix 3**: p. 3g.

353. Malmström, J., H. Lindberg, C. Lindberg, C. Bratt, E. Wieslander, E.-L. Delander, B. Särnstrand, J.S. Burns, P. Mose-Larsen, S. Fey, and G. Marko-Varga, *Transforming Growth Factor-β1 Specifically Induce Proteins Involved in the Myofibroblast Contractile Apparatus.* Molecular & Cellular Proteomics, 2004. **3**(5): p. 466-477.

354. Thannickal, V.J., D.Y. Lee, E.S. White, Z. Cui, J.M. Larios, R. Chacon, J.C. Horowitz, R.M. Day, and P.E. Thomas, *Myofibroblast differentiation by transforming growth factor-beta1 is dependent on cell adhesion and integrin signaling via focal adhesion kinase.* J Biol Chem, 2003. **278**(14): p. 12384-9.

355. Merck KGaA, S.-A. *D-Val-Leu-Lys 7-amido-4-methylcoumarin, V3138.* March 31, 2022]; Available from: https://www.sigmaaldrich.com/DE/de/product/sigma/v3138.

356. Kato, H., N. Adachi, Y. Ohno, S. Iwanaga, K. Takada, and S. Sakakibara, *New fluorogenic peptide substrates for plasmin.* J Biochem, 1980. **88**(1): p. 183-90.

357. Michael, I.P., G. Sotiropoulou, G. Pampalakis, A. Magklara, M. Ghosh, G. Wasney, and E.P. Diamandis, *Biochemical and Enzymatic Characterization of Human Kallikrein 5 (hK5), a Novel Serine Protease Potentially Involved in Cancer Progression*.* Journal of Biological Chemistry, 2005. **280**(15): p. 14628-14635.

358. Schuliga, M., T. Harris, and A.G. Stewart, *Plasminogen activation by airway smooth muscle is regulated by type I collagen.* Am J Respir Cell Mol Biol, 2011. **44**(6): p. 831-9.

359. Skehan, P., R. Storeng, D. Scudiero, A. Monks, J. McMahon, D. Vistica, J.T. Warren, H. Bokesch, S. Kenney, and M.R. Boyd, *New colorimetric cytotoxicity assay for anticancer-drug screening.* J Natl Cancer Inst, 1990. **82**(13): p. 1107-12.

360. Kiernan, J., *Histological and histochemical methods : theory and practice / J. A. Kiernan.* SERBIULA (sistema Librum 2.0), 1999.

361. Laemmli, U.K., *Cleavage of Structural Proteins during the Assembly of the Head of Bacteriophage T4.* Nature, 1970. **227**(5259): p. 680-685.

362. Smith, B.J., *SDS Polyacrylamide Gel Electrophoresis of Proteins.* Methods Mol Biol, 1984. **1**: p. 41-55.

363. Fire, A., S. Xu, M.K. Montgomery, S.A. Kostas, S.E. Driver, and C.C. Mello, *Potent and specific genetic interference by double-stranded RNA in Caenorhabditis elegans.* Nature, 1998. **391**(6669): p. 806-11.

364. Dupont, S., L. Morsut, M. Aragona, E. Enzo, S. Giulitti, M. Cordenonsi, F. Zanconato, J. Le Digabel, M. Forcato, S. Bicciato, N. Elvassore, and S. Piccolo, *Role of YAP/TAZ in mechanotransduction.* Nature, 2011. **474**(7350): p. 179-183.

365. Breit, A., K. Wicht, I. Boekhoff, E. Glas, L. Lauffer, H. Mückter, and T. Gudermann, *Glucose Enhances Basal or Melanocortin-Induced cAMP-Response Element Activity in Hypothalamic Cells.* Molecular endocrinology (Baltimore, Md.), 2016. **30**(7): p. 748-762.

366. Peskin, A.V. and C.C. Winterbourn, *A microtiter plate assay for superoxide dismutase using a water-soluble tetrazolium salt (WST-1).* Clin Chim Acta, 2000. **293**(1-2): p. 157-66.

367.	Horowitz, J.C., D.S. Rogers, R.H. Simon, T.H. Sisson, and V.J. Thannickal, *Plasminogen Activation–Induced Pericellular Fibronectin Proteolysis Promotes Fibroblast Apoptosis.* American Journal of Respiratory Cell and Molecular Biology, 2008. **38**(1): p. 78-87.

368.	Ard, S., E.B. Reed, L.V. Smolyaninova, S.N. Orlov, G.M. Mutlu, R.D. Guzy, and N.O. Dulin, *Sustained Smad2 Phosphorylation Is Required for Myofibroblast Transformation in Response to TGF-β.* American Journal of Respiratory Cell and Molecular Biology, 2019. **60**(3): p. 367-369.

369.	Gu, L., Y.J. Zhu, X. Yang, Z.J. Guo, W.B. Xu, and X.L. Tian, *Effect of TGF-beta/Smad signaling pathway on lung myofibroblast differentiation.* Acta Pharmacol Sin, 2007. **28**(3): p. 382-91.

370.	Li, S., A. Xu, Y. Li, C. Tan, G. La Regina, R. Silvestri, H. Wang, and W. Qi, *RS4651 suppresses lung fibroblast activation via the TGF-β1/SMAD signalling pathway.* European Journal of Pharmacology, 2021. **903**: p. 174135.

371.	Life-Technologies. *Episomal iPSC Reprogramming Vectors.* 2012 May 11, 2022]; Available from: https://tools.thermofisher.com/content/sfs/manuals/episomal_iPSC_reprogramming_vectors_man.pdf.

372.	Quax, P.H.A., I.L.A. Boxman, C.A.M. van Kesteren, J.H. Verheijen, and M. Ponec, *Plasminogen activators are involved in keratinocyte and fibroblast migration in wounded cultures in vitro.* Fibrinolysis, 1994. **8**(4): p. 221-228.

373.	Zhu, S., C.L. Gladson, K.E. White, Q. Ding, J. Jerry Stewart, T.H. Jin, J. Harold A. Chapman, and M.A. Olman, *Urokinase receptor mediates lung fibroblast attachment and migration toward provisional matrix proteins through interaction with multiple integrins.* American Journal of Physiology-Lung Cellular and Molecular Physiology, 2009. **297**(1): p. L97-L108.

374.	Santibanez, J.F., H. Obradović, T. Kukolj, and J. Krstić, *Transforming growth factor-β, matrix metalloproteinases, and urokinase-type plasminogen activator interaction in the cancer epithelial to mesenchymal transition.* Dev Dyn, 2018. **247**(3): p. 382-395.

375.	Lian, G.Y., Q.M. Wang, T.S. Mak, X.R. Huang, X.Q. Yu, and H.Y. Lan, *Inhibition of tumor invasion and metastasis by targeting TGF-β-Smad-MMP2 pathway with Asiatic acid and Naringenin.* Mol Ther Oncolytics, 2021. **20**: p. 277-289.

376.	Masuda, T., N. Hattori, T. Senoo, S. Akita, N. Ishikawa, K. Fujitaka, Y. Haruta, H. Murai, and N. Kohno, *SK-216, an Inhibitor of Plasminogen Activator Inhibitor-1, Limits Tumor Progression and Angiogenesis.* Molecular Cancer Therapeutics, 2013. **12**(11): p. 2378-2388.

377.	Stillfried, G.E., D.N. Saunders, and M. Ranson, *Plasminogen binding and activation at the breast cancer cell surface: the integral role of urokinase activity.* Breast Cancer Research, 2007. **9**(1).

378.	Mauro, C.D., A. Pesapane, L. Formisano, R. Rosa, V. D'Amato, P. Ciciola, A. Servetto, R. Marciano, R.C. Orsini, F. Monteleone, N. Zambrano, G.

Fontanini, A. Servadio, G. Pignataro, L. Grumetto, A. Lavecchia, D. Bruzzese, A. Iaccarino, G. Troncone, B.M. Veneziani, N. Montuori, S.D. Placido, and R. Bianco, *Urokinase-type plasminogen activator receptor (uPAR) expression enhances invasion and metastasis in RAS mutated tumors.* Scientific Reports, 2017. **7**(1): p. 9388.

379. Hooglugt, A., M.M. van der Stoel, R.A. Boon, and S. Huveneers, *Endothelial YAP/TAZ Signaling in Angiogenesis and Tumor Vasculature.* Frontiers in Oncology, 2021. **10**.

380. Hayashida, T., M. Decaestecker, and H.W. Schnaper, *Cross-talk between ERK MAP kinase and Smad signaling pathways enhances TGF-beta-dependent responses in human mesangial cells.* Faseb j, 2003. **17**(11): p. 1576-8.

381. Lamy, C., S.J. Goodchild, K.L. Weatherall, D.E. Jane, J.F. Liégeois, V. Seutin, and N.V. Marrion, *Allosteric block of KCa2 channels by apamin.* J Biol Chem, 2010. **285**(35): p. 27067-27077.

382. Kaitsuka, T., C. Katagiri, P. Beesetty, K. Nakamura, S. Hourani, K. Tomizawa, J.A. Kozak, and M. Matsushita, *Inactivation of TRPM7 kinase activity does not impair its channel function in mice.* Scientific reports, 2014. **4**: p. 5718-5718.

383. Nandakumar, V., L. Kelbauskas, R. Johnson, and D. Meldrum, *Quantitative characterization of preneoplastic progression using single-cell computed tomography and three-dimensional karyometry.* Cytometry A, 2011. **79**(1): p. 25-34.

384. Mitsui, Y. and E.L. Schneider, *Relationship between cell replication and volume in senescent human diploid fibroblasts.* Mech Ageing Dev, 1976. **5**(1): p. 45-56.

385. Pluskota, E., D.A. Soloviev, D. Szpak, C. Weber, and E.F. Plow, *Neutrophil apoptosis: selective regulation by different ligands of integrin alphaMbeta2.* J Immunol, 2008. **181**(5): p. 3609-19.

386. Godier, A. and B.J. Hunt, *Plasminogen receptors and their role in the pathogenesis of inflammatory, autoimmune and malignant disease.* J Thromb Haemost, 2013. **11**(1): p. 26-34.

387. Sandberg, R. and I. Ernberg, *Assessment of tumor characteristic gene expression in cell lines using a tissue similarity index (TSI).* Proceedings of the National Academy of Sciences, 2005. **102**(6): p. 2052-2057.

388. Keski-Oja, J., F. Blasi, E. Leof, and H. Moses, *Regulation of the synthesis and activity of urokinase plasminogen activator in A549 human lung carcinoma cells by transforming growth factor-beta.* Journal of Cell Biology, 1988. **106**(2): p. 451-459.

389. Santibáñez, J.F., M. Iglesias, P. Frontelo, J. Martínez, and M. Quintanilla, *Involvement of the Ras/MAPK Signaling Pathway in the Modulation of Urokinase Production and Cellular Invasiveness by Transforming Growth Factor-β1 in Transformed Keratinocytes.* Biochemical and Biophysical Research Communications, 2000. **273**(2): p. 521-527.

390. Nakao, T., S. Kim, K. Ohta, H. Kawano, M. Hino, K. Miura, N. Tatsumi, and H. Iwao, *Role of mitogen-activated protein kinase family in serum-induced leukaemia inhibitory factor and interleukin-6 secretion by bone marrow stromal cells.* Br J Pharmacol, 2002. **136**(7): p. 975-84.

391. Subramanian, R., C.S. Gondi, S.S. Lakka, A. Jutla, and J.S. Rao, *siRNA-mediated simultaneous downregulation of uPA and its receptor inhibits angiogenesis and invasiveness triggering apoptosis in breast cancer cells.* Int J Oncol, 2006. **28**(4): p. 831-9.

392. Syrovets, T., M. Jendrach, A. Rohwedder, A. Schüle, and T. Simmet, *Plasmin-induced expression of cytokines and tissue factor in human monocytes involves AP-1 and IKKbeta-mediated NF-kappaB activation.* Blood, 2001. **97**(12): p. 3941-50.

393. De Sousa, L.P., B.S. Brasil, B.M. Silva, M.H. Freitas, S.V. Nogueira, P.C. Ferreira, E.G. Kroon, and C.A. Bonjardim, *Plasminogen/plasmin regulates c-fos and egr-1 expression via the MEK/ERK pathway.* Biochem Biophys Res Commun, 2005. **329**(1): p. 237-45.

394. Miki, K., H. Tanaka, Y. Nagai, C. Kimura, and M. Oike, *Transforming Growth Factor β1 Alters Calcium Mobilizing Properties and Endogenous ATP Release in A549 Cells: Possible Implications for Cell Migration.* Journal of pharmacological sciences, 2010. **113**: p. 387-94.

395. Zhao, L., S. Liu, X. Che, K. Hou, Y. Ma, C. Li, T. Wen, Y. Fan, X. Hu, Y. Liu, and X. Qu, *Bufalin inhibits TGF-β-induced epithelial-to-mesenchymal transition and migration in human lung cancer A549 cells by downregulating TGF-β receptors.* Int J Mol Med, 2015. **36**(3): p. 645-652.

396. Feng, H.-T., W.-W. Zhao, J.-J. Lu, Y.-T. Wang, and X.-P. Chen, *Hypaconitine inhibits TGF-β1-induced epithelial–mesenchymal transition and suppresses adhesion, migration, and invasion of lung cancer A549 cells.* Chinese Journal of Natural Medicines, 2017. **15**(6): p. 427-435.

397. Ryazanova, L.V., M.V. Dorovkov, A. Ansari, and A.G. Ryazanov, *Characterization of the protein kinase activity of TRPM7/ChaK1, a protein kinase fused to the transient receptor potential ion channel.* J Biol Chem, 2004. **279**(5): p. 3708-16.

398. Ryazanova, L.V., L.J. Rondon, S. Zierler, Z. Hu, J. Galli, T.P. Yamaguchi, A. Mazur, A. Fleig, and A.G. Ryazanov, *TRPM7 is essential for Mg(2+) homeostasis in mammals.* Nat Commun, 2010. **1**: p. 109.

399. Yogi, A., G.E. Callera, S. O'Connor, T.T. Antunes, W. Valinsky, P. Miquel, A.C. Montezano, A.L. Perraud, C. Schmitz, A. Shrier, and R.M. Touyz, *Aldosterone signaling through transient receptor potential melastatin 7 cation channel (TRPM7) and its α-kinase domain.* Cell Signal, 2013. **25**(11): p. 2163-75.

400. Yu, M., C. Huang, Y. Huang, X. Wu, X. Li, and J. Li, *Inhibition of TRPM7 channels prevents proliferation and differentiation of human lung fibroblasts.* Inflamm Res, 2013. **62**(11): p. 961-70.

401. Wicks, S.J., S. Lui, N. Abdel-Wahab, R.M. Mason, and A. Chantry, *Inactivation of smad-transforming growth factor beta signaling by Ca(2+)-calmodulin-dependent protein kinase II.* Mol Cell Biol, 2000. **20**(21): p. 8103-11.

402. Zimmerman, C.M., M.S. Kariapper, and L.S. Mathews, *Smad proteins physically interact with calmodulin.* J Biol Chem, 1998. **273**(2): p. 677-80.

403. Su, C., Y. Tang, C. Wang, H. Huang, and H. Hou, *Platyconic acid A-induced PPM1A upregulation inhibits the proliferation, inflammation and extracellular matrix deposition of TGF-β1-induced lung fibroblasts.* Mol Med Rep, 2022. **26**(5).

404. Rössig, A., K. Hill, W. Nörenberg, S. Weidenbach, S. Zierler, M. Schaefer, T. Gudermann, and V. Chubanov, *Pharmacological agents selectively acting on the channel moieties of TRPM6 and TRPM7.* Cell Calcium, 2022. **106**: p. 102640.

405. Zeitlmayr, S., S. Zierler, C.A. Staab-Weijnitz, A. Dietrich, F. Geiger, F.D. Horgen, T. Gudermann, and A. Breit, *TRPM7 restrains plasmin activity and promotes transforming growth factor-β1 signaling in primary human lung fibroblasts.* Arch Toxicol, 2022. **96**(10): p. 2767-2783.

The following illustrations were designed using Biorender.com:

Figures created with BioRender.com:
fig 1, fig 14, fig 15, fig 24, fig 44, fig 79

Figures adapted from "Canonical and Non-canonical TGFb Pathways in EMT", by BioRender.com (2022). Retrieved from https://app.biorender.com/biorender-templates:

fig 2, fig 3, fig 4, fig 76, fig 77

Figure adapted from "RNAi Mechanism", by BioRender.com (2022). Retrieved from https://app.biorender.com/biorender-templates:

fig 10

Figure adapted from "COVID-19 Diagnostic Test through RT-PCR", by BioRender.com (2022). Retrieved from https://app.biorender.com/biorender-templates:

fig 12

9. Appendix

List of abbreviations

ANOVA	analysis of variance
AP-1	activator protein 1
AUC	Area under curve
BSA	Bovine serum albumin
cDNA	complementary DNA
Co-SMAD	co-mediator SMAD
Cp	Crossing point
DLC1	deleted in liver cancer 1
DMSO	dimethyl sulfoxide
ECM	extracellular matrix
EDTA	Disodium ethylenediaminetetraacetic acid
EGFR	Epidermal growth factor receptor
ELISA	Enzyme-linked Immunosorbent Assay
EMT	epithelial to mesenchymal transition
ERK1/2	extracellular signal-regulated kinase 1/2
FCS	Fetal calf serum
GDP	guanosine diphosphate
GEF	guanine nucleotide exchange factor
Grb2	growth factor receptor bound protein 2
GTP	guanosine triphosphate
HAI2	hepatocyte growth factor activator inhibitor 2
HCl	Hydrochlorid

HPAEC	primary human pulmonary artery endothelial cells
HRP	horseradish-peroxidase
ILD	interstitial lung disease
IPF	idiopathic pulmonary fibrosis
I-SMAD	inhibitory SMAD
JNK	c-Jun amino terminal kinase
kDa	Kilo dalton
LATS1/2	large tumor suppressor kinase 1/2
LB	lysogeny broth
MAPK	mitogen activated protein kinase
MEK1/2	MAP2K MAPK/ERK1/2 kinase
MH2	Mad homology 2
MMP	matrix-metalloproteinase
NSCLC	non-small cell lung cancer
OD	Optical density
PAGE	polyacrylamide gel electrophoresis
PAI1	plasminogen activator inhibitor 1
PBS	phosphate buffered saline
PF	pulmonary fibrosis
pHPF	primary human pulmonary fibroblasts
PI3K/Akt	phosphoinositide 3-kinase/ protein kinase B
PLG	plasminogen
pMPF	Primary mouse pulmonary fibroblasts

PPM1A	protein phosphatase, Mg^{2+}/Mn^{2+} dependent 1A
qRT-PCR	Quantitative real-time reverse transcriptase polymerase chain reaction
RFU	Random fluorescence unit
RhoA	Ras homolog family member A
RISC	RNA-induced silencing complex
RLU	Random light unit
ROCK	Rho-associated kinase
R-SMAD	receptor-regulated SMAD
RT	room temperature
SARA	SMAD anchor for receptor activation protein
SDHA	succinate dehydrogenase complex, subunit A
SDS	sodium dodecyl sulfate
SEM	standard error of the mean
siRNA	small interfering RNAs
SK channels	small conductance Ca^{2+}-activated K^+ channels
SRB	sulforhodamine B
TAK1	TGF-β-activated kinase 1
TAZ	WW domain-containing protein
TBST	TRIS-buffered saline
TEAD	TEA domain family member
TGF-β	transforming growth factor β
TMB	3,3′,5,5′-tetramethylbenzidine

tPA	tissue-type plasmin activator
TRIS	Tris-(hydroxymethyl)-aminomethan
TRP	transient receptor potential
TRPM7	transient receptor potential cation channel, subfamily M, member 7
uPA	urokinase-type plasmin activator
uPAR	urokinase-type plasmin activator receptor
WST-1	Water soluble tetrazolium 1
WT	Wild type
YAP	Yes-associated protein
α-sma	α-smooth muscle actin

List of figures

List of tables

List of publications

Zeitlmayr S, Zierler S, Staab-Weijnitz CA, Dietrich A, Geiger F, Horgen FD, Gudermann T, Breit A, *TRPM7 restrains plasmin activity and promotes transforming growth factor-β1 signaling in primary human lung fibroblasts*. Arch Toxicol, 2022 Oct; **96**(10):2767-2783

Geiger F, Zeitlmayr S, Staab-Weijnitz CA, Rajan S, Breit A, Gudermann T, Dietrich A, *An Inhibitory Function of TRPA1 Channels in TGF-β1-driven Fibroblast to Myofibroblast Differentiation*. Am J Respir Cell Mol Biol, 2022 Nov

Webert L, Faro D, Zeitlmayr S, Gudermann T, Breit A, *Analysis of the Glucose-Dependent Transcriptome in Murine Hypothalamic Cells*. Cells, 2022 Feb; **11**(4):639

The following figures contain already published results in the above-mentioned article in Archives of Toxicology and were reproduced with permission from Springer Nature [405]:

Fig 17

Fig 23

Fig 36-43

Fig 53-67

Fig 73

Fig 78

Conference contributions

Zeitlmayr S, Gudermann T, Breit A, *Effects of TRPM7 on TGF-β-induced signaling in lung cells*, annual GRK 2338 retreat, 2019

Zeitlmayr S, Gudermann T, Breit A, *Effects of TRPM7 on TGF-β-induced signaling in lung cells*, 5th German Pharm-Tox Summit, 2020

Zeitlmayr S, Gudermann T, Breit A, *A role for TRPM7 in plasmin activation in lung cells*, annual GRK 2338 retreat, 2020

Zeitlmayr S, Gudermann T, Breit A, *TRPM7 activity restrains plasmin activity and promotes transforming growth factor-β1 signaling in primary human lung fibroblasts (pHPF)*, annual GRK 2338 retreat, 2022

Affidavite

Affidavit

Zeitlmayr, Sarah
_____
Surname, first name

_____
Address

I hereby declare, that the submitted thesis entitled

is my own work. I have only used the sources indicated and have not made unauthorised use of services of a third party. Where the work of others has been quoted or reproduced, the source is always given.

I further declare that the dissertation presented here has not been submitted in the same or similar form to any other institution for the purpose of obtaining an academic degree.

Munich, 18.07.2023
_____
Place, Date

Sarah Zeitlmayr
_____
Signature doctoral candidate

Confirmation of congruency

LMU | LUDWIG-MAXIMILIANS-UNIVERSITÄT MÜNCHEN | Dekanat Medizinische Fakultät Promotionsbüro

Confimation of congruency between printed and electronic version of the doctoral thesis

Doctoral Candidate: Sarah Zeitlmayr

Address:

I hereby declare that the electronic version of the submitted thesis, entitled

is congruent with the printed version both in content and format.

Munich, 18.07.2023

Place, Date

Sarah Zeitlmayr

Signature doctoral candidate

Danksagung

An erster Stelle möchte ich meinem Doktorvater Prof. Dr. med. Gudermann danken, dass ich diese Arbeit am Walther-Straub-Institut anfertigen durfte.

Danke an alle Mitglieder meines *thesis advisory committee* für die Anregungen und Diskussionen in den TAC Meetings. Für die Bereitstellung von Plasmiden und die Methodenvorschläge möchte ich PD Dr. habil. med. Claudia Staab-Weijnitz, PhD, danken. Dankeschön an Prof. Dr. rer. nat. habil. Susanna Zierler für das Bereitstellen der Mäuse und Waixenicin A.

Ein herzliches Dankeschön an die mir noch unbekannten Gutachter für die Mühe bei der Begutachtung meiner Arbeit.

Ein besonders großer Dank geht an Dr. Andreas Breit. Danke für deine Geduld, deinen Ideenreichtum, für alle wissenschaftlichen und nicht-wissenschaftlichen Diskussionen und für alles, was ich von dir lernen durfte. Danke, dass du jederzeit helfend zur Seite stehst und dass du deine Studenten an erste Stelle stellst. Nicht zu vergessen: Danke für die Burger und deine Künste am Grill.

Weiterhin möchte ich mich bei Prof. Dr. rer. nat. Alexander Dietrich und bei Fabienne für die Zusammenarbeit und die Hilfe bei der Fibroblasten-Isolierung bedanken. Für die Finanzierung des Projekts und die vielseitigen Möglichkeiten das Programm zu strukturieren möchte ich dem GRK2338 danken.

Ein riesiges Dankeschön an alle Kolleginnen und Kollegen im WSI und an alle Mitglieder des GRK2338, die ich über die Jahre kennenlernen durfte und die zu der tollen Arbeitsatmosphäre beigetragen haben.

Liebe Steffi, ganz großen Dank für deine Hilfe über die Jahre, deine herzliche Art, dein Engagement und für legendäre Momente auf der Weihnachtsfeier. Herr Eggerbauer, merce für die Landshut Tour und dafür, dass du mein Lieblings-Niederbayer bist! Kuss auf die Nuss! Lieber Alex, danke für den smarten Stuhl, für deine sensationellen YouTube Kenntnisse, fürs Kasten schleppen und für deine wunderbar ansteckende Fröhlichkeit. Danke an Luisa für all die kleinen Aufmerksamkeiten, die Obstversorgung und den Burrito Tag. Ein besonders großes Dankeschön geht an alle ehemaligen und aktuellen Mitglieder der AG Breit. Lieber Dennis, danke für eine unvergessliche Bürozeit und deine Hilfe bei jeder Art von Problemen. Deine Spinnereien sind der Stoff aus dem Träume gemacht sind!

Danke Hardy fürs Aufessen meiner zu großen Portionen. Tila, danke für deine Hilfe, für viele lustige Momente und dass du mir meine verrückten Anwandlungen nicht krumm nimmst. Liebe Franzi, danke für die schöne (wenn auch viel zu kurze) Zeit im Büro, danke für jedes Feierabendbier und danke, dass du mich mit Koffein versorgst. Du bist ein würdiger Nachfolger für die AG Bright!

Ein besonderes Dankeschön an Ute, für deine Hilfe, deinen Optimismus und deine herzliche Art. Deine Labor-Organisation hat mir sehr oft Schlamassel erspart.

Chief Doris - vielen Dank für die Büro-Begrünung. Danke an Frau Schreier, dass Sie immer Zeit zum Helfen finden. Danke an die IT-Crowd für die schnelle Hilfe bei PC-Problemchen und für die gute Büro-Nachbarschaft! Danke Markus für Puddingpausen, Ü-Eier und dass du die beste Konditorin der Welt geheiratet hast! Liebe Franziska, danke fürs Kuchen backen, obwohl du mich nicht mal kanntest.

Liebe Janina, danke für deine Freundschaft und dass du jederzeit ein offenes Ohr für mich hast. Danke für die Weinauswahl und deine psychologischen Analysen. Edler Markus, danke, dass du stets meinen Horizont erweiterst, danke für abstruse und tiefsinnige Gespräche auf deinem Balkon und dass ich in deiner Wohnung rumwobbeln darf! Ein herzliches Dankeschön an Fr. Hafner für zahlreiche und anschauliche Ratschläge. Balduin und Lennox, danke für unzählige schöne und erholsame Stunden mit euch.

Der größte Dank geht an meine Eltern, Großeltern und meinen Bruder. Danke euch allen für eure Unterstützung, obwohl ihr keinen Plan hattet was ich da eigentlich mache. Dafür danke ich ebenso meinen Schwiegereltern Sigrid und Franz. Danke Oma und Opa, dass ihr immer ans Telefon geht. Mama und Papa, ich bin euch unendlich dankbar. Dafür, dass ihr immer an mich glaubt und für eure bedingungslose Hilfe in allen Lebenslagen. Ihr seid die Besten! Buale, ich könnte mir keinen besseren Bruder wünschen und bin froh, dass wir beide den gleichen Knacks haben!

Lieber Flo, dir kann ich zweifellos nicht genug danken. Danke für deine Liebe, deinen unerschütterlichen Optimismus und Glauben an mich. Merce für alles!